UNIVERSIDADE DO ALGARVE

The activity of mouse *Cerberus like 2* during cardiogenesis – genetic and morphogenetic studies

Ana Carolina Borges de Araújo

Tese para obtenção do grau de Doutor em Ciências Biomédicas

Trabalho efetuado sob a orientação de Professor Doutor

José António Belo

2013

Dissertação de Candidatura ao Grau de Doutor em Ciências Biomédicas, pela Universidade do Algarve.

PhD Thesis Proposal in Biomedical Sciences, by the University of Algarve (Portugal).

O trabalho apresentado nesta tese foi realizado com o apoio financeiro da Fundação para a Ciência e Tecnologia (bolsa de referência SFRH/BD/62081/2009).

Foundation of Technology and Science supported the work presented in this thesis (SFRH/BD/62081/2009).

The activity of mouse *Cerberus like 2* during cardiogenesis – genetic and morphogenetic studies

Declaração de autoria de trabalho

Declaro ser a autora deste trabalho, que é original e inédito. Autores e trabalhos consultados estão devidamente citados no texto e constam da listagem de referências incluída.

Recife minha cidade

"Vem cá que eu quero te mostrar
A minha cidade, o meu lugar
Recife tem um coração
Tem muito calor, muita emoção
O povo daqui gosta de cantar
Tem religião, gosta de rezar
Tem cristianismo, tem candomblé
Tem Luiz Gonzaga, Rei do Baião
Tem Alceu Valença, anunciação
E em Olinda o carnaval
É o melhor do mundo
É sensacional

Recife tem encantos mil
É... É um pedacinho do Brasil
É um paraíso tropical
Tem... Tem um acervo cultural
Ela é a Veneza desse Brasil
É intercortada por muitos rios
A capital do meu Pernambuco
Capitania que deu mais lucro

O Brasil, eu sei, tem muita beleza
Mas sou de Recife e devo cantar
A minha cidade, o meu lugar"

Reginaldo Rossi

Acknowledgements

Antes de mais queria agradecer em primeiro lugar ao meu orientador, Professor Doutor José A. Belo por ter possibilitado que este trabalho tenha sido feito no seu laboratório, por toda a supervisão e apoio.

Um grande obrigada aos membros do comité, os Professores Doutores José Bragança e Luís Rosário pelas discussões e incentivos.

Agradeço à Fundação para a Ciência e a Tecnologia pelo apoio financeiro.

À Universidade do Algarve e aos membros do Comité Científico do Programa Doutoral em Ciências Biomédicas queria agradecer por terem-me aceite como estudante de doutoramento.

Ao Centro de Biomedicina Molecular e Estrutural e ao Departamento de Ciências Biomédicas e Medicina pelo óptimo laboratório e por todo apoio que me foi prestado o qual possibilitou a elaboração deste trabalho.

Queria agradecer aos ex-membros do laboratório, especialmente à Salomé Almeida e João Facucho e aos atuais membros Fernando Cristo, João Furtado, Elizabeth Correia, Margaret Soares, Marta Burlacu, Rubina Perestrelo e Tiago Justo. Um grandessíssimo obrigada ao José Inácio, ao Paulo Pereira e à Sara Marques pela leitura crítica da tese.

Obrigada às minhas colegas do Programa Doutoral em Ciências Biomédicas Marinella Guezzo, Mónica Fernandes e Rita Costa pelo apoio e amizade.

Obrigada pelo suporte técnico prestado dos técnicos Ana Tatá, André Mozes, Claudia Florindo e Neusa Miguel. Um agradecimento especial a Maurícia Vinhas, por pacientemente ter seccionado grande parte das minhas amostras e de termos partilhado conhecimento e trabalho a cerca da ecocardiografia.

Por último às pessoas mais importantes da minha vida. Ao meu querido marido Nuno, que esteve sempre ao meu lado a dar-me suporte incondicional. Também não posso deixar de agradecer aos meus sogros Sr. Álvaro e D. Teresa, e ao meu cunhado Ricardo pelo suporte e encorajamento. Aos meus amigos e família que estão do outro lado do oceano. E por fim, nada na minha vida seria possível sem o grande apoio da minha amada mãe Sônia e das manas Luciana e Silvana nestes tantos anos de distância e ausência. Um agradecimento especial ao meu padrasto Zé Torres e ao cunhado Vinícius. Amo muito vocês e obrigada!

Resumo

Sendo o coração o primeiro órgão a ser formado, é também o primeiro a funcionar com o objectivo de suprir as necessidades do embrião vertebrado. No entanto, a morfogénese cardíaca é bastante complexa, e perturbações podem originar doenças cardíacas congénitas, sendo os defeitos com maior incidência à nascença. Com o objectivo de melhor compreender a intrincada base molecular que controla a formação e o desenvolvimento deste órgão e assim promover a união entre prevenção e tratamento, é de importância fundamental aprofundar os conhecimentos nesta área de investigação.

Apesar das óbvias diferenças entre o humano e o ratinho, o coração nos dois modelos animais é constituído por quatro câmaras (dois átrios e dois ventrículos) e os respectivos funcionamentos são semelhante tendo contudo algumas ressalvas ao serem equiparados. Além disto, 99% dos genes no ratinho têm equivalentes em humanos, logo o ratinho é considerado um ótimo modelo para o estudo de doenças humanas.

Durante o desenvolvimento, o coração recebe informação para se posicionar ao longo dos três eixos do corpo. É o terceiro eixo, o esquerdo-direito (E/D), que determina a direção de rotação do coração e que portanto influencia a sua morfologia final, como exemplo, ventrículo e átrio esquerdo posicionados no lado esquerdo do embrião. Embora já se saiba através de recentes estudos em peixe-zebra como o sinal assimétrico do eixo E/D direciona a rotação cardíaca, ainda é desconhecido a influência deste eixo no posicionamento dos outros órgãos viscerais.

Nodal, membro da família de factores de crescimento TGF-ß, tem sido reconhecido como um elemento chave durante o estabelecimento do eixo E/D e do desenvolvimento do embrião sendo especialmente requerido para a formação da mesoderme. O membro da família Cerberus/Dan, mouse *cerberus-like2 (Cerl2)*, é expresso assimetricamente no lado direito do nó em ratinhos e codifica a proteína que uma vez secretada é capaz de se ligar diretamente a Nodal. Dessa maneira, o antagonismo entre Cerl2 e Nodal é essencial para restringir assimetricamente a atividade do Nodal para o lado esquerdo do nó levando a indução da sua cascata de sinalização na placa lateral da mesoderme esquerda. Esta restrição assimétrica para o lado esquerdo do embrião vai determinar a orientação assimétrica dos órgãos.

Em ratinhos *knock-out* para o gene *Cerl2 (Cerl2*$^{-/-}$*)* foi demonstrado que o gene *Nodal* também pode ser expresso no lado direito do nó levando a indução da cascata de sinalização *Nodal* na placa lateral da mesoderme direita. Como consequência os ratinhos *Cerl2*$^{-/-}$ manifestam uma variedade de defeitos de lateralidade (DL) conhecidos como *situs inversus*, isomerismo e heterotaxia. Adicionalmente estão associadas aos DL malformações cardiovasculares, sendo as mais comuns rotação alterada do eixo cardíaco, defeitos no septo ventricular e atrial, bem como alterações na rotação e diferenciação das artérias, estas últimas conhecidas como transposição das grandes artérias, tronco arterioso comum, dupla saída do ventrículo direito e dupla via de saída do ventrículo esquerdo. Assim, estes fenótipos podem ser a causa de morte nos primeiros dias de vida dos animais *Cerl2* mutantes. Adicionalmente, resultados preliminares revelaram um novo fenótipo nos *Cerl2*$^{-/-}$ recém-nascidos caracterizado pelo aumento da espessura das paredes do ventrículo esquerdo ao qual nestes animais não foram associados defeitos de lateralidade.

De forma a caracterizar detalhadamente este fenótipo e identificar o papel do *Cerl2* durante a formação do coração, procedeu-se à análise do fenótipo cardíaco em embriões e em ratinhos no começo da vida pós-natal 0 (P0).

Com os dados apresentados neste estudo, demonstrou-se que o aumento da espessura do miocárdio no ventrículo esquerdo (VE) e no septo interventricular (SIV) em *Cerl2* mutantes sem DL é causado pela hiperplasia dos cardiomiócitos no ventrículo esquerdo. Além disso, nos mutantes de *Cerl2* o aumento da expressão relativa de ciclina D1 no VE foi detectada no estádio embrionário 13 (E13). Este resultado pode estar relacionado com a expressão específica de *Cerl2* no VE, tal como detectada em animais controlo, indicando assim um possível papel regulatório do Cerl2 durante a formação do coração e mais especificamente, do ventrículo esquerdo. Além disso, os ratinhos *Cerl2*$^{-/-}$ apresentaram expressão alterada de genes cardíacos durante o estádio embrionário e nas primeiras horas após o nascimento, o que é incompatível com a função cardíaca normal também confirmada pela redução da função sistólica em ratinhos neonatais de *Cerl2*$^{-/-}$. Para além de investigarmos o mecanismo celular responsável pelo aumento da massa ventricular esquerda, também sugerimos dois mecanismos moleculares pelos quais o Cerl2 pode estar envolvido. Sendo Cerl2 antagonista da via de sinalização TGFßs/Nodal/Activin/Smad2, em corações embrionários (E13) e neonatais de *Cerl2*$^{-/-}$ observou-se um aumento da fosforilação de Smad2 (pSMAD2). Estes resultados sugerem que a via de sinalização TGFßs/Nodal/Activin/Smad2 pode estar ativamente aumentada na ausência de Cerl2. Interessantemente, tem sido relatado que esta

via é essencial para a regulação da cardiogénese uma vez que também desempenha um papel relevante como mediador na patogénese cardíaca em corações de ratinho adulto após lesão.
A segunda hipótese tem como base dados recentes os quais reportam que a via de sinalização Wnt e Cerl2 estão interligadas no nó através de um *feedback* negativo, onde o *mRNA* do *Cerl2* é regulado após a transcrição por Wnt3 levando à degradação de *Cerl2* no lado esquerdo do nó e portanto estabelecendo a sua expressão de forma assimétrica. Em contrapartida, Cerl2 é capaz de inibir a auto-regulação da proteína Wnt3. Adicionalmente, também foi revelado que a via de sinalização Wnt/ß-catenin é essencial para estimular a proliferação de cardiomiócitos na camada compacta de ambos os ventrículos. Apesar de em nenhum estudo até agora ter sido demonstrada a relação entre Wnt/ß-catenin e Cerl2 no coração e de serem necessárias confirmações adicionais, sugerimos que a hiperplasia do VE encontrado em *Cerl2*$^{-/-}$ pode também ser devida ao aumento da via de sinalização Wnt/ß-catenin.

Uma vez que as células estaminais embrionárias derivadas da estirpe 129 de ratinho colonizam eficientemente as linhas germinativas, esta linhagem celular tem sido utilizada com frequência para a produção de linhas de animais geneticamente modificados. Como diferentes fundos genéticos podem originar diferentes fenótipos, o estabelecimento de valores de referência para cada estirpe de ratinhos é uma ferramenta útil nos dias atuais.

A ecocardiografia não-invasiva permite avaliar a função cardíaca e a morfometria ventricular esquerda e o seu uso tem crescido na última década. Dessa maneira, foram criados valores de referência para a estirpe 129/Sv de ratinhos juvenis (3 semanas) e adultos (8 semanas).

Com o objectivo de analisar se os ratinhos *Cerl2*$^{-/-}$ continuam a manifestar um aumento da massa ventricular esquerda com a redução da função cardíaca, procedeu-se à monitorização, através de ecocardiografia, de ratinhos recém-nascidos até à fase de jovens adultos (P60).

Uma parte significante dos mutantes *Cerl2* morrem no primeiro dia de vida, na presença e na ausência de DL. Tem sido relatado que a presença de DL é incompatível com um longo tempo de vida e portanto é esperado que a grande maioria destes mutantes com DL não sobrevivam. Já nos mutantes de *Cerl2* que morrem nas primeiras horas de vida e não apresentaram defeitos de lateralidade, foi detectada uma tendência para o aumento da massa ventricular esquerda a qual é indicativa de hipertrofia. Além disto este grupo revelou uma

dramática redução da função cardíaca como foi demonstrado pela diminuição dos batimentos cardíacos por minuto e pela diminuição do pico da velocidade da artéria pulmonar. Curiosamente, os mutantes de *Cerl2* que sobrevivem conseguem recuperar a sua função cardíaca como também demonstrado pela fração de ejeção, a fração de encurtamento e a fração de alteração das áreas (sistólica e diastólica) quando comparados com os animais controlo. Este resultado foi confirmado pela manutenção dos níveis de expressão dos indicadores de hipertrofia e stress (como por exemplo o *Anp*, *Bnp* e *Ankrd1*). Dessa maneira, concluiu-se que o primeiro dia de vida pós-natal é determinante para os mutantes que não apresentam DL. Contudo é desconhecido o(s) factor(es) que determina(m) a morte ou sobrevivência destes animais.

Apesar da melhora na função cardíaca nos adultos de *Cerl2*$^{-/-}$, o débito cardíaco obtido no ventrículo esquerdo quando normalizado pelo peso do corpo, revelou uma redução quando comparado com animais *wild-type*, indicando portanto que a recuperação da função sistólica não é completa. Curiosamente os ratinhos adultos *Cerl2*$^{-/-}$ quando comparados com os ratinhos controlo apresentaram diferentes padrões de dimensão nas paredes do VE, como exemplo afinamento da parede anterior e posterior. De acordo com a literatura tem sido sugerido que a alteração aeróbica regional do metabolismo cardíaco pode levar á uma diferença assimétrica na espessura das paredes dos ventrículos, sendo no entanto necessária uma investigação detalhada.

Embora ainda seja desconhecido o mecanismo pelo qual os ratinhos *Cerl2*$^{-/-}$ conseguem adaptar-se a vida pós-natal, sugerimos que o estes ratinhos mutantes podem ser um modelo interessante para estudar os mecanismos moleculares, celulares e fisiológicos que estão por trás da restauração da função cardíaca. Portanto análises detalhadas neste modelo poderia ajudar a desenvolver abordagens terapêuticas para o tratamento de insuficiência cardíaca.

Em conclusão, os resultados apresentados nesta tese proporcionam um conjunto importantes de novos dados relacionados com a cardigénese, durante e após a vida intrauterina, os quais revelam a importância de Cerl2 na regulação da formação do coração independentemente da sua bem conhecida função no estabelecimento do eixo E/D.

Palavras chave: *Cerl2,* cardiogénese, hiperplasia, função cardíaca

Abstract

Cardiogenesis is a delicate and complex process that requires the coordination of an intricate network of pathways and the different cell types. Therefore, understanding heart development at the morphogenetic level is an essential requirement to uncover the causes of congenital heart disease and to provide insight for disease therapies.

Mouse *Cerberus like 2* (*Cerl2*) has been defined as a *Nodal* antagonist in the node with an important role in the Left-Right (L/R) axis establishment, at the early embryonic development. As expected, *Cerl2* knockout mice *(Cerl2*$^{-/-}$*)* showed multiple laterality defects with associated cardiac failure. In order to identify the endogenous role of *Cerl2* during heart formation independent of its described functions in the node, we accurately analyzed animals where laterality defects were not present. We thereby unravel the consequences of *Cerl2* loss-of-function in the heart, namely increased left ventricular thickness due to hyperplasia of cardiomyocytes and de-regulated expression of cardiac genes. Furthermore, the *Cerl2* mutant neonates present impaired cardiac function. Once that the cardiac expression of *Cerl2* is mostly observed in the left ventricle until around midgestration, this result suggest a specific regulatory role of Cerl2 during the formation of the left ventricular myoarchitecture. Here, we present two possible molecular mechanisms underlying the cardiac Cerl2 function, the regulation of Cerl2 antagonist in activation of the TGFßs/Nodal/Activin/Smad2 signaling identified by increased Smad2 phosphorilation in *Cerl2*$^{-/-}$ hearts and the negative feedback between Cerl2 and Wnt/ß-catenin signaling in heart formation.

In this work and since embryonic stem cells derived from 129 mice strain is extensively used to produce targeted mutants, we also present echocardiographic reference values to progressive use of juveniles and young adult 129/Sv strain in cardiac studies. In addition, we investigate the cardiac physiology of the surviving *Cerl2* mutants in 129/Sv background over time through a follow-up study using echocardiographic analysis. Our results revealed that *Cerl2*$^{-/-}$ mice are able to improve and maintain the diastolic and most of systolic cardiac physiologic parameters as analyzed until young adult age. Since *Cerl2* is no longer expressed in the postnatal heart, we suggest that an intrinsic and compensatory mechanism of adaptation may be active for recovering the decreased cardiac function found in *Cerl2* mutant neonates. Altogether, these data highlight the role of *Cerl2* during embryonic heart development in mice. Furthermore, we also suggest that *Cerl2*$^{-/-}$ may be an interesting model to uncover the molecular, cellular and physiological mechanisms behind the improvement of

the cardiac function, contributing to the development of therapeutic approaches to treat heart failures.
Keywords: mouse; *Cerl2*; cardiogenesis; hyperplasia; cardiac function

List of Contents

List of Figures

List of Tables

Abbreviations

a.a.	amino acids
AHF	anterior heart field
Ao	aorta
ALK	activin like receptor
Ankrd	ankyrin repeat domain
AVE	anterior visceral endoderm
A/P	anterior/posterior
AVE	cnterior visceral endoderm
AW	anterior wall
BMP	bone morphogenetic protein
BSA	bovine serum albumin ·
BW	body weight
cDNA	complementary DNA
CNCc	cardiac neural crest cells
CRD	cystein Rich Domain
Cer	cerberus
Cerl1	*Cerberus like 1*
Cerl2	*Cerberus like 2*
CO	cardiac output
DAN	differential screening-sellected gene aberrative in neuroblastoma
DAPI	4',6-diamidino-2-phenylindole
DEPC	diethyl pyrocarbonate
DNA	Deoxyribonucleic Acid
D/V	dorso-ventral
E	embryonic day
E/A	early and late diastolic waves ratio
EDTA	sodium ethylenediamine tetraacetate
EF%	ejection fraction
EGF-CFC	epidermal growth factor-cripto,frl-1,cryptic
FAC%	fractional area change
FHF	first heart field

FGF	fibroblast growth factor
FS%	fraction shortening
GATA	GATA binding protein
ID	internal diameter
IVS	interventricular septum
HRP	horseradish peroxidase
KCl	Potassium Cloride
KO	knock-out
LA	left atrium
LD	laterality defects
Lefty	Left right determination factor
LPM	lateral plate mesoderm
L/R	Left/Right
LV	left ventricle
mRNA	Messenger Ribonucleic Acid
Mef2c	myocyte enhancer factor 2C
MV	mitral valve
Nkx2.	Nk2 transcription factor related
Notch	Notch gene homologue
NCc	neural crest cells
OFT	outflow tract
O/N	over night
P	postnatal
PA	pulmonary artery
PBS	Phosphate buffered saline
PBSw	Phosphate buffer saline tween
PFA	paraformaldehyde
Pitx	Paired-like homeodomain transcription factor
PS	primitive streak
PVDF	polyvinylidene fluoride
PW	posterior wall
qRT-PCR	quantivative real-time – polymerase chain reaction
RA	right atrium

R-Smad	Receptor-regulated Smad
RV	right ventricle
RT	room temperature
SDS-PAGE	Sodium dodecyl sulfate polyacrylamide gel electrophoresis
SHF	secondary heart field
Smad	Sma and MAD-related
SV	stroke volume
TF	transcription factor
TGF-β	transforming growth factor β
TL	tibia length
Tween	polyoxydethylene-sorbitan monolaurate
VSD	ventricular septal defect
Wnt	Wingless/Integrated family members
WT	wild-type

1 General Introduction

1.1 Developmental Biology

The study of developmental biology consists in understanding the processes by which organisms grow and develop. This field integrates many areas of biology such as genetic, physiology, molecular and cellular biology. Three main concepts compose Developmental Biology: Morphogenesis, where a specific cell lineage originates a complete organized tissue; Cell Growth, where several pathways are coordinated to control cell size and cell proliferation; and Cell Differentiation, the mechanisms that controls a diversity of cellular lineages originating from a pluripotent cell. Furthermore, the environment (epigenetic influences) and evolution of organisms (transmission of inheritability) are also integrated in those concepts. The multiplicity of the field of Developmental Biology comprehends the use of several models such as plants and animals. In addition, recent emerging discussions argue for highlighting the broadness of Developmental Biology's concepts to include the field of stem cells. As a mammal, the mouse model is the one that has been more extensively used to study mammalian development. Mice are relatively easy to breed throughout the year, have large litters, and can be housed easily. Other advantages of using mice are a well characterized genome and the existence of several sophisticated techniques to manipulate their genes.

1.2 Early Mouse Development (pre- and implantation phase)

In mouse, from pre- to implantation period, the single fertilized egg will first be cleaved in 2 and then 8 cells. At 8- to 16-cell stage, known as morula stage, the embryo starts to lose pluripotency (Krupinski et al., 2011). Through consecutive divisions, the morula generates the blastocyst, composed by two distinct cell types, the inner cell mass (ICM) and the trophectoderm (TE). The ICM give rises to the embryo, meanwhile the TE is involved in the initial contact of the embryo with the uterine wall (Marikawa and Alarcón, 2010) (Figure 1.1). Recent data has described the different genetic pathways that control the early cell fate of the ICM, such as *Nanog* and *Oct3/4*, as well as fate of the TE, where *Cdx2* and *Gata-3* are involved in (Morris et al., 2010; Takaoka and Hamada, 2012) (Figure 1.2).

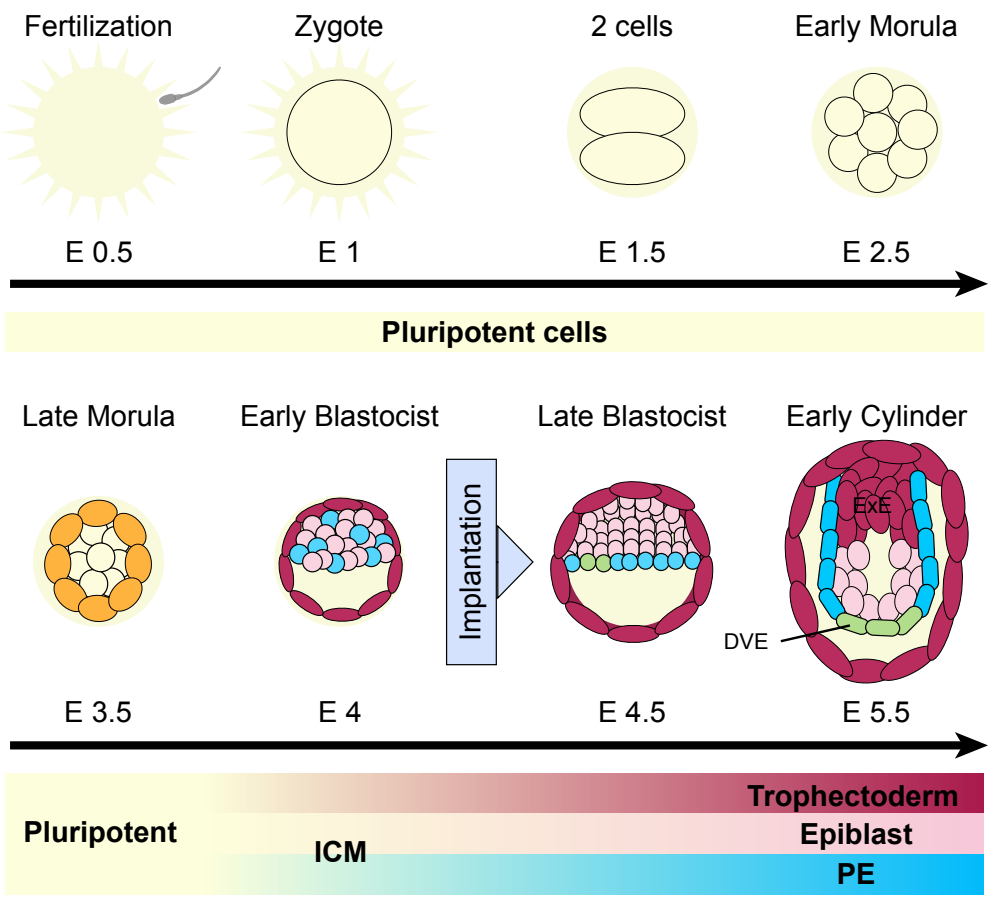

Figure 1.1 The pre- and peri-implantation period in mouse.
After fertilization, the zygote begins the cleavage process, into two (E1.5), eight (E2.5), sixteen (E3.5) and thirty-two cells (E4). At this stage, the embryo is divided into trophectoderm and inner cell mass (ICM). When more than 100 cells compose the embryo (E4-E4.5) the embryo is implanted in the mother's uterus. In late blastocyst phase, the ICM originates the epiblast and primitive endoderm, which ultimately gives rise to the visceral endoderm (green) and later to the distal visceral endoderm (DVE) at E5.5. ExE, extraembryonic ectoderm (Adapted from Krupinski et al., 2011; Takaoka and Hamada, 2012).

The ICM gives rise to the Epiblast and Primitive Endoderm (PE). The epiblast gives rise to the embryo itself and some extraembryonic structures. Meanwhile, the PE cells contribute to the formation of the Distal Visceral Endoderm (DVE) (E4.2) that later will generate the Anterior Visceral Endoderm (AVE) (E5.7) (Takaoka and Hamada, 2012). The DVE cells migrate to the future anterior side of the embryo and after changes in its genetic pattern, differentiate into the AVE, marking the prospective anterior side of the embryo. The expression of the Nodal antagonists *Lefty1* and *Cer1* in DVE is fundamental to the establishment of the primitive Anterior/Posterior (A/P) axis and the modulation of Nodal

expression and signaling in that region (Torres-Padilla et al., 2007; Rossant and Tam, 2009; Takaoka et al., 2011).

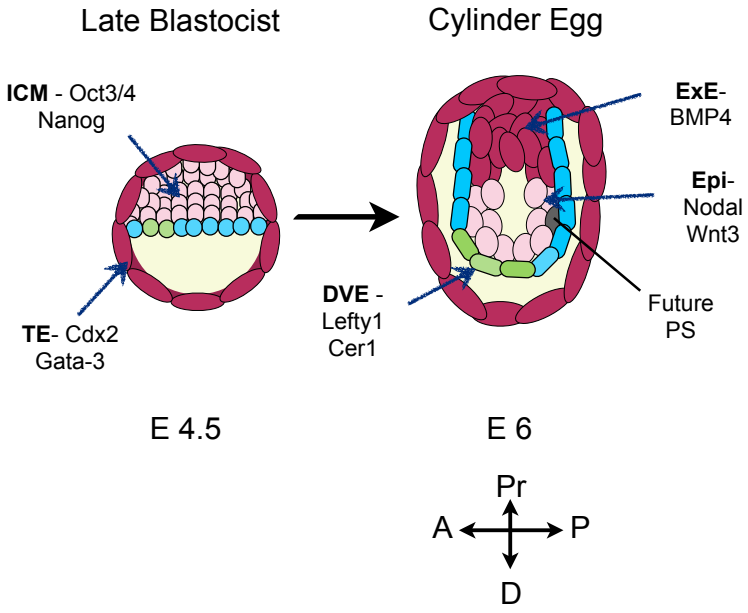

Figure 1.2 The genetic diversity in the early embryogesis.
In blastocyst, *Oct3/4* and *Nanog* are expressed in the ICM, while *Cdx2* and *Gata-3* are found in the TE. Signals from Nodal and Wnt pathway (*Wnt3*) are crucial to formation of the PS, meanwhile signals from the DVE (*Cer1* and *Lefty1*) inhibit Nodal and Wnt pathways. BMPs (*BMP4*) activate *Wnt3* expression in the Epiblast and the A/P axis is generated. A, anterior; D, distal; DVE, distal visceral endoderm; ICM, inner cell mass; Epi, epiblast; ExE, extraembryonic ectoderm; P, posterior; Pr, proximal; PS, primitive streak and TE, throphectoderm (Adapted from Takaoka and Hamada, 2012).

1.3 The establishment of the three body axes

1.3.1 The Anterior/Posterior and the Dorso/Ventral axes

The implantation of the embryo in the uterus occurs around E4.2-4.5 and the early events of the formation of the A/P axis described above begin even prior to gastrulation. During gastrulation (E6), epiblast cells ingress through primitive streak (PS) to form mesoderm at the opposite side of the AVE, thus forming the morphologic landmark of the establishment of the A/P axis (Tam and Behringer, 1997; Beddington and Robertson, 1998). Nodal signaling is active in the posterior side of the embryo, with the role of inducing and maintaining the PS (Hoodless et al., 2001) (Figure 1.2). The PS contributes to the formation of the embryo organizer, the node, that orchestrates the formation of diverse embryonic cell fates such as

the primitive mesodermal structures and the notochord, from where the neural tube and somites are originated (Davidson and Tam, 2000). The formation of the node characterizes the formation of the second axis of the body, the Dorso/Ventral (D/V) axis (Beddington and Robertson, 1999). Other contributions from PS will be discussed later.

The mouse node is a transient structure essential to the establishment of the second (D/V) and third body axes, the Left/Right (L/R). The ventral node cells constitute the notochord and the definitive endoderm, whereas the dorsal node cells constitute the floor plate in the neural tube (Beddington, 1994). Molecular breaking of symmetry occurs during the formation of the L/R axis, due to directional leftward laminar flow of extraembryonic fluid referred as nodal flow, which is responsible for the asymmetric orientation of the organs (Nonaka et al., 2002; Nakamura and Hamada, 2012). Therefore, understanding the molecular mechanisms underlying the establishment of the L/R axis as well as its physiological consequences is of paramount relevance for the translation of Developmental Biology to Medicine.

1.3.2 L/R axis and Nodal signaling

1.3.2.1 Nodal

Nodal is a member of Transforming Growth Factor (TGF) type β superfamily, having several roles during embryogenesis, among which mesendoderm induction (Kawasumi et al., 2011; Nakamura and Hamada, 2012) as well as modulation of tumor cell plasticity and aggressiveness (Minchiotti, 2005; Strizzi et al., 2011). Several components of the Nodal signaling pathway have been implicated in L/R axis development. Initially, Nodal is expressed bilaterally in crown cells of the mouse node, and shortly after the symmetry-breaking event, Nodal becomes asymmetrically expressed in the left side of the node and later in the left lateral plate mesoderm (L-LPM) (Schier, 2003). The association of Nodal with GDF1 (Growth/Differentiation Factor 1), another member of TGFß superfamily, is necessary to Nodal activity in the crown cells. Moreover, the node-specific enhancer (NDE) is a Nodal promoter which is activated by Notch signaling, and is necessary to the early symmetrical Nodal expression at the node (Tanaka et al., 2007). In addition, Nodal generates a positive feedback loop (auto-regulatory) mediated by Foxh1-dependent intronic enhancer (ASE) (Brennan et al., 2002), which is responsible for expansion of *Nodal* expression to the left LPM. Nodal generates also a negative feedback loop (inhibitory) by activating the expression of its antagonist *Lefty1* and *Lefty2*. Lefty1 is expressed in the midline and it acts as

a barrier to avoid Nodal migration to the right (R-) LPM whereas Lefty2 prevents excessive Nodal expression by inhibiting the Nodal autoregulatory loop (Meno et al., 2001; Hamada et al., 2001). Both of these Nodal antagonists, together with Cerl2 prevent Nodal expression in the R-LPM contributing to the sideness specific morphology (Marques et al., 2004; Hamada et al., 2001; Shiratori and Hamada, 2006). Nodal signaling activation results in the induction of Nodal target gene *Pitx2* in L-LPM (Shiratori and Hamada, 2006). Moreover, failure in L/R axis commonly leads to laterality defects (LD), anomalies known as *situs inversus, isomerisms,* and heterotaxia, which will be discussed later. Studies of patients with congenital LD have suggested that the role of Nodal signaling might extend to humans (Bamford et al., 2000).

1.3.2.2 Cerberus Family

Cerberus like (Cerl) family belongs to the TGF-beta superfamily and encodes for small secreted proteins (272 a.a., Xcer and Cerl1, and 185 a.a., Cerl2) (Belo et al., 1997; Marques et al., 2004). The Cerl family is characterized by 9 cysteines (Cystein-Rich Domain) at the C-terminal and a signal peptide at the N-terminal (Belo et al., 2009). Despite the conserved cysteine-knot domain, the patterns of Cerl expression is different between vertebrate species (Bouwmeester et al., 1996; Belo et al., 1997; Zhu et al., 1999). Cerl1 was first identified in Xenopus (Xcer) being localized in the organizer (node equivalent in mouse) and acts as an antagonist of some signaling pathways in that region (Bouwmeester et al., 1996). Furthermore, studies have shown that injection of Xcer mRNA in blastomeres resulted in formation of additional heads (Bouwmeester et al., 1996). After that, Cerl associated proteins were found in other vertebrate species, such as the mouse mCerl1 (José A Belo et al., 1997) and mCerl2 (Pearce, 1999; Marques et al., 2004); chicken (cCerl1 or Caronte; Rodríguez Esteban et al., 1999), zebrafish (zCharon; Hashimoto et al., 2004) and humans (Dand5; Mouse Genome Informatics). Cerl1 is expressed in AVE and together with Lefty-1 determines the establishment of the A/P axis in mouse restricting the PS to the prospective posterior side of the embryo (Belo et al., 1997; Belo et al., 2000; Yamamoto et al., 2004).

1.3.2.3 Cerberus like 2

Cerl2, another member of Cerl family was identified as a nodal antagonist in the mouse node, and has a fundamental role in L/R formation (Marques et al., 2004; Oki et al., 2009). At early head fold, the secreted Cerl2 protein is expressed in both sides of crown cells of the node. At 2-somite pairs, Cerl2 is accumulated on the right side and later, between 3-4-somite pairs,

Cerl2 was found on the left. It remains there until 6-somite pairs, after which Cerl2 is no longer expressed in that region (Inácio et al., 2013). Due to the small size of this protein, Cerl2 might be transported through the nodal flow, suggesting that Cerl2 is dynamically expressed over time (2- to 6-somite pairs) and dependent of nodal flow. This study also revealed the precise time point at which Cerl2 controls the asymmetric Nodal signal in the node. Furthermore, recent studies revealed that the asymmetric expression of *Cerl2* mRNA is regulated posttranscriptionally via its 3'UTR (untranslated region) through Wnt signaling induced by Notch signaling leading to *Cerl2* degradation on the left side of the crown node cells (Nakamura et al., 2012; Kitajima et al., 2013). In addition, growing evidence suggests that Cerl2 might have a specific role during cardiac development, but this far its role remained unknown.

1.3.2.4 L/R establishment

In mice, the generation of the L/R axis is dependent on the asymmetric signal generated by the motile cilia present in the node region from early somite stage (2 somite pairs), i.e. the Nodal flow. Around E7.5, the ciliated pit cells localized on the ventral surface of the node create by a clockwise rotational movement, the leftward unidirectional Nodal fluid flow (Hirokawa et al., 2012), characterizing the first step of the symmetry-breaking process. Our lab revealed that in crown cells of the perinodal region, the secreted Cerl2 protein binds to Nodal restricting its signal to the left side of the node (Marques et al., 2004) The second step of L/R establishment is constituted by the migration of the asymmetric nodal signal to the left lateral plate mesoderm (L-LPM) (Shiratori and Hamada, 2006). The exact mechanism of this molecular transport remains however unknown. The third step of L/R axis establishment is the situs-specific morphogenesis of internal organs mediated by asymmetric expression of Nodal target gene, Pitx2 (Hamada, 2010) (Figure 1.3). Pitx2 is a bicoid-type homeobox transcription factor that encodes a transcription factor required for correct L/R morphogenesis (Yoshioka et al., 1998; Shiratori et al., 2001). The first morphological evidence of the correct L/R asymmetry is observed by the rightward looping of the heart at E8.5.

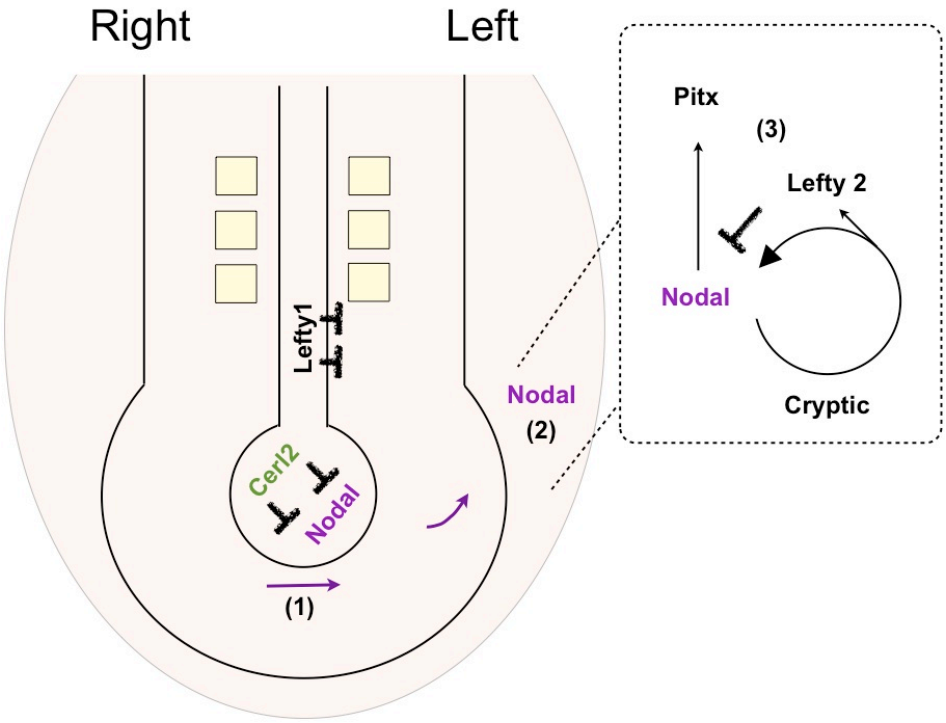

Figure 1.3 Nodal signaling during the L/R axis establishment in mouse.
At early somitogenesis (2 somite pairs) starts the breaking of the L/R symmetry in the mouse embryo (~E7.5). In the node, Cerl2 binds to Nodal and together with nodal flow the initial asymmetric Nodal signal is generated to the left side (1). The Nodal signal migrates to the L-LPM and the Nodal signaling cascade is then induced (2). Nodal activates its own expression (auto-regulatory mechanism) as well as target genes, which include its own antagonists (such as Lefty1/2) (3) (Adapted from Marques et al., 2004; Inácio et al., 2013).

1.3.2.5 Models of symmetry-breaking generated by nodal flow

Three hypotheses have been postulated to explain the first breaking of symmetry in the mouse node. The first considers the size of proteins with morphogenic properties (15-50kDa), such as Nodal, Cerl2 and Fibroblast Growth Factor (FGF) 8. These are secreted in the node cavity where they can be transported through the laminar nodal flow (Okada et al., 2005). Another possibility might be that extracellular particles secreted from the ventral node, the Nodal Vesicular Parcels (NVPs), may transport the morphogens to the left side of the node through the nodal flow leading to the activation of Nodal in the L-LPM (Tanaka et al., 2005). Also a mechanism known as "two-cilia" has been proposed, where the symmetry-breaking signal is sensed at the left side of the mouse node. In this model, the node comprises two types of cilia, motile and immotile monocilia (Mcgrath et al., 2003). The motile monocilia localize in the pit ventral node region rotate in the clockwise direction generating the nodal

flow which is sensed by immotile monocilia (Satir and Christensen, 2008). The immotile sensory cilia are localized in the perinodal crown region and contain the Ca^{2+} permeable channel Polycystin-2 (Pkd2) exclusively on the left side of the node (Satir and Christensen, 2007; Norris, 2012). Thus, Nodal flow establishment is immediately followed by elevation of the concentration of intracellular calcium on the left hand side of the node, which in turn may activate the asymmetric expression of Nodal and its target genes on the L-LPM. Indeed, Pkd2 is essential for establishment of correct L/R asymmetry (Babu and Roy, 2013) and to further regulate the asymmetric expression of *Cerl2* in the crown cells (Yoshiba et al., 2013). Moreover, the integrity of ciliary components are also essential to generate the asymmetric nodal flow as observed in mouse mutants for genes encoding the motor protein Kinesin 3 (Kif3), and for cilia motility (Hirokawa et al., 2009) such as the Left-right dynein (Lrd) (Supp et al., 1997). These mutants revealed absence or abnormal nodal flow and these exhibit randomized expression in LPM and in visceral organs (Hamada, 2010).

1.3.2.6 Nodal Signaling Pathway

After the first role of Nodal in A/P axis formation, Nodal is re-expressed in the node and then in the L-LPM (Nakamura and Hamada, 2012) where its signaling cascade is asymmetrically activated. The classical Nodal pathway occurs through types I and II serine/threonine kinase receptors (I and II Activin Receptor Like Kinase, ActRIB or ALK4/7 and ActRIIB, respectively) (Schier, 2009). Nodal binds with heteromeric complex co-receptor Epidermal Growth Factor (EGF)-like and cysteine-rich domain (Cripto-FRL1- Cryptic, CFC) motifs, EGF-CFC, which provides specificity to the receptors ALK4 and ActRIIB (ten Dijke and Hill, 2004). The Nodal pathway is transduced by phosphorylation of receptor-associated Smads (R-Smad) Smad2 and Smad3. Then these receptors interact with Smad4 forming a transcriptional complex which ultimately translocate to the nucleus and together with transcription factors (FoxH1, Mixer) regulates the expression of downstream target genes (Shen, 2007) (Figure 1.4).

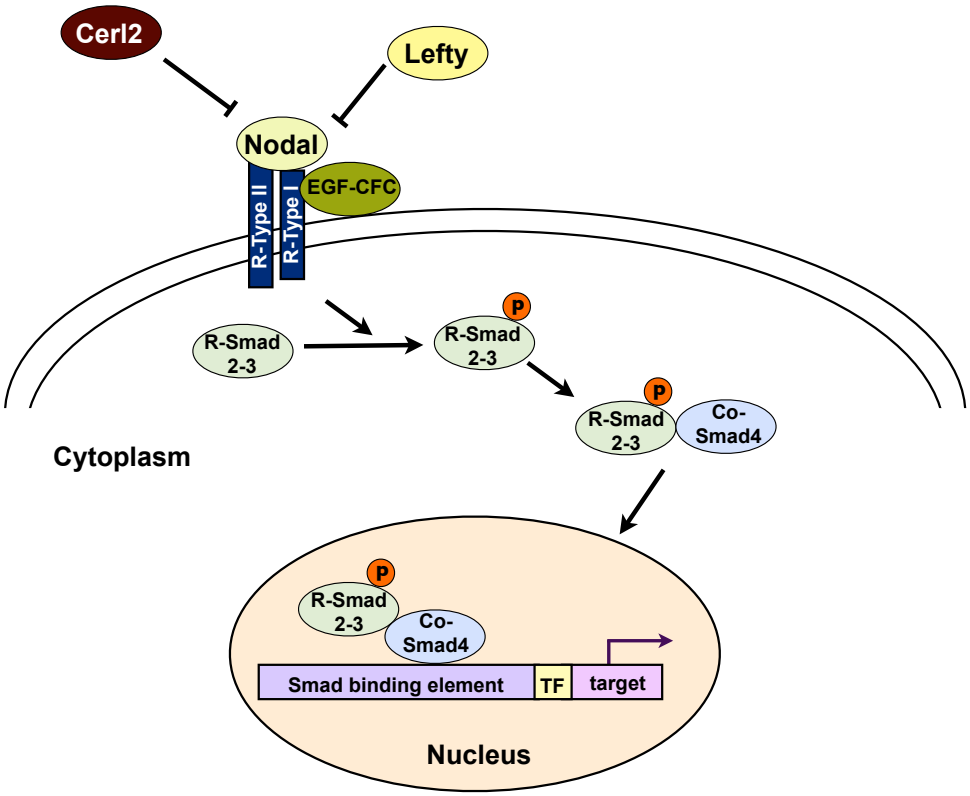

Figure 1.4 Nodal signaling activation.
Nodal interacts with its cofactor (EGF-CFC) and receptors (Receptor type I and II). After receptor activation, receptor-associated (R) Smad 2 and/or 3 are phosphorylated. Activated R-Smads form a heteromeric complex with Smad4, which is translocated to the nucleus in order to activate and control the transcription of Nodal target genes. P, phosphorylation; TF, transcription factor (Adapted from Villapol et al., 2013).

Recent emerging data have suggested the mechanisms by which Nodal activity is converted in orientation of the cardiac looping through the Nodal related gene in zebrafish, Southpaw (Spaw) (Lenhart et al., 2013; Veerkamp et al., 2013). These reports demonstrated that Nodal and its target genes (*FoxH1* and *Has2*) induce the motility of cardiac cells, but more in the left side than in the right side, resulting in the movement of the cardiac tissue towards the left. These findings provide a significant explanation to enhance the understanding by which the visceral organs are oriented. Furthermore, taking into account that the functions of Nodal signaling during embryonic development are conserved between species, these mechanisms may possibly exist in other animal models.

1.3.2.7 Failure in L/R axis and laterality defects

As described above, the asymmetric activation of the downstream target genes of Nodal determines the arrangement of the internal organs. Therefore, altered activation of Nodal signaling results in randomized organ's positioning, known as laterality defects (LD). These include complete or partial organ's reversal, *situs inversus totalis* or *parcialis,* respectively; and heterotaxia, which is characterized by the failure in the arrangement of one or more organs. The heterotaxia is normally composed by single organ inversions and symmetry of internal organs, classified as isomerism. In humans, laterality defects normally compromise health due to failure to establish correct connections between organs leading to defective function (Vandenberg and Levin, 2013) (Figure 1.5).

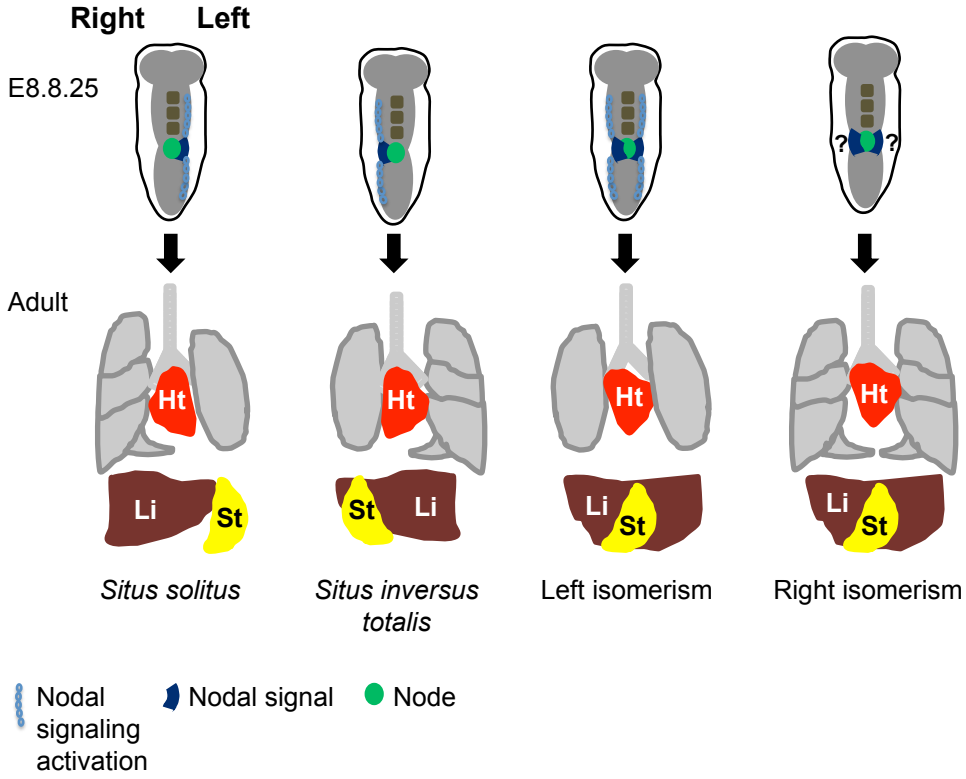

Figure 1.5 Nodal signaling controls visceral organs' positioning.
Correct organ's arrangement is defined as *Situs solitus* where the heart normally points to the left; the right lung is composed by 4 lobes and the left lung, by one lobe; the liver is on the right side, opposite to the stomach, meaning that the Nodal signaling was activated in the L-LPM. *Situs inversus* indicates that Nodal signaling was activated in the right (R-) LPM, and normally causes the complete inversion of the organs. The isomerisms are a herotaxy form. Left and Right isomerisms denote that Nodal signaling is activated on both sides of the LPM, and weak or no activation respectively; which might result in two left or two right body sides. In these cases, the liver and stomach tends to symmetric positions (Adapted from Mcgrath and Brueckner, 2003).

The brain is asymmetric in humans and, curiously, symmetry in the brain leads to dyslexia and diseases such as schizophrenia (Gesmhwnd and Levitsky, 1968; Crow, 2008; Leonard and Eckert, 2009). Since asymmetrical heart and is the first organ to be formed (Buckingham et al., 2005), the first evidence of failure in L/R axis establishment can be observed in the orientation of the cardiac loop (Ramsdell, 2005). Furthermore, typical cardiac defects associated with laterality defects include atrial and ventricular septal defects (ASDs and VSDs, respectively), double outlet right ventricle (DORV), transposition of the great arteries (TGA) and aortic arch anomalies (Bowers et al., 1996) leading ultimately to abnormal cardiac function. Therefore, congenital heart diseases (CHDs) are frequently related with laterality defects (Shiraishi and Ichikawa, 2012).

1.4 General view of the layer's contributions to heart development

Shortly after gastrulation, the prospective cardiac cells commit to the cardiac fate. In the following section, the contribution of three germ layers to heart development will be exposed.

1.4.1 Ectoderm

The ectodermal layer surrounds the embryo and originates the skin and neural tissues. Furthermore, the ectodermal layer contributes to some mesodermal tissues which will give rise to anterior heart field (Xu et al., 1999). In addition, the cardiac neural crest cells, which derive from the neural crest cells (NCc) formed at the junction between the neuroepithelium and the surface ectoderm at E9, contribute to the arterial pole development (Kelly and Buckingham, 2002; Randall et al., 2009).

1.4.2 (Visceral) Endoderm

The endoderm is primary germ-cell layer that forms the gut tube, liver, pancreas, gallbladder and lungs. Studies in mice have shown the role of the anterior visceral endoderm (AVE) as a cardiogenic inducer due the proximity with the pre-cardiac mesoderm and the capacity of the visceral endoderm to secrete Bone Morphogenetic Proteins (BMPs), Fibroblast Growth Factors (FGFs), Wnt8c and Cerl1 (Lough and Sugi, 2000; Uosaki et al., 2012).

1.4.3 Mesoderm

During embryonic development, the formation of the mesoderm requires the spatiotemporal expression and signaling of Wnt, BMP, and Nodal (Abu-issa and Kirby, 2007) resulting in extensive cell rearrangements of gastrulation in the early embryo. The mesoderm can be

divided into four regions i.e. chordamesoderm, paraxial mesoderm, intermediate mesoderm, lateral plate mesoderm. The lateral plate mesoderm (LPM) gives rise to multiple cell types including connective tissue, the cardiovascular system and skeletal and smooth muscle (Kelly and Buckingham, 2002). For cardiogenesis, the LMP splits into splanchnic and somatic layers, which will migrates into the heart contributing to the three main cell lineages, the endocardium, myocardium and epicardium (Buckingham et al., 2005).

1.4.4 Endocardium

The endocardium delineates the trabecular layer and forms the vascular endothelium lining of the heart (Evans et al., 2010). Furthermore, it plays an essential role in the formation of the cardiac conduction system and in the cardiac valves (Harris and Black, 2010). During cardiac looping, the myocardium induces the endocardial cells to migrate into the cardiac cushions. The endocardial cushion development is essential for atrial and ventricular septation, therefore failure in septation leads to atrial and ventricular septal defects (ASD and VSD, respectively) (Smith and Bader, 2007). The development of the atrial-ventricular (AV) and outflow tract (OFT) endocardial cushions will give rise to the AV valves (tricuspid and mitral) and OFT valves (pulmonary and aortic) (Lavine and Ornitz, 2008). Members of Epidermal growth factor (Neuregulin 1), FGF (FGF-4, -9, -16 and -20), Endothelin-converting enzyme (ECE-1 and 2) and Neurofibromin (Nf1) families were shown to have an essential role during the endocardial formation (Harris and Black, 2010; Odiete et al., 2012).

1.4.5 Myocardium

The myocardium is the proper cardiac muscle, being composed by multiple cell lineages. Furthermore, myocardium originates the chamber and non-chamber structures (Sedmera, et al., 2000). Myocardial growth is attributable to increase in proliferation (physiological hyperplasia) and in size (physiological hypertrophy) of cardiomyocytes. At early heart development (E7.5-E10.5), the cardiomyocyte proliferation is dependent on cardiac-specific transcriptional regulators such as NKX2.5, GATA4, MEF2C and TBX5 (Dunwoodie, 2007). Exogenous factors derived from the epicardium and endocardium (E11.5 and E13.5) regulate the myocardial growth through cardiomyocyte proliferation (Sedmera et al., 2002). Retinoic acid (RA) signaling and one of its receptors (RXR-α) derivating from the epicardium regulates the expression of FGF (FGF-9, -16 and -20) to control the midgestation myocardial growth and to suppress myocardial differentiation (Xavier-Neto et al., 2000; Chen et al., 1998; Lavine et al., 2005) (Figure 1.6). The endocardial layer proliferates to generate a

spongy network of myocardial cell or the well-known trabecular layer which allows for adequate oxygenation of the developing heart (McNally and Dellefave, 2009). However in late midgestation (E14 – E16.5) the decreased proliferation is related with conduction system differentiation (Sedmera et al., 2003).

In adult hearts, recent studies point to continued DNA synthesis and therefore to neomyocardialization potential (Graham and Harvey, 2011; Sedmera and Thompson, 2011; Porrello et al., 2011; Mollova et al., 2012). Despite the knowledge regarding the activation of cell cycle machinery as cyclins and cyclin-dependent kinases (CDKs) during cardiogenesis and in postnatal life, the mechanisms underlying proliferative regulation remain unknown (Ikenishi et al., 2012).

1.4.6 Epicardium

Epicardium is derivative from a cluster of mesothelial cells called proepicardium and consists a single layer of cells that are in direct contact with the pericardial fluid, overlaying the myocardium (Zamora et al., 2007; Schlueter and Brand, 2011). These cluster is present at the base of the venous pole or inflow-tract and arises from septum transversum mesenchyme (Männer et al., 2001). The epicardium originates cardiac fibroblasts, the epithelial mesenchymal transition (EMT) and the smooth muscle cells of the coronary vessels (Mikawa and Brand, 2010) (Figure 1.7). In addition, it has been discussed the potential capacity of the epicardium to induce the proliferation of cardiomyocytes (Zhou et al., 2008; Bochmann et al., 2010).

During gastrulation in mouse, the splanchnic layer of the anterior lateral plate mesoderm, derivative of the anterior primitive streak (PS), contributes to cardiac progenitors (Kirby, 2007; Tam and Behringer, 1997). Thus, in the anterior side of the embryo, the heart forming region fuses forming a horseshoe-shape called as cardiac crescent (DeRuiter et al., 1992). That region give rises to the first heart field (FHF) (Pérez-Pomares et al., 2009) which ultimately will contribute to the left ventricle (LV), atria ventricular canal, atria and inflow tract (Zaffran and Frasch, 2002; van den Berg et al., 2009). Hereafter, the second population of cardiac progenitors were identified and divided into two subpopulations the anterior heart field (AHF) and Secondary Heart Field (SHF). The AHF will give rise to the right ventricle (RV) and outflow tract (OFT) (Kelly et al., 2001).

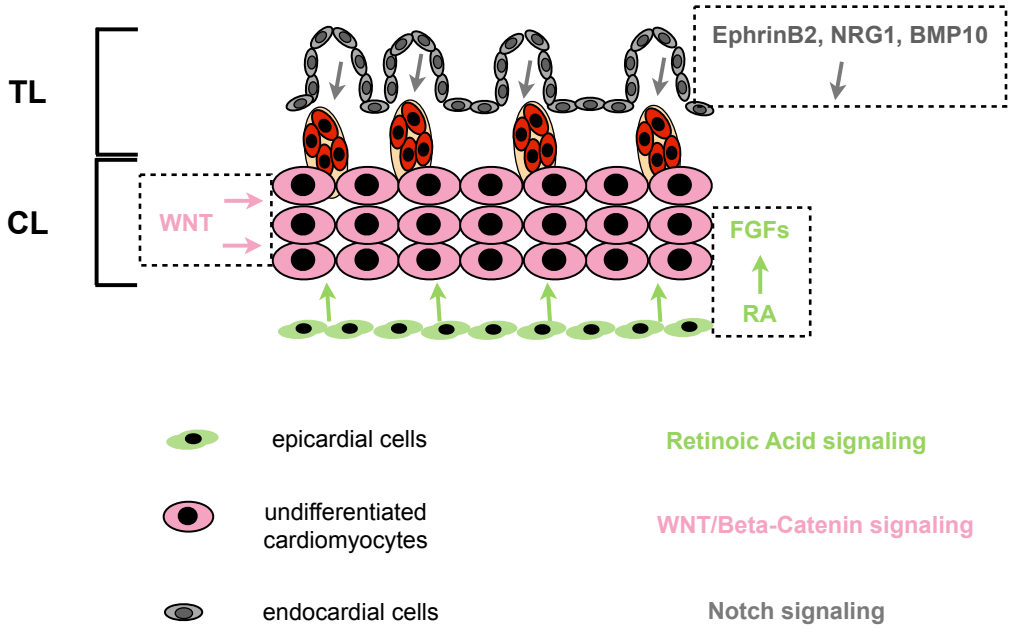

Figure 1.6 Three signals control the myocardial growth during the midgestation.
The epicardium induces cardiomyocyte proliferation by stimulating RA signaling and consecutively activating FGFs. Wnt signaling via activation of beta-catenin stimulates the preferential proliferation of CL myocardium. Notch signaling coordinates the trabecular growth through the mediation by the EphrinB2-dependent, endocardial paracrine factor NRG1, and the maintenance of a BMP10 in proliferating cardiomyocyte population. CL, compact layer; RA, retinoic acid; TL, trabecular layer (Adapted from Grego-Bessa et al., 2007; Lavine and Ornitz, 2009; Buikema et al., 2013).

1.5 Basic Heart development

The SHF provides cells to the myocardium and smooth muscle to compose the definitive arterial pole (Waldo et al., 2001; Waldo et al., 2005). Cells from respective cardiac fields migrate to the ventral side of the embryo and fuse forming a linear heart tube (Moorman et al., 2003) (Figure 1.7). Shortly after, the heart tube loops to the right of the embryo (Icardo, 1988) under information from the L/R patterning (Kathiriya and Srivastava, 2000). During cardiac looping it's already possible to distinguish two myocardial layers, the trabeculae and the compact layers. The trabeculae are myocardial projections outlined by endocardial cells, being the result of interactions between primitive myocardium and endocardium (Ben-Shachar et al., 1985). Its main function is to give support to myocardial sustenance prior to the development of coronaries (Sedmera et al., 2000). Notch supports the proliferation in trabeculation by controlling production of Neuregulin, EphrinB2, and Bmp10 in the

endocardium (Grego-Bessa et al., 2007; Mercola et al., 2011). Thus, prolonged Notch1 activation leads to excessive cardiomyocyte proliferation with formation of ectopic trabecular structures (Niessen and Karsan, 2008; Luxán et al., 2013). The compact myocardium is the proper cardiac muscle localized in the extreme proliferative ventricular zone (Risebro and Riley, 2006). After the development of coronary arteries, the trabecular myocardium is compacted towards the compact myocardial wall leading the increased thickness, this process is referred as compaction and occurs between E13 and E14 (Wessels and Sedmera, 2003; Pennisi et al., 2003).

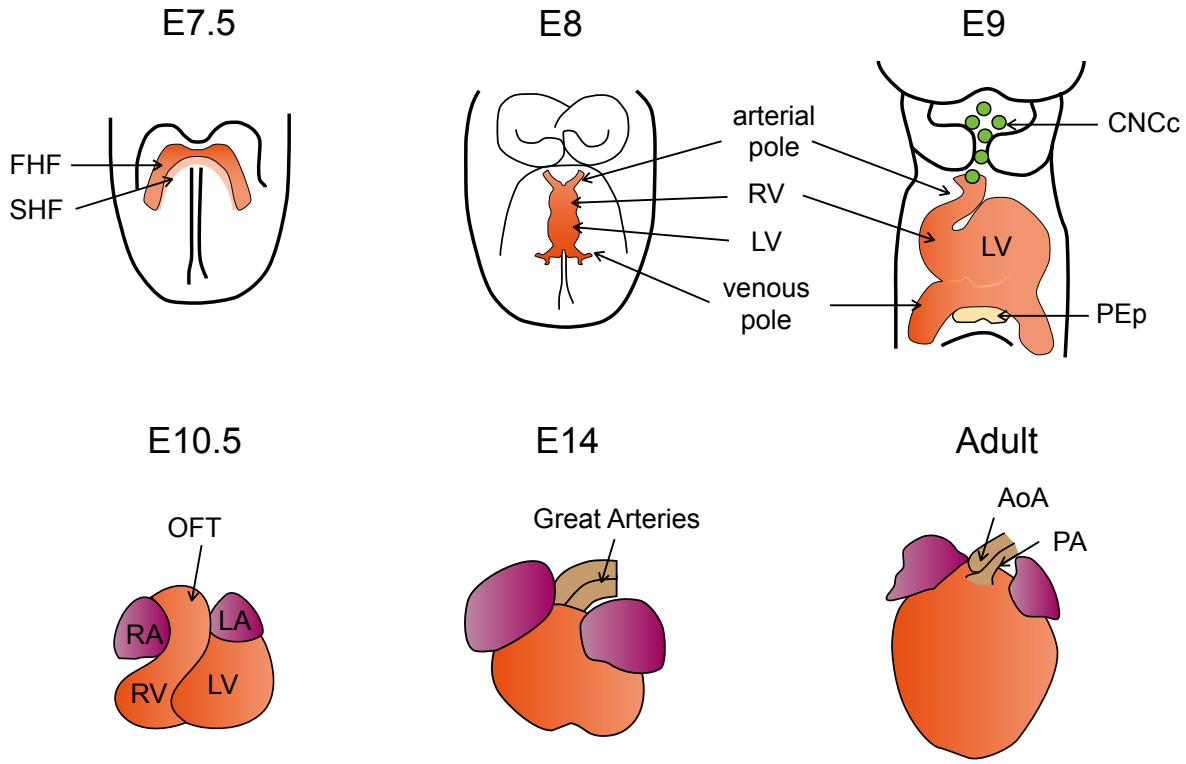

Figure 1.7 The steps of heart development in mouse.
Initially the cardiac progenitors leave the primitive streak and migrate to the anterior position forming two heart fields (E7-E7.5). Those fuse to form a heart tube (E8). At E8.5 the heart loops rightward and then the future atria and ventricles assume their definitive positions. In the midgestation (E9), the CNCc contribute with smooth muscle components to the OFT formation and development. At E10.5 to E14.5 the atrial and ventricular septa are formed, and differentiation of the OFT occurs within aorta and pulmonary arteries. From fetal phase to adult age, the cardiac cells become differentiated and mature. AoA, aorta artery; CNCc, cardiac neural crest cells; FHF, first heart field, LA, left atrium; LV, left ventricle; OFT, outflow tract; PA, pulmonary artery; Pep, proepicardium; RA, right atrium; RV, right ventricle; SHF, second heart field (Adapted from Buckingham et al., 2005).

During development, cardiomyocytes from the compact layer have a higher proliferation rate than cardiomyocytes in the trabecular layer (Ieda et al., 2010). A mechanism has been proposed to explain these differences in cardiomyocytes proliferation rates where the differential activation of canonical Wnt signaling/β-catenin signaling promotes the preferential proliferation of compact versus trabecular layer (Buikema et al., 2013) (Figure 1.6 and Figure 1.8).

With further development, the heart becomes differentiated to a four-chambered organ and the high contractility can already be observed (Christoffels et al., 2004). Simultaneously the atrio-ventricular septation is established and the precise alignment between arteries and their respective ventricles occurs, allowing proper development of the conduction and circulatory systems (Dunwoodie, 2007). In the late gestational period (E16.5 – E19.5), the last phase of the complex cardiac morphogenesis, begins the maturation phase. That phase comprehends, at the cellular level, the pattern of differentiated cardiomyocytes that persists until the first weeks of birth (Bersell et al., 2009).

1.5.1 Main steps of cardiogenesis

Midgestational heart development (from 10.5 to E16.5) begins after the looping, during which occurs the epicardium and endocardial cushion formation, myocardial growth, coronary vascular development and ventricular septation (Horsthuis et al., 2009). Since we previously discussed about the epicardium and endocardium cushion formation, we will describe other steps of the heart development.

1.5.1.1 Myocardial growth

During development, mitotic events, which are associated with the augment of proliferation, are frequent during heart growth and in the first days after birth, resulting in binucleated cardiomyocytes (Li et al., 1996; Soonpaa et al., 1996; Pasumarthi and Field, 2002). When the heart reaches maturity (in the post natal phase), the progressive proliferative capacity (physiological hyperplasia) decreases until it stops completely. Then, the cardiomyocytes grow mainly through cellular enlargement (physiological hypertrophy). Physiological hypertrophy has been considered to be the result of an increase in size of preexisting fetal cardiomyocytes which occurs in the developing and adult heart (Rubart and Field, 2006). Peptide growth factors, such as insulin-like growth factor (IGF) and epidermal growth factor, coupled to the phosphatidylinositol 3-kinase (PI3K)/Akt pathway are frequently associated with physiological hypertrophy where the cardiomyocyte enlarges by increasing the synthesis

of their cardiac contractile proteins (Mlc2v, myosin light chain two ventricles; and cardiac alpha-actin), by induction of early genes such as c-fos, c-jun, and erg-1 (Dorn Il, 2007; Rohini et al., 2010).

1.5.1.2 Coronary vascular development

Coronary vascular system formation occurs simultaneously with the period of rapid cardiac growth and can be divided into two stages: vascular plexus formation and vascular remodeling. The coronary plexus is formed between E11.5 and E13.5 and is remodeled between E14.5 and E16.5 to give rise to the mature coronary vascular system (Lavine and Ornitz, 2008).

1.5.1.3 Ventricular septation

Cardiac septation is the closure of direct communications between left and right atria, ventricles and subarterial channels, and the development of the right atrioventricular junction

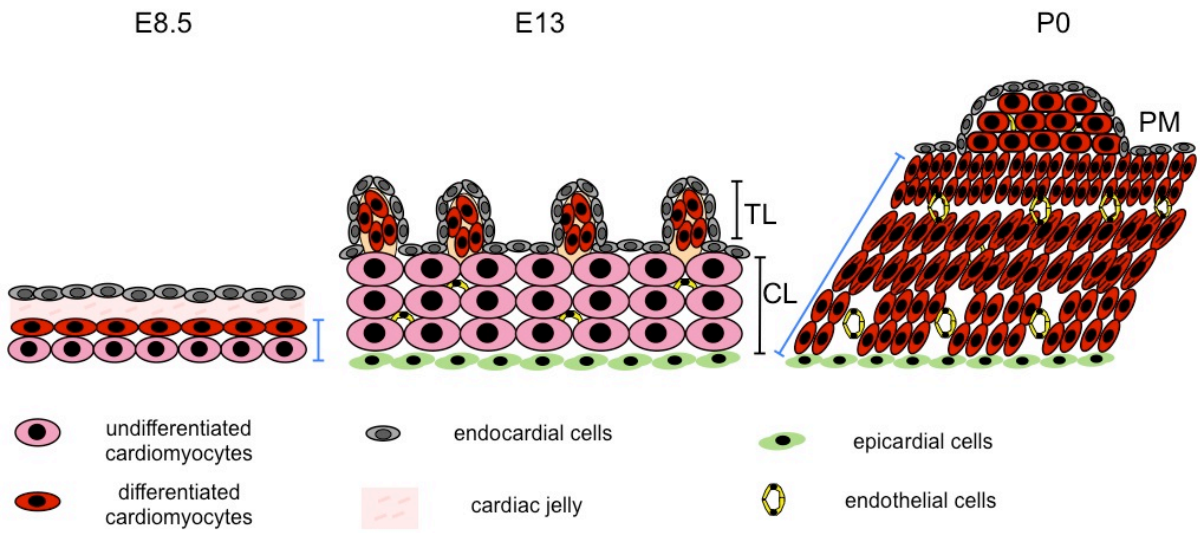

Figure 1.8 The process of myocardium formation.
In early heart development, a thin layer of the cardiomyocytes surrounded internally by the endocardium composes the myocardial muscle. The cardiac jelly separates both layers (E8.5). In early midgestation (E10.5), the mesothelial cells originates the outmost cardiac layer, the epicardium. At midgestation (E13), the myocardium is divided in compact (CL) and trabecular layer (TL). In neonatal heart (P0), the myocardium is thicker, the coronary cells are visible and the most differentiated cardiomyocytes composes the papillary muscle (PM). Note in blue line the CL expansion at E8 and P0, respectively (Adapted from Sedmera et al., 2000) .

and left ventriculoarterial junction (Lamers and Moorman, 2002). At E10.5, the embryonic RV and LV can be distinguished morphologically by the interventricular sulcus, which marks the site of the forming IVS (Zaffran et al., 2004). Ventricular septation (VS) is regulated by Tbx genes (Tbx5 and Tbx20) and occurs between E14.5 and E16.5 (Takeuchi et al., 2003). Its formation arises from the interface between cardiomyocytes derived from the cardiac crescent and those derived from the pharyngeal mesoderm of the AHF, which ultimately gives rise to the LV and RV respectively, suggesting a dual origin for the septum (Meilhac et al., 2004).

1.5.2 Cardiac Cell Types

The diverse cellular lineages that compose the heart are divided in muscle (cardiomyocytes and smooth muscle cells) and non-muscle cells (cardiac fibroblasts and endothelial cells) (Figure 1.9). From genetic manipulation has been known the cardiac progenitors which will give rise to the diverse cardiac cellular lineage (Martin-Puig et al., 2008; Van Vliet et al., 2012; Laugwitz et al., 2008; Miquerol et al., 2011; Lin et al., 2012). The cardiac cells are derived from a multipotent mesodermal progenitor (van Weerd et al., 2011) that through the control of complex genetic pathways drives to a specific differentiated cardiac cell. The cardiomyocytes are the workhorse cells of the heart and although occupy the majority of heart volume, non-myocytes (cardiac fibroblasts) are present in large number (Camelliti et al., 2005; Kohl et al., 2005).

1.5.2.1 Other cardiac cellular sources

Additionally, two other sources were identified that do not come from the cardiogenic mesoderm, but are derivatives of the cardiac neural crest cells (CNCc) and the proepicardial organ (Figure 1.9). The dorsal neural tube originates the neuro-ectoderm, which contributes to the CNCc. The CNCs migrates into the arterial pole from the caudal pharyngeal arches and has an important function in arterial pole maturation (Vincent and Buckingham, 2010). The proepicardium forms the outmost layer of the epicardium (Schlueter and Brand, 2011), as reported above the epicardium originate the coronary vascular smooth muscle, the endothelial cells and the fibroblasts (see detailed information on the topic General layers contribution to heart development).

1.5.3 Cardiac Genetic Program

From early morphogenetic signals of cardiac precursors in the anterior region of mouse embryos until the well-known four-chambered heart, a precise and harmonious arrangement between genetic cardiac network and different cell types is required. Therefore, even subtle perturbations during heart formation could result in congenital heart defects (CHD) (Nemer, 2008), being the most common congenital malformation worldwide (Hoffman and Kaplan, 2002; Garne et al., 2012).

The cardiac progenitors are determined early at E6.5 in the lateral epiblast, and these cells then migrate to the primitive streak where they originate the cardiac fields (Arai et al., 1997; Van Vliet et al., 2012). Several cardiac signaling pathways have been published and recent emerging information has been elucidating the cardiac genetic program.

Here we present the summarized view about the three major pathways of cardiac inducers that control the cardiogenic mesoderm, such as the Transforming Growth Factor β (TGFβ)/

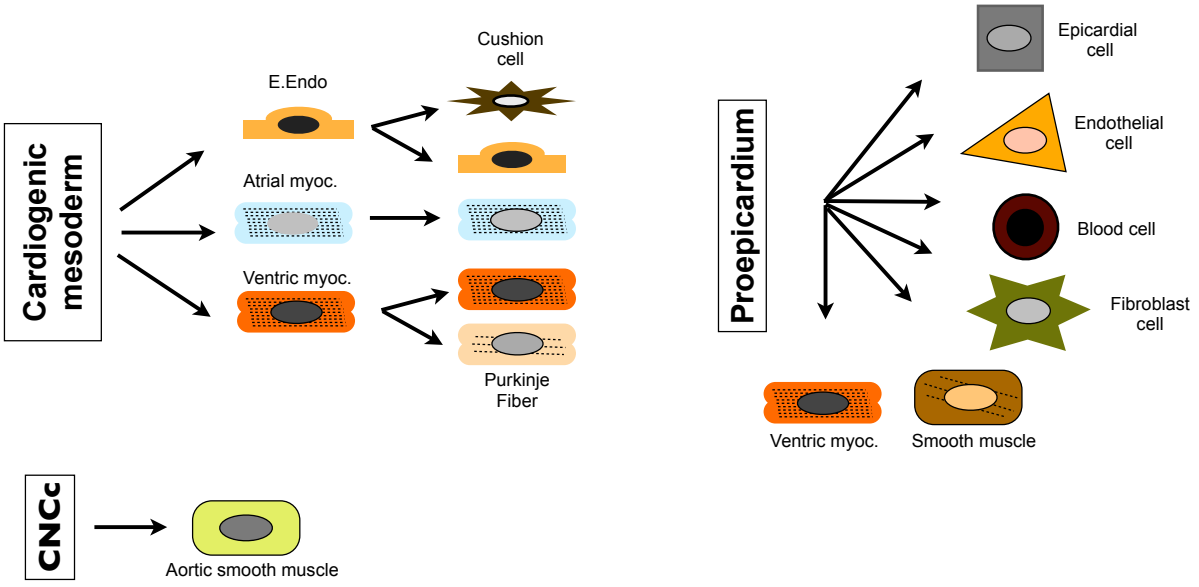

Figure 1.9 The cardiac cell lineage.
Representation of the three main sources that compose the heart. These give rise to several types of cardiac cells. CNCs, cardiac neural crest cells; e. endo, endocardial endothelial cells; myoc., myocardium (Adapted from Martin-Puig et al., 2008).

Bone Morphogenetic Proteins (BMPs), Fibroblast Growth Factors (FGFs) and Wnt (Wagner and Siddiqui, 2007; Vincent and Buckingham, 2010) (Figure 1.10). We also present the main transcription factors and its target genes fundamental to correct cardiogenesis.

1.5.3.1 TGFβ signaling

TGFβ family members, such as Nodal and BMP, have a role in inducing mesendoderm in mouse embryos (Schier, 2003). In addition, Nodal is able to induce mouse embryonic stem cells to form cardiac progenitors (Cai et al., 2012). Indeed, recent work has been investigating the role of Cer/Dan family as a heart inducer, as described with Cerl1 in Xenopus (Foley et al., 2007), chicken (Bento et al., 2011) and in mouse embryonic stem cells (Cai et al., 2013).

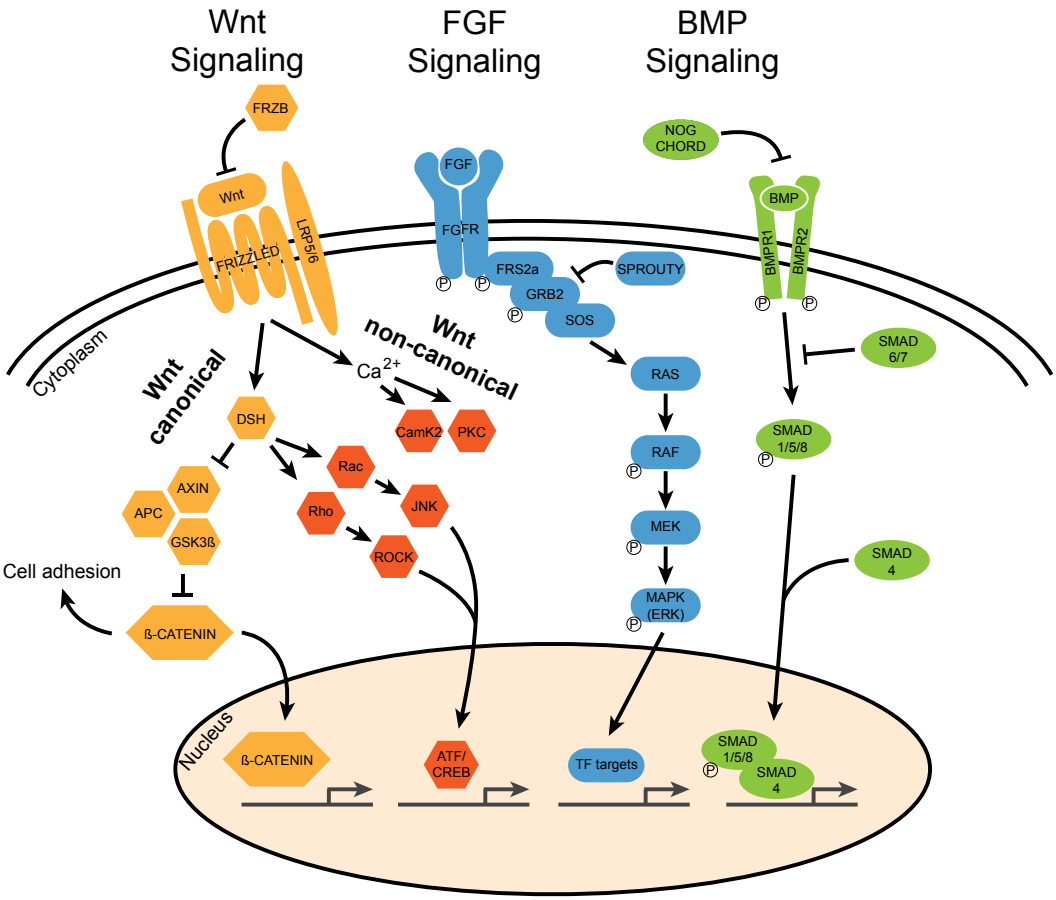

Figure 1.10 The three main signaling pathways to induce the heart formation.
The canonical and non-canonical Wnt signaling, FGF and BMP signaling are depicted respectively (Adapted from Rochais et al., 2009). For detailed information, see the text.

1.5.3.2 BMP Signaling Pathway

Secreted Bone Morphogenetic Proteins (BMPs) belong to the TGFβ superfamily (Kawabata et al., 1998) with important roles in embryonic pattern formation and in regulation of proliferation, differentiation, migration and survival of many different cell types (van Wijk et al., 2007). BMPs (BMP2, BMP4, BMP5, BMP7) are able to induce the formation of early heart forming region in chicken (van Wijk et al., 2007). BMP2 and BMP4 are related with early endocardial formation of the AV canal and OFT in mouse (Keyes et al., 2003). Furthermore, several experiments have shown the role of BMP signaling in valve development as the induction of Epithelial-Mesenchymal Transformation (EMT) which originates the cardiac valve primordia (Guo and Xiao-Fan, 2009).

Activation of the BMP signaling begins when BMP binds to type II receptor (ActRIIA, ActRIIB). This receptor recruits the type I receptor (BMPRIA, BMPRIB) by phosphorylation of this receptor and then to phosphorylate receptor-regulated Smad1, Smad5 and Smad8, which are the immediate downstream molecules of BMP signaling. This complex binds with Co- Smad4 to form a transcription factor complex that translocates to the nucleus, regulating target gene expression (Kawabata et al., 1998; Yuan and Jing, 2010).

1.5.3.3 FGF Signaling

Fibroblast Growth Factors (FGFs) are involved in the assortment of cellular processes, such as angiogenesis, differentiation, apoptosis, chemotaxis, cell migration and cell survival (Böttcher and Niehrs, 2005). It has been reported to have a fundamental role in the induction of cardiogenic precursors (FGF4 and FGF8), proliferation, septation and alignment of the OFT (FGF8 and FGF10) (Park et al., 2008; Nakajima, 2010). The inactivation of Fgf10 results in cardiac defects mainly in OFT and RV. However other FGF family members such as Fgf8/Fgf15 could partially rescue the phenotype caused by the loss of Fgf10 (Abu-Issa et al., 2002; Vincentz et al., 2005). In addition, it has also been reported that BMP and FGF signaling pathways interact resulting in a proliferative undifferentiated state of the SHF cells in chicken (Hutson et al., 2010).

FGFs bind with its receptors then initiating the signaling. This dimerization leads to cross-phosphorylation of tyrosine residues in the intracellular domain of the tyrosine kinase receptor. These residues activate the cytoplasmic signal transduction pathways as the Ras/ERK, PLCgama/CamKII, PI3K/PKB (Dorey and Amaya, 2010).

1.5.3.4 WNT Signaling

Wingless/Integrated family (WNT) encodes secreted glycoproteins which have an important role in regulating cell proliferation, differentiation, survival, polarity and migration (Nusse, 2005). In cardiogenesis, the Wnt signaling has a dual role, as an inhibitor (Wnt3a and Wnt8) and as an inductor (Wnt11) through activation of the Wnt canonical/β catenin dependent and Wnt non-canonical/β catenin independent signalings, respectively (Huelsken and Birchmeier, 2001; Brade et al., 2006). The canonical Wnt signaling regulates Bmp4 in SHF; promotes cell proliferation through regulation of Cyclin D2 and regulates the expression of Fgf10 while it inhibits FHF precursors (Ai et al., 2007; Rochais et al., 2009).

To initiate the Wnt canonical signaling pathway, Wnt binds to its cell surface receptor (Frizzle, Fzd) and co-receptor (lipoprotein low-density-lipoprotein receptor-related protein, LRP) phosphorylating Dishevelled (Dsh) which prevents the degradation of β-catenin through inhibition of the protein complex Gsk3β-APC (Glycogen synthase kinase 3β and the member of Axin family, Adenomatous polyposis coli protein). Thus β-catenin is translocated to the nucleus and interacts with the transcription factors family known as LEF/TCF (Lymphoid enhancer-binding and T- cell factors) to activate the transcription of Wnt target genes expression (Hsu et al., 1998; Miller, 2001).

The Wnt non-canonical/ Ca^{2+} pathway is activated independently of β-catenin. These Wnts bind to a distinct group of Fzd receptors (Fzd2) and activate a heterotrimeric G protein. Thus, increasing intracellular Ca^{2+} levels and subsequent stimulation of Ca^{2+}/calmodulin-dependent kinase II (CamKII) and protein kinase C (PKC). The activation of the non-canonical pathway might modulate the activation of Wnt canonical signaling in a cell context-dependent manner (Kohn and Moon, 2005; Wagner and Siddiqui, 2007).

1.5.3.5 Transcription Factors

Cardiac transcription factors (TF) drive the regulation of cardiac gene expression and therefore play a fundamental role in transcriptional regulation during development (Akazawa and Komuro, 2003). Here we describe the major TFs in cardiogenesis and some target genes.

1.5.3.5.1 GATA family

The GATA family is characterized by the zinc finger domain, in which the DNA binds to the nucleotide sequence 5'- A/T GATA A/G – 3' of target promoters. Gata-4 has been known as the most important TF of the GATA family (Pikkarainen et al., 2004), being the first TF to be express in cardiac cells (Franco et al., 1998). Deletion of *Gata-4* in humans results in failure

of atrial and ventricular septation (ASD and VSD respectively), double-outlet right ventricle (DORV) and hypoplastic left heart syndrome (Matsuoka, 2007), which is ultimately is related with decreased proliferation (Pu et al., 2004). Consistently in response to hypertrophic stimulation, the overexpression of *Gata-4* generated cardiac hypertrophy in mice, since cyclin type D2 is a direct transcriptional target indicating that Gata-4 is crucial for cell proliferation (Liang et al., 2001; Misra et al., 2012). Gata-4 activates the expression of *α-Mhc*, *Troponin C* and *I*, *Anp* and *Bnp* which will be discussed later (Ip et al., 1994; Franco et al., 1998; Durocher et al., 1997).

1.5.3.5.2 NKX2.5

The presumptive homologue of Tinman in *Drosophila melanogaster,* Nkx2.5 was identified in mice with expression in myocardium. Furthermore NKX2.5 promotes the cardiac morphogenesis and maturation (Durocher et al., 1997; Targoff et al., 2008). Nkx2.5 is required for specification and definition of the four chambers and to formation and maintenance of the correct conduction system (Pashmforoush et al., 2004; Prall et al., 2010). Nkx2-5 mutation in mice and humans leads to the ASD, DORV (Biben et al., 2000; Mcelhinney et al., 2003). In addition, it was published that deficiency of Nkx2.5 in mice leads to a failure of SHF cells to proliferate (Prall et al., 2010). Interestingly, members of the Gata and Nkx family physically interact to activate target genes in the lung, heart and vascular smooth muscle as reported in *in vitro* studies (Durocher et al., 1997).

1.5.3.6 Target genes

1.5.3.6.1 α-MHC

Myosin is a major protein component of the heart being responsible to generate the force for cellular movements ranging from cytokinesis to muscle contraction (Hang et al., 2010). Myosin heavy chain (MHC) is divided into two isoforms, α and β, both expressed in the early heart development. In adult mice, α-MHC becomes specific in the atria and β-MHC in the ventricles (Wessels and Sedmera, 2003). However, the α/β-MHC function varies in response to physiological and pathological signaling (van Rooij et al., 2007). During development, heart growth by cardiomyocyte proliferation and by physiological hypertrophy, increases the expression of contractile proteins (Hirschy et al., 2006). In mice, ablation of one α-MHC allele leads to depressive cardiac function and lethality (Jones et al., 1996). In humans, dilated cardiomyopathy is related with decrease of some contractile proteins, such α-Mhc and

decreased systolic function (Chen et al., 2008).

1.5.3.6.2 ANP and BNP

Atrial and Brain Natriuretic Peptide (ANP and BNP respectively) are synthetized and secreted hormones from the heart in response to stretching (pressure or volume load) of muscles that characterizes an increase in blood volume (Mäkikallio et al., 2006). During development, ANP and BNP are actively expressed in the ventricles, whereas in adults ANP is mainly produced in the atria, and BNP, in the ventricles (Cameron and Ellmers, 2003). The pattern of expression of both genes during the main steps of heart formation suggests a role for these genes in cardiogenesis (Christoffels et al., 2000). Studies in isolated ANP and BNP knockout mice revealed that both genes provide an important role in controlling cardiac hypertrophy by playing an anti-hypertrophic effect (Nishikimi et al., 2006). The levels of BNP mRNA in the heart are closely related to its biological activity, since BNP secretion is dependent of continuous synthesis (Magga et al., 1997). In contrast, the amount of biological activity may not reflect ANP mRNA levels, since the amount of ANP storage is bigger, which indicates that the production of ANP is active after prolonged stimulus (de Bold et al., 1996).

1.5.3.6.3 c-TNT

Troponin (Tn) complexes are localized along the thin filaments of the sarcomere acting as an intracellular Ca^{2+} sensor and playing a role in the regulation of the force generated by the interaction of thin filaments with myosin heads (Wang et al., 1994). The troponins which integrate that complex are the troponin I (TnI), troponin C (TnC), troponin T (cTNT). We focus on the cTnt that is an essential component for muscle contraction while anchoring other troponins (Nishii et al., 2008). In humans, alteration of c-Tnt leads to hypertrophic cardiomyopathy which is characterized by increased myocardial mass with myocyte and myofibrillar disarray (Thierfelder et al., 1994). In zebrafish, the c-Tnt knockdown (Tnnt2) resembles the phenotype found in humans (Becker et al., 2011). In contrast, mutation of cTnt in mouse was observed to cause systolic and diastolic dysfunction with decreased ventricular mass due to reduced of myocytes size (Tardiff et al., 1999).

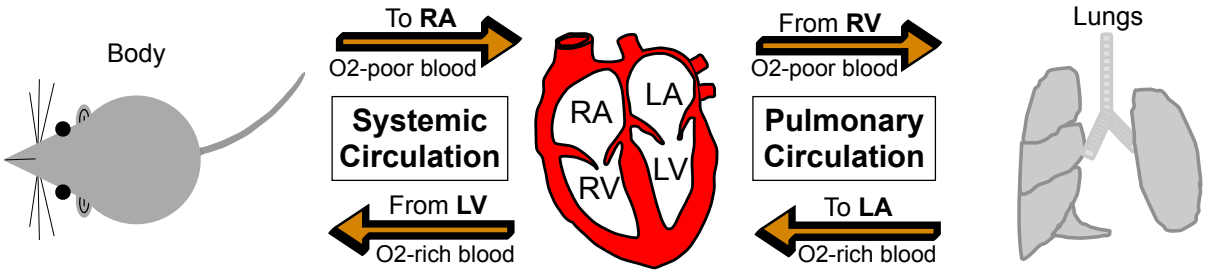

Figure 1.11 The Systemic and Pulmonary circulations.
The systemic circulation consists in providing oxygenated blood to the body (and organs as well) meanwhile through the pulmonary circulation, the oxygen poor blood is exchanged in the lungs. LA represents the left atrium, LV, left ventricle, RA, right atrium and RV, right ventricle.

1.6 Heart Physiology

The basic function of the heart is to pump blood through blood vessels by repeated and rhythmic contractions and maintaining the arterial blood pressure in order to provide a correct perfusion of the organs (Kirby, 2007). Two types of circulation characterize the circulatory system in mammalians. The pulmonary circulation starts from the vena cava (superior and inferior), which brings poor oxygenated blood from the body to the right atrium (RA). That blood arrives at the RV through the tricuspid valve (tv), where is then pumped to the pulmonary artery passing through the pulmonary valve in direction to the lungs. From the lungs, the oxygenated blood flows through the pulmonary veins (right and left) and arrives at the left atrium (LA). From LA, blood passes through the mitral valve (mv) and then there is rapid inflow of blood into the LV. The LV pumps arterial blood to the aorta through the aortic valve, and then to the rest of the body. Venous blood (poorly oxygenated) returns to the RA completing the known systemic circulation (Moorman and Christoffels, 2003) (see Figure 1.11).

That continuous event is possible due to the cardiac cycle that comprises the systole, which refers to the period of ventricular contractions and ejection of blood out of the ventricles and diastole, and the phase of ventricular relaxation and filling (Kusunose et al., 2012; Anderson, 2012). Despite the obvious differences in morphology and anatomy between mouse and human hearts, cardiac physiology concepts could be related to both species (Constantinides, 2012).

The cardiac cycle is divided in four phases (Fuster et al., 2000):

1.The filling phase of diastole: the ventricles receive blood from their respective atria; the A-V valves (inlet valves) are open while the pulmonary and aorta valves (outlet valves) are closed;

2.Isovolumetric contraction phase of systole: the cardiac muscle increases pressure and all the four valves are shut.

3.Ejection phase of systole: the heart reaches the maximum pressure and shortens length while the outlet valves are opened and the ventricles eject blood.

4.Isovolumetric relaxation phase: the cardiac muscle decreases pressure and all the four valves are shut.

To more details see the Figure 1.12.

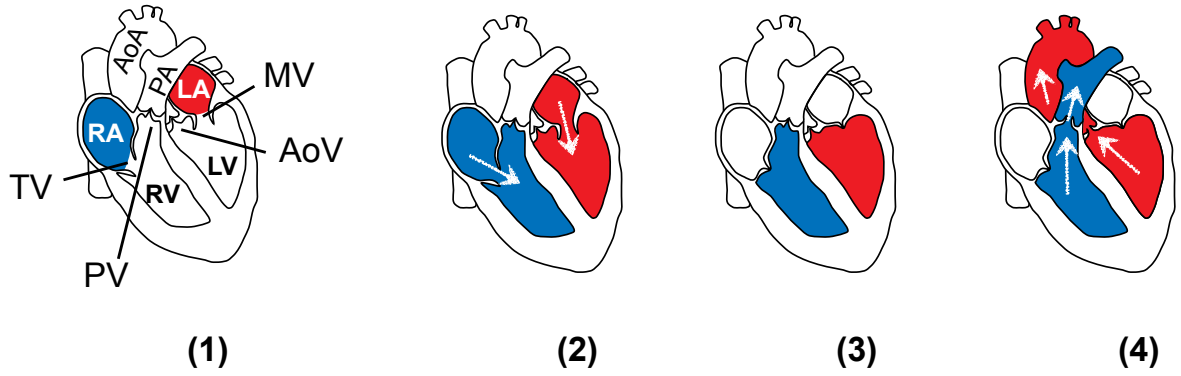

Figure 1.12 The cardiac cycle.
In ventricular filling phase, the blood pressure in the atria increases leading to the TV and MV opening. The blood flow goes to the ventricles (1, 2). The pressure between atria and ventricles at this time characterizes the early diastolic wave (E-wave). The atrial contraction is followed by the atrial diastolic wave (A-wave). Thus, the E/A waves ratio is an important parameter to indicate the diastolic function obtained from echocardiography. In the isovolumetric contraction time, the valves are closed and the pressure in the ventricles increases (3). With high pressure, the aorta and pulmonary valves open, and the ventricles eject blood to their respective arteries, characterizing the ejection phase of systole (4). After that, the valves (aorta and pulmonary) are closed, the ventricles become relaxed and the ventricular pressure drops comprising the isovolumetric relaxation time. MV, mitral valve; TV, tricuspide valve (Adapted from Tortora, G. & Grabowski, S. 2000; Nihoyannopoulos and Kisslo, 2009).

1.6.1 Heart electrophysiology – the signal propagation

The conduction pathway of the heart proceeds thought the transmission of electrical excitation based in membrane-depolarization and -repolarization current known as action potential (AP). The AP begins in the sino-atrial node (RV) and spreads to both atria and then to the ventricles reaching therefore individual atrial and ventricular myocytes. To best understanding we summarize the propagation of conduction system using the human as a model (Wilkins, 2011) (Figure 1.13).

1. **Sinoatrial (SA) node** is a pacemaker of the heart, being responsible for the atrial propagation of the AP;
2. **Atrioventricular (AV) node** avoid the ventricles do not contracting fast in order to allows the filling phase of diastole;
3. **Bundle of His** allows the rapid conduction of the impulse through the ventricles;
4. **Purkinge fibers** conduct impulses through the muscle to assist in its depolarization and contraction.

The electrocardiogram (ECG) records the electrical potential differences generated by the heart where waveforms represent the heart's depolarization- repolarization cycles. Thus, understanding the ECG is fundamental to analyze the cardiac function (Wilkins, 2011).

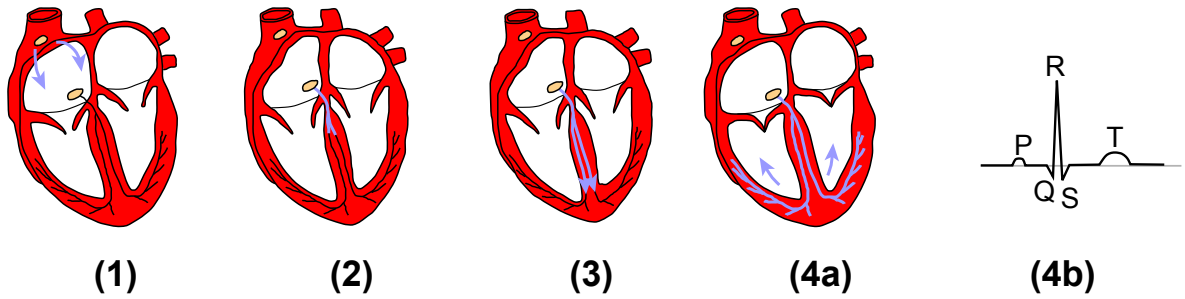

Figure 1.13 The propagation of the conduction system.
(1) The signal from the SA node (cardiac pacemaker) spreads to the AV node. (2) The AV node attenuates the transmission velocity and transmits the impulse to the bundle of His in the septum (3) and then through Purkinje fibers to both ventricles (4a). The depolarization and repolarization time in each cellular segment of the heart is different from one another. We can observe (4b) the curve standard of the ECG, which represent the conduction of electrical impulses from the atria to the ventricles. The ECG is mainly divided in three parts. P wave represents the depolarization of the atria; QRS complex indicate the ventricular depolarization; and ventricular repolarization produces the T wave. Note the phases of

propagation of cellular depolarization represented by purple arrows (Adapted from Tortora, G. & Grabowski, S. 2000; Nihoyannopoulos and Kisslo, 2009).

The heart muscle depends on the intrinsic cellular automaticity to spontaneously initiate an impulse, which characterizes the myogenic capacity. Furthermore, individual cardiomyocytes have rhythmical depolarization and repolarization capacities, which is dependent on the action potentials (AP) to initiate the contraction (contractility capacity) (Figure 1.13). The AP are generated by ion transport through the ion channels present in the membrane, where the cell responds to an electrical stimulus (excitability) (Grant, 2009). These signals are spread out through the cells (conductivity) generating a continuous AP in the cardiomyocytes and therefore resulting in systole (contraction) and diastole (relaxation) of the heart (Wilkins, 2011).

The membrane potential (mV) is depicted in 5 phases (Figure 1.14):

Phase 0 - the rapid depolarization phase (Na^+ and Ca^{2+} currents move into the cell, fast and slow respectively);

Phase 1- the early repolarization phase, inactivation of fast Na^+ channels (K^+ current outward from the cell);

Phase 2 - plateau phase (Ca^{2+} current moves into the cell and slow K^+ current outwards);

Phase 3 - rapid repolarization phase (fast K^+ outward current; Ca^{++} channels are closed, Sodium and Potassium pumps actively pump Na^+ outwards and K^+ inwards in the cell);

Phase 4 - the resting potential, the spontaneous depolarization brings the cell to the threshold of the next AP.

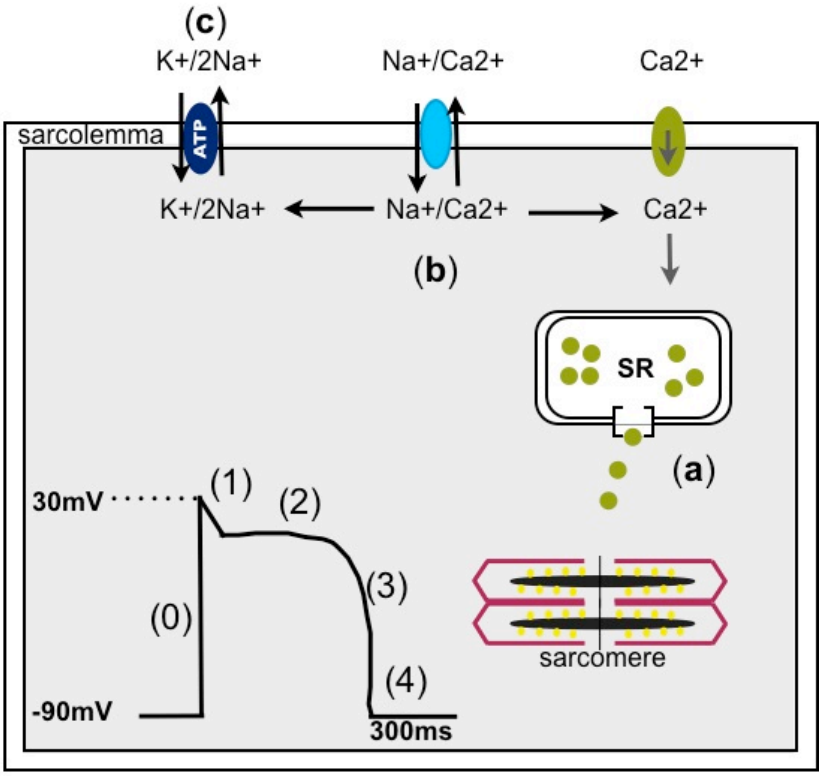

Figure 1.14 The action potential of the ventricular sarcomere and sarcomere contraction.
The AP is depicted from (0) to (4) phases and the sarcomere contraction, from (a) to (c). In resting membrane potential, the cells are not being stimulated. In Phase (0), the Na+ channels open causing a fast Na^+ inward current (cellular excitation). Phase (1), the Na^+ channels are closed due to the small efflux of K^+. Phase (2), the permeability of the Ca^{2+} channels increases leading to increased Ca^{2+} current inwards and a plateau is established, the cell contracts. Phase (3), the Ca^{2+} channels are closed and the K^+ channels are still open causing repolarization of the cell and cardiomyocyte relaxation (Phase 4). Ca^{2+} enters the cell and triggers the release of large quantities Ca^{2+} from the sarcoplasmic reticulum (a). Increased Ca^{2+} concentration initiates the contractile process, since Ca^{2+} binding to a component of troponin, actin and myosin can lead to interactions producing force and shortening. Ca^{2+} is removed by reuptake into the SR and by extrusion from the cell by a Ca^{2+}/Na^+ exchange, the relaxation occurs (b). Sodium balance is restored by Na^+/K^+ ATPase, which uses energy from ATP hydrolysis to pump Na^+ out of the cytoplasm (c). SR, sarcoplasmic reticulum (Adapted from Bers, 2002).

1.6.2 Echocardiography

Echocardiography has been explored as a routine method to evaluate the cardiac structure and functionality in humans. Indeed, echocardiography performance is a noninvasive and reliable method to follow the patient's clinic evolution after cirurgical procedures, which makes this technic an important tool nowadays (Sutton and Maniet, 2003).

To avoid the possible limitations of echocardiography in mice, due to small heart size, high heart rate and heart position (Chen et al., 2012), important advances have been done to improve accurate echocardiography images.

High-resolution echocardiography has been currently performed in mice, in order to improve the understanding of the cardiac abnormalities underlying diseases as well as the monitoring of the cardiac remodeling after induced myocardial infarction (Collins et al., 2003).

1.6.2.1 Basic principles of echocardiography

Sound is defined as mechanical waves, which are an oscillation of pressure transmitted through gases, liquids and solids. Ultrasound is a sound wave with high-frequency, normally above 20kHz (Hatfield and Bodenham, 1999).

Echocardiography employs ultrasound waves to generate images of the heart together with quantitative data of the blood flow within the cardiac chambers and blood vessels (Nihoyannopoulos and Kisslo, 2009).

In order to obtain echocardiographic images the ultrasound system depends mainly on:

1. The characteristic of the tissues, which determines the velocity propagation;
2. Radio frequency in which raw data is converted in gray-scaled images;
3. The transducer designs. Transducers use a piezoelectric crystal to generate and receive ultrasound waves, induced by an ultrasound pulse (Goldberg and Smith, 1994; Nihoyannopoulos and Kisslo, 2009) (Figure 1.15). The transducer converts one type of energy into another (electrical energy into mechanical energy and vice-versa). We have used the linear transducer in which the beam travels perpendicularly to the surface of the transducer, resulting in a rectangular image.

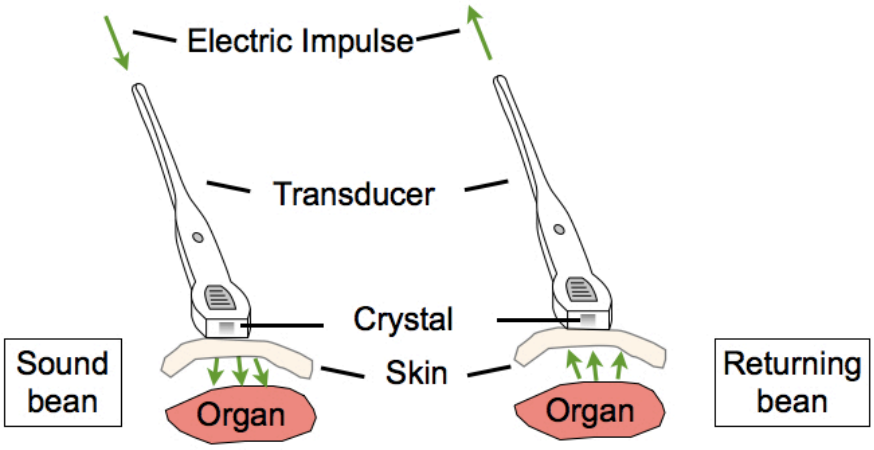

Figure 1.15 The summary of ultrasound technique to obtain images.
The transducer generated pulse wave into the body, reflected of the tissue and returned to the transducer and the raw data system (radiofrequency) is converted into gray-scaled images. Through crystal piezoelectric, electrical energy is converted into mechanical and then sound energy and vice versa (piezoelectric effect) generating therefore an ultrasound image (Adapted from Tortora, G. & Grabowski, S. 2000; Nihoyannopoulos and Kisslo, 2009).

1.6.2.2 Evaluation of cardiac function

1.6.2.2.1 Heart position

The human and mouse hearts have a pyramidal and ellipsoid shape, respectively. Its greater axis oriented obliquely to the left, which means that the long axis of the body does not coincide with the long axis of the heart (Figure 1.16). Thus, in order to obtain the diverse echocardiography measurements previous experience with animal manipulation and echocardiography performance is a mandatory requirement to a good practice. See in Figure 1.17, the several parameters that might be obtained from echocardiography.

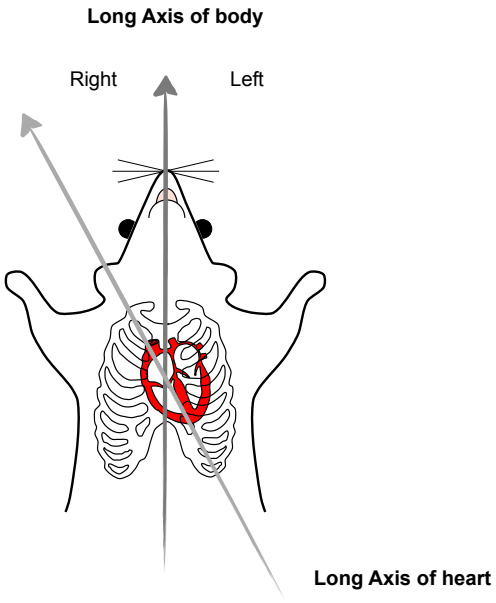

Figure 1.16 The heart position.
The long heart axis is not equivalent to the long axis of the body. The long axis of the heart is at an angle to the long axis of the body. Approximately, two-thirds of the heart is to the left of the body midline (Adapted to mouse from Ho et al., 2005).

1.6.2.2.2 Parasternal echocardiography views

Initially the parasternal long axis (PLAX) is the first position to be performed though bi- (B-) dimensional view. The B-mode view is useful to visualize and quantify the structural morphology at real-time image of the heart (Figure 1.17 B). The M-(motion-) mode represents the temporal image of the heart walls and the motion along a single dimension. Through M-mode view is possible to obtain the quantification of the wall's thickness and internal diameters of the cavities that comprise the heart structure (Figure 1.17 A).

The Pulse wave Doppler imaging is used for the quantitative blood flow from valves (mitral and tricuspid) and arteries (aorta and pulmonary) (Figure 1.17 C, D and E).

1.6.2.2.3 Cardiac index

1.6.2.2.4 LV structure

The end-systolic and diastolic LV anterior wall (AW), posterior wall (PW), interventricular septal (IVS) thicknesses and LV internal dimensions (LVID) are parameters to measure the LV morphology. Due the RV morphometry in mouse (banana shape), the echocardiography performance is hard and therefore less usual.

1.6.2.2.5 Global cardiac function

The global cardiac function is represented by the heart rate (HR), which normally is obtained from R wave to R wave interval (RR interval) from electrocardiogram or by four-five consecutive beats from M-Mode of aortic or pulmonary peak velocities. The HR is typically expressed by beats per minute (bpm). Myocardial performance index (MPI), also known as TEI index, also indicates the global cardiac function, since it combines systolic (ejection time and isovolumic contraction time) and diastolic (isovolumic relaxation time) parameters.

1.6.2.2.6 LV systolic function

The parameters that determine the LV hemodynamic index (systolic function) are: the Cardiac output (CO), which indicates the amount of blood pumped in one minute by the LV or RV, is a product of the stroke volume and heart rate; the Stroke volume (SV) is a blood volume pumped per each beat by ventricle; Ejection Fraction (EF) is employed to indicate the volume fraction pumped from the ventricle in each cardiac cycle; and Fractional Shortening (FS) represents the fraction of internal diameter reduction in cardiac cycle. These parameters were calculated by using formulas (See Table 2.4).

1.6.2.2.7 LV diastolic function

The ratio of peak velocity of early (E) to late (A) filling of mitral inflow (E/A), and the isovolumetric relaxation time (IVRT) represent the diastolic parameters (to more detail see the Figure 1.12).

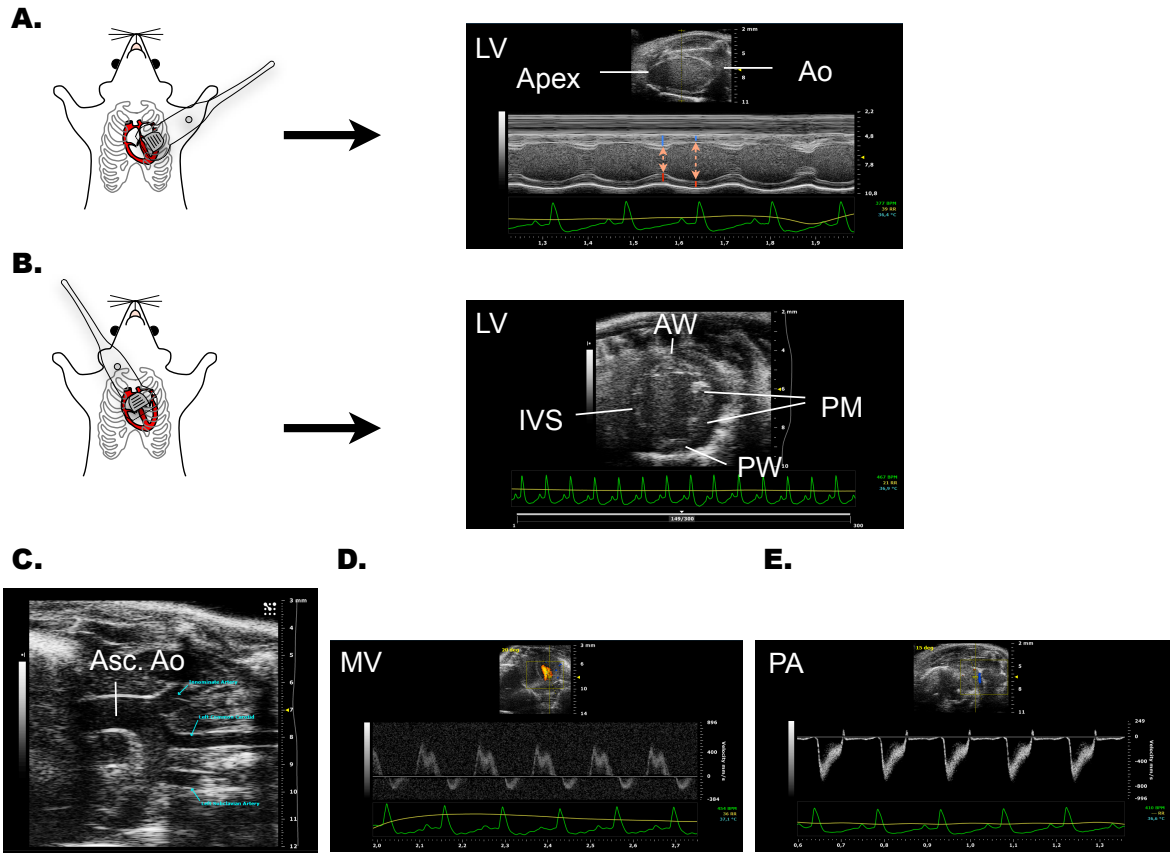

Figure 1.17 Several echocardiography measurements performed in mice.
The parasternal long axis view (PLAX) is represented in (A). On the left in order to obtain the PLAX, the transducer positioned to aorta artery (Ao) and the left ventricular apex stay in the same horizontal level, represented on the right through M- (motion-) mode view. Note in blue and red lines and orange arrows, the IVS; LVPW and LVID in the systole and diastole, respectively. In (B) the parasternal short axis view (PSAX) and the transduction position (on the left). Note the transversal axis view of the LV (on the right) depicted by B- (bidimensional-) mode view. The aortic arch B-mode view is represented in (C). The M-mode of the mitral valve (MV) was obtained from four-chamber view (D). The adapted PLAX view is represented in (E) where we obtained from Color Doppler, the peak of pulmonary velocity. Asc. Ao, indicates the ascendant aorta; AW, anterior wall; IVS, interventricular septum; MV, mitral valve; PA, pulmonary artery; PM, papillary muscles; PW, posterior wall.

1.7 Aim of the present thesis

In the last decade, the use of transthoracic echocardiography has become a current technique in the analysis of cardiac malformations and in the monitoring of cardiovascular diseases in humans and in genetically modified mice. Therefore, the establishment of the reference values for the most commonly used mouse inbred strains in whose genetic background those mutations are generated is essential for helping in results interpretation. Thus, we create a

standard echocardiographic protocol and reference values using juvenile (3 weeks) and adult (8 weeks) mice 129/Sv strain (Chapter 3.1). Furthermore the improvement of our experience in performing echocardiography was very useful to the following experiments with the *Cerl2* null mutants.

Previously in our lab it was reported that the subset of *Cerl2*$^{-/-}$ mice dying during the first hours after birth mainly due to heart defects. Therefore, in order to access the endogenous role of *Cerl2* in cardiogenesis we characterized the *Cerl2* mutants without laterality defects as described in Chapter 3.2.

After characterization of the cardiac *Cerl2*$^{-/-}$ phenotypes during embryogenesis and in early neonatal age, we detected marked increase of the left ventricular wall thickness. In addition, the *null* mutants neonates revealed impaired cardiac function, which consequently compromises the survival of these animals. However, whether the surviving *Cerl2* mutants present and develop further the latter phenotype remained unclear. Therefore, in order to analyze the cardiac physiology of surviving *Cerl2*$^{-/-}$ mutants over time, we performed echocardiography at postnatal days (P) 0, P30 and P60 (Chapter 3.3).

We expect that these studies contribute to the understanding of the the role of Cerl2 during cardiogenesis and how its absence affects the cardiac function in postnatal age.

2 Material and Methods

2.1 Mice

All animal work performed in this study was conducted compliant with the Portuguese law and approved by the Consultive Commission of the Veterinary Agency (Portuguese Ministry of Agriculture), the sole Agency/Committee in Portugal responsible to issue the ethical approval for these type of studies, following the EU guidelines for animal research and welfare.

The animals were housed in an air-conditioned room at 22°C with a 12:12 hours light-dark cycle and fed with standard mouse food and tap water *ad libitum*. After echocardiography recordings, neonates (Chapter 3.2) and young adult mice (Chapter 3.3) were euthanized under profound isoflurane anesthesia (5% isoflurane inhalant mixed with 1 L/minutes 100% Oxygen). The chest was opened and subsequently the cardioplegic solution (1.5% KCl) was injected in the LV to induce cardiac arrest. The young adult mice (Chapter 3.1) were euthanized under profound isoflurane anesthesia and then sacrificed by cervical dislocation.

In the Chapter 3.1 was used 30 wild type (WT) male 129/Sv mice (Harlan Laboratories) divided by two groups, 15 juvenile mice (3 weeks) and 15 adult mice (8 weeks). In the Chapter 3.2, the mice line used were WT, *Cerl2*$^{-/-}$ :: *Mlc1v-nLacZ24* and *Cerl2*$^{-/-}$ on background 129/Sv. In the Chapter 3.3, males WT and *Cerl2*$^{-/-}$ (5 and 4, respectively) were evaluated from postnatal (P) 0 to P60. Furthermore, the dead neonates (2 WT and 10 *Cerl2*$^{-/-}$) were analyzed.

Noon of the day of detection of the vaginal plug was considered as embryonic stage 0.5. Pregnant females were sacrificed by cervical dislocation. The uterine horns were immediately removed and the embryos were dissected in Phosphate Buffered Saline (PBS) DEPC.

2.2 Samples preparation

After the echocardiography recordings, the neonates and young adults mice under deep anesthesia (5% isoflurane mixed with 1L/minutes 100% Oxygen) were euthanized with cardioplegic solution (1.5% KCl) injected in the LV. We weighted the wet organs such as heart (In this thesis, on Chapter 3.2 and 3.3) and lungs and liver (In this thesis, on Chapter 3.3). The left tibia from adults were removed from every animal, the surrounding tissues removed and measured with calipers

For paraffin and frozen embedding the embryos and neonatal hearts were fixed in 4% paraformaldehyde (PFA) overnight (O/N). For qRT-PCR and Western Blot the whole embryos and isolated hearts were frozen directly in dry ice and stored at -80ºC.

2.3 Histology

Whole Embryos and neonatal hearts were fixed in 4% paraformaldehyde (PFA) in phosphate-buffered saline (PBS) for over night (O/N) at 4ºC, dehydrated in a series of methanol (25%, 50%, 75%, 95% and 100%), cleared in isopropanol (30 minutes at 65ºC) and embedded in paraffin wax.

The hearts were sectioned transversally in 10 and 5µm thickness (embryos and neonatal hearts respectively) using microtome (Leica RM2135). Haematoxylin and Eosin (H&E) and Masson's Trichrome (TRI) staining were performed on paraffin-embedded sections, according to standard practices (2.3.1 and 2.3.2, respectively).

For measuring wall thickness, in embryonic hearts, the three sections having as guideline the same level of the conduction system in order to best visualize the four-chambers (Ieda et al., 2010) were choose and five parts per section were randomly selected. The proportion of the compact and trabecular layers to the heart size was the ratio between their respective lengths and the longest diameter of the ventricle (Stankunas et al., 2008). To neonatal hearts, five sections at the level of mid-papillary muscle were chosen to measure the anterior, lateral and posterior LV and RV walls, and the IVS as well. The data were normalized by the body weight. A blinded observer to mouse genotypes conducted the data analysis. Axiom Vision Image Software (Zeiss Company) was used for measurements.

2.3.1 Hematoxylin and Eosin Staining Protocol

1. Deparaffinize sections, 2 times in xylene, 20 minutes each
2. Re-hydrate through series of ethanol (100%, 95%, 75% and 50%), for 5 minutes each
3. Wash in distilled water for 5 minutes
4. Stain in Gill Hematoxylin Number 3 (Sigma-Aldrish, GHS316) solution, for 15 seconds
5. Wash in running tap water, for 2 minutes
6. Counterstain in 1% Eosin Scarlet (Fluka, 45260), for 2 minutes
7. Rinse in distilled water, for 2 minutes
8. Dehydrate through 75%, 85%, 95% and 100% ethanol, for 5 minutes each
9. Clear in 2 changes of xylene, for 10 minutes each
10. Mount with xylene based mounting medium

2.3.2 Masson's Trichrome Staining

1. Deparaffinize sections, 2 times in xylene, 20 minutes each

2. Re-hydrate through series of ethanol (100%, 95%, 75% and 50%), for 5 minutes each
3. Wash in distilled water for 5 minutes
4. Mayer`s acid hematoxilin fo 10 minutes
5. Running tap water 10 minutes
6. Rinse in distilled water
7. Xylidine ponceau (0.5% Xylidine ponceau 2R in 1% acetic acid + 0.5% acid fucsin in 1% acetic acid) for 2 minutes
8. Rinse in distilled water
9. 1% phosphomolybdic acid 4 minutes
10. Rinse in distilled water
11. Light green (2% light green SFY in 2% citric acid, dilute 1/10 in distilled water before use) 90 seconds
12. Dehydrate through 75%, 85%, 95% and 100% ethanol, for 5 minutes each
13. Clear in 2 changes of xylene, for 10 minutes each
14. Mount with xylene based mounting medium

2.3.3 β-Galactosidase Staining Hearts

In order to detect the protein ß-Galactosidase (ß-Gal) in *Mlc1v-nLacZ24* neonatal hearts, we performed the ß-Gal staining which is based on the ß-Galactosidase cleavage of the chromogenic substrate X-Gal (5-bromo-4-chloro-3-indolyl-b-D-Galactosidase) leading to a blue reaction product in the cardiac cells.

1. Neonatal hearts were harvested in cold PBS and fixed for 30 minutes in 4% PFA and 0,2% Glutaraldehyde (freshly prepared)
2. Incubate in Wash Solution 3 times for 30 minutes (PBS+2mM MgCl2 + 0.01% Deoxycholate + 0.02% NP-40 + 5mM K-Ferricyanide + 5mM K-ferrocyanide, kept out of the light)
3. The staining was achieved by incubation at 37°C for a few hours or O/N in wash buffer with 1mg/ml X-Gal (dissolve X-Gal in DMF at 100mg/ml)
4. After staining, rinse twice in PBS and to preserve the stain postfix the samples in 4%PFA O/N at 4ºC
5. Wash in PBS for 30 minutes

6. Dehydrate through methanol series 25, 50, 75% (with PBS) and twice 100% methanol for 30 minutes each, cleared in isopropanol (30 minutes at 65ºC) and embedded in paraffin wax for sectioning.

2.4 Immunohistochemistry

2.4.1 Frozen Sections

After fixation, the embryonic hearts, remove excess PFA with PBS rinse. Begin sucrose infiltration for cryoprotection (following steps: 30% Sucrose 1x PBS O/N 4ºC; 1:1 30% Sucrose 1x PBS and OTC (TissueTek) O/N 4ºC, then embedding the samples in OCT compound); Snap frozen samples in liquid nitrogen or isopentane pre-cooled in liquid nitrogen, embedded in OCT compound in cryomolds. Store frozen blocks at - 80 ºC.

The embryos (were cryosectioned in transversal axis (10 μm) through cryostat (Leica CM3050S) The immunohistochemistry (IHC) was performed according adapted from Abcam protocols:

1. Rinse 3x in PBS during 5 minutes each.
2. Permeabilization with 0.1% Triton in PBS for 10 minutes only
3. Blocking with 1% BSA in PBSw for 1 hour at RT
4. Apply primary antibody diluted in PBSw with 1% BSA.
5. Incubate overnight at 4°C.
6. Rinse 2 X 10 minutes in PBSw with gentle agitation
7. Apply secondary antibody diluted in PBSw with 1% BSA, and incubate for 1 hour at RT in the dark.
8. Rinse 3 X 5 minutes in PBSw in the dark.
9. For DNA stain, incubate the slides with 0.3% 4',6-diamidino-2-phenylindole (DAPI) in PBSw for 2 minutes at RT
10. Rinse with PBS, 1x 5minutes
11. Mount coverslip with a drop of anti-fade mounting medium (32 μL) and wait 10 minutes.
12. Seal coverslip with nail polish to prevent drying and movement under microscope.
13. Store in the dark at -20°C.

2.4.2 Paraffin Sections

After fixation the neonatal hearts were embedded in paraffin wax (see details in Hystology section) and sectioned in transversal axis (5 μm). Then the samples were dewaxed (in xylene

substitute, 2x10minutes), hydrated with serial decreasing concentrations of ethanol (100%, 95%, 75%, 25%, 3 minutes each) and then rinse in distilled water. For antigen retrieval, the sections were boiled in Tris-EDTA buffer (10mM Tris Base, 1mM EDTA Solution, 0.05% Tween 20, pH 9.0) for 20 minutes. When 20 minutes has elapsed, remove the vessel and run cold tap water into it for 10 minutes. The endogenous peroxidase activity was blocked by incubation with 3% hydrogen peroxide at RT for 40 minutes. Continue with the immunohistochemical staining protocol as described above.

Table 2.1 Antibodies used in this study

Aplication	Antibody	Dilution	Company
IHC	Laminin	1:150	Abcam, ab11575
IHC	pH3	1:800	Cell Sig., #9701
IHC	MF20	1:200	Abcam, ab15
IHC	α-Actinin Sarcomeric	1:500	Sigma, A7811
IHC	Caspase-3	1:200	R&D, AF835
IHC	Goat anti-mouse	1:1000	Invitrogen,A21235
IHC	Goat anti-rabbit	1:1000	Invitrogen,A11012

IHC means immunohistochemistry

2.5 Cell counting and measurements

The quantification of proliferating cardiomyocytes in embryonic hearts was performed on 9 fields per ventricle (three fields by each three sections) divided by the total of cardiomyocytes counted per ventricle (n= 4-5 per genotype). Meanwhile to neonatal hearts, the mitotic index was obtained from 3 fields per each ventricular wall (AW, LW, and PW) and IVS in total of 3-4 sections divided by the total of cardiomyocytes counted per each ventricular wall (n=4-5 per genotype). All the images were obtained using confocal microscope (LSM 710, Zeiss Company; 63X to embryonic and 40X magnification to fetal and neonatal hearts). To each stage were determined random areas with fixed size. Adobe Photoshop CS4 software was used to determine fixed sizes and to count the cardiomyocytes. The guidelines to choose the respective sections were the same to measure the myocardial thickness as reported above (in Histology section). A blinded observer quantified the hyperplasia assay.

Cardiomyocyte area was assessed from the LVAW, LVPW and IVS (6-8 sections by each heart, n=3). We used the microscope with Apotome (Axio Imager Z2 Fluorescence, Zeiss Company; 63X magnification). The relative cell area of 100 cardiomyocytes was traced to each group (Zen software, Zeiss Company). A blinded observer quantified the hypertrophy assay.

2.6 Western Blotting (WB)

For total protein extracts, embryonic and neonatal hearts were lysed in protein extraction buffer (10mM TRIS-HCl pH 7.5; 150mM sodium chloride; 2mM EDTA; 10% Glicerol, 1% NP 40 diluted in water), and the complete phosphatase inhibitor cocktail (Roche). Protease inhibitor (Calbiochem) was also added. The lysates were homogenized on ice, centrifuged for 5 minutes at 4ºC. Following extraction, total proteins were separated by their molecular weight using denaturing on 8% SDS-PAGE polyacrylamide gels and then transferred onto an Immun-Blot PVDF membranes (Bio-Rad), blocked with 3% skim milk in Tris-Buffered Saline Tween-20 (TBST) for RT/1hour, and blotted with primary antibodies (see Table 2.2) for O/N 4ºC. For normalization purposes, blots were also probed with antibodies against mouse α-tubulina. To identify the primary antibody protein complexes, secondary anti-rabbit and anti-mouse antibodies coupled to horseradish peroxidase was used. Western blots were developed with Immun–Star WesternC Chemiluminescence Kit (Bio-Rad) and exposed to Quemi-Doc (Bio-Rad). Densitometry measurements of relative protein were determined by Image Lab 4.0 software (Bio-Rad).

Table 2.2 Antibodies used in this study

Aplication	Antibody	Dilution	Company
WB	pSmad2	1:500	Cell Sig., #3101
WB	pSmad1 5 8	1:1000	Cell Sig., #9511
WB	α-Tubulin	1:50000	Sigma, T6199
WB	Goat anti-mouse HRP	1:25000	Sigma, A4416
WB	Goat anti-rabbit HRP	1:25000	Sigma, H6908

WB means Western Blotting

2.7 RNA Isolation, Reverse Transcription and qRT-PCR

From whole embryos, isolated hearts (atria and ventricles combined), isolated right and left ventricles we obtained total RNA using 1000 µl TRI Reagent® (Sigma-Aldrich). Chloroform was added (200 µl) and samples were centrifuged at 13,000 g for 15 minutes at 4°C. Next we treated the RNA with RNAse free DNA-free™ kit (Ambion AM1906) prior to reverse transcription for 20 minutes at 37ºC. RNA quantity, quality and integrity were evaluated using a spectrophotometer (Nano Drop, Thermo Scientific) and Experion™ (Bio-Rad).

To all genes analysed, 3-5 distinct samples were used to perform the corresponding qRT-PCR experiments. First strand cDNA was synthesized at 42ºC for 1h using 0,5 µg of RNA, oligo-dT primers (Thermo-Scientific), Ribo-Lock RNA inhibitor (Thermo-Scientific), 5x first strand buffer (Invitrogen) and M-MLV reverse transcriptase (Invitrogen) according to manufacture's guidelines. Negative controls to assess genomic contamination were performed for each genotype, without reverse transcriptase. Non-template control (without RNA template) also was included in the reaction as a negative control, in which resulted in all cases in no detectable amplification product.

Triplicate reactions were performed in 96-well plates with optical sealing tape (Microseal® B Adhesive Sealer, Bio-Rad) in 15 µL total volume containing water, SsoFast™ EvaGreen® Supermix (Bio-Rad), the corresponding primers and 2µL cDNA. Oligonucleotide primer sequences and PCR annealing temperatures are given in Table 2.3. Amplification of target sequences was detected with CFX96 Real time PCR Detection System (Bio-Rad) and analyzed with Bio-Rad CFX Manager 3.0. Amplification conditions were as follows: a hot start at 95 °C was performed for 1 minutes followed by 30 cycles of denaturation at 95 °C for 15 seconds, annealing for 15 seconds at the gene-specific annealing temperature and extension at 72 °C for 20 seconds. The cycle threshold (Ct) was determined as the number of PCR cycles required for a given reaction to reach an arbitrary fluorescence value within the linear amplification range. Relative quantification was performed according to the $2^{-\Delta\Delta Ct}$ method (Livak and Schmittgen, 2001), and normalized to GAPDH and HPRT1 as reference genes.

Table 2.3. qRT-PCR primers used in this study.

Gene	Primers	Annealing Temperature (ºC)
Anp	Fwd 5' GAACCTGCTAGACCACCT 3' Rev 5' CCTAGTCCACTCTGGGCT 3'	56
Ankrd1	Fwd 5' GTAACAGGCAAAAAGAACAGCAATGGG 3' Rev 5' TTTTTCTTTTTGAGCTCTGCCTCTCG 3'	63
Bnp	Fwd 5' AAGCTGCTGGAGCTGATAAGA 3' Rev 5' GTTACAGCCCAAACGACTGAC 3'	56
Cerl2	Fwd 5' GCAGAGAGTAGCTGCTGGTGTGCCTTT 3' Rev 5' CGGCACACAGCTGTTGCAGAAGACTAC 3'	66
Ccnd1	Fwd 5' CAAATGGAACTGCTTCTGGTGAACAA 3' Rev 5' GGAGGGTGGGTTGGAAATGAACTT 3'	63
Ccnd2	Fwd 5' CTGTGCGCTACCGACTTCAA 3' Rev 5' CACATCAGTGTGGGTGATCTTG 3'	55
cTnT	Fwd 5' GGAAATCCAAGATCACTGCCTCC 3' Rev 5' GGGCACTGAGGGACAGACCA 3'	60
Gata-4	Fwd 5' GCACTGAAGAGATGCGCCC 3' Rev 5' CACCGCGTAATCAGCGCC 3'	59
Gapdh	Fwd 5' GGGAAGCCCATCACCATCTTC 3' Rev 5' AGAGGGGCCATCCACAGTCT 3'	60
Hprt1	Fwd 5' GCTGGTGAAAAGGACCTCT 3' Rev 5' CACAGGACTAGAACACCTGC 3'	60
α-Mhc	Fwd 5' GATGGCACAGAAGATGCTGA 3' Rev 5' CTGCCCCTTGGTGACATACT 3'	60
Nkx2.5	Fwd 5' CCACTCTCTGCTACCCACCT 3' Rev 5' CCAGGTTCAGGATGTCTTTGA 3'	60

2.8 Echocardiography

2.8.1 Animal Preparation for echocardiography

Body weight (BW) was determined for each period prior to cardiac examination. The anesthesia was induced in juveniles and young adults animals in a chamber supplied with 3%

isoflurane inhalant mixed with 1L/min 100% Oxygen. Thus, the animals were maintained anesthetized with a facemask with isoflurane, 1.5-1.7% for P30 and 1.8-2% for P60 animals to allow a minimal sedation level during the procedures. Neonatal mice were anesthetized using the facemask supplied with 2% isoflurane mixed with 1L/min 100% Oxygen and then the anesthesia was maintained with 1% isoflurane. They were immobilized on a heating platform ventral side up. In order to prevent any undesired anesthesia effects in body temperature (Hartley et al., 2002), the body temperature was maintained at 37ºC ±1ºC with a heating lamp. The body temperature, heart and respiration rates were constantly monitored. We applied a conductive gel and tape to adhere the paws to electrodes leads. To avoid the ultrasound attenuation, we shaved the animal's chest using a chemical hair remover and a warming acoustic gel was placed at the animal chest. To prevent eye irritation caused by the isoflurane, we used a lubricant eye ointment. The distance between the thorax and the transducer was continuously monitored to prevent reflexive bradycardia. Images were captured on cine loops at the time of the study and afterward measurements were done off-line.

2.8.2 Echocardiography assessment and measurements

We performed echocardiography through Vevo 2100 using a high-frequency transducer (40MHz; Visual Sonics, Canada). The heart was first imaged in B-mode in the parasternal long axis view to examine the left ventricle (LV). The measurements included LV endocardial and epicardial length (LVEndoL and LVEpiL, respectively) in diastole and systole. LV lengths were measured from the aortic annulus to the apex level. For long axis view in B-mode, image depth was 11 mm and image width was 12.08 mm. Moreover, parasternal short axis view was obtained at the level of papillary muscles to measure LV endocardial and epicardial area (LVEndoA and LVEpiA, respectively) in diastole and systole. These measurements were obtained by tracing the endocardial and epicardial border of the LV, where the papillary muscles were excluded from the endocardial tracings. In order to estimate LV mass (LVM) and LV volume (LVV), the area-length method was used (Kiatchoosakun, et al., 2002; Collins, et al, 2001). LVM was normalized to BW and represented as LVM index (LVMi). Endocardial area change (EAC) and fractional area change (FAC) were also calculated. For short axis view in B-mode, image depth was 10 mm and image width was 9.08 mm.

In order to acquire accurate measurements of cardiac dimensions, M-mode images were obtained from long axis and short axis B-mode images by placing the M-mode sample gate

perpendicular to the interventricular septum (IVS) and LV walls, respectively, at the level of papillary muscles. M-mode sample gate depth, length and angle for long axis view were 8-11 mm, 4.6-7.6 mm and 0 dg, respectively. For short axis view, M-mode sample gate depth, length and angle were 8-10 mm, 4.6-7.6 mm and 0 dg, respectively. M-mode from long axis view was performed to measure IVS thickness, while M-mode from short axis view was performed to measure thickness of LV anterior wall (LVAW), LV posterior wall (LVPW) and LV internal diameter (LVID). All M-mode measurements were performed in end-diastole (-d) and end-systole (-s) according to the leading-edge method of the American Society of Echocardiography (Sahn et al., 1978) End-diastolic and end-systolic measurements were obtained at the time of maximal internal chamber dimensions and at the minimal internal chamber dimensions, respectively (Stypmann et al., 2006). The LV structural parameters measured from short axis view in M-mode were used in the calculation of LV ejection fraction (EF) and LV fractional shortening (FS). M-mode from right parasternal long axis view was performed to evaluate the right ventricle internal diameter (RVID) and thickness of right ventricle anterior wall (RVAW). M-mode sample gate depth, length and angle for the right ventricle (RV) view were 7-9 mm, 2.6-4.6 mm and 0 dg, respectively.

By positioning the Doppler sample volume parallel to flow direction, which was assisted by Color Doppler-mode. From a modified short axis view of the pulmonary valve (PV) we measured pulmonary artery diameter (PAD) and PV peak velocity (PVPV). PV peak pressure gradient (PVPPG) was calculated. For pulmonary artery view in B-mode, image depth was 10-11 mm and image width was 9.08 mm. For Doppler mode of pulmonary artery view, Doppler sample volume depth, size and angle were 5-8 mm, 0.22 mm and 5-30 dg, respectively. Ascending aorta valve (AoV) flow was obtained from a suprasternal view to measure AoV peak velocity (AoVPV). The aortic arch view was performed to measure the ascending aorta diameter (AoD) and the descending aorta peak velocity (DAoPV). AoV peak pressure gradient (AoVPPG) was calculated. All arterial diameters were measured in systole, at the time of maximal artery diameter. For aorta view in B-mode, image depth was 8-12 mm and image width was 6-11 mm. Doppler sample volume depth, size and angle for ascending aorta were 6-10 mm, 0.27 mm and 20-55 dg, respectively. For descending aorta, Doppler sample volume depth, size and angle were 6-9 mm, 0.27 mm and 5-30 dg, respectively. Stroke volume (SV) and cardiac output (CO) were calculated using aortic outflow as previously described by others (Collins et al., 2003). CO was normalized to BW and

represented as CO index (COi). HR was determined from spectral Doppler tracings of the pulmonary artery and ascending aorta flow.

Mitral valve (MV) and tricuspid valve (TV) inflow were assessed from the apical 4 chamber view. The MV measurements performed were the following: MV early wave peak (MVE), MV atrial wave peak (MVA), no flow time (NFT), aortic ejection time (AET), isovolumic relaxation time (IVRT), isovolumic contraction time (IVCT) and MV ejection time (MVET). The MV peak pressure gradient (MVPPG), LV myocardial performance index (LVMPI) and MVE/A ratio were calculated. For mitral valve view, Doppler sample volume depth, size and angle were 7-11 mm, 0.22 mm and 5-30 dg, respectively. TV measurements included TV early wave peak (TVE) and TV atrial wave peak (TVA). The TV peak pressure gradient (TVPPG) and TVE/A ratio were calculated. For tricuspid valve view, Doppler sample volume depth, size and angle were 6-12 mm, 0.29 mm and 5-50 dg, respectively.

All measurements were performed excluding the respiration peaks and obtained in triplicate; the mean or median value was used for data analysis. All calculated parameters were automatically computed by the Vevo 2100 standard measurement package. The equations used by the system are shown in detail (see Table 2.4).

2.9 Intra and inter observer variability

The variability of LV B-mode (In this thesis, on Chapter 3.3), M-mode (In this thesis, on Chapter 3.1 and 3.3) measurements were determined. For intra-observer variability, one examiner analyzed all animals twice, in different occasions. For inter-observer variability, all animals were re-analyzed by a blinded examiner. The percentage of error and the observer variation were calculated. The percentage of error is the difference between two observations divided by the mean and expressed as percentages, while the observer variation is the difference between the two measurements.

Table 2.4 Equations automatically computed by the Vevo 2100 system

Description	Equation
Left ventricle volume in diastole (µl)	$\mathrm{LVVd} = \frac{3}{4} \times \mathrm{LVEndoLd} \times \mathrm{LVEndoAd}$
Left ventricle volume in systole (µl)	$\mathrm{LVVs} = \frac{3}{4} \times \mathrm{LVEndoLs} \times \mathrm{LVEndoAs}$
Left ventricle mass (mg)	$\mathrm{LVM} = 1.05 \times \left(\frac{5}{6} \times \mathrm{LVEpiAd} \times (\mathrm{LVEpiLd} + \mathrm{Td})\right) - \left(\frac{5}{6} \times \mathrm{LVEndoAd} \times \mathrm{LVEndoLd}\right)$
Endocardial area change (mm^2)	$\mathrm{EAC} = \mathrm{LVEndoAd} - \mathrm{LVEndoAs}$
Fractional area change (%)	$\mathrm{FAC} = \frac{\mathrm{LVEndoAd} - \mathrm{LVEndoAs}}{\mathrm{LVEndoAd}} \times 100$
Ejection fraction (%)	$\mathrm{EF} = 100 \times \left(\frac{\mathrm{LVVd} - \mathrm{LVVs}}{\mathrm{LVVd}}\right)$
Fractional shortening (%)	$\mathrm{FS} = 100 \times \left(\frac{\mathrm{LVIDd} - \mathrm{LVIDs}}{\mathrm{LVIDd}}\right)$
Stroke Volume (µl)	$\mathrm{SV} = 0.785 \times (\mathrm{AoD})^2 \times \mathrm{AoVTI}$
Cardiac output (ml/min)	$\mathrm{CO} = \frac{\mathrm{SV} \times \mathrm{HR\ (from\ AoD)}}{1000}$
Aortic valve peak pressure gradient (mmHg)	$\mathrm{AoVPPG} = 4 \times \left(\frac{\mathrm{AoVPV}}{1000}\right)^2$
Pulmonary valve peak pressure gradient (mmHg)	$\mathrm{PVPPG} = 4 \times \left(\frac{\mathrm{PVPV}}{1000}\right)^2$
Mitral valve peak pressure gradient (mmHg)	$\mathrm{MVPPG} = 4 \times \left(\frac{\mathrm{MVPV}}{1000}\right)^2$
Left ventricle myocardial performance index	$\mathrm{LVMPI} = \frac{\mathrm{IVRT} + \mathrm{IVCT}}{\mathrm{AET}}$
Tricuspid valve peak pressure gradient (mmHg)	$\mathrm{TVPPG} = 4 \times \left(\frac{\mathrm{TVPV}}{1000}\right)^2$

LVEndoL = Left ventricle endocardial length. LVEndoA = Left ventricle endocardial area. LVEpiA = Left ventricle epicardial area. LVEpiL = Left ventricle epicardial length. T = Average wall thickness. LVV = Left ventricle volume. LVID = Left ventricle internal diameter. AoD = Ascending aorta diameter. AoVTI = Ascending aorta velocity time integral. SV = Stroke volume. HR = Heart rate. AoVPV = Ascending aorta valve peak velocity. PVPV

= Pulmonary valve peak velocity. MVPV = Mitral valve peak velocity. IVRT = Isovolumic relaxation time. IVCT = Isovolumic contraction time. AET = Aortic ejection time. TVPV = Tricuspid valve peak velocity. -d = In diastole. -s = In systole.

2.10 Statistical Analysis

Statistical analysis was performed using SPSS software (Version 20) in Chapter 3.1. Shapiro-Wilk test was used to assess normality of data. The following parameters were not normally distributed: AoVPV, DAoPV, AoVPPG and RVIDs from juvenile data and LVEndoAs, LVEndoLd and LVEpiLd from adult data. Data are presented as mean ± standard deviation or median with interquartile range (IQR), whenever appropriate. To compare results between the two groups, juvenile and adult mice, Student's unpaired t-test was used for the normally distributed data, while Mann–Whitney U test was used for not normally distributed data. Paired t-test was used for within group comparison. Bland-Altman analysis was performed to assess agreement between measurements of intra- and inter-observer measurements variability; in addition Pearson's correlation was used. For BW and HR association with all the measured parameters, Pearson's correlation or Spearman's correla- tion were used depending if data followed a linear model and if it was normally distributed or not, respectively. * P-value < 0.05 was considered significant.

The data obtained from all analyses in Chapter 3.2 and Chapter 3.3 was performed using GraphPad PRISM 6 software (GraphPad Software; San Diego, CA). Statistical differences were determined by unpaired Student's t test or one-way ANOVA to compare more than two groups (Chapter 3.2). Kaplan–Meier analysis, assessed survival data. To One-way ANOVA, Tukey test was used to compare the follow-up values. Bland-Altman analysis (bias plot) and Pearson was performed to assess the agreement between intra and inter-observer measures (Chapter 3.3). Values are depicted as mean ± SEM or ±SD. *P<0.05 was considered statistically significant.

3 Results

Results

3.1 Part I

Transthoracic echocardiography reference values in juvenile and adult 129/Sv mice

Maurícia Vinhas[1], Ana Carolina Araújo[1,2], Sónia Ribeiro[3], Luís Brás Rosário[3] and José António Belo[1,2*]

1. Regenerative Medicine Program, Department of Biomedical Sciences and Medicine (DCBM), University of Algarve (UALG), Campus of Gambelas, Edf.8, 8005-139, Faro, Portugal.
2. Institute for Biotechnology and Bioengineering, Center for Molecular and Structural Biomedicine (CBME), University of Algarve, Campus of Gambelas, Edf.8, 8005-139, Faro, Portugal.
3. Santa Maria Hospital, Cardiology Service, Lisbon Academic Medical Centre (CCUL), Lisbon, Portugal.

Published in Cardiovascular Ultrasound (2013) 11: 1-10

Authors' contribution

MV performed the image acquisitions and measurements, performed statistical analysis, analyzed and interpreted the ultrasound data and wrote the manuscript. ACA performed the measurements for the inter-observer variability, participated in the interpretation of the results and contributed to the writing of the manuscript. SR participated in the interpretation of the results and contributed to the writing of the manuscript. LBR participated in the interpretation of the results and contributed to the writing of the manuscript. JAB designed the study and wrote the manuscript.

3.1.1 Abstract

Background

In the recent years, the use of Doppler-echocardiography has become a standard non-invasive technique in the analysis of cardiac malformations in genetically modified mice. Therefore, normal values have to be established for the most commonly used inbred strains in whose genetic background those mutations are generated. Here we provide reference values for transthoracic echocardiography measurements in juvenile (3weeks) and adult (8weeks) 129/Sv mice.

Methods

Echocardiographic measurements were performed using B-mode, M-mode and Doppler-mode in 15 juvenile (3 weeks) and 15 adult (8 weeks) mice, during isoflurane anesthesia. M-mode measurements variability of left ventricle (LV) was determined.

Results

Several echocardiographic measurements significantly differ between juvenile and adult mice. Most of these measurements are related with cardiac dimensions. All B-mode measurements were different between juveniles and adults (higher in the adults), except for fractional area change (FAC). Ejection fraction (EF) and fractional shortening (FS), calculated from M-mode parameters, do not differ between juvenile and adult mice. Stroke volume (SV) and cardiac output (CO) were significantly different between juvenile and adult mice. SV was 31.93 ± 8.67 µl in juveniles vs 70.61 ± 24.66 µl in adults, $\rho < 0.001$. CO was 12.06 ± 4.05 ml/min in juveniles vs 29.71 ± 10.13 ml/min in adults, $\rho < 0.001$. No difference was found in mitral valve (MV) and tricuspid valve (TV) related parameters between juvenile and adult mice. It was demonstrated that variability of M-mode measurements of LV is minimal.

Conclusions

This study suggests that differences in cardiac dimensions, as wells as in pulmonary and aorta outflow parameters, were found between juvenile and adult mice. However, mitral and tricuspid inflow parameters seem to be the similar between 3 weeks and 8 weeks mice. The reference values established in this study would contribute as a basis to future studies in post-natal cardiovascular development and diagnosing cardiovascular disorders in genetically modified mouse mutant lines.

Keywords: Echocardiography, juvenile, adult, 129/Sv mouse, reference values, Doppler

3.1.2 Background

Cardiac ultrasound, also known as echocardiography, is one of the most commonly used diagnostic techniques in human cardiology for possible pathology or lesion. This technique uses high frequency ultrasound waves for visualizing the heart and can provide information on the heart anatomy, blood flow pattern and function of heart muscle, vessels and valves. Until recently, echocardiographic application in animals was limited primarily to larger, non-rodent species. Due to advances in ultrasound imaging technology, ultrasound systems have now the spatial and temporal resolution to obtain accurate and reliable images of mouse hearts (Tanaka et al., 1996). As a result, it has become a valuable non-invasive imaging tool to visualize and evaluate cardiac morphology and function *in vivo of mice. It was demonstrated by others that e*chocardiography is becoming a useful technique for studying cardiovascular development and diagnosing cardiovascular disorders in small animals (Fox et al., 1999).

Knowledge of findings in healthy animals is important for interpretation of results in genetically modified and surgical animals. Most of the available mouse ES cell lines have been generated using the 129/Sv strain. Therefore, the purpose of this study is to provide reference values for transthoracic echocardiography measurements and calculated parameters using B-mode, M-mode and Doppler-mode in juvenile (3 weeks) and adult (8 weeks) 129/Sv mice, obtained during isoflurane anesthesia.

3.1.3 Results

Satisfactory images could be captured in all animals. Cardiac examination time was around 30 min, in all animals. All echocardiographic measurements performed in juvenile and adult mice were summarized (Table 3.1, 3.2 and 3.3).

The RV could only be assessed in 7 juvenile and in 11 adult mice. The TV inflow could only be assessed in 12 juvenile and in 6 adult mice.

BW was significantly lower in the juvenile (7.68 ± 1.33 g) as compared to adult mice (19.84 ± 2.84 g; $p < 0.001$). In the same way, HR was significantly lower in the juvenile (387.34 ± 44.12 bpm) as compared to adult mice (421.82 ± 25.34 bpm; $p = 0.015$). Table 3.1 summarizes B-mode echocardiographic measurements. This table shows that all parameters have higher values in the adult mice than juvenile, except for FAC and LVMi.

Table 2.5 Echocardiographic measurements from B-mode images.

Measurement	Juvenile	n	Adult	n	*p*
LVEndoLd (mm)	6.18 (0.57)	15	7.40 (0.58)	15	< 0.001
LVEndoLs (mm)	4.99 ± 0.38	15	6.58 ± 0.45	15	< 0.001
LVEpiLd (mm)	6.38 (0.56)	15	7.65 (0.67)	15	< 0.001
LVEpiLs (mm)	5.35 ± 0.34	15	7.03 ± 0.44	15	< 0.001
LVEndoAd (mm^2)	6.06 ± 0.87	15	9.87 ± 1.20	15	< 0.001
LVEndoAs (mm^2)	3.06 (0.98)	15	4.25 (1.12)	15	< 0.001
LVEpiAd (mm^2)	11.85 ± 1.73	15	19.47 ± 1.71	15	< 0.001
LVEpiAs (mm^2)	8.84 ± 1.83	15	14.46 ± 1.57	15	< 0.001
EAC (mm^2)	3.22 ± 0.81	15	5.62 ± 1.16	15	< 0.001
FAC (%)	52.89 ± 10.07	15	56.87 ± 7.80	15	ns
LVVd (µl)	29.57 ± 6.04	15	59.90 ± 8.78	15	< 0.001
LVVs (µl)	11.85 ± 3.19	15	23.32 ± 5.31	15	< 0.001
LVM (mg)	39.68 ± 8.64	15	81.90 ± 9.69	15	< 0.001
LVMi (mg/g)	5.26 ± 1.27	15	4.16 ± 0.42	15	0.005
AoD (mm)	0.93 ± 0.09	15	1.27 ± 0.13	15	< 0.001
PAD (mm)	1.34 ± 0.11	15	1.59 ± 0.13	15	< 0.001

Values are mean ± SD or median (IQR), as appropriate. *p* = statistical significance; ns = not significant. n=15 for all measurements. LVEndoL = Left ventricle endocardial length. LVEpiL = Left ventricle epicardial length. LVEndoA = Left ventricle endocardial area. LVEpiA = Left ventricle epicardial area. EAC = Endocardial area change. FAC = Fractional area change. LVV = Left ventricle volume. LVM = Left ventricle mass. LVMi = LVM index. AoD = Ascending aorta diameter. PAD = Pulmonary artery diameter. -d = In diastole. -s = In systole.

Table 3.2 summarizes M-mode echocardiographic measurements. This table shows that EF and FS are considered the same in the two groups. Representative images and measurements of echocardiographic B-mode and M-mode are shown in Figure 3.1.

Table 3.3 summarizes Doppler echocardiographic measurements. SV and CO were lower in the juvenile as compared to adult mice. No significant difference was found in MV and TV related data between juvenile and adult mice, except for IVRT. Representative images of echocardiographic PW Doppler-mode are shown in Figure 3.2.

Table 2.6 Echocardiographic measurements from M-mode images.

Measurement	Juvenile	n	Adult	n	*p*
LVAWd (mm)	0.61 ± 0.09	15	0.74 ± 0.14	15	0.005
LVAWs (mm)	0.85 ± 0.13	15	1.08 ± 0.18	15	< 0.001
LVIDd (mm)	2.84 ± 0.20	15	3.56 ± 0.19	15	< 0.001
LVIDs (mm)	1.96 ± 0.21	15	2.44 ± 0.28	15	< 0.001
LVPWd (mm)	0.59 ± 0.15	15	0.64 ± 0.13	15	ns
LVPWs (mm)	0.81 ± 0.17	15	0.88 ± 0.19	15	ns
EF (%)	59.63 ± 9.05	15	59.91 ± 8.15	15	ns
FS (%)	30.76 ± 6.15	15	31.45 ± 5.63	15	ns
IVSd (mm)	0.41 ± 0.08	15	0.47 ± 0.15	15	ns
IVSs (mm)	0.50 ± 0.13	15	0.62 ± 0.25	15	ns
RVIDd (mm)	1.08 ± 0.15	7	1.42 ± 0.19	11	0.001
RVIDs (mm)	0.65 (0.31)	7	0.89 (0.21)	11	ns
RVAWd (mm)	0.50 ± 0.11	7	0.32 ± 0.08	11	0.001
RVAWs (mm)	0.66 ± 0.16	7	0.57 ± 0.13	11	ns

Values are mean ± SD or median (IQR), as appropriate. *p* = statistical significance. ns = not significant. n=15 for all measurements, except for RV measurements (n=7 for the juveniles and n=11 for the adults).
LVAW = Left ventricle anterior wall. LVID = Left ventricle internal diameter. LVPW = Left ventricle posterior wall. EF = Ejection fraction. FS = Fractional shortening. IVS = Interventricular septum. RVID = Right ventricle internal diameter. RVAW = Right ventricle anterior wall. -d = In diastole. -s = In systole.

The most important values of tables 3.1, 3.2 and 3.3 are also summarized in Figure 3.3.

We also found that some of the structural parameters analyzed, such as AoD, EpiLs and EndoLd, had a strong positive correlation with BW, both in juvenile and adult mice (see Additional file, Table 3.6 and 3.7). Both CO and SV correlated strongly with BW in juveniles and adults ($p < 0.01$). In 3 weeks mice, NFT had a moderately strong negative correlation with HR ($p < 0.01$) (see Additional file, Table 3.6). In 8 weeks mice, also NFT and AET had a strong negative correlation with HR ($p < 0.01$) (see Additional file, Table 3.7).

Table 3.4 summarizes intra- and inter-observer variability of LV M-mode measurements. No significant differences between measurements were found, except for intra-observer measurement of LVPWd from adult mice ($p < 0.05$ by paired *t*-test).

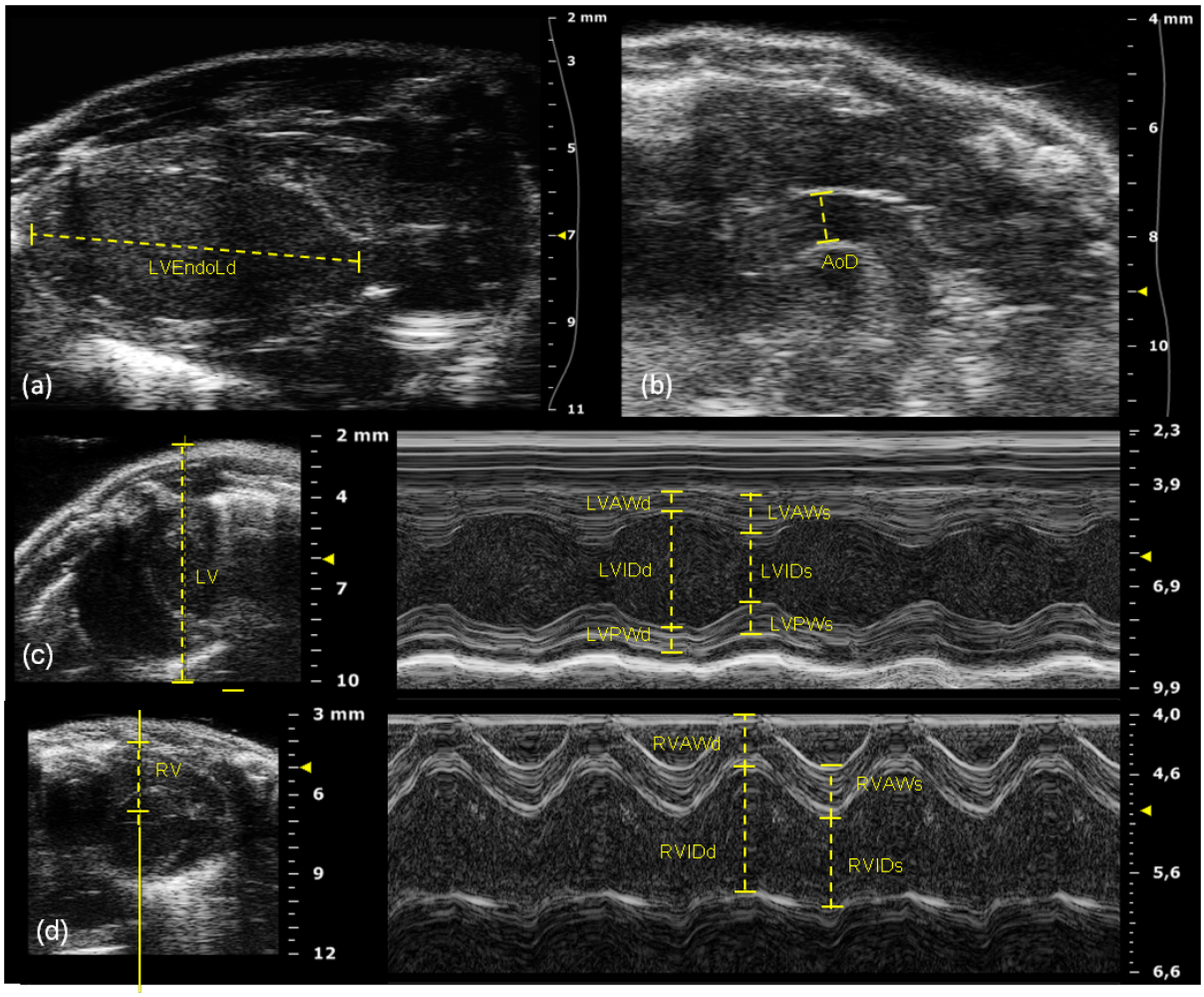

Figure 2.1 Representative B-mode and M-mode echocardiographic images and measurements.
(A) Parasternal long axis view of left ventricle (LV) in B-mode. (B) Aortic arch view in B-mode. (C) Short axis view in 2D (left panel) and M-mode tracing (right panel) of the LV, at the level of papillary muscle. (D) Right parasternal long axis view in 2D (left panel) and M-mode tracing (right panel) of the righ ventricle (RV). LVEndoL = Left ventricle endocardial length. AoD = Ascending aorta diameter. LVAW = Left ventricle anterior wall. LVID = Left ventricle internal diameter. LVPW = Left ventricle posterior wall. RVAW = Right ventricle anterior wall. RVID = Right ventricle internal diameter; -d = In diastole. -s = In systole.

Table 2.7 Echocardiographic measurements from Doppler images.

Measurement	Juvenile	n	Adult	n	*p*
AoVPV (mm/s)	1055.28 (327.21)	15	1557.67 (693.61)	15	0.003
AET (ms)	50.37 ± 4.56	15	49.59 ± 4.50	15	ns
AoVPPG (mmHg)	4.45 (3.13)	15	9.76 (9.46)	15	0.003
DAoPV (mm/s)	747.59 (162.89)	15	1049.88 (321.15)	15	0.002
SV (µl)	31.93 ± 8.67	15	70.61 ± 24.66	15	< 0.001
CO (ml/min)	12.06 ± 4.05	15	29.71 ± 10.13	15	< 0.001
COi (ml/min.g)	1.54 ± 0.36	15	1.48 ± 0.39	15	ns
PVPV (mm/s)	663.34 ± 141.08	15	810.62 ± 149.55	15	0.01
PVPPG (mmHg)	1.83 ± 0.77	15	2.71 ± 0.96	15	0.01
MVE (mm/s)	673.53 ± 149.31	15	747.08 ± 92.31	15	ns
MVA (mm/s)	456.51 ± 73.29	15	500.17 ± 85.14	15	ns
IVCT (ms)	10.90 ± 2.76	15	12.91 ± 3.45	15	ns
IVRT (ms)	16.52 ± 3.29	15	12.48 ± 2.49	15	0.001
MVET (ms)	61.05 ± 9.74	15	59.24 ± 8.34	15	ns
NFT (ms)	77.45 ± 5.66	15	75.66 ± 7.57	15	ns
MVPPG (mmHg)	1.98 ± 0.76	15	2.30 ± 0.52	15	ns
MVE/A	1.50 ± 0.37	15	1.53 ± 0.27	15	ns
LVMPI	0.55 ± 0.14	15	0.51 ± 0.07	15	ns
TVE (mm/s)	241.72 ± 30.57	12	252.83 ± 77.42	6	ns
TVA (mm/s)	400.90 ± 47.96	12	386.53 ± 123.06	6	ns
TVPPG (mmHg)	0.74 ± 0.21	12	0.68 ± 0.39	6	ns
TVE/A	0.60 ± 0.06	12	0.66 ± 0.13	6	ns

Values are mean ± SD or median (IQR), as appropriate. *p* = statistical significance. ns = not significant. n=15 for all measurements, except for TV measurements (n=12 for the juveniles and n=6 for the adults).

AoVPV = Ascending aorta valve peak velocity. AET = Aortic ejection time. AoVPPG = Ascending aorta valve peak pressure gradient. DAoPV = Descending aorta peak velocity. SV = Stroke volume. CO = Cardiac output. COi = CO index. PVPV = Pulmonary valve peak velocity. PVPPG = Pulmonary valve peak pressure gradient. MVE = Mitral valve early wave peak. MVA = Mitral valve atrial wave peak. IVCT = Isovolumic contraction time. IVRT = Isovolumic relaxation time. MVET = Mitral valve ejection time. NFT = Non-filling time. MVPPG = Mitral valve peak pressure gradient. LVMPI = Left ventricle myocardial performance index. TVE = Tricuspid valve early wave peak. TVA = Tricuspid valve atrial wave peak. TVPPG = Tricuspid valve peak pressure gradient.

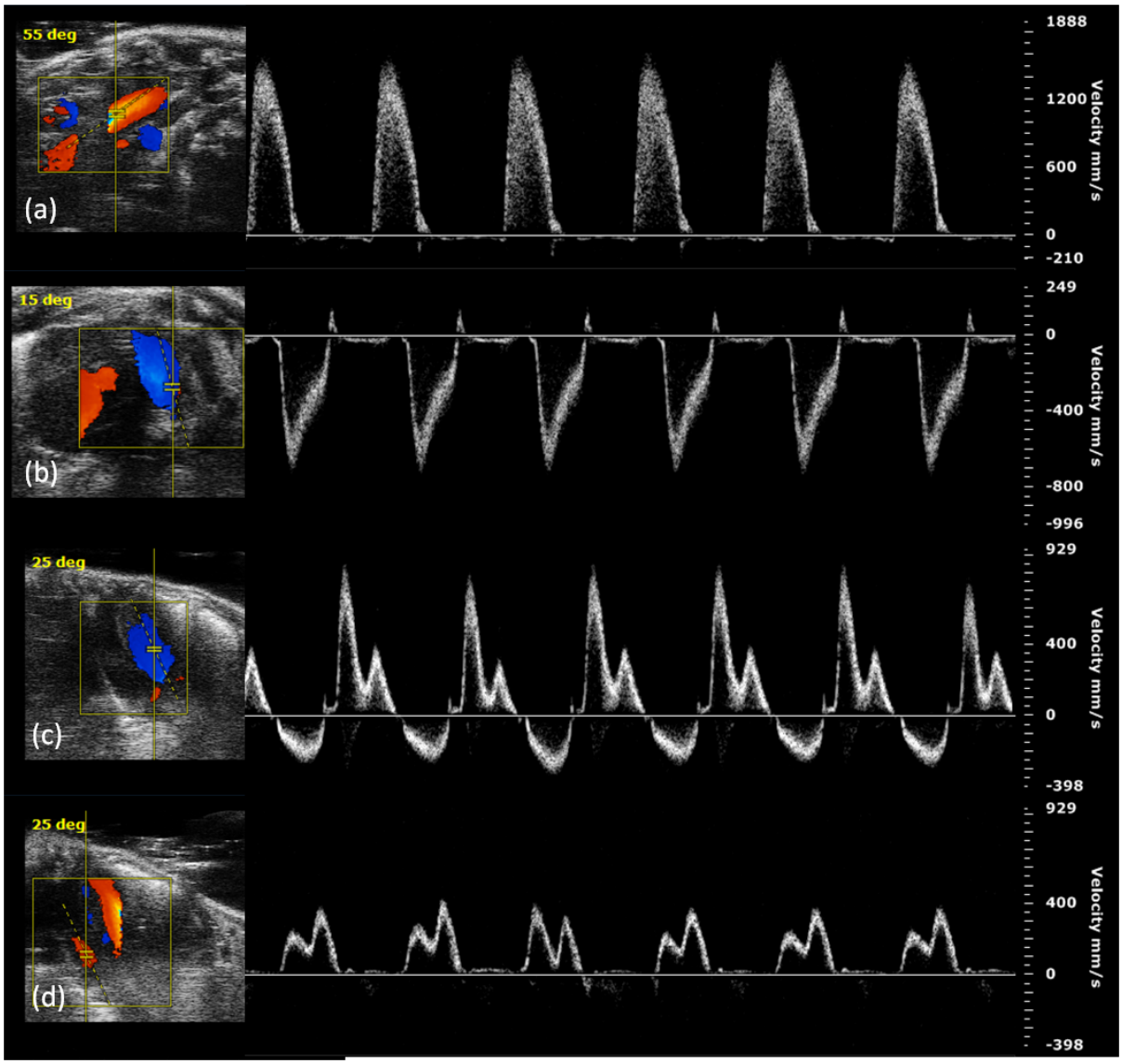

Figure 2.2 Representative Doppler echocardiographic images.
(A) Suprasternal view (left panel) and PW Doppler tracing (right panel) of aortic outflow. (B) Modified short axis view (left panel) and PW-Doppler tracing (right panel) of pulmonary outflow. (C) Apical 4 chamber view (left panel) and PW-Doppler tracing (right panel) of mitral valve (MV) inflow. (D) Apical 4 chamber view (left panel) and PW-Doppler tracing (right panel) of tricuspide valve (TV) inflow.

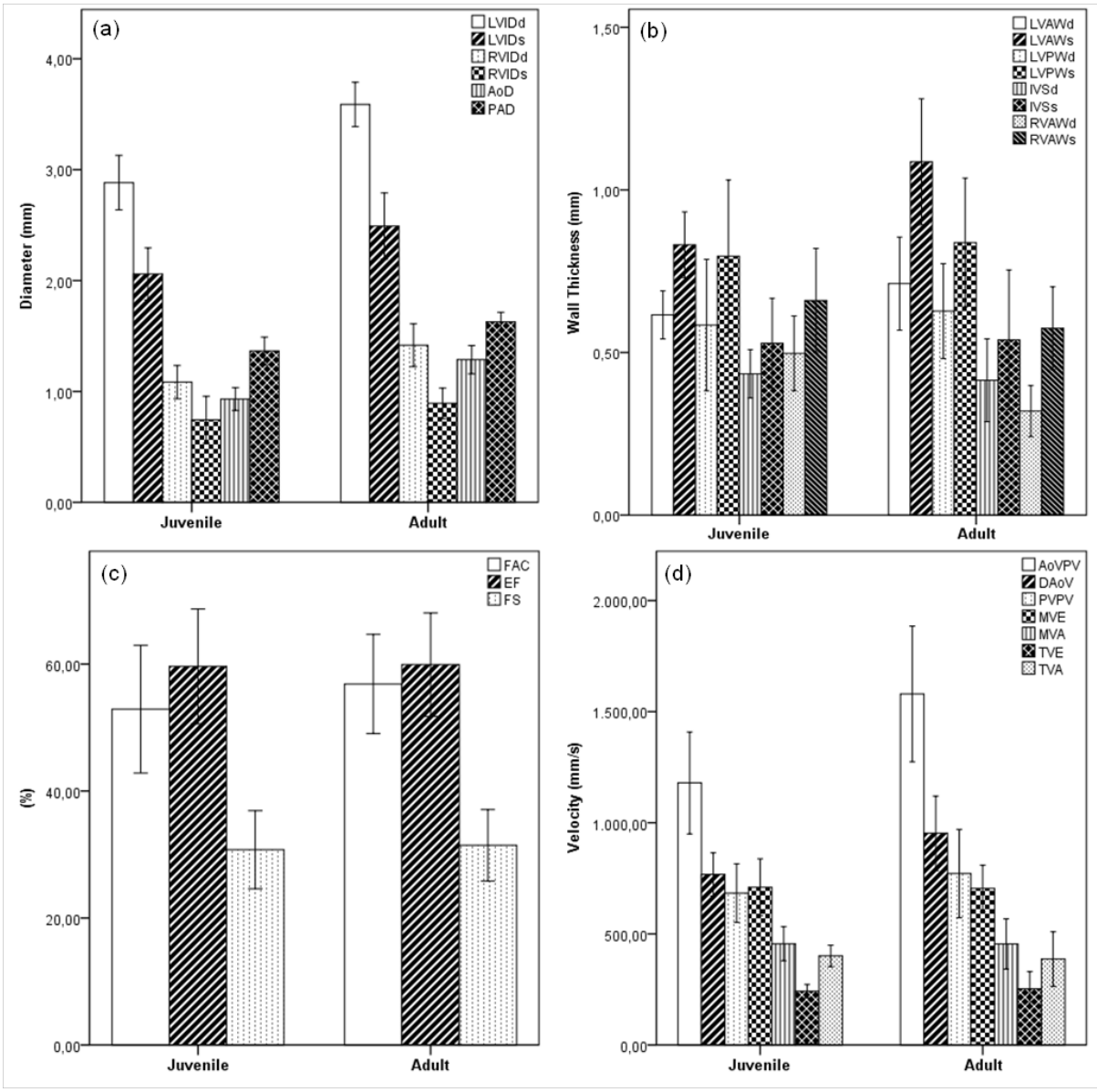

Figure 2.3 Bar graphs showing overview over the results of juvenile (n=15) vs adult mice (n=15).

(A) Thicknesses of left ventricle (LV) walls and interventricular septum (IVS). (B) Diameters of LV and arteries. (C) Percentages of fractional area change (FAC), ejection fraction (EF) and fractional shortening (FS). (D) Peak velocities of arterial outflow and mitral valve (MV) inflow. * Statistically significant. LVID = Left ventricle internal diameter. AoD = Ascending aorta diameter. PAD = Pulmonary artery diameter. LVAW = Left ventricle anterior wall. LVPW = Left ventricle posterior wall. AoVPV = Ascending aorta valve peak velocity. DAoPV = Descending aorta peak velocity. PVPV = Pulmonary valve peak velocity. MVE = Mitral valve early wave peak. MVA = Mitral valve atrial wave peak. -d = In diastole. -s = In systole.

Table 2.8 Variability of LV M-mode measurements.

	Intra-Observer		Inter-Observer	
Juvenile	**Error (%)**	**Observer Variation (mm)**	**Error (%)**	**Observer Variation (mm)**
LVAWd	1.08 ± 6.66	-0.01 ± 0.04	3.05 ± 11.36	0.02 ± 0.06
LVAWs	3.74 ± 5.11	-0.03 ± 0.04	4.88 ± 12.02	0.04 ± 0.10
LVIDd	1.07 ± 3.30	0.03 ± 0.10	0.32 ± 6.29	0.01 ± 0.18
LVIDs	3.11 ± 7.32	0.06 ± 0.16	1.11 ± 14.40	0.02 ± 0.29
LVPWd	1.78 ± 7.11	-0.01 ± 0.04	13.82 ± 27.87	0.07 ± 0.14
LVPWs	0.78 ± 9.52	0.00 ± 0.08	9.15 ± 30.98	0.06 ± 0.20
IVSd	4.96 ± 11.52	0.02 ± 0.04	8.83 ± 24.40	0.05 ± 0.11
IVSs	2.40 ± 13.61	0.00 ± 0.07	2.07 ± 23.71	0.02 ± 0.13
Adult	**Error (%)**	**Observer Variation (mm)**	**Error (%)**	**Observer Variation (mm)**
LVAWd	4.18 ± 8.30	-0.03 ± 0.07	3.24 ± 12.83	0.03 ± 0.10
LVAWs	2.40 ± 8.69	-0.02 ± 0.10	1.70 ± 9.05	0.02 ± 0.10
LVIDd	1.49 ± 3.52	0.05 ± 0.12	-0.43 ± 2.77	-0.02 ± 0.10
LVIDs	1.13 ± 5.56	0.03 ± 0.14	0.57 ± 5.44	0.01 ± 0.15
LVPWd	5.68 ± 7.16 *	-0.03 ± 0.04*	-5.64 ± 20.58	-0.05 ± 0.19
LVPWs	2.10 ± 6.29	-0.01 ± 0.05	-8.86 ± 21.86	-0.10 ± 0.24
IVSd	2.73 ± 8.55	-0.01 ± 0.04	-2.88 ± 21.07	-0.01 ± 0.09
IVSs	2.04 ± 10.62	0.00 ± 0.06	-0.84 ± 18.54	0.01 ± 0.10

Values are mean ± SD. p = statistical significance. All $p > 0.05$, except * $p = 0.01$. LVAW = Left ventricle anterior wall. LVID = Left ventricle internal diameter. LVPW = Left ventricle posterior wall. IVS = Interventricular septum. -d = In diastole. -s = In systole.

However, Bland-Altman analysis showed a good agreement of both measurements (Figure 3.4), linear regression LVPWd (intra_Obs.1) = 0.885 × LVPWd (intra_Obs.2) + 0.107, r^2 = 0.89, Pearson's correlation 0.94, $p < 0.01$. The agreement between intra- and inter-observer measurements was considered high, as illustrated in Bland-Altman analysis (Table 3.5).

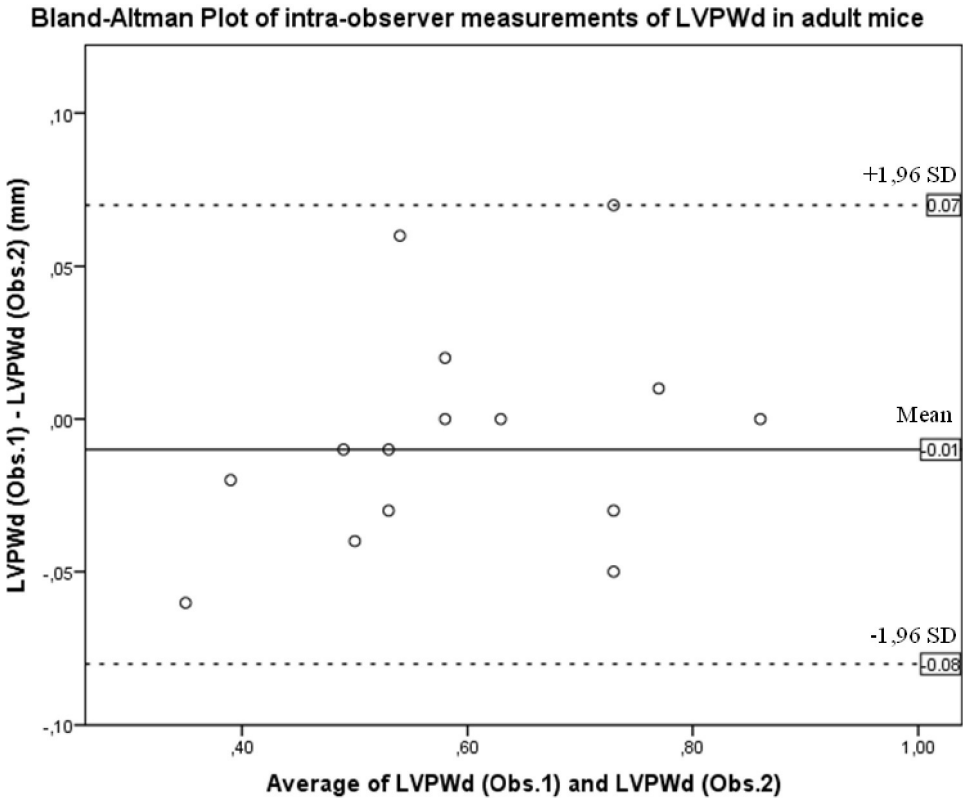

Figure 2.4 Bland-Altman correlation of intra-observer measurements of LVPWd in adult mice.
LVPWd = Left ventricle posterior wall in diastole. Obs.1 = Measurement 1 of observer 1. Obs. 2 = Measurement 2 of observer 1.

3.1.4 Discussion

In order to understand and analyze *studies* that use *transgenic animals or animals that undergo surgical procedures,* the cardiac characterization of normal/wild type and healthy animals is considered extremely important. To our best knowledge, echocardiographic evaluation of reference values of B-mode, M-mode and Doppler-mode in juvenile (3 weeks) and adult (8 weeks) 129/Sv wild-type mice has not been reported. In the present study, cardiac dimensions were significantly different between juvenile and adult mice, as expected. Diastolic function does not differ between juvenile and adult mice. Additionally, we demonstrate that the variability of LV measurements in M-mode is minimal, indicating that this method is reliable.

Table 2.9 Agreement between measurements of intra- and inter-observer variability.

	Intra-Observer				Inter-Observer			
Juvenile	**Mean difference ± SD**	**Limits of agreement**	***r***	***p****	**Mean difference ± SD**	**Limits of agreement**	***r***	***p****
LVAWd	-0.01 ± 0.04	-0.09 to 0.08	0.91	<0.01	0.02 ± 0.06	-0.11 to 0.14	0.82	<0.01
LVAWs	-0.03 ± 0.04	-0.12 to 0.06	0.94	<0.01	0.04 ± 0.10	-0.16 to 0.24	0.72	<0.01
LVIDd	0.03 ± 0.10	-0.17 to 0.23	0.89	<0.01	0.01 ± 0.18	-0.36 to 0.38	0.64	<0.05
LVIDs	0.06 ± 0.16	-0.25 to 0.38	0.77	<0.01	0.02 ± 0.29	-0.55 to 0.60	0.20	ns
LVPWd	-0.01 ± 0.04	-0.08 to 0.07	0.97	<0.01	0.07 ± 0.14	-0.21 to 0.36	0.50	ns
LVPWs	0.00 ± 0.08	-0.16 to 0.15	0.89	<0.01	0.06 ± 0.20	-0.34 to 0.46	0.42	ns
IVSd	0.02 ± 0.04	-0.07 to 0.11	0.83	<0.01	0.05 ± 0.11	-0.17 to 0.26	0.39	ns
IVSs	0.00 ± 0.07	-0.13 to 0.14	0.91	<0.01	0.02 ± 0.13	-0.24 to 0.27	0.57	<0.05
Adult	**Mean difference ± SD**	**Limits of agreement**	***r***	***p****	**Mean difference ± SD**	**Limits of agreement**	***r***	***p****
LVAWd	-0.03 ± 0.07	-0.17 to 0.10	0.90	<0.01	0.03 ± 0.10	-0.18 to 0.23	0.70	<0.01
LVAWs	-0.02 ± 0.10	-0.22 to 0.17	0.84	<0.01	0.02 ± 0.10	-0.19 to 0.23	0.82	<0.01
LVIDd	0.05 ± 0.12	-0.18 to 0.28	0.87	<0.01	-0.02 ± 0.10	-0.22 to 0.18	0.91	<0.01
LVIDs	0.03 ± 0.14	-0.24 to 0.30	0.89	<0.01	0.01 ± 0.15	-0.29 to 0.30	0.91	<0.01
LVPWd	-0.03 ± 0.04	-0.12 to 0.05	0.94	<0.01	-0.05 ± 0.19	-0.42 to 0.32	0.47	ns
LVPWs	-0.01 ± 0.05	-0.12 to 0.10	0.96	<0.01	-0.10 ± 0.24	-0.57 to 0.38	0.49	ns
IVSd	-0.01 ± 0.04	-0.08 to 0.06	0.97	<0.01	-0.01 ± 0.09	-0.18 to 0.17	0.83	<0.01
IVSs	0.00 ± 0.06	-0.11 to 0.11	0.98	<0.01	0.01 ± 0.10	-0.18 to 0.21	0.93	<0.01

r = Pearson's coefficient. **p*-value for correlation coefficient. LVAW = Left ventricle anterior wall. LVID = Left ventricle internal diameter. LVPW = Left ventricle posterior wall. IVS = Interventricular septum. -d = In diastole. -s = In systole.

3.1.4.1 Body weight and heart rate

The BW was significantly lower in the juvenile than in the adult mice, as expected. Similar results were observed in other mice strains, as C57BL/6 and CD1 mice (Stypmann et al., 2006;Hinton et al., 2008; Tiemann et al., 2003). Nevertheless, BW of 3 weeks 129/Sv mice was lower than 3 weeks C57BL/6 mice (7.68g vs 10.2g) (Tiemann et al., 2003) and 8 weeks 129/Sv mice were lower than 8 weeks CD1 mice (19.84g vs 32.4g) (Stypmann et al., 2006), showing the influence of mouse backgrounds in body weight. In addition, HR was significantly lower in the younger animals, despite the similar isoflurane concentration used for both groups, which is inconsistent with some studies (Stypmann et al., 2006; Hinton et al., 2008; Rottman et al., 2007). One study shows that HR in C57BL6 mice is constant between 1 month and 2 months mice and decreases between 2 months and 16 months (Hinton et al., 2008), while other studies show that HR in C57BL6 conscious mice and CD1 mice decreases with age (Stypmann et al., 2006; Tiemann et al., 2003). We found one study in accordance with our result, where HR was higher in old vs young C57BL/6 mice (Tiemann et al., 2003). The higher HR observed in the adult mice might be explained possibly due to a higher thoracic compression in the adult animals during echocardiography, to allow a better access to the heart.

3.1.4.2 Cardiac dimensions parameters

We observed a significant difference in LV lengths and LV areas in 3 weeks mice vs 8 weeks mice, which could be explained by the significantly higher BW of adult mice, due to the continuous increase of the heart and body weight between these ages.

A higher value of EAC was observed in the adult mice, but we couldn't find any data to correlate with our result. While FAC, a parameter that represents LV systolic function does not differ between juvenile and adult. According to previous studies in C57BL6 mice, FAC does not differ between these ages, which correlate with our result. However the value found is lower than in our study, around 46% (Hinton et al., 2008). Together, these results reinforce the influence of mice background on cardiac parameters.

As expected, LVV and LVM were different between 3 weeks mice and 8 weeks mice, since the animals are still in growth. However, when LVM was normalized to BW (LVMi), we noticed that LVMi was higher in the juveniles due to the higher BW of the adult mice. These results are consistent with the literature found for other strains (Stypmann et al., 2006; Li et al., 2000).

We observed no significant difference in thickness of IVS and LVPW between juvenile and adult mice. A similar result was obtained in a previous study with other mice strain between 6 and 12 weeks old (Tiemann et al., 2003). LVAW thickness and LVID were significantly different in the two groups. The literature found for these parameters showed a tendency toward an increase of LVAW (Stypmann et al., 2006) and LVID (Hinton et al., 2008; Semeniuk et al., 2002) with age, although no statistical significance was reached.

Our data suggests that EF and FS, parameters of systolic function, does not differ between 3 weeks and 8 weeks mice, which match with previous results found for other mice strains (Stypmann et al., 2006; Hinton et al., 2008; Semeniuk et al., 2002). The values found for EF in other studies with anesthetized animals were around 53 – 55% for 129/Sv mice (Yang et al., 1999) and around 60 – 63% for CD1 mice (Stypmann et al., 2006). EF in conscious animals was around 65% for C57BL6 mice (Popović et al., 2005) and 84 % for 129/Sv mice (Yang et al., 1999). The values found for FS in other studies with anesthetized animals were around 37 – 40% for CD1 mice (Stypmann et al., 2006), around 33 – 35% for 129/Sv mice (Yang et al., 1999) and around 35% for C57BL6 mice (Hinton et al., 2008). In another study, a FS value of 45% was observed for 6-8 months C57BL6 mice (Gao et al., 2000). FS in conscious animals were around 51% for 129/Sv mice (Yang et al., 1999).

3.1.4.3 Outflow-related parameters

Concerning the aorta and pulmonary artery, their respective diameters, peak velocities and peak pressures were different between juvenile and adult mice. The higher arterial diameters in the adults, due to higher body surface in older animals, go along with the literature found (Hinton et al., 2008). AET was the only arterial-related parameter that did not show a significant difference between the two groups.

SV and CO, calculated by the aortic outflow method, were significantly higher in 8 weeks mice. On the other hand, COi was considered the same in the two groups due to BW normalization of CO resulted from higher BW in the adult mice compared to lower BW in the juvenile mice. Parameters that are constant when indexed to BW indicate that these values are related to body size. Our CO result is inconsistent with the data found for other strain (Stypmann et al., 2006), which shows no difference between different ages. This could be explained by the older ages tested in the referred study (between 8 and 52 weeks). The values found in other studies for CO were around 18 – 20 ml/min for 129/Sv mice (Yang et al., 1999) and 16 – 17 ml/min for CD1 mice (Stypmann et al., 2006).

3.1.4.4 Inflow-related parameters

We did not find any significant difference in MV and TV inflow parameters between the two groups, except for IVRT that was significantly lower in the 8 weeks mice. E wave and A wave are diastolic parameters that depend mainly on myocardial relaxation, LV geometry and loading conditions. Therefore during maturation of the LV, from juvenile to adult, these parameters evolve in parallel, keeping the resulting E and A wave constant. IVRT is dependent of LV relaxation, loading conditions and HR. Bearing in mind the constant values of A and E wave, IVRT changes could be dependent on intrinsic myocardial relaxation. A similar result was obtained for MVE, MVA, MVPPG, IVRT and MVE/A for other mice strains in previous studies (Stypmann et al., 2006; Hinton et al., 2008).

3.1.5 Limitations

One limitation of this study is the influence of anesthetic agent as depressor of cardiovascular function. However the use of anesthesia during echocardiography is crucial to facilitate data acquisition, by providing sedation and immobility of animals, avoiding the animal stress during the procedure. We used the isoflurane, since it's one of the most common inhalant anesthetics, and has many advantages when compared with other anesthetics. It produces minimal cardiac depression and has higher molecular stability (Brunson DB, 1997). Also, isoflurane was considered the most reproducible anesthetic in repeat studies at 12 days (Roth et al., 2002).

It would have been advantageous to consider more than two time points, in order to analyze data during the entire life span of these animals.

Also, it would be interesting to analyze, in the future, global and regional strain data for deformations reference values.

3.1.6 Conclusions

Since mice are a common model system for studying cardiac development and disease, cardiac characterization of normal/wild type and healthy animals is considered extremely important *for interpretation of results in transgenic and surgical animals.* And so, this study defines reference echocardiographic measurements and calculated parameters for juvenile (3 weeks) and adult (8 weeks) 129/Sv wild type mice.

The work presented here suggests a significant difference of almost all cardiac dimensions as well as outflow-related parameters (pulmonary and aorta flow) of 3 weeks vs 8 weeks 129/Sv

wild type mice. While inflow-related parameters (mitral and tricuspid flow) do not differ between weeks 3 and 8. In addition, when comparing with the literature, we can detect some differences in the parameters studied, suggesting the great influence of genetic background of each mice strain on the results obtained.

The reference values reported in this study could contribute as a basis to further comparative results between strains and to the future studies in cardiovascular postnatal development and diagnosing cardiovascular disorders using murine models in the 129Sv genetic background.

Table 2.10 Correlation analysis between BW or HR and all echocardiographic parameters measured in juvenile mice.

Juvenile Mice (3 Weeks)									
	BW		HR			BW		HR	
Parameter	Correlation Coefficient	*p*	Correlation Coefficient	*p*	Parameter	Correlation Coefficient	*p*	Correlation Coefficient	*p*
AoD	0.80*	< 0.001	0.26	ns	**IVSd**	0.20	ns	0.29	ns
PAD	0.32	ns	0.18	ns	**IVSs**	0.43	ns	0.28	ns
CO	0.80*	< 0.001	0.43	ns	**RVIDd (n=7)**	-0.09	ns	-0.52	ns
SV	0.63	< 0.05	0.11	ns	**RVIDs (n=7)**	0.07	ns	-0.46	ns
LVEndoLd	0.47	ns	0.02	ns	**RVAWd (n=7)**	0.43	ns	0.86	< 0.05
LVEndoLs	0.75	0.001	0.36	ns	**RVAWs (n=7)**	0.56	ns	0.20	ns
LVEpiLd	0.52	< 0.05	0.02	ns	**AoVPV**	0.39	ns	0.12	ns
LVEpiLs	0.80	< 0.001	0.32	ns	**AET**	-0.04	ns	-0.53	< 0.05
LVEndoAd	0.61	< 0.05	0.09	ns	**AoVPPG**	0.39	ns	0.12	ns
LVEndoAs	0.02	ns	0.02	ns	**DAoPV**	0.57	< 0.05	0.49	ns
LVEpiAd	0.52	< 0.05	0.45	ns	**PVPV**	0.63	< 0.05	0.40	ns
LVEpiAs	0.38	ns	0.43	ns	**PVPPG**	0.63	< 0.05	0.40	ns
EAC	0.56	< 0.05	0.21	ns	**MV E**	0.18	ns	0.21	ns
FAC	0.35	ns	0.00	ns	**MV A**	0.51	ns	0.13	ns
LVVd	0.64	0.01	0.07	ns	**MVPPG**	0.06	ns	0.18	ns
LVVs	0.24	ns	0.11	ns	**IVCT**	-0.23	ns	-0.20	ns
LVM	0.53	< 0.05	0.44	ns	**IVRT**	-0.23	ns	-0.18	ns
LVAWd	0.21	ns	0.01	ns	**MV ET**	-0.11	ns	-0.57	< 0.05
LVAWs	0.16	ns	0.04	ns	**NFT**	-0.30	ns	-0.66	< 0.01
LVIDd	0.65	< 0.01	0.32	ns	**MV E/A**	-0.13	ns	-0.13	ns
LVIDs	0.18	ns	-0.03	ns	**LV MPI**	-0.07	ns	0.14	ns
LVPWd	0.48	ns	-0.27	ns	**TV E (n=12)**	-0.57	ns	0.01	ns
LVPWs	0.71	< 0.01	0.11	ns	**TV A (n=12)**	-0.75	< 0.01	0.12	ns
EF	0.34	ns	0.33	ns	**TVPPG (n=12)**	-0.51	ns	0.13	ns
FS	0.34	ns	0.33	ns	**TV E/A(n=12)**	0.13	ns	-0.20	ns

Table showing correlation analysis between BW or HR and all echocardiographic parameters measured in juvenile mice. For all parameters correlation coefficient are from Spearman's correlation, except *. *Pearson's correlation coefficient. *p* = statistical significance. ns = not significant. n=15 for all measurements, except for RV measurements (n=7 for the juvenile mice) and for TV measurements (n=12 for the juvenile mice).
BW = Body weight. HR = Heart rate. AoD = Ascending aorta diameter. PAD = Pulmonary artery diameter. CO = Cardiac output. SV = Stroke volume. LVEndoL = Left ventricle endocardial length. LVEpiL = Left ventricle epicardial length. LVEndoA = Left ventricle endocardial area. LVEpiA = Left ventricle epicardial area. EAC = Endocardial area change. FAC = Fractional area change. LVV = Left ventricle volume. LVM = Left ventricle mass. LVAW = Left ventricle anterior wall. LVID = Left ventricle internal diameter. LVPW = Left ventricle posterior wall. EF = Ejection fraction. FS = Fractional shortening. IVS = Interventricular septum. RVID = Right ventricle internal diameter. RVAW = Right ventricle anterior wall. AoVPV = Ascending aorta valve peak velocity. AET = Aortic ejection time. AoVPPG = Ascending aorta valve peak pressure gradient. DAoPV = Descending aorta peak velocity. PVPV = Pulmonary valve peak velocity. PVPPG = Pulmonary valve peak pressure gradient. MVE = Mitral valve early wave peak. MVA = Mitral valve atrial wave peak. MVPPG = Mitral valve peak pressure gradient. IVCT = Isovolumic contraction time. IVRT = Isovolumic relaxation time. MVET = Mitral valve ejection time. NFT = Non-filling time. LVMPI = Left ventricle myocardial performance index. TVE = Tricuspid valve early wave peak. TVA = Tricuspid valve atrial wave peak. TVPPG = Tricuspid valve peak pressure gradient. -d = In diastole. -s = In systole.

Table 2.11 Correlation analysis between BW or HR and all echocardiographic parameters measured in adult mice.

Adult Mice (8 Weeks)									
	BW		HR			BW		HR	
Parameter	Correlation Coefficient	*p*	Correlation Coefficient	*p*	Parameter	Correlation Coefficient	*p*	Correlation Coefficient	*p*
AoD	0.75*	0.001	0.23	ns	**IVSd**	-0.30	ns	-0.14	ns
PAD	0.30	ns	0.35	ns	**IVSs**	-0.07	ns	0.03	ns
CO	0.67	< 0.01	0.22	ns	**RVIDd (n=11)**	0.56	ns	0.48	ns
SV	0.73	< 0.01	0.05	ns	**RVIDs (n=11)**	0.31	ns	-0.09	ns
LVEndoLd	0.81	0	-0.01	ns	**RVAWd (n=11)**	0.21	ns	-0.40	ns
LVEndoLs	0.71*	< 0.01	-0.14	ns	**RVAWs (n=11)**	0.39	ns	-0.06	ns
LVEpiLd	0.79	0.001	0.01	ns	**AoVPV**	0.58	< 0.05	-0.02	ns
LVEpiLs	0.72*	< 0.01	-0.09	ns	**AET**	-0.05	ns	-0.75	0.001
LVEndoAd	0.33	ns	0.38	ns	**AoVPPG**	0.58	< 0.05	-0.02	ns
LVEndoAs	0.15	ns	0.02	ns	**DAoPV**	-0.09	ns	0.24	ns
LVEpiAd	0.51	ns	0.27	ns	**PVPV**	-0.07	ns	0.38	ns
LVEpiAs	0.24	ns	0.07	ns	**PVPPG**	-0.07	ns	0.38	ns
EAC	0.30	ns	0.42	ns	**MV E**	-0.29	ns	0.04	ns
FAC	0.07	ns	0.24	ns	**MV A**	-0.11	ns	0.52	< 0.05
LVVd	0.40	ns	0.34	ns	**MVPPG**	-0.37	ns	0.05	ns
LVVs	0.24	ns	0.03	ns	**IVCT**	0.34	ns	-0.37	ns
LVM	0.71*	< 0.01	0.10	ns	**IVRT**	0.40	ns	-0.31	ns
LVAWd	0.20	ns	0.16	ns	**MV ET**	0.10	ns	-0.53	< 0.05
LVAWs	0.23	ns	0.16	ns	**NFT**	0.20	ns	-0.64	0.01
LVIDd	0.23	ns	0.24	ns	**MV E/A**	-0.17	ns	-0.22	ns
LVIDs	0.01	ns	-0.08	ns	**LV MPI**	0.64	0.01	-0.10	ns
LVPWd	0.49	ns	-0.16	ns	**TV E (n=6)**	-0.43	ns	-0.03	ns
LVPWs	0.19	ns	0.12	ns	**TV A (n=6)**	-0.14	ns	0.09	ns
EF	0.11	ns	0.28	ns	**TVPPG (n=6)**	-0.14	ns	0.09	ns
FS	0.11	ns	0.28	ns	**TV E/A (n=6)**	-0.82*	< 0.05	0.75	ns

Table showing correlation analysis between BW or HR and all echocardiographic parameters measured in adult mice.. For all parameters correlation coefficient are from Spearman's correlation, except *. *Pearson's correlation coefficient. *p* = statistical significance. ns = not significant. n=15 for all measurements, except for RV measurements (n=11 for the adult mice) and for TV measurements (n=6 for the adult mice).

BW = Body weight. HR = Heart rate. AoD = Ascending aorta diameter. PAD = Pulmonary artery diameter. CO = Cardiac output. SV = Stroke volume. LVEndoL = Left ventricle endocardial length. LVEpiL = Left ventricle epicardial length. LVEndoA = Left ventricle endocardial area. LVEpiA = Left ventricle epicardial area. EAC = Endocardial area change. FAC = Fractional area change. LVV = Left ventricle volume. LVM = Left ventricle mass. LVAW = Left ventricle anterior wall. LVID = Left ventricle internal diameter. LVPW = Left ventricle posterior wall. EF = Ejection fraction. FS = Fractional shortening. IVS = Interventricular septum. RVID = Right ventricle internal diameter. RVAW = Right ventricle anterior wall. AoVPV = Ascending aorta valve peak velocity. AET = Aortic ejection time. AoVPPG = Ascending aorta valve peak pressure gradient. DAoPV = Descending aorta peak velocity. PVPV = Pulmonary valve peak velocity. PVPPG = Pulmonary valve peak pressure gradient. MVE = Mitral valve early wave peak. MVA = Mitral valve atrial wave peak. MVPPG = Mitral valve peak pressure gradient. IVCT = Isovolumic contraction time. IVRT = Isovolumic relaxation time. MVET = Mitral valve ejection time. NFT = Non-filling time. LVMPI = Left ventricle myocardial performance index. TVE = Tricuspid valve early wave peak. TVA = Tricuspid valve atrial wave peak. TVPPG = Tricuspid valve peak pressure gradient. -d = In diastole. -s = In systole.

Results

3.2 Part II

Targeted inactivation of Cerl2 leads to cardiac hyperplasia and systolic dysfunction in the mouse

Ana Carolina Araújo[1,2,3] and José António Belo[1,2,*]

[1] Embryology and Genetic Manipulation Laboratory, Regenerative Medicine Program, Department of Biomedical Sciences and Medicine, Universidade do Algarve, Portugal.

[2] Institute for Biotechnology and Bioengineering - LA, Centro de Biomedicina Molecular e Estrutural, Universidade do Algarve, Portugal.

[3] PhD Program in Biomedical Sciences, Universidade do Algarve, Portugal

(manuscript submitted)

Authors' contribution

ACA performed almost all experiments, analyzed and interpreted the data and wrote the manuscript. JAB designed the study and wrote the manuscript.

3.2.1 Abstract

Background: Previous analysis of the *Cerberus like 2* knockout (*Cerl2*$^{-/-}$) mouse revealed a significant mortality during the first day after birth, mostly due to cardiac defects apparently associated with randomization of the left-right axis. We therefore analyzed the cellular and molecular mechanisms underlying the cardiac phenotypes found in *Cerl2*$^{-/-}$ without a laterality phenotype, in order to access the endogenous role of *Cerl2* in cardiogenesis.

Methods and Results: We have however identified *Cerl2*-associated cardiac defects, notably a large increase in the left ventricular myocardial walls in neonates that cannot be explained by laterality abnormalities. Moreover, embryonic and fetal *Cerl2*$^{-/-}$ hearts show a progressive increase of the left ventricular thickness. The compound mouse line *Cer2*$^{-/-}$*::Mlc1v-nLacZ24,* in which the right ventricle is genetically marked, displayed a massive enlargement of the left ventricle myocardium in animals absent of laterality defects. In addition, echocardiography analysis reveals an impaired cardiac function in *Cerl2*$^{-/-}$ neonates due to left ventricular systolic dysfunction. We found in *null* mutants a high cardiomyocyte mitotic index in compact myocardium and increased *cyclin D1* expression in the left ventricle at embryonic day (E) 13, which correlate with specific ventricular expression of *Cerl2*. In addition, we observed an increase of Smad2 phosphorylated (pSmad2) levels at E13 and neonatal hearts indicating a prolonged TGFßs/Nodal/Activin/Smad2 signaling activation. Analysis by qRT-PCR, revealed an impaired expression of cardiac genes in *Cerl2*$^{-/-}$ hearts.

Conclusion: Taken together we can conclude that the increase of the LV myocardial walls in *Cerl2*$^{-/-}$ is due to cardiomyocyte hyperplasia and these features are independent of LD. According to recent data, we also suggest that Cerl2 may relate with Wnt signaling leading to directional left ventricular cardiomyocyte hyperplasia in *Cerl2* null mutants.

Keywords: Cerl2, cardiogenesis, hyplerplasia; systolic disfunction

3.2.2 Introduction

The heart is the first organ to be formed to allow the efficient supply of the increasing nutritional requirements of the growing embryo (Buckingham et al., 2005). A series of processes orchestrated by a complex genetic network and interplay of the diverse cardiac cell lineages is essential for a successful cardiogenesis (Garry and Olson, 2006). Subtle perturbations during heart formation usually lead to congenital heart defects (CHD) (Nemer, 2008) which are the most common congenital malformations worldwide (Garne et al., 2012).

In mice, the heart starts to be formed at gastrulation with the formation of the cardiac crescent at the anterior side of the embryo (DeRuiter et al., 1992), which contribute to the heart primordium or first heart field (FHF) (Pérez-Pomares et al., 2009). Cells from FHF will mainly give rise to the left ventricle (LV) (Buckingham et al., 2005). Later, another region can be identified, the secondary heart field (SHF) that will contribute to the right ventricle (RV) and outflow tract (OFT) (Kelly and Buckingham, 2002). The heart primordium region fuses at the embryonic midline to form a primitive heart tube (Abu-issa and Kirby, 2007). In this primitive tubular phase, heart loops to the right side of the embryo under the control of the signals that regulate left–right axis (L/R) (Brand, 2003). Two myocardial layers compose the primitive heart, the trabecular and compact layers. The trabeculae is a bundle of cardiomyocytes outlined by endocardial cells that project across the lumen of the ventricular chamber (Ben-Shachar et al., 1985), and the compact layer is an organized multilayer that comprises the outmost ventricular region (Ieda et al., 2010). The cardiomyocytes that compose the compact layer have higher proliferative and low differentiation capacities and the reverse is found in trabeculae (Rumiantsev and Bruce, 1991). Recent emerging data revealed that the activation of Wnt canonical/ß-catenin signaling controls the regional increased proliferation in the compact myocardium (Buikema et al., 2013) contributing to the discrepancy in proliferation rates between the both myocardial layers. As development proceeds, the heart expands towards a four-chambered organ and the atrio-ventricular septation is established simultaneously with the correct alignment between arteries and their respective ventricles. This allows the development of the conducting and circulatory systems (Christoffels et al., 2004). At the cellular level, the cardiomyocytes proliferate regulated by cyclins and cyclin-dependent kinase (CDKs) (Li and Brooks, 1999; Walsh et al., 2010) reaching two distinct high rates of DNA synthesis. The first occurs around midgestation (E12.5) and is associated with increased cardiomyocyte proliferation (Li et al., 1996). Later, in the first days after birth (P3-P4), a second peak of DNA synthesis is observed which ultimately results in binucleated cardiomyocytes (Ikenishi et al., 2012). Nonetheless, recent

studies point to continued DNA synthesis and therefore to neomyocardialization potential in adult hearts (Porrello et al., 2011; Mollova et al., 2012). On the other hand, the patterning of differentiated cardiomyocytes occurs in the early heart morphogenesis and persists until the first weeks of birth (Francou et al., 2013).

Thus the balance between proliferation and differentiation during the heart formation is therefore crucial to provide the progressive thickening of the cardiac myoarchitecture (Sedmera et al., 2000).

Cerberus like 2 (*Cerl2*) is a member of the Cer/Dan family, and has been show to antagonize signals from the Transforming Growth Factor (TGF) type β superfamily (Marques et al., 2004). The secreted protein Cerl2 binds to Nodal and contributes to asymmetric initiation of the left/right (L/R) patterning (Marques et al., 2004; Inácio et al., 2013). Accordingly, *Cerl2* knockout (*Cerl2*$^{-/-}$) mice display L/R axis randomized and a significant mortality rate within a few hours after birth, mostly due to cardiac defects (Marques et al., 2004). It has been reported that animals with laterality defects (LD) frequently have impaired cardiac function correlated with cardiac malformations (Kathiriya and Srivastava, 2000).

The main goal of this study is to investigate the consequences of *Cerl2* loss-of-function in heart development, independent of the influence of LD on cardiac performance. We therefore analyzed exclusively animals that did not show LD. In addition, emerging data have elucidated the role of *Cerl-1*, another member of Cer/Dan family, for cardiogenesis initiation, as reported in Xenopus (Foley et al., 2007), chicken (Bento et al., 2011) and in mouse embryonic stem cells (Cai et al., 2013). Whether *Cerl2* has a specific role in cardiogenesis independent of its known role during establishment of L/R asymmetry will be investigated.

Here, we demonstrate that enlargement of the LV myocardial walls and interventricular septum (IVS) in *Cerl2* null mutants without LD is caused by left ventricular cardiomyocyte hyperplasia. Moreover, the increased relative expression of *cyclin D1* in midgestation is related with specific expression of *Cerl2* in the LV. We also observed an increase of phosphorylated Smad2 (pSmad2) in *Cerl2*$^{-/-}$ embryonic and neonatal hearts, suggesting that the TGFßs/Nodal/Activin/Smad2 signaling cascade is sustained in the absence of *Cerl2*. Moreover, these animals showed impaired expression of cardiac genes, which is incompatible with normal cardiac function. Our study provides the first detailed description of the cardiac phenotype in *Cerl2*$^{-/-}$ mice without LD. We postulate a role for Cerl2 in cardiac development independent of its role during establishment of L/R asymmetry.

3.2.3 Results

3.2.3.1 *Cerl2*$^{-/-}$ neonates display left ventricular hypertrophy with increased left ventricular mass and severe cardiac dysfunction

It has been extensively reported that laterality defects are characterized by failure in the L/R axis establishment followed by randomized positioning of the asymmetrical visceral organs (Kathiriya and Srivastava, 2000). We therefore observed the relative positions of the heart and arteries, lung lobulation, liver and stomach.

In contrast to the wild-type (WT) controls, a third of *Cerl2*$^{-/-}$ neonates die immediately after birth and a few more until the time of weaning (data not shown). From the 52 living animals analyzed, 38 (73%) did not display LD. We started our analysis by performing a histological examination of *Cerl2*$^{-/-}$ neonatal hearts without LD, and complemented it with a histomorphometric analysis of the anterior (AW), lateral (LW) and posterior wall (PW) of the LV and RV. The IVS was also measured.

Histological analysis showed an enlarged LV myocardium and IVS in the *Cerl2*$^{-/-}$ neonates (Figure 3.5 A and B). Additionally, at higher magnifications we observed an increased cardiomyocyte number thought the number of nuclei by section (Figure 3.5 A' and B'). Histomorphometric evaluation showed a massive thickening of the walls that constitute the LV myocardium and the IVS (Figure 3.5 C). However, no significant differences were found in the RV of *null* mutants as compared to WT controls.

In order to validate that the increased LV and IVS myocardial walls found in *Cerl2*$^{-/-}$ neonates without LD is not related with the laterality phenotype, we crossed our *null* mice with the *Mlc1v-nlacZ-24* transgenic mouse line. This transgenic line contains enhancer-trap *nlacZ* transgene upstream of the *Fgf10* and therefore expresses ß-galactosidase activity in the RV/pulmonary ventricle and OFT (Kelly et al., 2001). We examined the organ placement, performing echocardiography analysis and ß-galactosidase staining in neonatal hearts to verify the position of the RV/pulmonary ventricle and OFT in these animals (data not shown). In Figure 3.5 D, the RV is marked. Thus we analyzed only the animals without LD, which were about half of the living neonates analyzed (6/11). From histomorphometry (Figure 3.5 E), our results confirm that in the *Cerl2* mutants the LV and IVS myocardium is hypertrophic, in the absence of LD.

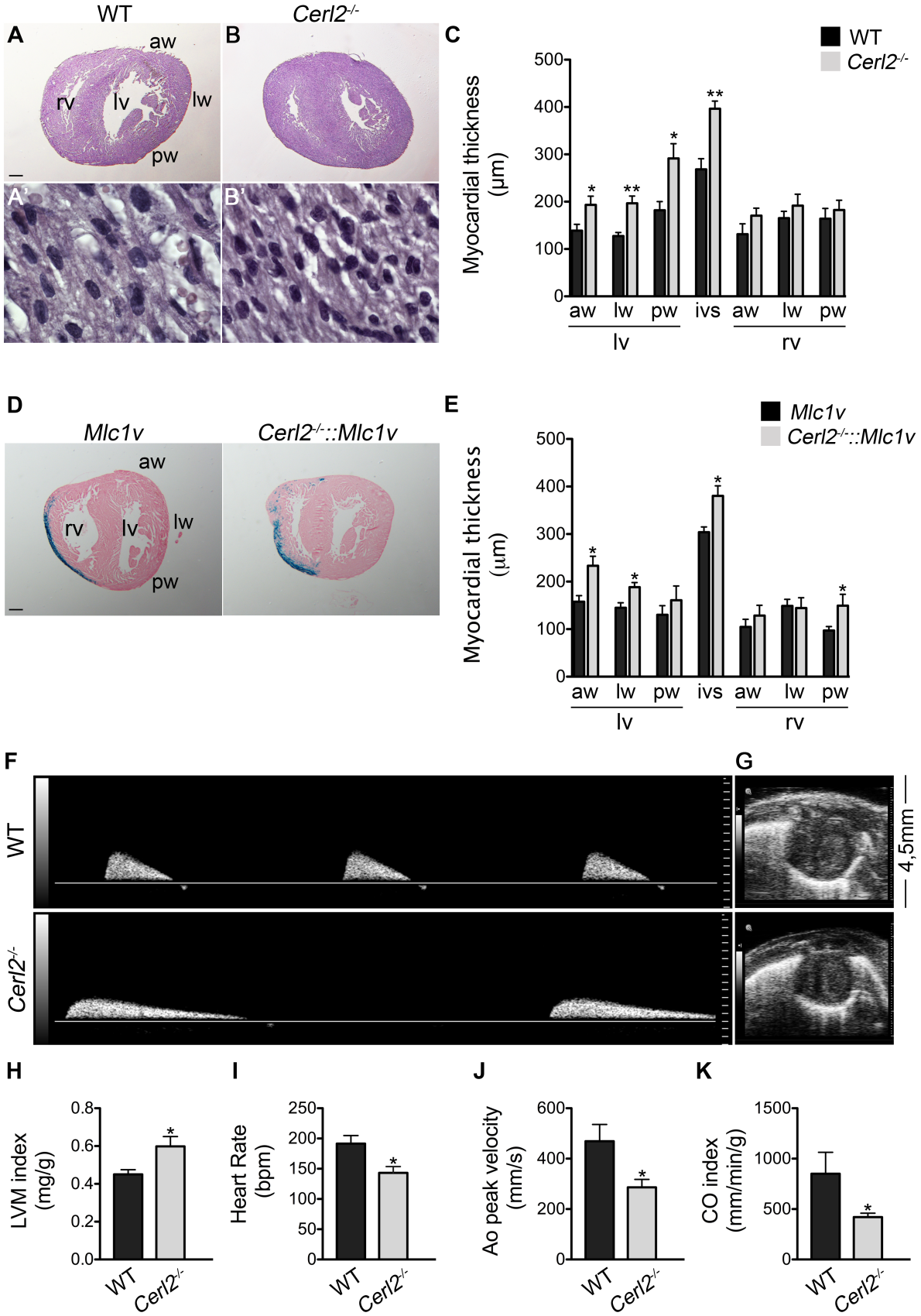

Figure 2.5 Increased compact myocardium and systolic dysfunction in *Cerl2*$^{-/-}$ neonates is independent of the LD phenotype.

(A, B and D) Transverse sections (5μm) of hearts stained with H&E (A and B) and LacZ staining counter stained with Eosin (D). (A' and B') Note the numbers of cardiomyocytes per field (100X). (C and E) Quantitative measures of myocardial thickness in the compact layer indicate increased LV and IVS thickness (n=5 and n=4, respectively). (F–K) Echocardiographic analysis (n= 5 or 6 for WT and n=7 for *Cerl2*$^{-/-}$). (F) Represents the Ao peak velocity by Colour Doppler. (G) Represents the PSAX in B-mode view. (H) LVM index (mg/g) is increased in *null* mutants; (I) Heart Rate (bpm, beats per minute), (J) Ao peak velocity (mm/s) and (K) CO index (ml/min/g) are reduced in *Cerl2*$^{-/-}$ neonates. Ao, aorta artery; aw, anterior wall; CO, cardiac output; ivs, interventricular septum; lw, lateral wall; lv, left ventricle; LVM, left ventricular mass; pw, posterior wall and rv, right ventricle. Scale bars: 200μm.* P<0.05 and ** P<0.01.

In order to complement the hypertrophic phenotype, we evaluated the left ventricular mass (LVM) and the cardiac function through non-invasive transthoracic echocardiography in neonatal mice (Figure. 3.5 F-K). According to our analysis the LVM index, a useful parameter to detect hypertrophy, is increased in *Cerl2*$^{-/-}$ neonatal hearts (Figure 3.5 H). Additionally, the wet heart weight/body weight ratio, also indicative of hypertrophy has been found to be imprecise in smaller mice (Ghanem et al., 2006). Therefore, we did not find significant differences when compared with WT (Table 3.8). We determined the heart rate (HR) using the time interval between four-five successive waveforms on Color Doppler mode tracings of the aorta artery (Ao) peak velocity. According to our data, *Cerl2*$^{-/-}$ neonatal mice have a decreased HR (Figure 3.5 I). Furthermore, the LV function was also affected as suggested by the decreased ascending aorta artery peak velocity in *Cerl2* null mutants (Figure 3.5 F,J). In addition, the pulmonary systolic performance was also analyzed by the pulmonary artery (PA) peak velocity (Zheng-Fischhöfer et al., 2006), and no significant differences were found in *Cerl2*$^{-/-}$ neonates (Table 3.8). The cardiac output (CO) index, a parameter which indicates the systolic function was calculated to the LV (Stypmann et al., 2009) and a reduced COi was found in *Cerl2* mutants (Figure 3.5 K). Taken together, these data indicates that the LV hypertrophy observed in *Cerl2*$^{-/-}$ without LD leads to abnormal cardiac physiology due to impaired systolic function.

Table 2.12 Echocardiographic parameters in *Cerl2*$^{-/-}$ neonates.

Parameters	WT	*Cerl2*$^{-/-}$	*P*
Vent./Body	5.27 ± 0.19	4.98 ± 0.3	ns
Pa (mm/s)	301.1 ± 48.2	332 ± 60.89	ns
Ao diameter (mm)	0.59 ± 0.04	0.52 ± 0.02	ns
LVSV (µL)	9.93 ± 2.8	3.96 ± 0.53	0.033*

Vent., ventricles; Vent/Body represents the ratio ventricles (without atria) and body; Pa, Pulmonary artery peak velocity; Ao, Aortic internal diameter was obtained at end-systole; LVSV, Left Ventricular Stroke Volume. Statistically significant result was considered when *P>0.05. ns, means no statistical significant results. Data are means ± standard error of the mean (SEM).

3.2.3.2 LV myocardial wall increases progressively during heart development in *Cerl2*$^{-/-}$ mice

In order to understand if the massive increase of the LV walls and IVS found in neonatal hearts originates during prenatal stages through of the known compaction process, which is characterized by compaction of the trabecular myocardium towards the compact layer leading to increased of thickness of the heart at E13-E14 (Sedmera et al., 2000), we analyzed both myocardial layers in embryonic and fetal hearts.

Histomorphometric analysis revealed that at E13-13.25, the trabecular layer of the LV is larger in *Cerl2*$^{-/-}$ (Figure 3.6 A-A'',B-B'',C). In contrast, no differences in compact and trabecular layer were found in the RV in *Cerl2* mutant (Figure 3.6 A-A',B-B',C).

At E15-15.25, *Cerl2*$^{-/-}$ hearts showed a thicker compact layer in the LV (Figure 3.6 D-D', E-E' and F). However, we did not find any difference on trabecular length. The compact layer in the RV of *Cerl2*$^{-/-}$ did not differ of WT thickness. In contrast, *Cerl2*$^{-/-}$ showed seemingly a significantly higher right ventricular trabeculation (Figure 3.6 F). This shift from thickened LV trabecular layer at E13 in *Cerl2*$^{-/-}$ to thickened compact layer at E15 may be likely related with the compaction process. Moreover, we did not measure the IVS at E13 and E15 since the septation is still incomplete at these stages. Nonetheless, we observed that the IVS in *Cerl2*$^{-/-}$ hearts seems to be already enlarged at E13 (Figure 3.6 A,B).

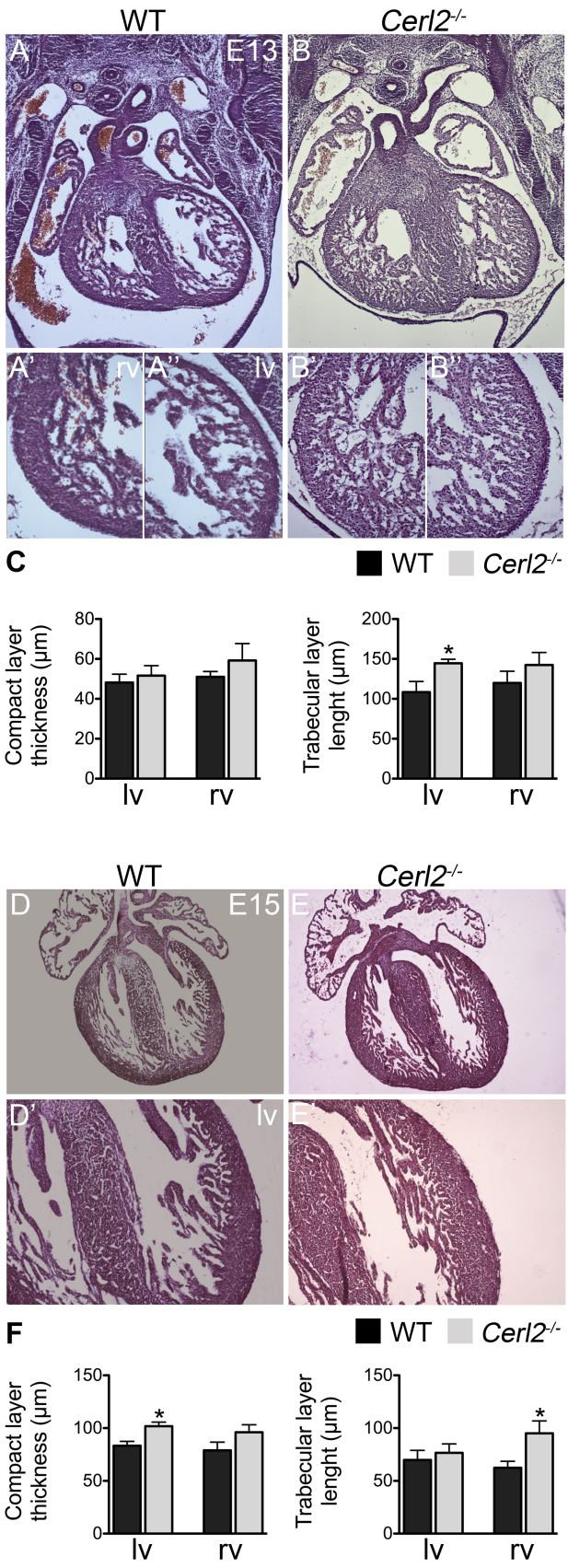

Figure 2.6 Progressive increase of compact myocardium in *Cerl2*$^{-/-}$ embryos.

(A-B and D-E) Transverse sections (10μm) stained with H&E at E13 and E15 respectively (5X). (C and F) Quantitative measures of myocardial thickness in the compact and trabecular layers (E13, n=4 and E15, n=5). Note the progressive increase of the compact myocardium after the compaction process. lv, left ventricle and rv, right ventricle. A'-A'' and B'-B''; 20X, and D'and E', 10X. * $P<0.05$.

3.2.3.3 Mitotic cardiomyocytes are increased in LV myocardium of *Cerl2*$^{-/-}$ embryonic and neonatal hearts

In order to investigate the cellular mechanism underlying the cardiac hypertrophy, we evaluated the number of mitotic cardiomyocytes in *Cerl2*$^{-/-}$ embryos (E13-13.25), fetuses (E15-15.25) and neonates (P0). To that end, we immuno-labeled cardiomyocytes with heavy chain cardiac myosin (MF-20) or α-actinin sarcomeric antibodies and co-labeled with the mitotic marker of phospho-Histone 3 (pH3) antibody. This allowed us to calculate the mitotic index as the ratio between proliferating cardiomyocytes and the total number of cardiomyocytes.

At E12.5, when the first peak of DNA synthesis in cardiomyocytes is normally observed (Soonpaa et al., 1996), the *Cerl2*$^{-/-}$ embryos revealed at E13-13.25 an increase of mitotic index in the LV of the compact myocardium (Figure 3.7 A-C). In contrast, no difference was observed in the compact RV myocardium. At E15-15.25, no statistically significant difference was found in the compact myocardium for any of the ventricles despite the tendency to maintain an increase in the mitotic index in *Cerl2* null mutants (Figure 3.7 D). Before the second peak of DNA synthesis that will lead to the formation of binucleated cardiomyocytes (P3-P4), we analyzed the ventricles at the early neonatal period (P0), sub-dividing them into AW, LW and PW to define the pattern of proliferation in each myocardial wall. The results showed a significantly higher proliferation index in all LV walls of *Cerl2*$^{-/-}$ (Figure 3.7 E). Unexpectedly, we found a variability of the mitotic index in the IVS. Regarding the RV of *Cerl2*$^{-/-}$, the AW and LW presented a significant increase in the proliferation. In addition, we performed immunohistochemistry with anti-cleaved Caspase-3 to compare the levels of apoptosis in *Cerl2*$^{-/-}$ neonatal hearts with WT. The results indicate that the general increase of the mitotic index observed in compact layer of the *Cerl2*$^{-/-}$ are not be related with alterations in levels of cellular death (data not shown).

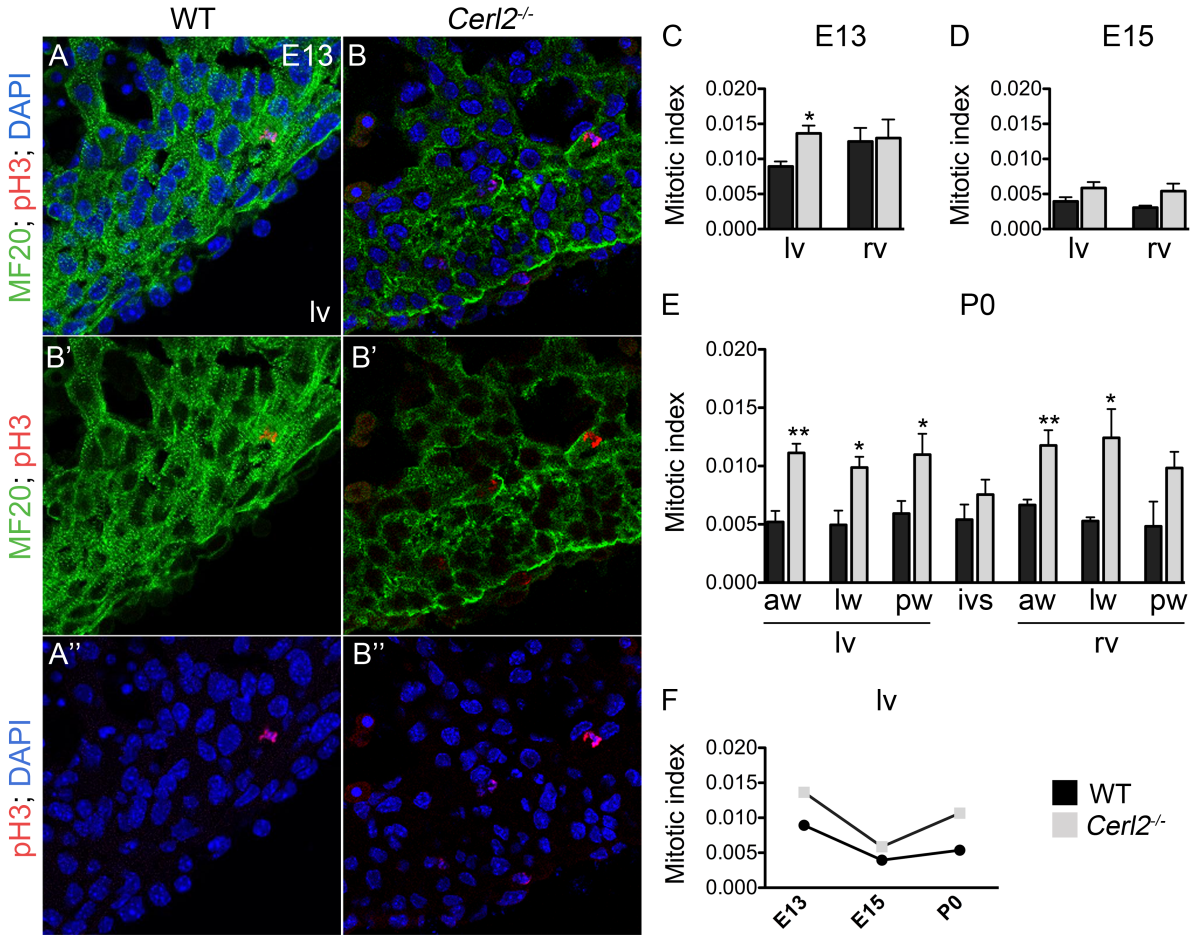

Figure 2.7 Increased left ventricular mitotic index in *Cerl2*$^{-/-}$.
(A and B) Corresponds to merged images at E13 of MF20 (green), pH3 (red) and DAPI (blue). (A' and B') MF20 and pH3; (A'' and B'') pH3 and DAPI (63X). (C-F) Proliferating cardiomyocyte observed in different stages of the heart development. (C) E13-13.25, n=4; (D) E15-E15.25, n=5; (E) P0 hearts, n=5. (F) The timeline of mitotic cardiomyocytes in the LV. aw, anterior wall; ivs, interventricular septum; lw, lateral wall; lv, left ventricle; pw, posterior wall and rv, right ventricle. * P<0.05 and ** P<0.01.

Cell growth can be caused by hyperplasia (increase in cell number) or hypertrophy (increase in cell size). Therefore, besides the hyperplasic cardiac phenotype found in *Cerl2*$^{-/-}$ neonates, we investigated whether hypertrophy is also involved in thickened LV walls and IVS as well. For that we evaluated the relative cardiomyocyte area of the AW and PW of the LV and of the IVS through co-immunostaining using MF20 and laminin as markers of cardiomyocyte and cardiomyocyte borders, respectively (Figure 3.8 B,C) Our analysis revealed no differences between the genoypes, suggesting that *Cerl2*$^{-/-}$ neonatal hearts do not display hypertrophy at the cellular level. Fibrosis is a classical feature of hypertrophy and cell death

(Manabe et al., 2002). Trichrome staining showed no evidence of fibrosis in *Cerl2*$^{-/-}$ neonatal hearts (Figure 3.8 A). Taken together we conclude that the increased LV thickness displayed by the *Cerl2*$^{-/-}$ is caused only by cardiomyocyte hyperplasia (Figure 3.7 F).

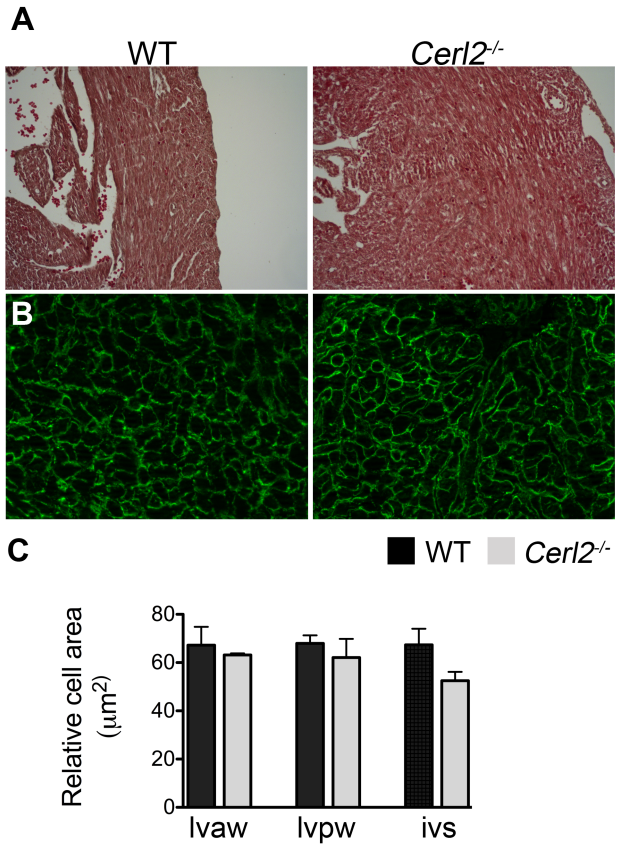

Figure 2.8 No evidence of fibrosis neither increased relative cardiomyocyte size in *Cerl2*$^{-/-}$ neonates. (A) Trichrome staining did not reveal fibrosis in *Cerl2* mutants (20X). (B) Represents the lvaw labeling with anti-laminin (*green*), 63X. (C) Relative cardiomyocyte area measured in 100 cells (μm^2), n=3. lvaw, left ventricle anterior wall, lvpw, left ventricle posterior wall and ivs, interventricular septum. Statistically significant result was considered when **P*>0.05. Data are means ± standard error of the mean (SEM).

3.2.3.4 The regional expression of *Cerl2* and Cyclin type D1 in the LV at E13 embryonic hearts

Previous work have shown the expression of *Cerl2* at the mouse node and its function in the initiation of the asymmetry breaking (Marques et al., 2004; Inácio et al., 2013). To evaluate if *Cerl2* is expressed during cardiac formation, we performed real time quantitative RT-PCR (qRT-PCR) analysis from isolated embryonic, fetal and neonatal mouse hearts. We used embryos at node stage (E8.25 - 8.5) and *Cerl2*$^{-/-}$ hearts as positive and negative controls,

respectively. Relative *Cerl2* mRNA expression was found in hearts at E10.5 and E13 even if seemingly lower than the expression in node stage embryos (Figure 3.9 A). In addition, we could not detect *Cerl2* expression beyond the midgestation, suggesting that *Cerl2* might be important during early cardiogenesis. We isolated part of the LV and RV at E13 in order to evaluate the *Cerl2* expression in each ventricle and we have found more expression in the LV than in the RV. Furthermore, in order to investigate the master regulators of cell cycle machinery, we also quantified the relative mRNA expression of the type D cyclin (D1 and D2) in isolated ventricles. From those, only the cyclin D1 was increased mainly in the LV of the *null* mutant (Figure 3.9 B). Therefore, we conclude that the LV phenotype showed by *Cerl2*$^{-/-}$ may be due to the localized absence expression of *Cerl2* in the LV. Accordingly, the LV hyperplasia confirmed by the increased of mitotic index evidenced in *Cerl2*$^{-/-}$ may be due to the overexpression of cyclin D1 in embryonic LV mutant hearts. As expected, we did not detect *Cerl2* expression in the *Cerl2*$^{-/-}$ hearts (data not shown).

3.2.3.5 Absence of *Cerl2* leads to increase of Smad2 phosphorylated signaling in embryonic and neonatal hearts

Since Cerl2 is a TGFßs/Nodal/Activin antagonist, we postulated that the absence of *Cerl2* might cause alteration in levels of TGFßs/Nodal/Activin signaling. Binding of TGFßs/Nodal/Activin to the receptors leads to the activation trough phosphorylation of downstream effector Smad2 (Feng and Derynck, 2005). To understand if TGFßs/Nodal/Activin signaling is altered in *Cerl2* null mutants, we evaluated the phosphorylation status of Smad2 (pSmad2) in protein extracts from embryonic (E13) and neonatal (P0) hearts. Quantification of pSmad2 by Western blot revealed increased phosphorylation of Smad2 embryonic E13 hearts (Figure. 3.10 A, top; B, left) suggesting an increase of TGFßs/Nodal/Activin signaling.

Surprisingly, we also observed increased phosphorylation of Smad2 in neonatal *Cerl2*$^{-/-}$ hearts (Figure 3.10 A, bottom; B, right), indicating that in the absence of *Cerl2* the TGFßs/Nodal/Activin /Smad2 signaling activity may persist until late heart development.

3.2.3.6 Expression of cardiac genes is affected in *Cerl2*$^{-/-}$ mice

To evaluate whether the absence of *Cerl2* affects the cardiac development at the molecular level, we performed qRT-PCR analysis of transcripts isolated from hearts at E13-E13.25,

E15-E15.25 and P0. We analyzed the expression of transcription factors that are important for normal heart development such as *Gata-4* and *Nkx2.5* (Durocher et al., 1997).

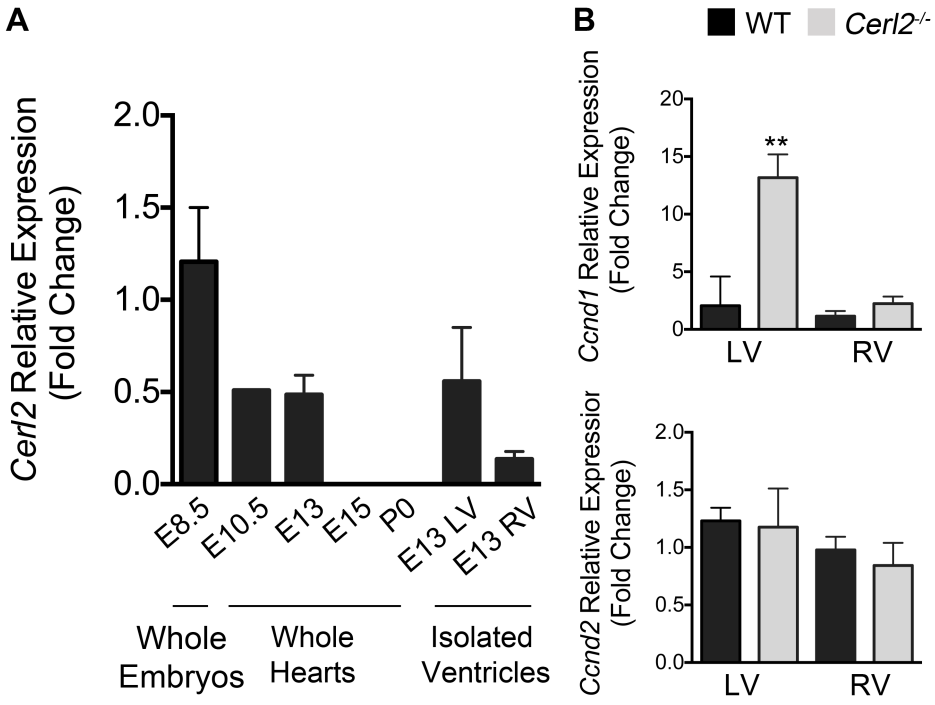

Figure 2.9 Regionalized left ventricular expression of *Cerl2* in WT and increased *Ccnd1* expression in *Cerl2*$^{-/-}$ at embryonic hearts.
(A) The relative expression of *Cerl2* in WT embryos by qRT-PCR. At E8.25-8.5, pull of two litters (whole embryos, n=6 each); E10.5, pull of one litter (isolated hearts n=6); E13, E15 and P0 isolated hearts (n=5); E13 isolated ventricles (n=3). The chart reveal expression of *Cerl2* until the midgestation and specifically more in the LV. (B) *Ccnd1* and *Ccnd2* relative expression in isolated ventricles at E13. qRT-PCR was performed in triplicate. lv and rv indicates left and right ventricles, respectively. Only the relative expression of *Ccnd1* in increased in the LV. ** $P<0.01$.

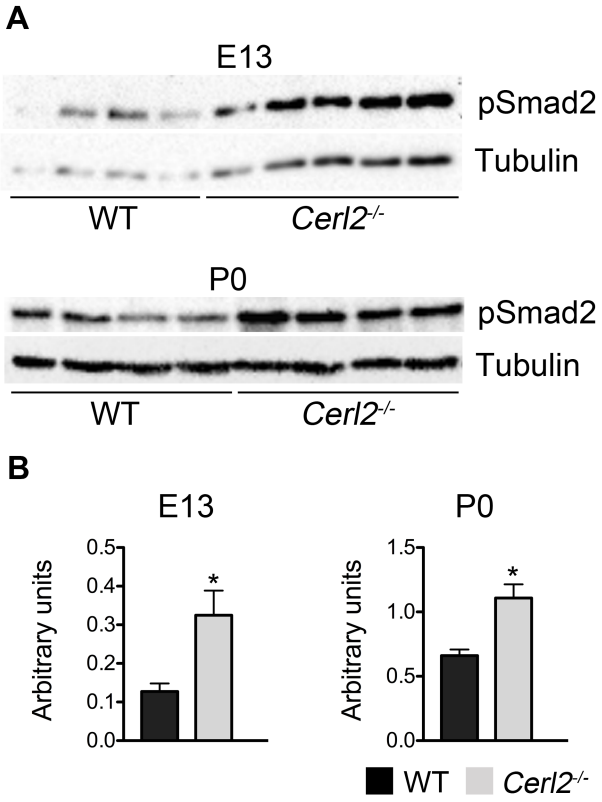

Figure 2.10 Increased pSmad2 levels in *Cerl2*$^{-/-}$ embryonic and neonatal hearts.
(A) Western blot at E13 (WT, n=4 and *Cerl2*$^{-/-}$ n=5) and P0 (n=4). (B) Quantitative analysis of anti-pSmad2 normalized with anti-tubulin (arbitrary units). * P<0.05.

In addition, we analyzed structural genes involved in contractility like *α-Mhc* and *cTnT*, which are activated by the above transcription factors (Durocher et al., 1997).
Furthermore, genes involved in hypertrophy program and cardiac stress were also evaluated, such as *Anp*, *Bnp* and *Ankrd1* (Arimura et al., 2009, Rohini et al., 2010). qRT-PCR analysis showed a dramatic reduction of *Gata-4* expression and a decrease of *c-TNT* in *Cer-2*$^{-/-}$ hearts at E13 (Figure 3.11 A). In contrast, we detected an increased *Nkx2.5* expression. At E15, *Cerl2*$^{-/-}$ hearts display decreased *Nkx2.5*, *α-Mhc* and *cTnT* expression (Figure 3.11 B). In *Cerl2*$^{-/-}$ neonatal hearts, we noticed increased *Bnp* and *Ankrd1* expression (Figure 3.11 C), suggesting early cardiac stress in neonates. However, no significant alteration was found for the other genes (*Gata-4*, *Nkx2.5*, *α-Mhc*, *c-Tnt* and *ANP*) at this stage. Taken together, these data indicate that the mRNA expression pattern of some cardiac genes is affected in *Cerl2*$^{-/-}$.

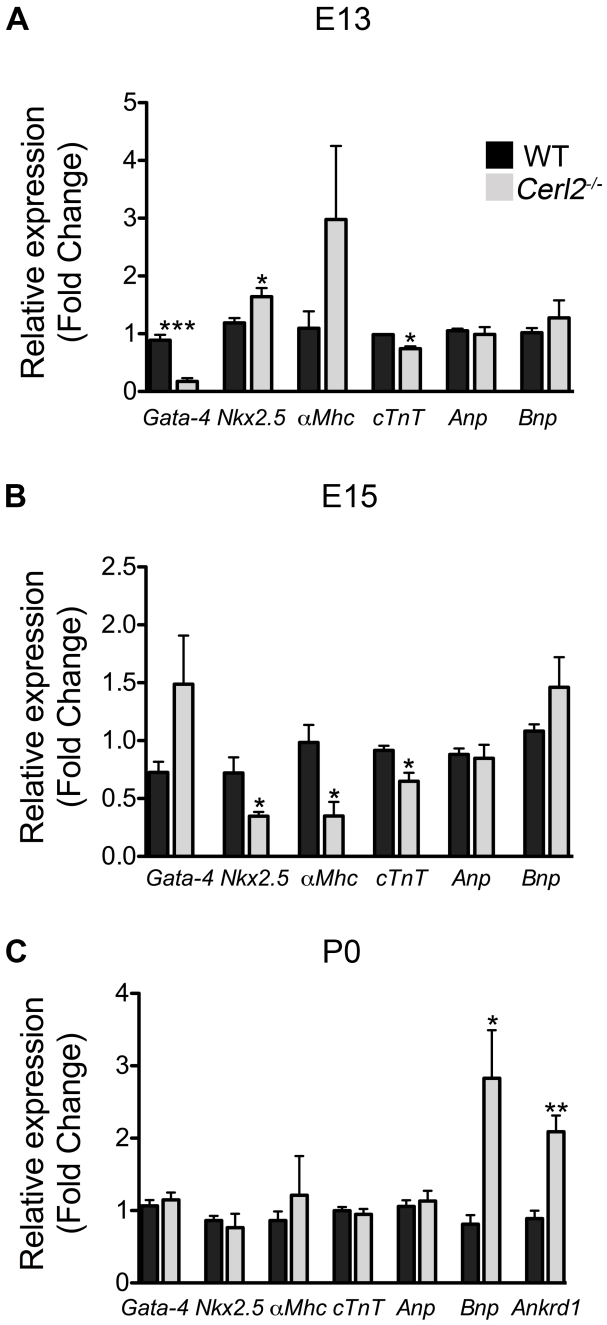

Figure 2.11 Relative mRNA expression of cardiac genes is altered in *Cerl2*$^{-/-}$ hearts.
qRT-PCR was performed in triplicate for *Gata-4*, *Nkx2.5*, *α-Mhc*, *c-Tnt*, *Anp, Bnp* and *Ankrd1*. Note the altered expression of cardiac genes during the development in absence of Cerl2 (A) E13, n=4. (B) E15-15.25, n=4 and (C) P0, n=5. * P<0.05, ** P<0.01 and *** P<0.001.

3.2.4 Discussion

In order to further characterize the effect of *Cerl2* loss-of-function during heart development we investigated the cardiac phenotype of *Cerl2*$^{-/-}$ mice without LD.

Previous study reported that before the compaction, the RV and LV shows the same thickness (Sedmera et al., 2000). Accordingly, at this stage the compact layer in either of the two ventricles of *Cerl2*$^{-/-}$ seems not to differ from WT. However, *Cerl2*$^{-/-}$ embryos showed increased LV trabecular expansion, in which could lead to an increased compact layer during the compaction process. As most of the trabeculae become compacted around E14 consequently at E16 onwards the myocardium is mainly constituted by compact layer (Sedmera et al., 2000; Risebro and Riley, 2006). In this context, we decided to investigate the *Cerl2*$^{-/-}$ hearts at E15-15.25. We observed that only the compact layer of the LV was enlarged. In addition, we observed that the trabecular layer is increased in the RV of the *Cerl2*$^{-/-}$, but it was not sufficient to generate a statistically significant abnormal enlarged RV myocardium. Usually, the hypertrabeculation is associated with noncompaction in the ventricles, resulting in thin a compact layer (Mysliwiec et al., 2011; Luxán et al., 2013). Despite the increased trabeculae expansion in the RV, the thinner RV myocardium was not observed in *Cerl2*$^{-/-}$. Taken together, these data suggest that the thickening of LV myocardium in *Cerl2*$^{-/-}$ starts to develop already during embryonic heart development.

Continuing the investigation of the time course on myocardial growth, we analyzed neonatal hearts at early postnatal life. *Cerl2*$^{-/-}$ neonates and the compound *Cerl2*$^{-/-}$*::Mlc1v-nlacZ-24* mouse line, which was generated to mark genetically the RV/pulmonary ventricle, displayed increased myocardial thickness in LV and IVS. These data suggest that in absence of Cerl2 the animals showed LV hypertrophy, and this finding is independent of the LD phenotype. The increased LVM index in *Cerl2*$^{-/-}$ also confirmed that result.

Evaluation of the cardiac function in neonates through determination of the heart rate and systolic filling parameters, such as aorta peak velocity and CO index, showed that *Cerl2*$^{-/-}$ cardiac function is compromised mainly due reduced LV systolic performance. Several studies have discussed the causes of the predominant increased LV muscle associated with impaired cardiac function instead of the RV. First, the workload on the LV is higher than the RV, leading to altered cardiac function in this ventricle (Sedmera et al., 2000). Second, the RV function becomes affected after the followed impaired LV function (Voelkel et al., 2006). Third, due to the complex shape and motion of the RV in mouse, scarce studies have been done in quantification of the right ventricular function (van Nierop et al., 2013). And lastly, the specific expression of *Cerl2* in the LV until the midgestation may in fact contribute to the

phenotype found in that ventricle. Although the cardiac phenotype of *null* mutants that displayed LD was not the main interest of our work, we did not observe increase of the LV and IVS myocardial walls neither increased of mitotic index in any of stages here analyzed.

In order to understand the cellular mechanism underlying the substantial increase of compact myocardium in *Cerl2*$^{-/-}$, we counted the mitotic cardiomyocytes at E13, E15 and P0. During embryonic mouse development, the cardiomyocytes are single nucleated (Ahuja et al., 2007). In *Cerl2*$^{-/-}$ at E13-13.25, we observe increased cardiomyocyte proliferating from the LV compact myocardium, but not statistically significant difference in the RV. The cardiomyocytes that composes the trabeculae are more differentiated than the ones of the compact (Rumiantsev and Bruce, 1991), then it has been proposed that the cardiomyocyes from compact myocardium migrates to the trabecular layer contributing to the its expansion (von Gise et al., 2012). After the compaction process, a natural reduction of the cardiac cell cycle occurs (Chen et al., 2004). Thus, at E15-15.25 despite the tendency to maintain increased cardiomyocyte proliferation in *Cerl2*$^{-/-}$, the proliferation of ventricular compact myocardium showed no significant difference between genotypes. The second DNA synthesis peak occurs during early neonatal period (P3-P4) resulting in bi-nucleated ventricular cardiomyocytes (Pasumarthi and Field, 2002). We analyzed neonates within few hours of birth (P0) to ensure that we would evaluate essentially the single nucleated cells. We detected a large increase of mitotic index in all LV walls of *Cerl2*$^{-/-}$. In contrast, the IVS showed no differences. According to literature, the proliferation capacity of the IVS decreases upon the completion of the septation process and, from midgestation onwards, it is mostly the LV myocardial population that contributes to IVS formation (Franco et al., 2006). Therefore, it is likely that the increased thickness found in IVS in *Cerl2* mutants is due to a substantial influence from the LV. Although, we observed an increased mitotic index in the RV, this event was not able to induce increased myocardial thickness. The distinct cell-lineage sources, roles and workloads between the ventricles, and the regionalized expression of *Cerl2* may explain why only the LV is enlarged. In addition, the right ventricular hypertrophic heart has been poorly described in mouse and humans.

Moreover, it was reported the role of Cer/Dan family to inhibit Wnt signaling (Piccolo et al., 1999). Emerging data revealed that mRNA *Cerl2* is regulated posttranscriptionally by Wnt3 leading to degradation of *Cerl2* in the left side of mouse node, thus Cerl2 and Wnt signaling seems to relate though negative feedback loop (Nakamura et al., 2012; Kitajima et al., 2013). In addition, Wnt canonical/ß catenin signaling was reported as essential to stimulate cardiomyocyte proliferation in the compact layer of the both ventricles through increase of

the *D-type cyclin 1* and *2*, *Ccnd1* and *Ccnd2*, respectively (Buikema et al., 2013). Therefore, we analyzed the level of *cyclins D1* and *D2*, key regulators of G1/S phase(Li and Brooks, 1999; Ikenishi et al., 2012) in order to investigate the key regulator of cell cycle in *Cerl2*$^{-/-}$. Our data revealed an increase of *Ccnd1* but not *Ccnd2* in the LV of *Cerl2*$^{-/-}$ at E13. Together, we can conclude that LV hyperplasia found in *Cerl2*$^{-/-}$ during the development and in early postnatal age may be regulated by the Wnt/ß-catenin signaling.

It has been reported that TGFßs/Nodal/Activin signaling is essential to regulate the cardiogenesis (Yuan and Jing, 2010). Furthermore, Smad2 pathway plays a relevant role as a mediator in the cardiac pathogenesis and ventricular remodeling in adult mouse hearts after injury (Euler-Taimor and Heger, 2006). Whereas *Cerl2* is expressed in the heart during development, it is possible that Cerl2 functions therein to regulate TGFßs/Nodal/Activin/Smad2 signaling. To our knowledge no data is available regarding antagonistic Cerl2 activity during cardiogenesis. Furthermore, in the same period we have found increased Smad2 phosphorylation in *Cerl2*$^{-/-}$ hearts indicating that in the absence of *Cerl2* ectopic TGFßs/Nodal/Activin/Smad2 signaling is activated. In addition, its signaling is increased in *Cerl2*$^{-/-}$ neonatal hearts. How this occurs in such a late stage when *Cerl2* is no longer expressed in the heart remains unclear. Nevertheless, we could anticipate two scenarios; first, Cerl2 may interact with other protein(s) that could extend that signaling activation in the early neonatal period; second, the autoregulatory loops are common in this type of signaling, being possible that the absence of *Cerl2* at earlier stages allows the prolongation of TGFßs/Nodal/Activin/Smad2 signaling until later stages.

To investigate whether the increased mitosis occurs in response to stimuli from increased cardiac cell death, we observed the apoptotic cells in *Cerl2*$^{-/-}$ neonatal mice. We did not find alterations in any sub-region of the LV or IVS. It has been recognized that apoptosis has a fundamental role during heart and vessel formation. However, its role during late fetal development and early postnatal life is still poorly investigated (Manabe et al., 2002). Additionally, evaluation of the relative cardiomyocyte cell area in neonatal mice did not reveal any differences in the LV and IVS. Furthermore, fibrosis was also not detected in *Cerl2*$^{-/-}$ neonatal hearts. Collectively, these data demonstrates that the increased myocardial thickness in *Cerl2*$^{-/-}$ is caused by cardiomyocyte hyperplasia and not by hypertrophy.

It has been reported that *Cerl1* is an early but not a late cardiac inductor in *Xenopus* and mouse embryonic stem cells (Foley et al., 2007; Bento et al., 2011; Cai et al., 2013). We hypothesized that *Cerl2* may share the same function that *Cerl1*. According to our qRT-PCR analysis, at E13 *Cerl2*$^{-/-}$ showed a severe decrease in *Gata-4* expression, however another

transcription factor *Nkx2.5* is increased. As Gata-4 interacts with Nkx2.5 (Durocher et al., 1997), we postulated that in absence of *Cerl2* a compensatory Nkx2.5 mechanism may be responsible to increase its expression and thus leading to unaltered expression of some *Gata-4 - Nkx2.5* target genes (*α-Mhc*, *ANP* and *BNP)* (Nemer, 2008) but reduced *cTnT* expression. In contrast, at E15 we observe a decreased *Nkx2.5* expression. Since alterations in this gene are associated with conduction abnormalities (Clark et al., 2006), we speculate that *Cerl2*$^{-/-}$ may have impaired cardiac function already during fetal development. Concurrently, we also detected reduction of the encoding contractile genes *α-Mhc* and *cTnT* but not altered *Gata-4* in *Cerl2*$^{-/-}$. In agreement with other reports, it is consistent that alterations of major transcription factors and their target genes compromise the cardiomyocyte differentiation program (Zheng et al., 2003). Furthermore, at this stage we also did not detect any alteration of *Anp* and *Bnp* expression in *Cerl2*$^{-/-}$, which indicates that the molecular mechanisms regulating the hypertrophic response in embryonic stages are not de-regulated (Rohini et al., 2010).

On the other hand, we did not find alteration in the expression on any of the structural cardiac genes in *Cerl2*$^{-/-}$ neonatal hearts. Nonetheless, we observed increased *Bnp* and *Ankrd1* expression that constitute the hallmark of cardiac stress genes. It has been recently demonstrated that *Ankrd1* is involved with the proliferation of cardiomyocytes and cardiomyopathy in humans (Arimura et al., 2009; Qiu et al., 2010). Therefore, it is possible that increased *Ankrd1* expression is associated with the ventricular hyperplasia in *Cerl2*$^{-/-}$ neonates. Collectively, the observed changes in the expression of essential genes for cardiogenesis indicate a de-regulation of the cardiac genetic program in *Cerl2* mutant embryos, which consequently compromises the cardiac function and survival of these animals. Interestingly, cardiac Smad4 deletion in mouse revealed alteration in pSmad2 levels, as well as in cardiomyocyte proliferation and in the expression of cardiac genes (Qi et al., 2007). Therefore we postulate that the activated Smad2/4 complex may have an important role in regulation of cardiogenesis in *Cerl2*$^{-/-}$.

In conclusion, our study provides the first evidence of the role of Cerl2 during cardiac development independently of its function in establishment of the L/R asymmetry. We demonstrate that specific expression of *Cerl2* in the LV may justify the hyperplasic left ventricular phenotype found in *Cerl2*$^{-/-}$. Additionally, this phenotype causes impaired systolic function in neonates, which may determine the cause of death. The Cerl2-Wnt/ß-catenin relation may leads to regulatory proliferative function of Wnt/ß-catenin signaling in compact

layer during the development and, therefore this study reveals an important break-through in the role of Cerl2 to control growth factor activity in cardiogenesis. However, the prolonged TGFßs/Nodal/Activin/Smad2 signaling in neonates when *Cerl2* in no longer expressed remains to be elucidated. In the future, a tissue-specific cardiac deletion of *Cerl2* would be relevant to determine its precise contribution during the heart formation.

Results

3.3 Part III

The improvement of cardiac performance in *Cerberus like 2* knockout mice – follow up study

Ana Carolina Araújo[1,2,3,4], Mauricia Vinhas[3], José A. Belo[1,2,3]

1. Laboratório de Embriologia e Manipulação Genética, Regenerative Medicine Program, Departamento de Ciências Biomédicas e Medicina, Universidade do Algarve, Portugal.
2. Institute for Biotechnology and Bioengineering - LA, Centro de Biomedicina Molecular e Estrutural, Universidade do Algarve, Portugal.
3. Regenerative Medicine Program, Departamento de Ciências Biomédicas e Medicina, Universidade do Algarve, Portugal.
4. PhD Program in Biomedical Sciences, Universidade do Algarve, Portugal

(manuscript in preparation)

Authors' contribution

ACA performed the image acquisitions and measurements, performed statistical analysis, analyzed and interpreted the ultrasound data and wrote the manuscript. MV performed the measurements for the inter-observer variability, participated in the interpretation of the results and contributed to the writing of the manuscript. JAB designed the study and wrote the manuscript.

3.3.1 Abstract

Background: The majority of the *Cerberus like-2* knockout (*Cerl2*$^{-/-}$) mice die during the first hours after birth and present two types of phenotypes. The first is characterized by the random positioning of the internal organs and heart defects, and the second by the increased left ventricular wall thickness and impaired cardiac function. However, whether the surviving *Cerl2* mutants present and develop further the latter phenotype remains unknown.

Methods: To investigate this, we monitored the left ventricular morphometry and examined the cardiac function from neonates until young adult age through non-invasive echocardiography. We compared 5 wild type and 4 *Cerl2*$^{-/-}$ males that survived through the complete analysis. In addition, qRT-PCR was performed in order to evaluate the relative expression of cardiac genes in the *Cerl2*$^{-/-}$ hearts.

Results: Here, we show that the *Cerl2* mutants that survive the critical first day of life recover from the impaired cardiac function. *Cerl2*$^{-/-}$ showed different pattern of LV dimension during the postnatal development, which affects systolic parameters such as the cardiac output. Furthermore, *Cerl2* expression was undetectable in adult mice and genetic markers linked to hypertrophy program (i.e. *Anp*, *Bnp* and *Ankrd1*) showed normal range of relative expression in adults indicating a recovery of the pathological hypertrophy.

Conclusions: *Cerl2* must be required during embryonic *cardiogenesis* mainly to the left ventricle. Its absence leads to abnormal increase of myocardial thickness, cardiac dysfunction and altered expression of cardiac genes. However, from fetal period onwards, *Cerl2* is no longer expressed in the heart and therefore likely dispensable. We also conclude that the global cardiac function is partially restored in *Cerl2* mutants.

Keywords: *Cerl2*$^{-/-}$, mice, postnatal, cardiac function

3.3.2 Introduction

Recent studies have been showing the powerfulness of assessing cardiac function in mice through echocardiography performance (Syed et al., 2005). Echocardiography is a non-invasive and inexpensive method which provides reliable information for the prognosis of cardiovascular diseases and for follow-up study purposes, such as for monitoring after myocardial infarction and pharmacological treatment in murine and humans (Mor-Avi et al., 2011; Benavides-Vallve et al., 2012). The secreted *Cerberus like-2* (*Cerl2*) is an antagonist of the Transforming Growth Factor type ß family (TGF-ß) that functions to dynamically control Nodal signal in the mouse node at early embryogenesis and then to establish proper Left/Right (L/R) asymmetry (Marques et al., 2004; Inácio et al., 2013). It has been extensively reported that failure in L/R axis determination leads to well known laterality defects (LD), which ultimately lead to randomized position of the visceral organs (Shiraishi and Ichikawa, 2012). Therefore, part of *Cerl2* knockout mice (*Cerl2*$^{-/-}$) die during the first hours after birth possibly due to LD (Marques et al., 2004). Moreover, we have reported that *Cerl2* is expressed in the heart until midgestation (embryonic day, E13) mainly in the left ventricle (LV). Upon careful analysis, we observed that some *Cerl2*$^{-/-}$ neonates displayed increased LV walls and interventricular septum (IVS) associated with impaired systolic function, even though these animals did not show evidences of LD (in this thesis, on chapter 3.2). This phenotype could indicate that progressive cardiac failure may develop in *Cerl2* mutants. However, whether at later ages the cardiac function declines further in these animals remains unknown. Therefore, we performed a serial follow up study using echocardiographic analysis from neonatal to young adult ages in order to evaluate the cardiac phenotype of the *Cerl2*$^{-/-}$ mice.

Here, we observed that the first day of birth is crucial to a significant percentage of the *Cerl2 null* mutants since part of these animals die due to defects described above. However, analysis of the mice that survived until the end of experiment showed that, even though they had decreased cardiac function at postnatal day (P) 0, they were able to improve their cardiac function and sustain most of the ameliorated cardiac physiologic parameters. We hypothesize that *Cerl2* mutant mouse may be an interesting model to study the molecular, cellular and physiological mechanisms behind the recovery of the cardiac function, which may help developing therapeutic approaches to treat heart failures.

3.3.3 Results

3.3.3.1 Survival analysis

Evaluation of the survival curve revealed that *Cerl2* mutants present a significantly reduced percentage of survival within the first day after birth when compared to WT (Figure 3.12 A). Phenotypic analysis revealed that the dead *Cerl2 null* mutants displayed LD, including inversion of a complete set or isolated organ(s) associated with structural cardiac failure, such as ventricular septal defects as analyzed by gross morphology (Figure 3.12 B, right). In addition, we identified another subset of dead *Cerl2* mutants that displayed normal organ arrangement and no evident signs of cardiac abnormalities (Figure 3.12 B, middle). Therefore, the dead *Cerl2* null mutants were divided and analyzed in animals that displayed or not LD (+LD and -LD, respectively). The newborn pups were weighted and the *Cerl2* mutants that died within the first day of life showed lower body weight (Figure 3.12 C). Echocardiographic analysis through bi-dimensional- (B-) mode view revealed end-systolic LV longitudinal length and end-systolic epicardial but not endocardial area were increased in the dead +LD *Cerl2*$^{-/-}$ and -LD *Cerl2*$^{-/-}$ respectively (Figure 3.12 D,E). However, the left ventricular mass index (LVMi) was similar to WT controls suggesting absence of hypertrophy (Figure 3.12 F). The global cardiac function was evaluated through the heart rate (HR) and the systolic peak of pulmonary artery velocity. Both of these parameters were reduced in -LD *Cerl2*$^{-/-}$ (Figure 3.12 G,H). We were unable to evaluate the aortic peak velocity in all *Cerl2 null* mutants, which could have been useful to contribute with other parameter to assess cardiac function. In addition, we analyzed the dead WT animals and, despite the low number of dead WT pups (n=2/12), which precluded the statistical analysis, these pups displayed reduced body weight (BW) and tendency to have decreased global cardiac function (Figure 3.12). Taken together these data indicate that in the first day of life, the *Cerl2* mutants absent of LD that die are likely the consequence of severely decreased heart function. Furthermore, all the *Cerl2 null* mutants with LD die shortly after birth despite the fact that they did not show statistically significant differences in LVMi and global cardiac function parameters, which is likely caused by the diversity of phenotypes in this category of mutants thus contributing to the variability observed in cardiac morphometry and physiology.

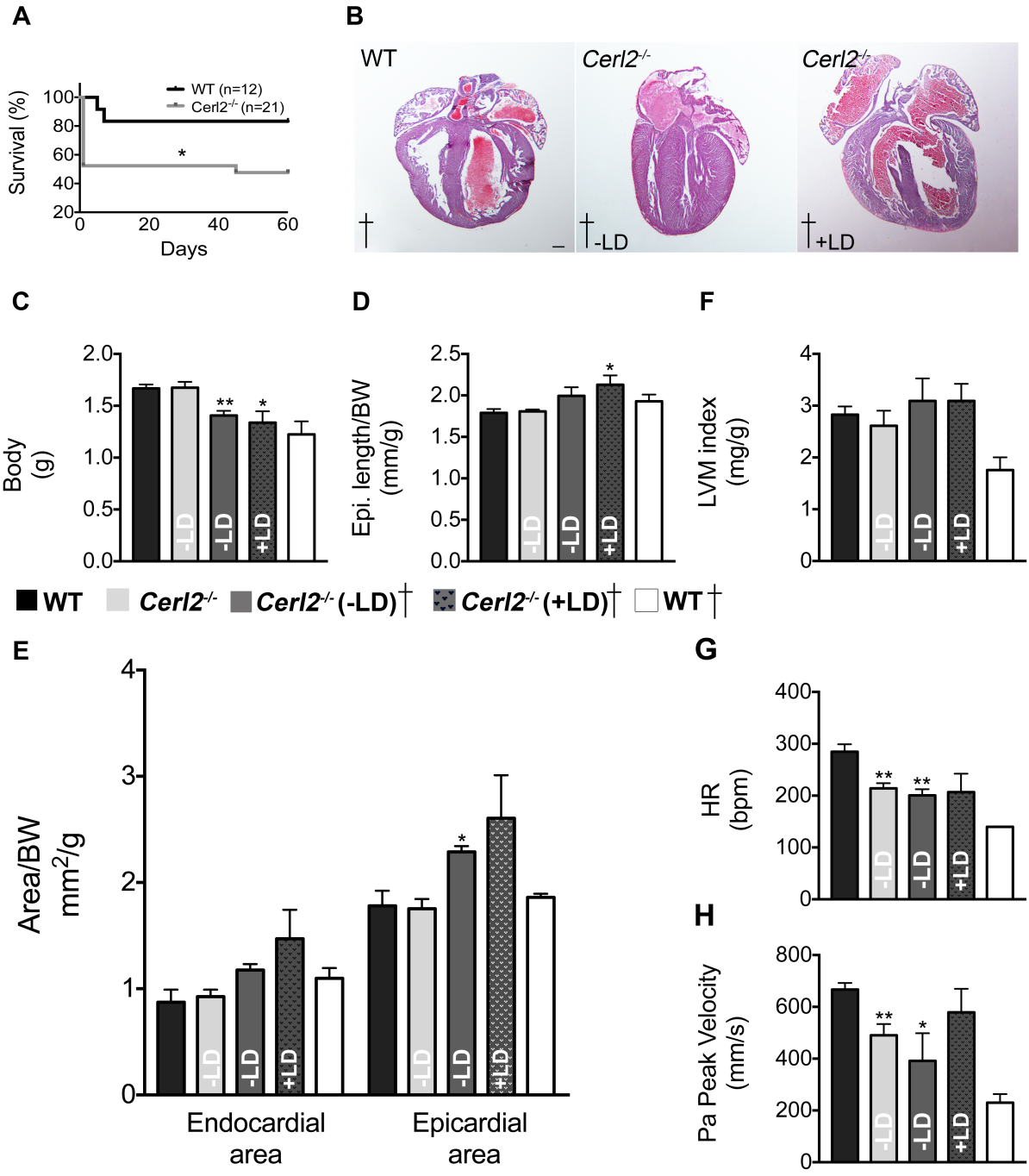

Figure 2.12 Survival percentage and echocardiographic analysis in died *Cerl2*$^{-/-}$ neonates.

Kaplan-Meier survival curves demonstrated significantly reduction of survival in *Cerl2*$^{-/-}$ mice compared to WT (A). Representative histological micrographs of died neonatal hearts (200µm) (B). Note the interventricular failure in +LD *Cerl2*$^{-/-}$ (right). The body weight in dead animals is decreased (C). Echocardiographic end-systolic parameters obtained from B-mode (D-F). Longitudinally, +LD *Cerl2*$^{-/-}$ neonates revealed increased LV length in PLAX view (D). In contrast, the epicardial area was only increased in -LD *Cerl2*$^{-/-}$, indicating therefore that transversally these animals displayed large area obtained from PSAX (E). The LVMi in *Cerl2* mutants were similar when compared with WT control (F). From pulsed-wave spectral Doppler, the HR was obtained in four-five consecutive peaks of the Pa peak

velocity and only -LD *Cerl2*$^{-/-}$ showed a reduced values in these parameters (G,H). BW, body weight; HR, heart rate; LVM, left ventricle mass; ns, non significant; Pa, pulmonary artery. +LD and –LD indicate the presence and absence of laterality defects, respectively. The results were indexed with BW in order to compare genotypes age-matched. Statistically significant result was considered when **P*<0.05 and ***P*<0.01. Results are expressed as mean ±SEM.

3.3.3.2 Echocardiographic Analysis of the surviving *Cerl2* mutants

The echocardiography was performed during 5 minutes to neonates and 20 minutes to juvenile (P30) and P60 (young adult). Females were excluded from the study, since we did not reach a sufficient number of *null* mutants surviving through the complete study to perform statistical analysis. In addition, one *Cerl2 null* mutant male died at day 45 and hence it was excluded from the analysis.

Prior to echocardiographic analysis, the body weight (BW) was obtained and averaged for each stage of interest for WT and *Cerl2* mutants. We did not observe significant differences in body mass at all time points (Table 3.9). Like in the control, young adult *Cerl2* mutants did not show loss of hair or weight, as well as any obvious evidence of behavioral alteration. Furthermore, at P60 *Cerl2*$^{-/-}$ did not show difference in their respective organ weights to tibia length (TL) or BW ratio (Table 3.10) when compared to the control.

Table 2.13 Body weight over time.

Measurement		Neonatal (P0)	Juvenile (P30)	Yng. Adt. (P60)
BW (g)	WT	1.66±0.03	9.13±0.55	21.64±0.88
	Cerl2$^{-/-}$	1.67±0.05^{ns}	10.71±0.85^{ns}	24.65±1.7^{ns}

BW, body weight; Yng. Adt, young adult mice; WT, wild type. Statistically significant result was considered when **P*<0.05. ^{ns} means no significant. Results are expressed as mean ±SEM.

Table 2.14 Body and wet organs weights and tibia length at P60.

Organs	WT	*Cerl2*$^{-/-}$
Heart (mg)	124 ±9.274	130±9.13^{ns}
Lungs (mg)	128±9.165	137.5±11.09^{ns}
Liver (mg)	996±73.53	1100±62.78^{ns}
Tibia (mm)	17.63±0.44	18.79±0.471^{ns}
Body (g)	21.64±0.88	24.65±1.705^{ns}
Heart/TL (mg/mm)	7.057±0.583	6.904±0.38^{ns}
Heart/BW (mg/g)	5.73±0.306	5.27±0.073^{ns}
Lungs/TL (g/mm)	7.29±0.59	7.31±0.53^{ns}
Lungs/BW (mg/g)	5.91±0.262	5.58±0.374^{ns}
Liver/TL (g/mm)	56.26±3.07	58.43±2.43^{ns}
Liver/BW (mg/g)	46.21±3.24	44.93±2.71^{ns}

Tibia length (TL), and organs weight were obtained at P60. BW, body weight; WT, wild type. Statistically significant result was considered when $*P<0.05$. ^{ns} means no significant. Results are expressed as mean ±SEM.

3.3.3.3 Left Ventricle structure

First, we performed transthoracic echocardiography to evaluate the dimensions of right and left ventricles (RV and LV, respectively) together with analysis of the cardiac function over time of *Cerl2*$^{-/-}$ (n=4) and WT (n=5) mice at defined ages. In contrast to adult mice, the precise way to measure small hearts is obtained from systole (Ghanem et al., 2006). Therefore, in order to compare the results from P0 to P60 we analyzed the end-systolic (s) values through B-mode view. Analysis over the time revealed that the LV endocardial and epicardial area obtained thought parasternal short axis view (PSAX) were continuously increased in WT and *Cerl2*$^{-/-}$ (Figure 3.13 A). Furthermore, both genotypes showed increased expansion of the left ventricular mass (LVM) and LV longitudinal length as expected to postnatal development (Figure 3.13 B,C). These data suggest that growth of the hearts of *Cerl2* mutants and WT accompanies their overall growth during the postnatal ages analyzed. However, while in WT the end-systolic aortic diameter significantly increased from P30 to

P60, in *Cerl2*$^{-/-}$ was maintained (Figure 3.13 D). This may compromise the pressure overload and consequently the stroke volume in *Cerl2* mutants.

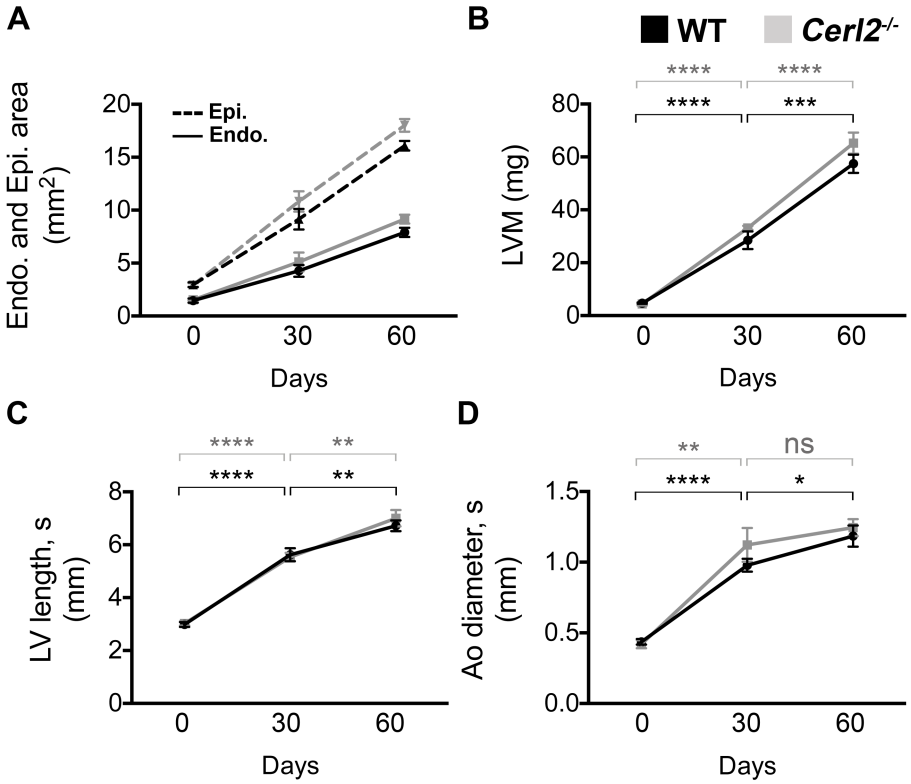

Figure 2.13 Bi-dimensional analysis over time at end-systole.
End-systolic endocardial and epicardial areas (represented by continuous and dashed lines respectively) were obtained from P0 to P60 in WT and *Cerl2*$^{-/-}$ (A). The both genotypes showed a progressive increase of the LVM as well the LV longitudinal length (B,C). However the aortic diameter did not increase in *Cerl2*$^{-/-}$ from P30 to P60 (D). Statistically significant result was considered when **P*<0.05; ***P*<0.01; ****P*<0.001 and *****P*<0.0001. Note, dark and gray asterisks indicate statistically significant results to WT and to *Cerl2*$^{-/-}$ over the time, respectively. ns, indicates no statically significant. Results are expressed as mean ±SEM. Ao represents the aorta; Endo, endocardial; Epi, epicardial; LVM, left ventricular mass; s, systole.

Next we analyzed the LV wall dimension at P30 and P60 by motion- (M-) mode including end –systolic (s) and -diastolic (d) measurements such as LV internal diameter (LVID), interventricular septum (IVS), and LV anterior and posterior walls (LVAW and LVPW, respectively). Analysis over the time revealed that the LVID,s and d (Figure 3.14 A), and IVS,s (Figure 3.14 B) increased from P30 to P60 in WT but not in *Cerl2 null* mutants. The LVAW thickness in WT and in *Cerl2*$^{-/-}$ was maintained (Figure 3.14 C). In contrast, during

the same period the LVPW thickness increased in *Cerl2*$^{-/-}$ but not in the WT (Figure 3.14 D). Additionally, the end-systolic and -diastolic LV volumes were increased only in WT (Figure 3.14 E). We also obtained information from the RV chamber by measuring the end-diastolic RV internal diameter (RVID,d) and despite the trends to increase in WT from P30 to P60, the both groups revealed the same RV dimension over the time. This morphometric analysis in M-mode demonstrated that *Cerl2* mutants display cardiac regional differences during the postnatal growth, which may indicate altered cardiomyocyte stimulation in the IVS and LV walls.

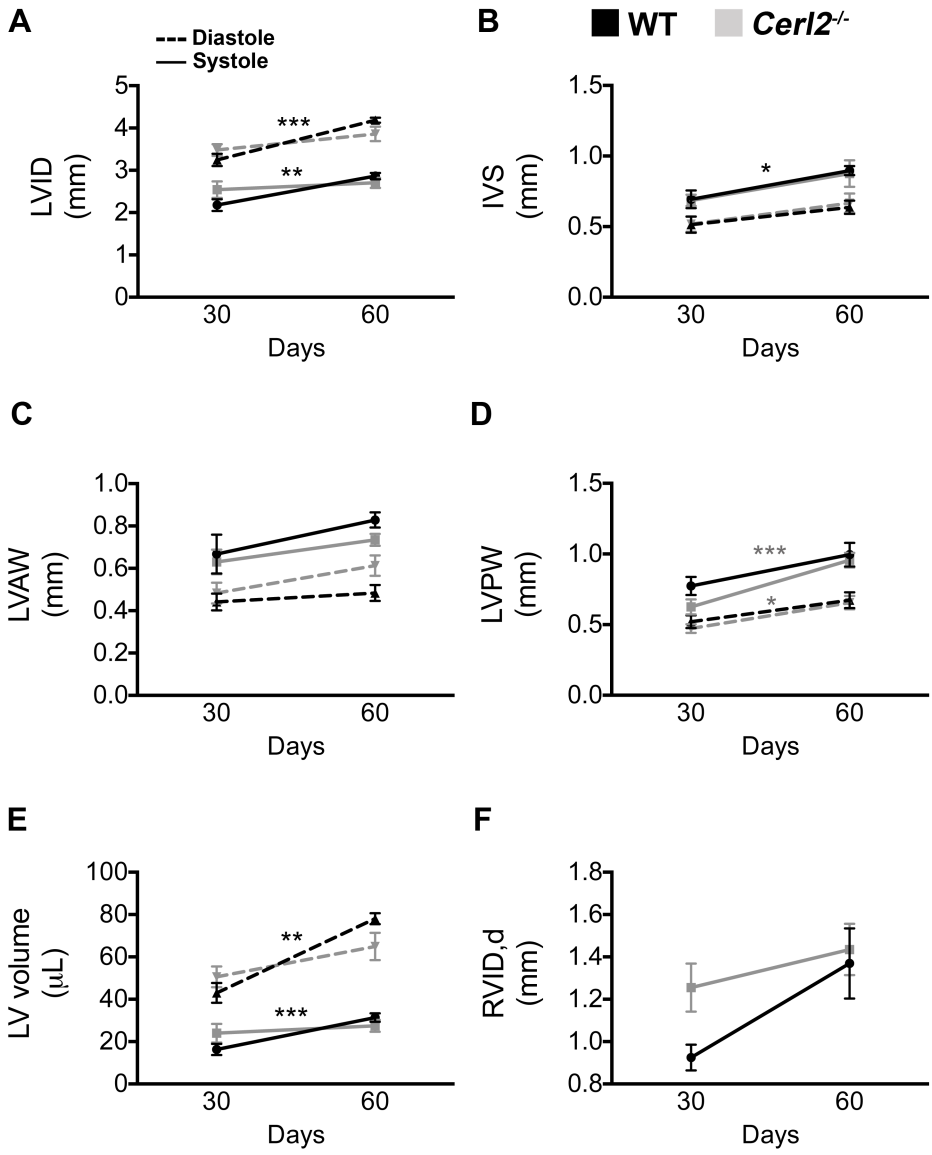

Figure 2.14 Motion-dimensional analysis at end-systole and diastole over time.

From P30 to P60 the LVID and IVS were progressive increased only in WT (A,B). The LVAW was maintained in both groups (C). However the *Cerl2 null* mutants displayed an increase of LVPW (D). LV volumes were increased only in WT (E). The RVID,d did not change to both genotypes (F). IVS, interventricular septum; LVAW, left ventricle anterior wall; LVID; left ventricle internal diameter; LVPW, left ventricle posterior wall; RVID,d right ventricle internal diameter at end-diastole. Continuous and dashed lines represent end-systole and end-diastole, respectively. Statistically significant result was considered when **P*<0.05; ***P*<0.01; ****P*<0.001. Note, dark and gray asterisks indicate statistically significant results to WT and to *Cerl2*$^{-/-}$ over time, respectively. Results are expressed as mean ±SEM.

Table 2.15 Serial PSAX measurements.

Day		Endo Area, s	Epi Area, s	LVMi	LV volume,s	LV volume,d
0	WT	0.87±0.12	1.78±0.14	2.8±0.15	ne	ne
	KO	0.92±0.06^{ns}	1.75±0.09^{ns}	2.6±0.3^{ns}	ne	ne
30	WT	0.46±0.05	1±0.06	3.08±0.2	1.78±0.26	4.7±0.37
	KO	0.48 ±0.08^{ns}	1.01±0.0^{ns}	3.15±0.22 ^{ns}	2.24±0.43^{ns}	4.79±0.55^{ns}
60	WT	0.37±0.03	0.75±0.04	2.67±0.2	1.47±0.14	3.64±0.22
	KO	0.37±0.01^{ns}	0.73 ±0.03^{ns}	2.65±0.06 ^{ns}	1.14±0.21^{ns}	2.7±0.36^{ns}

Endo area, endocardial area (mm^2); EPI area, epicardial area (mm^2); LVMi, left ventricle mass index (mg/g); s and d indicates values obtained from end-systole and end-diastole, respectively. KO, represent the *Cerl2*$^{-/-}$ and WT, wild type. The values were normalized with the body weight in order to compare genotypes age-matched. Statistically significant result was considered when **P*<0.05; ne, no evaluated; ^{ns} means no statistically significant. Results are expressed as mean ±SEM.

The morphometric values are indexed to BW for proper comparison of the mice of the different genotypes at the individual age-matched time points. Measures obtained from B-mode view revealed that LVM index, LV endocardial and epicardial area, end-systolic aortic diameter and LV longitudinal length did not show significant differences between WT and *Cerl2*$^{-/-}$ in all time points analyzed (Table 3.11 and Table 3.12). Similarly, through M-Mode view, the LVID (Figure 3.15 A) and the IVS (Figure 3.15 B) values were similar between WT and *Cerl2* mutants at all time points. Nevertheless, analysis of the LV wall thickness revealed that at P30 the LVPW and at P60 the LVAW were reduced in *Cerl2* mutants when compared to the WT (Figure 3.15 C,D). This demonstrates that *Cerl2*$^{-/-}$ have a thinner LVAW and LVPW without however compromising the LVID excluding, therefore, the possibility

that these mutants develop dilated cardiomyopathy. The LV volumes (LVV) were also indexed and the end-diastolic but not end-systolic LV volume was tendencially reduced in *Cerl2*$^{-/-}$ at P60 suggesting that the LV filling may be affected in *Cerl2*$^{-/-}$ young adult mice (Table 3.11). In addition, we also obtained information from the RV chamber by measuring the RV end-diastolic internal diameter (RVID,d), and we did not find differences between genotypes at each time point (Table 3.12) suggesting that WT and *null* mutants revealed similar RV filling. Together, the data from our detailed morphometric analysis indicate that *Cerl2*$^{-/-}$ hearts have discrete but significant alterations restricted to the LV walls and the aortic internal diameter that could lead to disturbed cardiac function.

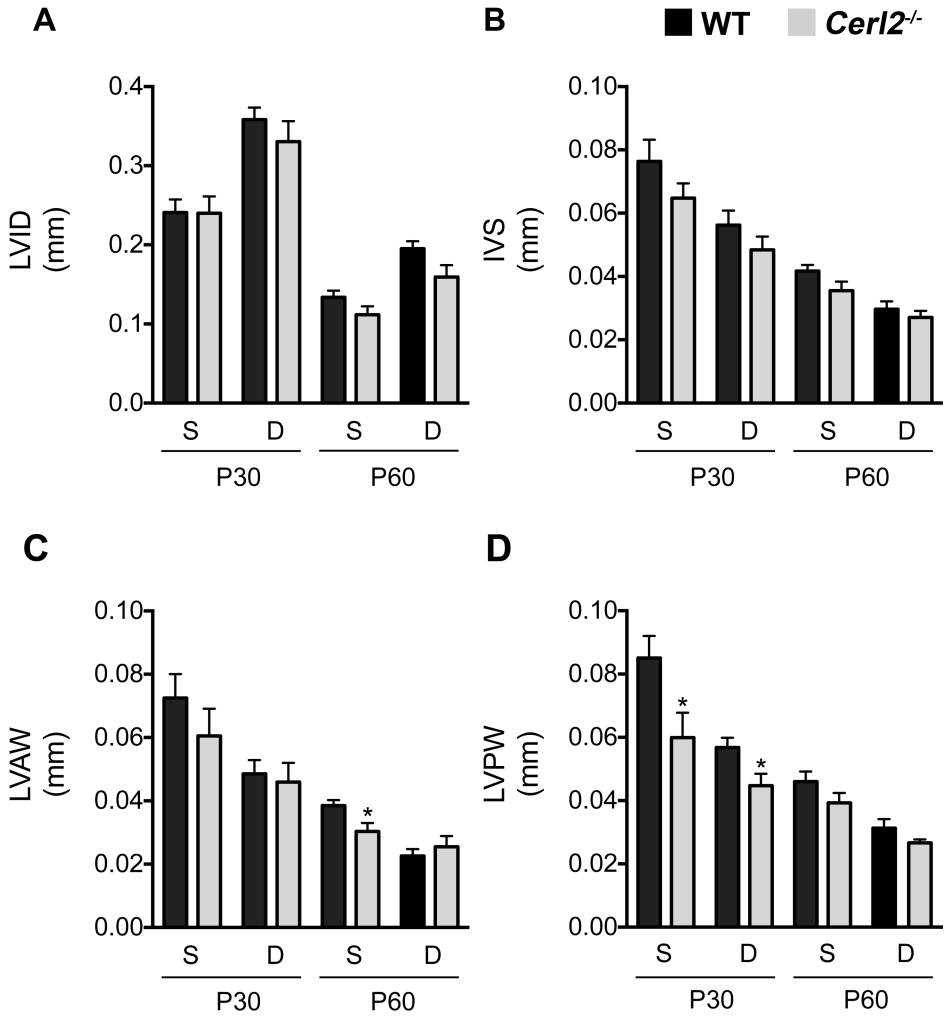

Figure 2.15 Motion-dimensional analysis at end-systole and -diastole in each time point. LVID and IVS was similar between the genotypes at P30 and at P60 (A,B). However, the LVAW,s, LVPW,s and ,d were reduced in *Cerl2*$^{-/-}$ at P30 and P60 respectively (C,D). The values were normalized with the body weight in order to compare genotypes age-matched. IVS, interventricular septum; LVAW, left ventricle anterior wall; LVID; left ventricle

internal diameter; LVPW, left ventricle posterior wall; D, end-diastole; S, end-systole. Statistically significant result was considered when **P*<0.05. Results are expressed as mean ±SEM.

Table 2.16 Serial PLAX measurements.

Day		Ao diam, s	LV length, s	RVID,d
0	WT	0.27±0.02	1.79±0.04	ne
	KO	0.25±0.005^{ns}	1.8±0.02^{ns}	ne
30	WT	0.1±0.002	0.62±0.04	0.1±0.013
	KO	0.1±0.003^{ns}	0.52±0.05^{ns}	0.12±0.014^{ns}
60	WT	0.05±0.005	0.31±0.008	0.063±0.006
	KO	0.05±0.003^{ns}	0.28±0.01^{ns}	0.06±0.008^{ns}

Ao diam., aortic internal diameter (mm); RVID, right ventricle internal diameter; ,s and ,d are obtained at the end-systole and -diastole, respectively. KO, represent the *Cerl2*$^{-/-}$ and WT, the wild type. The values were normalized with the body weight in order to compare genotypes age-matched. Statistically significant result was considered when **P*<0.05; ne, no evaluated; ^{ns} means no statistically significant. Results are expressed as mean ±SEM.

3.3.3.4 Global cardiac function

We started analyzing cardiac function by determining the heart rate (HR) from five consecutive spectral Doppler tracings from the aortic flow. According to our measurements, the HR was lower in *Cerl2*$^{-/-}$ at P0 (Figure 3.16 A). In addition, we evaluated the right and left ventricular physiology by determining, respectively, the pulmonary and aortic arteries peak velocities (Zheng-Fischhöfer et al., 2006; Stypmann et al., 2009) (Figure 3.16 B,C). We found decreased artery peak velocities at P0, which is consistent to what has been previously reported (in this thesis, on chapter 3.2). However, at P30 and at P60 all these parameters were similar between the *Cerl2 null* mutant and WT animals, suggesting that the *Cerl2*$^{-/-}$ animals were able to recover the normal cardiac function. To understand further the extent of the cardiac function recovery observed at P30 and at P60, we analyzed diastolic and systolic parameters, such as isovolumic relaxation time (IVRT), and isovolumic contraction time (IVCT) and ejection time (ET) (Table 3.13). Furthermore, myocardial performance index (MPI), also known as TEI index, was calculated to evaluate the global cardiac function, since it combines systolic and diastolic parameters (Parthenakis et al., 2002). The IVRT, IVCT, ET

and MPI from age-matched WT and *Cerl2* mutants were not significantly different at P30 and at P60. Taken together, these data indicate that the *Cerl2*$^{-/-}$ recovered from the impaired cardiac function observed at P0.

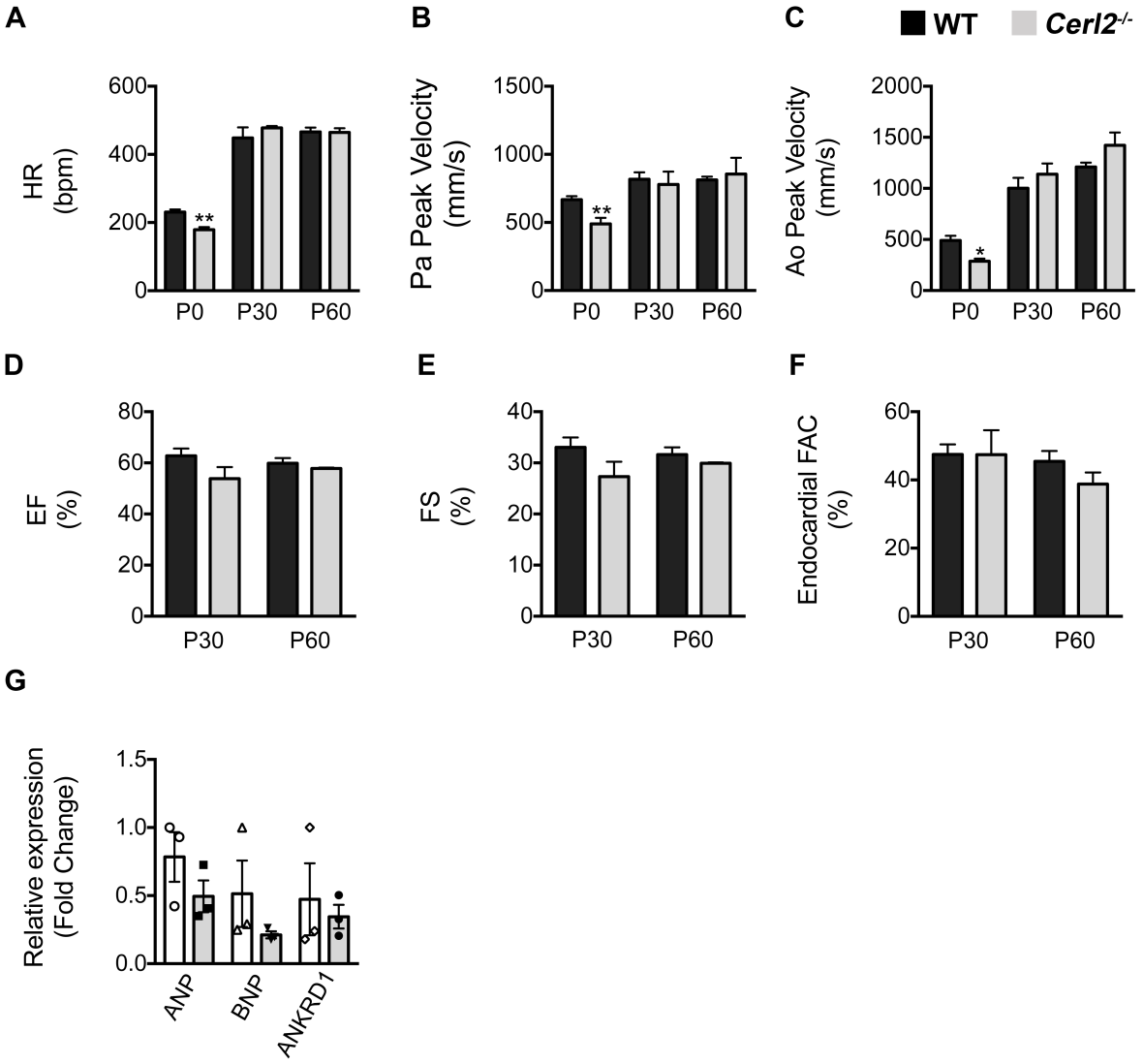

Figure 2.16 Cardiac function evaluation.
HR, Pa and Ao peak velocities were reduced in *Cerl2*$^{-/-}$ neonates. After that the *null* mutants are able to recover the cardiac dysfunction and maintain until the end of experiment (A-C). Left ventricular systolic parameters were evaluated (D-F). EF%, FS% and FAC% were maintained between WT and *Cerl2*$^{-/-}$ at all time points. qRT-PCR revealed normal relative expression of *Anp*, *Bnp* and *Ankrd1* between WT and *Cerl2*$^{-/-}$ at P60 (G). Ao; aorta artery; EF, ejection fraction; FAC, fractional area change; FS, fraction shortening; HR, heart rate; ns, non significant; Pa, pulmonary artery; Statistically significant results were considered when **P*<0.05, ***P*<0.01 and ****P*<0.001. Results are expressed as mean ±SEM.

Table 2.17 Global cardiac function.

Day		MPI	IVCT	IVRT	ETmv
30	WT	10.54±1.3	10.25±1.32	13.04±0.7	45.7±3.8
	KO	11.85±1.7^{ns}	11.5±1.84^{ns}	15.19±2.1^{ns,}	45.3±3.6^{ns}
60	WT	10.35±1.5	10.06±1.55	11.61±0.6	40.7±4.5
	KO	12.18±2.4^{ns}	11.58±2.4^{ns}	18.8±4.1^{ns}	32.7±2.9^{ns}

ETmv, ejection time of the mitral valve; IVCT, isovolumic contraction time; IVRT, isovolumic relaxation; MPI, myocardial performance index. The times are depicted in ms. Statistically significant result was considered when **P*>0.05; ^{ns} means no significant. Results are expressed as mean ±SEM.

3.3.3.5 Systolic function

Through PSAX at the level of the papillary muscles, we obtained systolic parameters, such as ejection fraction (EF%), fractional shortening (FS%) and fractional area change (FAC%). The *Cerl2* mutants showed normal systolic function when compared to WT at all time points (Figure 3.16 D-F). In addition, we calculated another systolic parameter, the cardiac output (CO) that is the product of the HR and stroke volume (SV). These can be evaluated in two ways. The first way is dependent of the aortic valve (AoV) values i.e. velocity time integral (AoV VTI) and AoV inner diameter. We revealed that only the WT increase the SV and the CO from P30 to P60 (Figure 3.17 A,B). We also calculate the SV index (SVi) and the CO index (COi) normalized by the BW, and no differences were found when comparing WT and *Cerl2*$^{-/-}$ (Figure 3.17 C,D). We can also evaluate the SV using the LV volume measurements (LV diastolic volume – LV systolic volume) if we assume the ellipsoidal morphology of the heart. According to our data, the SV and the CO was increased in both genotypes over the time (Figure 3.17 E,F) and, when indexed to BW, the SVi and the COi were reduced in *Cerl2*$^{-/-}$ at P60 (Figure 3.17 G,H). Even though the SVi and COi obtained from AoV parameters suggest that the systolic function seems not to be compromised by the maintenance of aortic lumen in *null* mutants, the LV volumetric changes showed to be effective in reduced SVi and COi indicating that echocardiographic measurements may be associated with biased statistical assumptions from both SV evaluations. Therefore, we can conclude that even though the decreased COi in *Cerl2*$^{-/-}$ at P60, the cardiac function of *null* mutants recovered significantly as demonstrated by other systolic parameters such as EF%, FS% and FAC%.

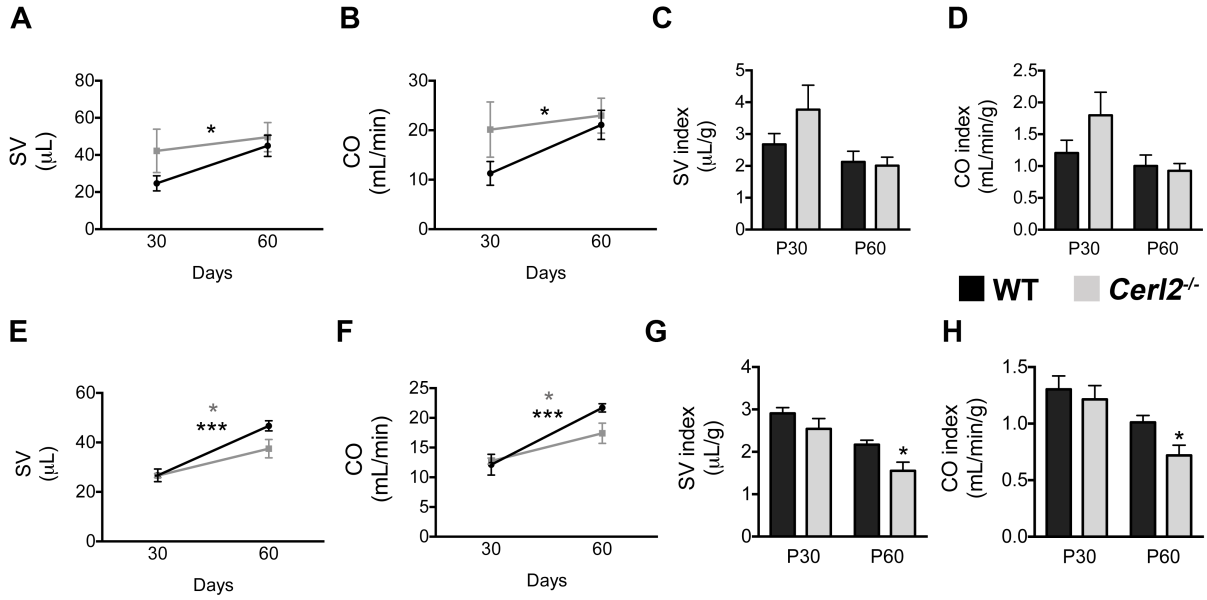

Figure 2.17 Systolic function.
SV and CO were calculated by aortic dimension (A-D) and by LV volumes (E-H). The SV and CO were only increased in WT from P30 to P60 (A,B). However *Cerl2*$^{-/-}$ animals did not revealed significant results when indexed (C,D). SV and CO calculated from LV volumes showed that the both genotypes increase the systolic function over the time (E,F). Although the *null* mutants displayed reduced SVi and COi (G,H). CO, cardiac output; i, index; SV, stroke volume. Statistically significant results were considered when **P*<0.05 and ****P*<0.001. Note, dark and gray asterisks indicate statistically significant results to WT and to *Cerl2*$^{-/-}$ over time, respectively (A,B,D,E). The values were normalized with the body weight in order to compare genotypes age-matched. Results are expressed as mean ±SEM.

3.3.3.6 Diastolic function

The diastolic function was assessed through ventricular inflow velocities such as peak velocity of early and late transmitral waves (E and A respectively) and by the ratio E/A. Furthermore, we measured the time in which all valves are closed and the ventricles relax without any change represented by the IVRT. We did not detect any significant differences regardless of the genotype between time points (Table 3.14) suggesting that the diastolic function was preserved in *Cerl2* mutants.

Table 2.18 Diastolic function through transmitral color Doppler.

Day		E	A	E/A
30	WT	700.8±92.6	536±68.6	1.3±0.03
	KO	588.9±63.9^{ns}	488.2±59.2^{ns}	1.21±0.02^{ns}
60	WT	703.8±119.5	562±104.3	1.26±0.02
	KO	604.7±51.03^{ns}	460±53.7^{ns}	1.33±0.07^{ns}

A, late diastolic wave; E early diastolic wave. E and A are depicted in mm/s. Statistically significant result was considered when **P*<0.05. ^{ns} means no significant. Results are expressed as mean ±SEM.

3.3.3.7 Relative genes expression

Cerl2 is expressed in the LV until midgestation as previously reported (in this thesis, on chapter 3.2). However, in further ages this expression is no longer detected (data not shown). Relative mRNA expression of hypertrophy markers such as *Anp*, *Bnp* and *Ankrd1* was quantified in WT and *Cerl2*$^{-/-}$ hearts at P60. Contrary to early neonatal age (in this thesis, on chapter 3.2), we did not detect any difference in the levels of these genes when compared to the WT (Figure 3.16 G). Together with cardiac function evaluation, these findings demonstrate that young adult *Cerl2* mutants are likely not under cardiac stress.

3.3.3.8 Intra- and inter-observer variability

Table 3.15 summarizes intra- and inter-observer variability measurements. Correlation analyses demonstrated excellent agreement between intra-observer measurement (LV EF% in the *Cerl2*$^{-/-}$ at P60) and inter-observer (LVMi in the *Cerl2*$^{-/-}$ at P0; LVMi in the *Cerl2*$^{-/-}$ at P30 and LV EF% in the *Cerl2*$^{-/-}$ at P60) in echocardiographic assessment.

Table 2.19 Variability of LV measurements obtained from B- and M-mode view.

	Intra-Observer			Inter-Observer		
P0	**Error (%)**	**Coefficient (mm)**	**r**	**Error (%)**	**Coefficient (mm)**	**r**
LVMi,s WT	-10.23 ± 23.68	-0.1 ± 0.23	-0.09	0.56 ± 9.05	0.002 ± 0.26	-0.63
LVMi,s KO	-6.33 ± 36.32	-0.19 ± 0.45	-0.18	8.3 ± 11.62	-0.24 ± 0.32	0.95*
P30	**Error (%)**	**Coefficient (mm)**	**r**	**Error (%)**	**Coefficient (mm)**	**r**
LVMi,s WT	-3.91 ± 24.38	0.14 ± 0.33	-0.33	-4.07 ± 19.44	0.15 ± 0.32	0.35
LVMi,s KO	-7.71 ± 12.41	0.25 ± 0.31	0.09	-2.18 ± 6.11	0.053 ± 0.26	0.98*
LVID,d WT	-1 ± 14.27	0.003 ± 0.02	0.07	-3.44 ± 17.3	0.013 ± 0.02	-0.27
LVID,d KO	0.19 ± 12.27	-0.003 ± 0.04	-0.07	3.05 ± 7.06	-0.01 ± 0.03	0.32
IVS, d WT	12.58 ± 18.55	-0.006 ± 0.006	-0.15	37.45 ± 33.8	-0.018 ± 0.006	-0.07
IVS,d KO	-6.3 ± 39.85	0.004 ± 0.007	-0.62	-4.22 ± 44.5	0.005 ± 0.01	-0.83
LVAW,d WT	2.23 ± 31.25	-0.001 ± 0.006	0.018	-38.53 ± 18.18	-0.016 ± 0.004	0.53
LVAW,d KO	-6.25 ± 31.83	0.002 ± 0.007	0.6	-10.7 ± 41.7	0.007 ± 0.01	-0.46
LVPW,d WT	15.02 ± 25.2	-0.007 ± 0.004	-0.27	20.16 ± 7.71	-0.01 ± 0.004	0.01
LVPW,d KO	1.63 ± 13.7	-0.001 ± 0.004	0.89	-14.48 ± 32.28	0.007 ± 0.007	-0.44
LV EF% WT	2.7 ± 11.32	-1.67 ± 2.78	0.006	7.7 ± 16.9	-4.5 ± 4.5	0.22
LV EF% KO	-1.63 ± 33.63	0.97 ± 6.65	-0.23	-12.11 ± 7.3	6.77 ± 6.2	0.31

LV COi WT	0.34 ± 29.64	-0.007 ± 0.16	0.07	-0.28 ± 37.3	0.005 ± 0.12	-0.06
LV COi KO	-1.09	-0.008 ± 0.16	0.21	-4.8 ± 15.9	-0.37 ± 0.5	0.004
P60	**Error (%)**	**Coefficient (mm)**	**r**	**Error (%)**	**Coefficient (mm)**	**r**
LVMi,s WT	-8 ± 15.73	0.22 ± 0.28	-0.07	-14.3 ± 11.6	0.41 ± 0.3	-0.1
LVMi,s KO	-6.43 ± 10.3	0.18 ± 0.1	-0.7	-6.8 ± 11.5	0.19 ± 0.13	-0.7
LVID,d WT	0.5 ± 16.75	0.0008 ± 0.01	-0.07	-2.6 ± 3.57	0.005±0.01	0.2
LVID,d KO	-0.25 ± 13.2	0.001 ± 0.02	-0.35	-1 ± 28.8	0.002 ± 0.02	-0.14
IVS, d WT	8.77 ± 14.21	-0.002 ± 0.004	-0.57	23.2 ± 15.46	-0.006 ± 0.002	-0.06
IVS,d KO	-21.9 ± 8	0.006 ± 0.003	0.6	3.3 ± 23.7	-0.0007 ± 0.003	-0.18
LVAW,d WT	-0.77 ± 42.4	0.0004 ± 0.004	-0.22	-0.2 ± 25.6	-0.00006 ± 0.003	-0.006
LVAW,d KO	-12.8 ± 34.4	0.0005 ± 0.004	-0.06	-3 ± 21.27	-0.001 ± 0.005	-0.11
LVPW,d WT	0.46 ± 42.2	-0.01 ± 0.01	-0.25	12.63 ± 14.6	-0.003 ± 0.004	-0.14
LVPW,d KO	1.05 ± 17.6	-0.0002 ± 0.002	-0.4	7.8 ± 16.02	-0.001 ± 0.003	-0.92
LV EF% WT	6.9 ± 12.3	-4.1 ± 2.54	0.35	11.35 ± 12.1	-6.1 ± 4	-0.64
LV EF% KO	-3.24 ± 8.6	2.11 ± 2.92	-0.99**	-6.3 ± 15	4.3 ± 4.4	-0.98*
LV COi WT	8.2 ± 17.2	-0.007 ± 0.1	-0.42	-2.1 ± 40.4	-0.02 ± 0.2	0.44
LV COi KO	-3.76 ± 3.5	-0.03 ± 0.14	-0.93	16.8 ± 17.6	-0.15 ± 0.13	0.23

Error % was obtained by Bland- Altman analysis, which showing the agreement as a percent difference between observers (±SD). Coefficient (mm) is the difference between two observations (±SEM). It was calculated by unpaired two-tailed Student's t-test. r, Pearson's coefficient. **P*-value for correlation coefficient (**P<0.05* and ***P<0.01*). IVS,

interventricular septum; LVAW, left ventricle anterior wall; LVID, left ventricle internal diameter; LVPW, left ventricle posterior wall; LV COi, left ventricular cardiac output index; LV EF%, left ventricular ejection fraction; LVMi, left ventricular mass index; ,s and ,d indicates that the measures were obtained at end- systole and diastole, respectively.

3.3.4 Discussion

According to our previous reports *Cerl2* mutants revealed two subsets of phenotypes, which in most cases leads to death of the mutants in their first day of life (Marques et al., 2004), (in this thesis, on chapter 3.2). To distinguish these subsets, we created two groups of dead *Cerl2* mutants, namely the ones with (+LD) and without laterality defects (-LD), which we used in histological and echocardiographic analysis. Heterotaxy in mice, in contrast with *situs inversus,* leads to an assortment of phenotypes with malpositioning of the great arteries and thinning of LV walls (Francis et al., 2012). In addition, failure in ventricular septation, transposition of the great arteries, double outlet right ventricle and common arterial trunk are common features that characterize the congenital heart disease (CHD) (Garne et al., 2012). Since the +LD *Cerl2*$^{-/-}$ neonates display a variable array of these cardiac abnormalities characteristic of CHD, we were unable to obtain statistically significant data regarding LV morphometry and global cardiac function. Moreover CHD is incompatible with a long lifespan, being the most common cause of death in childhood (Shiraishi and Ichikawa, 2012),(Bentham and Bhattacharya, 2008). Thus, we postulate that together with other systemic defects, the cardiac related abnormalities may contribute for the lethality observed in this group of animals.

On the other hand, echocardiographic analysis of the –LD *Cerl2*$^{-/-}$ neonates, which died in the first day of life, revealed increased end-systolic LV epicardial area when compared to the WT controls. However, when indexed, the LVMi was similar between both genotypes likely due to the observed slight increases in endocardial area and epicardial length, which can interfere with the LVM calculations. This data suggests that the *Cerl2*$^{-/-}$ neonates seemingly do not display LV hypertrophy. Nonetheless, dead -LD *Cerl2*$^{-/-}$ also showed decreased cardiac function as measured by the HR and pulmonary artery peak velocity. Even though we do not known precisely what determines the death/survival of these animals, based on our findings we can conclude that the first day of birth is critical to *Cerl2*$^{-/-}$ neonates. From our echocardiographic analysis, we could also not detect significant evidence of LV hypertrophy in the surviving -LD *Cerl2* mutant neonates. In small hearts (<50mg), the echocardiographic analysis has to be however validated with hystomorphometric analysis (Ghanem et al., 2006).

Since in this study we intended to do a follow up of the surviving *Cerl2* mutants, we could not sacrifice the animals at neonatal age to perform the histological measures in the hearts. Despite this, in our previous report we showed through histomorphometric analysis that the *Cerl2*$^{-/-}$ neonates have a marked increase of the LV walls thickness, which can be already detected at fetal stages (in this thesis, on chapter 3.2). This leads to increased LVMi in the *Cerl2* mutants and since this parameter is an indicator of LV hypertrophy (Barrick et al., 2007), these data is consistent with the presence of LV hypertrophy in *Cerl2* mutant neonates without LD.

According to literature, the cardiac muscle continues to grow until around P60 when it reaches a plateau (Wiesmann et al., 2000). We observed that end-systolic LV epicardial and endocardial area, LV epicardial length and the LVM were progressively increased both in WT and surviving –LD *Cerl2* mutants during the analyzed time points. It is known that the mechanical stiffness and the geometric properties of aorta, such as the wall thickness, diameter and length, increase after birth in response to the increased systemic blood pressure and cardiac output (Heymann et al., 1981; Huang et al., 2006). In contrast with the WT, the inner diameter of the aorta was maintained in *Cerl2*$^{-/-}$ from P30 to P60 may leading the maintenance of the SV and CO as measured by the inner diameter and VTI of the aortic valve. However, when indexed to the BW, the epicardial and endocardial area, LV epicardial length, inner aortic diameter revealed no differences between *Cerl2* mutants and WT at all time points analyzed, suggesting that the postnatal cardiac development of the surviving *Cerl2* mutants progresses similarly to the WT. In addition, we did not find significant differences between the genotypes at P60 of the wet heart/ liver/ lungs to BW or TL ratio. These data suggest that the adult *Cerl2* mutants do not have hypertrophy, neither have any characteristic symptoms of cardiac failure such as congestion or edema (Liao et al., 2002; Swynghedauw, 1999; Sugihara et al., 2013).

Evaluations obtained from M-mode over the time revealed that the LV dimensional parameters are quite different in WT and in *Cerl2*$^{-/-}$, except for the LVAW thickness that was maintained from P30 to P60 in both. In WT animals the LVPW is maintained over the time, but the IVS thickness and LVID diameter increases. In contrast, in *Cerl2* mutants we observed the opposite, i.e. maintenance of IVS and LVID, and increased LVPW. These regional morphometric differences could be caused by divergent myocardial blood flow (MBF) resulting in altered aerobic metabolism of cardiomyocytes in certain LV walls, which may alter the cardiac workload. Indeed, it has been demonstrated that when pacemakers are inserted in dogs this leads to asynchronous electrical activation, leading ultimately to the

reduction of the cardiac mass in the stimulated area due to reduced regionalized MBF (Oosterhout et al., 1998; Oosterhout et al., 2002). Upon indexation, we observed that *Cerl2*$^{-/-}$ displayed reduced end-systolic and -diastolic LVPW thickness at P30 and reduced end-systolic LVAW thickness at P60. When compared with WT, we did not detected significant differences in IVS thickness and LVID at all time points. This suggests that, despite the observed reductions of the LV walls thickness, the LVID was maintained in *Cerl2*$^{-/-}$. The assessment of RV function in mice is a great challenge due to its morphology (Vitarelli and Terzano, 2010). Evaluation of the end-diastolic RVID revealed that the RV filling is similar between the control and the *Cerl2* mutants over the time. Upon indexation, these values also were not different between both genotypes at P30 and at P60. Altogether, these data demonstrate that *Cerl2* mutants manage to avoid developing dilated cardiomyopathy, which is normally characterized by the thinning of the LV walls, increased LV dilation and concomitant reduced systolic function (Seidman and Seidman, 2001).

Even though echocardiography has been frequently performed in adult mice and human for serial measurements of the LV dimensions and cardiac functional analysis (Reffelmann and Kloner, 2003; Vinhas et al., 2013), the use of this technique for analysis of small hearts is limited. Accordingly, we were unable to obtain systolic (EF%, FS% and FAC%) and diastolic parameters (IVRT and E/A) in neonatal mice. Nonetheless, and like it is performed in humans (Kolettis et al., 1976; Yared et al., 2011), we assessed the global cardiac function using the HR, and the systolic functions of the LV and RV by the aortic and pulmonary artery peak velocities, respectively. In *Cerl2*$^{-/-}$ neonates, we observed a severe decrease of cardiac function, which is consistent with what we have previously shown (in this thesis, on chapter 3.2). However, from P30 we observed similar values for these parameters in WT and *Cerl2*$^{-/-}$, suggesting that there was an improvement of the cardiac function in *null* mutants. This is consistent with what we observed from our B- and M-mode measurements. In addition, this improvement at P30 and P60 was further confirmed by the analysis of diastolic parameters (IVRT, and E/A) and by other systolic parameters such as the EF%, FS% and FAC%. Furthermore, analysis of the expression of the hypertrophy markers *Anp*, *Bnp* and *Ankrd1* (Nishikimi et al., 2006; Mikhailov and Torrado, 2008; Das et al., 2009; Qiu et al., 2010) showed that unlike in neonatal heart (in this thesis, on chapter 3.2), there were absolutely no differences in the expression of these genes at P60 between WT and *Cerl2*$^{-/-}$ hearts. Taken together, these data indicate that the surviving *Cerl2* mutants recover cardiac performance after early neonatal age.

To analyze more in detail the systolic function of *Cerl2* mutants, and assuming the cardiac ellipsoidal shape, we evaluated also the SV by the LV volume measurements. Even though the preload is usually measured by the LV pressure, we evaluated it through the end-diastolic LV volume, which is a widely accepted parameter to estimate the preload (Norton, 2001). In contrast with the WT, the LV volumes (systolic and diastolic) were maintained from P30 to P60 in *Cerl2* mutants. Furthermore, when indexed the end-diastolic LV volume showed a trend to be reduced in *Cerl2*$^{-/-}$ at P60 when compared with the WT. This may be symptomatic of altered SV in the *Cerl2* mutant according to the Frank–Starling law (Moss and Fitzsimons, 2002). Furthermore, the preload seems to affect the SVi and COi since these values were reduced in *Cerl2*$^{-/-}$ at P60. Altogether, these data indicate that, despite the recovery of the cardiac performance of *Cerl2* mutants at P30 and P60, the systolic function is still affected in the *Cerl2*$^{-/-}$ heart.

We have previously shown that *Cerl2* is required mainly in the LV during embryonic *cardiogenesis*. Its absence leads to abnormal increase of LV myocardial thickness due to hyperplasia, cardiac dysfunction and altered expression of cardiac genes (in this thesis, on chapter 3.2). However, from midgestation onwards, *Cerl2* is no longer expressed in the heart and therefore likely dispensable, and the cardiac function is able to partially restore. To our knowledge, this is the first report demonstrating through serial echocardiography the functional improvement of the cardiac function using a *null* mutant as a model. We hypothesize that these animals must have a compensatory mechanism of adaptation in order to improve the cardiac function during the first months of life. Understanding the mechanism underlying the *Cerl2*$^{-/-}$ recovery could provide valuable insights to improve therapies to treat heart failure conditions in humans.

3.3.5 Limitations

Despite the echocardiography advances in the last decades, the accuracy in smaller hearts is still a great challenge, thus the morphometric values obtained from echocardiography should to be confirmed with histomorphometry (Ghanem et al., 2006). Since sacrificing the animals at each time point is incompatible with a follow up study such as this one, we do not have information from histomorphometry. Therefore, we could not confirm the neonatal morphometry by echocardiography for the analyzed animals.

It has been reported that the alteration in artery components, and variation in lumen and outer diameter may affect the blood pressure, causing the hipo- or hypertension in murine

(Giummelly et al., 1999; Le et al., 2011). We did not monitor the blood pressure during the follow up.

This study involved a small number of animals WT and *Cerl2*$^{-/-}$, our data suggests that the absence of *Cerl2* may severely affect the cardiac function, contributing to increase the mortality in early postnatal life.

Despite the fact that isoflurane inhalant has been reported to depress the cardiac function, it is one of the most common agent used with low hemodynamic effects (Wu et al., 2010).

3.3.6 Conclusion

Here, we observed that the surviving *Cerl2* mutants partially recover cardiac performance after birth. However, what determines the survival of some *Cerl2 null* mutants absent of LD and the mechanism orchestrating the recovery of the surviving mutants remains unknown. Being a follow-up study, each animal served as its own control, providing a great statistical analysis and significantly reducing the number of mice required to conduct the experiment. We believe that *Cerl2*$^{-/-}$ mice are a good model to investigate the mechanisms underlying heart adaptations and cardiac function recovery during early postnatal age. Using our model may allow obtaining insights towards the identification of potential therapeutic approaches to treat (early) heart failure.

4 General Discussion

Although obvious differences are found between the murine and the human heart such as the cardiac weight and shape (ellipsoidal and pyramidal shape, respectively), the four-chambered hearts are anatomically very similar (Wessels and Sedmera, 2003). Functionally, smaller animals require more energy consumption per body weight, reflecting in variability of heart rate, ejection time and intra-ventricular pressure when compared with humans (Kusunose et al., 2012). Genetically, mice and humans share 99% of conserved genes and molecular pathways (Yutzey and Robbins, 2007), making the mouse a good model to understand human diseases. Also, mice have been modified genetically for biomedical research purposes.

The heart is the first organ to be formed in order to supply adequate nourishment to the developing embryo (Vincent and Buckingham, 2010). The cardiac myoarchitecture formation undergoes multiple and coordinated morphogenetic processes, such as the establishment cardiac polarity which is mainly regulated by the third body axes (L/R) (Francis et al., 2012). Therefore, understanding the intricate heart development at the morphogenetic level is crucial to find the causes of congenital heart diseases, which are the most common type of birth defects in humans (Garne et al., 2012), and for the identification of new specific targets for the treatment of cardiac failures.

4.1 Targeted inactivation of Cerl2 leads to left ventricular cardiac hyperplasia

It was reported that ~ 40% of the *Cerl2*$^{-/-}$ mice display L/R axis randomized and a significant mortality rate within a few hours after birth, mostly due to cardiac defects (Marques et al., 2004). In addition, preliminary results revealed a large increase in the left ventricular myocardial walls in neonates where the laterality abnormalities were not evidenced. Therefore, through observation of the organs positioning, histological and echocardiographic analysis, we defined two groups of *Cerl2 null* mutants, namely with laterality defects (+LD) and without laterality defects (-LD). In order to assess the endogenous role of *Cerl2* in cardiogenesis, we analyzed the cardiac phenotypes presented in -LD *Cerl2*$^{-/-}$ at the level of cellular growth and the signaling pathways in which Cerl2 has been proposed to be involved. At midgestation, the position of the organs and their respective lobules, such as the lungs and liver, are established, allowing us to identify the animals displaying LD from midgestation until the early postnatal age (P0). During cardiac looping (E8.5 – E10.5), the myocardium becomes divided into two layers, the trabeculae and the compact, with singular characteristics being possible to distinguish them (Ben-Shachar et al., 1985; Risebro and Riley, 2006). The

trabeculae are myocardial projections outlined by endocardial cells and the compact layer is an organized multilayer that comprises the outmost ventricular region (Ieda et al., 2010). Furthermore, at cellular level, the cardiomyocytes that compose the compact layer have higher proliferative and low differentiation capacities and the reverse is found in trabeculae (Rumiantsev and Bruce, 1991).

At midgestation, the compaction process occurs, in which the trabecular layer contributes, through condensation towards the compact myocardial wall, to the majority of the increase in myocardial thickness during cardiogenesis (Wessels and Sedmera, 2003; Pennisi et al., 2003). In order to evaluate the marked increase of myocardium previously found in preliminary studies with *Cerl2 null* neonates, we measured both layers slightly before and after the compaction process (E13 and E15, respectively). At E13, accurate histomorphometry revealed that the right and left ventricular compact layer thickness of *Cerl2*$^{-/-}$ are equal among themselves and seems not to differ from the respective WT ventricles. This result is in accordance with literature which reveals that before the compaction process, both ventricles show similar thickness (Sedmera et al., 2000; Risebro and Riley, 2006). However, *Cerl2*$^{-/-}$ embryos displayed increased LV trabecular expansion suggesting increase in the compact layer after the compaction process. At E15, we observed that only the left ventricular compact myocardium was enlarged in *Cerl2*$^{-/-}$ when compared with WT, concluding that the trabeculae enhance significantly the LV thickness. Additionally, we also observed that the trabecular layer is increased in the RV of the *Cerl2 null* mutant. This particular finding in the RV may indicate a failure in right ventricular compaction, which ultimately results in the thinning of the RV myocardium, however this phenotype was not found. Studies have demonstrated that the endocardium and epicardium regulate the myocardial growth before the compaction process (E9.5-E12.5) (Lai et al., 2010; Mikawa and Brand, 2010). Therefore, signals from the endocardium and epicardium are crucial to prevent excessive trabeculation by allowing trabeculae maturation and promoting an increase in thickness in the compact layer. Such signals come for instance from ADAMTS1, member of the matrix metalloproteinase family (Stankunas et al., 2008) and MIB1 (mindbomb homolog 1), which encodes an E3 ubiquitin ligase promoting endocytosis of the NOTCH ligands DELTA and JAGGED (Luxán et al., 2013). Meanwhile, *Fgf-9* is expressed in the epicardium and its deletion leads to an hypoplasic and dilated heart in mice (Lavine et al., 2005). Although we don't know the reason by which *Cerl2*$^{-/-}$ presented increased trabeculation slightly before the compaction process, we postulate that a coordinate mechanism between endo- and epicardium is active in order to prevent the excessive trabeculation and subsequently

originating the thick compact layer, which provides the extensive muscular power required onwards to heart development. Measurements in neonatal hearts confirmed the preliminary results where *Cerl2*$^{-/-}$ showed increased IVS and LV myocardial thickness. Furthermore, we revealed that a regional increase of LV myocardial walls in absence of *Cerl2* is already detected during cardiogenesis.

In order to accomplish that the LV hypertrophy found in -LD *Cerl2*$^{-/-}$ neonates is not associated with the laterality phenotype, we crossed our *null* mice with the *Mlc1v-nlacZ-24* transgenic mouse line. This transgenic line has integrated upstream of *Fibroblast Growth Factor 10* (*Fgf10*) and consequently acts as an *Fgf10* enhancer-trap showing a highly similar pattern to that of *Fgf10* i.e. a genetic marker of the RV/pulmonary ventricle (Kelly et al., 2001). In the compound *Cerl2*$^{-/-}$*::Mlc1v-nlacZ-24* mouse line, by combining our analysis of the arrangement of visceral organs with ß-galactosidase staining, which in these mutants marks the right or pulmonary ventricular position of neonatal hearts, we were able to identify the animals displaying cardiac LD. These data confirmed the results described above, where -LD *Cerl2*$^{-/-}$ presented increased myocardial thickness in the IVS and LV, indicating that left ventricular hypertrophy is independent of the LD phenotype.

Contrarily to the RV in early postnatal period, the LV develops significantly due to increased haemodynamic loading i.e. LV pressure and volume, contributing therefore to the thicker LV myocardium (Sedmera, 2010). Although the causes that determines the marked increase of the left ventricular thickness in *Cerl2 null* neonates remains unknown, we hypothesized that the regional LV phenotype presented during the development combined with the LV requirement to the cardiac function may leads to this finding. According to our knowledge, no gene's germline ablation neither conditional knockout revealed a left ventricular phenotype as the one evidenced in the target inactivation of *Cerl2*. We therefore cite some examples by which demonstrate through the specific gene deletion in the hearts leading to assortment of phenotypes that may affect the RV or the both ventricles; Gata-4 is a transcription factor with important role in the early cardiogenesis (Molkentin et al., 1997), the early conditional Gata-4 deletion by Cre recombinase driven by the Nkx2.5 cause a right ventricular hypoplasia and selective reduced proliferation in this ventricle (Zeisberg et al., 2005). In mice, the transcription factor Hand1 is expressed in segments of the linear heart tube, which ultimately contributes to form the conotruncus and left ventricle (LV) (Thomas et al., 1998). Transgenic expressing Cre under the control of the αMHC promoter excised Hand1 in the heart. Therefore, these mutants displayed defects in the left ventricle and endocardial cushions associated with de-regulated ventricular gene expression, however no

alteration in proliferation range was found (McFadden et al., 2005). The conditional deletion of c-Abl, the nonreceptor tyrosine kinase involved in the regulation of cell proliferation, survival, and migration, displayed cardiac hyperplasia associated with increased genes expression of cell cycle regulators and cardiac stress (Qiu et al., 2010). Smad 4 is a common mediator of Smad complexes transactivation in the nucleus (Moustakas et al., 2001), thus the selective Smad4 deletion in the cardiomyocytes causes lethality in the midgestation and the embryos display hypoplasia of ventricles due to reduced proliferation (Moustakas et al., 2001).

Since *Cerl2 null* mutants presented increased LV walls thickness, we decided to investigate the cellular growth underlying this marked cardiac muscle hypertrophy. Besides during the heart formation, the cellular mechanisms that control the proliferation, differentiation, migration, and cell death, play an important role in cardiomyocytes maturation and expansion of the ventricular chambers (Stennard and Harvey, 2010; Sedmera, 2011). Although the cell growth can be caused by physiological hyperplasia (increase in cell number) and hypertrophy (increase in cell size; Hirschy et al, 2006), some studies revealed that the major contribution to the heart size during the intrauterine period is due to the high cardiomyocyte proliferation rate (Li et al., 1996; Sedmera and Thompson, 2011). Moreover, according to literature the peaks of mitotic cardiomyocytes are detected during midgestation (E12.5) and early postnatal age (P3-P4) resulting in increased proliferation and in the formation of binucleated cardiomyocytes, respectively (Soonpaa et al., 1996; Pasumarthi and Field, 2002). Therefore, proliferative cardiomyocytes were counted and the relative cardiomyocyte's area was measured. Curiously, at E13 - E15 - P0, *Cerl2*$^{-/-}$ revealed an increased mitotic index in the LV when compared with the controls and no increase of relative cardiomycyte area was found in *Cerl2*$^{-/-}$ neonates. From those evaluations we conclude that in absence of Cerl2, the massive LV phenotype occurs due to cellular hyperplasia and not hypertrophy. This result leads us to investigate the expression of *Cerl2* during heart formation. Therefore, we performed qRT-PCR in whole WT hearts at E10.5, E13, E15, P0 and P60, where we only detected expression until around E13. Moreover, in order to obtain deep insight into the ventricular *Cerl2* mRNA expression, after microdissection we observed that WT hearts express more *Cerl2* in the LV than in the RV. Altogether, we can conclude that Cerl2 may have a specific regulatory role during formation of the left ventricular myoarchitecture, thus elucidating the differential phenotype between the ventricles in *Cerl2 null* mutants.

In order to confirm the left ventricular increase in cardiomyocyte proliferation during the period where *Cerl2* seems to be required during cardiogenesis, we quantified in embryonic hearts (E13), the relative expression of mRNA of *type D cyclins* (*D1* and *D2*) - the cell cycle regulators of G1/S phase (Li and Brooks, 1999; Ikenishi et al., 2012). We found an increase of relative *cyclin D1* (*Ccnd1*) expression in the LV of the *null* mutants. Our data confirmed that in absence of *Cerl2* there's an increase of mitotic events in the left ventricular compact myocardium.

The target deletion of Cerl2 results in a significant percentage of lethality at the early neonatal age. In order to evaluate whether the absence of *Cerl2* affects the cardiac development at early stages we quantified the relative mRNA expression of cardiac genes essential to proper heart formation (*Gata-4* and *Nkx2.5*), contraction (*alpha-Mhc* and *c-Tnt*) and indicators of stress and hypertrophy (*Anp*, *Bnp* and *Ankrd1*) at E13, E15 and P0. According to literature, the transcription factor Gata-4 interacts with Nkx2.5 in a cooperative crosstalk essential for early cardiogenesis (Durocher et al., 1997). Therefore, in embryonic *Cerl2*$^{-/-}$ hearts, we found a severe reduction of *Gata-4* and an increase of *Nkx2.5* expression levels. However, that interaction does not alter the expression of *Gata-4* - *Nkx2.5* target genes such *α-Mhc*, *ANP* and *BNP*. In addition *Mef2,* a transcriptional activator of *cTnT*, interacts cooperatively with *Gata-4* and *Nkx2.5* (Akazawa and Komuro, 2003; Vincentz et al., 2008). Despite increased Nkx2.5 expression, we observed reduced expression of *cTnT* in embryonic hearts. At E15, we detected a decreased *Nkx2.5* expression compensated by an increased *Gata-4* expression. Concomitantly, a reduction of the encoding contractile genes *α-Mhc* and *cTnT* was also detected in *Cerl2*$^{-/-}$ when compared to WT control. Interestingly the levels of *cTnT* in *Cerl2* mutants seem to be independent of the *Gata-4* - *Nkx2.5* expression during cardiogenesis suggesting that other transcription factors control the cardiac genetic program. Furthermore, at fetal stage we did not detect any alteration of *Anp* and *Bnp* expression in *Cerl2*$^{-/-}$, which indicates that the molecular mechanisms regulating the hypertrophic response in embryonic stages are not de-regulated.

In *Cerl2*$^{-/-}$ neonatal hearts, we did not find alteration in the expression on any of the structural cardiac genes (*Gata4*, *Nkx2.5*, *α-Mhc* and *cTnT*). Nonetheless, we detected increased *Bnp* expression which constitutes the hallmark of a cardiac stress gene. Other cardiac stress marker, *Ankrd1,* was recently involved with cardiomyopathy in humans (Arimura et al., 2009). In addition it has been reported that the *Ankrd1* may be associated with cardiomyocyte

proliferation (Qiu et al., 2010), although its specific role has not been completely defined. Therefore, it is possible that increased expression of *Ankrd1* may be associated with ventricular hyperplasia in *Cerl2*$^{-/-}$ neonates. Collectively our observations of alterations in the expression of essential cardiac genes may indicate a deregulation of the cardiac genetic program in *Cerl2* mutant embryos. In agreement with previous reports, the alterations of major transcription factors and their target genes may compromise the cardiomyocyte differentiation program and therefore it may lead to impaired cardiac function (Zheng et al., 2003; Clark et al., 2006).

After characterization of cardiac *Cerl2*$^{-/-}$ phenotype, we start to analyze the signaling pathways by which Cerl2 was previously reported to be involved. Cerl2 antagonize the signals from the Transforming Growth Factor (TGF) type β superfamily (Marques et al., 2004). In order to activate the Tgfβs/Nodal/Activin/Smad2 signaling, the intracellular Smad2/3 protein are phosphorylated (Schier, 2003). Then these receptor-regulated Smads interact with the co-factor Smad4 forming a transcriptional complex, which will translocate to the nucleus to regulate the downstream target genes (Shen, 2007). Our results revealed an increase of Smad2 phosphorylated (pSmad2) levels at E13 and neonatal hearts indicating that in absence of Tgfβs/Nodal/Activin antagonism more activation occurs in this signaling cascade. Although the expression of *Cerl2* is no longer detected from E13 WT hearts onwards, indicating therefore the main role of this gene during cardiogenesis, we hypothesize that the cumulative effects might explain the elevated phosphorylation of Smad2 found in *Cerl2*$^{-/-}$ neonatal hearts. Furthermore, studies have demonstrated a bimodal role of Tgfβs/Nodal/Activin/Smad2 signaling activation to the heart formation. First, Nodal/Cripto are responsible for mesodermal and endodermal induction to promote cardiac induction and late, Tgfβs control cardiomyocytes differentiation activating Smad2 phosphorylation as demonstrated by in vitro studies with mouse embryonic stem cells (Parisi et al., 2003; Kitamura et al., 2007; Cai et al., 2012). In injured adult mouse hearts, the Smad2 activation indicate that Tgfβs plays a relevant role as a mediator in the cardiac pathogenesis and ventricular remodeling (Euler-Taimor and Heger, 2006; Bujak and Frangogiannis, 2007). Taken together, we can conclude that the Tgfβs/Nodal/Activin/Smad2 signaling cascade is ectopically sustained in neonatal *null* mutants hearts and this finding may be responsible for the cardiac phenotype in *Cerl2*$^{-/-}$ mice.

Previous data reported that Xenopus Cerl-1 protein binds to Xnr-1 (Xenopus Nodal-related-1), Bmp and XWnt-8 (Piccolo et al., 1999). However, in mouse Cer-l binds to Nodal and Bmp4 but does not inhibit Wnt signals confirming that Cerl-1 protein in mouse has biochemical activities from Xenopus Cerl-1 (Belo et al., 2000). Furthermore, Cerl-2 was also shown to bind to Nodal and to Bmp4 (Marques et al., 2004). Recent emerging data revealed that *Cerl2* mRNA is regulated posttranscriptionally by Wnt3 in the left side of the node leading to *Cerl2* degradation and therefore contributing to the asymmetrical expression of *Cerl2* (Nakamura et al., 2012). Moreover, Cerl2 inhibits the Wnt self-activating loop, then establishing a double negative loop between Cerl2 and Wnt (Nakamura et al., 2012; Kitajima et al., 2013). In addition, it was recently reported that the ß-catenin protein is symmetrically expressed in both ventricles, and thus the Wnt canonical/ß catenin signaling promotes the proliferation of cardiomyocytes mainly in the compact layer by increased *D-type cyclin 1* and *2* levels (Buikema et al., 2013). To the best of our knowledge, no data was reported considering the conexion between *Cerl2* and *Wnt* canonical/*ß-catenin* signals in the heart. Since we showed that the LV expresses *Cerl2* during midgestation, we hypothesize that in *Cerl2*$^{-/-}$, Wnt self-activating loop is increased and then may stimulate the proliferation more in the LV than the RV, however experiments need to confirm this interlinked feedback loops connecting Cerl2 and Wnt.

Our study provides the first evidence of the function of Cerl2 during cardiac development independently of its known role in establishment of the L/R asymmetry. Despite of the extensive results here described, we still need to elucidate the possible links between Cerl2 and Wnt canonical/ß catenin signaling during cardiogenesis and the sustained increased phosphorylation levels of Smad2 when *Cerl2* in no longer present.

4.2 Transthoracic echocardiography reference values in juvenile and adult 129/Sv mice.

Embryonic stem cells derived from 129 mice strain are extensively used to generate targeted mutants (Simpson et al., 1997). Nevertheless, the influence of each strain background on gene expression has become particularly apparent and therefore the establishment of reference values for each strain is useful nowadays.

To this matter, we established reference values to juvenile (3 weeks) and young adult mice (8weeks) through transthoracic echocardiography. We also expanded our experience in

echocardiography by performing it in neonates, who due to smaller size, we were not able to maintain the control of body temperature, respiration and heart rates resulting in shortened times for execution of this technique. This imaging diagnostic technique have been currently used in follow-up studies of therapeutic treatments and after cardiac intervention i.e. induction of myocardial infarction and aorta constriction as well (Rottman et al., 2007; Benavides-Vallve et al., 2012). Moreover, the use of non-invasive echocardiography to evaluate the cardiac function and the LV morphometry has become a very common technique since it presents several advantages such as readiness and low cost if compared to computed tomography (CT) and magnetic resonance imaging (MRI) (Nahrendorf et al., 2007; Gao et al., 2011; van Nierop et al., 2013). From this work, we created an internal standard protocol to assess the cardiovascular structures and to evaluate the cardiac function from neonatal to adult mice, considering the relation isoflurane concentration and body weight.

Even though anesthetic agents are required for experimental interventions and phenotypic evaluations, adult mice have been reported to have reduced cardiac function under these conditions (Rottman et al., 2003). However, the effects of isoflurane are modest and the evaluation of the cardiac function is more reproducible in when compared with another inhalants or with injectable anesthetics (Janssen et al., 2004). Nevertheless, the prolonged isoflurane use causes neurodegeneration as demonstrated in neonates (P7, 6 hours of 1,5% isoflurane exposure during 7 days) (Loepke et al., 2009). Furthermore, our reference values must only be applied to male and with the same isoflurane concentration (1,5-2%). As previously reported, using C57Bl6 and BalbC strains age-matched (1-2% isoflurane) revealed gender-related differences in left ventricular systolic and diastolic function (Baumann et al., 2008). Moreover, female mice revealed the predisposition to develop heart failure. A recent study demonstrated that the cardiac energy substrate metabolism might be implicated (Foryst-Ludwig et al., 2011).

4.3 The assessment of the cardiac function in *Cerl2*$^{-/-}$ mice

Cerl2 mutants present within the first day after birth a significantly reduced percentage of survival when compared to WT. Moreover, here we report the possible cause of death such as the massivly increased LV walls' thickness caused by hyperplasia. Furthermore, this phenotype is associated with impaired cardiac function.

From the early neonatal period to adult age, some developmental processes still occur in the heart, such as the growth of the cardiac muscle, mostly due to an increase of cardiomyocyte size (Ahuja et al., 2007). In addition, recent studies indicate a potential proliferative capacity of cardiomyocytes at postnatal ages in mice and humans (Porrello et al., 2011; Mollova et al., 2012). From a physiological point of view, a progressive increase of cardiac workload is required to sustain the dramatic demand of the animal's metabolism (Greyson, 2010). In this context, whether the surviving *Cerl2*$^{-/-}$ mutants develop further the gross hypertrophy and impaired systolic function remains unknown. Therefore, in order to evaluate the morpho-physiology in *Cerl2* null mutants, we performed echocardiography in neonates.

The LV mass, which is commonly used to indicate a cardiac status, i.e cardiac stress and hypertrophy (Collins et al., 2001; Ghanem et al., 2006) was calculated and our results showed an increase of the LV mass index in *Cerl2*$^{-/-}$ neonates. According with the histomorphometry described above combined with the LVM measurements, our data revealed that the in absence of *Cerl2* the neonates displayed increase of the LV walls. Also in the early neonatal age, *Cerl2*$^{-/-}$ display decreased heart rate and left ventricular systolic function as evidenced in systolic filling parameters, such as aortic peak velocity and cardiac output index. We can conclude that in the absence of *Cerl2*, neonatal mice display left ventricular systolic dysfunction indicating that blood is not being pumped optimally from this ventricle. Furthermore, the assessment of the LV systolic function provides valuable information in diagnosis of cardiac disease (Hartley et al., 2002; Baumann et al., 2008) since these animals presented increased thickness in LV walls associated with high mortality in the first day after birth.

The accurate establishment of reference values using 129Sv strain background together with the findings obtained from *Cerl2*$^{-/-}$ characterization during cardiac development and at early neonatal age, lead us to follow the *null* mutant until the young adult age in order to evaluate the morpho-volumetric and cardiac function phenotype.

The monitoring of the *Cerl2* null mutants over the time revealed that the neonates with LD phenotype died within the first day of birth confirming previous results (Marques et al., 2004) and (in this thesis, on chapter 3.2). Although, +LD *Cerl2*$^{-/-}$ did not show statistically significant differences in LVM index and global cardiac function parameters when compared with surviving WT controls, the presence of LD has been reported as incompatible with long

lifespan (Ramsdell, 2005; Shiraishi and Ichikawa, 2012). Moreover, we assume that the diversity of the phenotypes such as *situs inversus*, isomerisms and heterotaxia contributes to the variability of results observed in cardiac morphometry and physiology. The –LD *Cerl2*$^{-/-}$ neonates, which died in the first day of life, displayed reduced cardiac function and revealed a tendency to increase the LVMi through echocardiographic analysis. In addition, during the follow up study, we observed that a number of *null* mutants survived until the end of experiment (P60) also presented impaired cardiac function in neonatal age. Based on our findings we revealed that the first day of birth is critical to *Cerl2*$^{-/-}$ neonates without LD, however what determines the death/survival of these animals remains unknown.

Follow-up analysis revealed that *Cerl2* mutants displayed distinct regional morphometric IVS and LV walls over the time. However, when compared with WT, *Cerl2*$^{-/-}$ displayed thinner LVAW and LVPW at time point P30 and P60, respectively. Moreover, the LV wall thinning did not compromise the LVID neither the FS%. The results revealed a singular LV phenotype is found in *null* mutants from juvenile age indicating that the LV systolic function seems to be recovered.

From early to later postnatal age, the external and internal aortic diameters increase due to increased SV and CO. Contrarily to WT, the end-systolic aortic lumen was maintained in *Cerl2*$^{-/-}$ from P30 to P60 and therefore it may affect the cardiac afterload. In humans with diabetes, hypertension and dilated cardiomyopathy, increased blood pressure is associated with reduced arterial diameter and compliance, leading to cardiac hypertrophy and systolic or diastolic dysfunction (Vinereanu et al., 2003). *Elastin* heterozygous mice revealed the same pattern of phenotypes as the ones found in humans (Le et al., 2011; Le and Wagenseil, 2012). Therefore the link between human and mice may be due to elasticity and endurance of arterial wall in some diseases (Wagenseil and Mecham, 2009). Although the SV and CO were maintained in *Cerl2*$^{-/-}$ over the ageing, the indexed values revealed no differences between the genotypes at P30 and at P60 suggesting that the parameters obtained from aorta did not interfere in systolic function.

In order to avoid statistical assumption, we also evaluated the SV assuming the ellipsoidal shape of the heart through the end-systolic and diastolic LV volumes. Although the LV volumes, SV and CO in *Cerl2 null* mutant did not follow the WT in postnatal ages analyzed,

when indexed these parameters resulted in reduced SVi and COi at P60. These data indicate that actually the systolic function is partially recovered in *Cerl2*$^{-/-}$ animals.

According to the literature, the HR stabilizes at P50 on mice from C57Bl6 background and at P60 on CD1 and 129Sv strains, respectively (Wiesmann et al., 2000; Tiemann et al., 2003; Stypmann et al., 2006; Hinton et al., 2008; Vinhas et al., 2013). The LV mass, LV volume, SV and CO increase with ageing, although the EF% is constant over time (Schneider et al., 2008). As expected the HR from P30 to P60 was maintained in the genotypes. Moreover the EF%, FS% and FAC%, were also maintained with aging indicating that these systolic parameters are similar between *Cerl2 null* mutants and controls.

We analyzed also the expression of the hypertrophy markers such as *Anp*, *Bnp* and *Ankrd1* (Nishikimi et al., 2006; Das et al., 2009; Mikhailov and Torrado, 2008; Qiu et al., 2010) at P60. Our results revealed no differences in the expression of these genes between WT and *Cerl2*$^{-/-}$. In contrast, *null* neonates showed increased *Bnp* and *Ankrd1* expression (in this thesis, on chapter 3.2). Taken together, these data indicate that young adult *Cerl2* mutants did not shown cardiac stress and therefore they seem to recover the cardiac performance likely demonstrated with the cardiac global and most of the systolic parameters.

The diastolic parameters are important to indicate diastolic dysfunction and it often precedes the onset of systolic dysfunction (Zhou et al., 2003). The evaluation of the ventricular diastolic filling did not reveal differences between the genotypes over time indicating normal diastolic function in *null* mutants.

This study revealed that surviving *Cerl2*$^{-/-}$ animals recover from cardiac dysfunction evidenced with the diastolic and most of the systolic parameters. Importantly, each animal served as its own control, providing a powerful statistical analysis and substantially reducing the number of mice required to conduct such a follow-up study. We conclude that these animals must adapt in order to improve the cardiac function during the first months of life. In addition, this work brings detailed and useful information about the improvement of *Cerl2*$^{-/-}$ cardiac function.

5 Concluding Remarks

The results presented in this work revealed the endogenous cardiac role of *Cerl2* through detailed characterization of the *Cerl2*$^{-/-}$ phenotype during the intra-uterine and early neonatal age. Furthermore, we demonstrated that the left ventricular phenotype in *Cerl2 null* mutants is independent of the role of *Cerl2* during the establishment of the L/R asymmetry.

We demonstrated that *Cerl2* is expressed in the embryonic heart mainly in the LV indicating its function during cardiogenesis. Therefore, the absence of *Cerl2* severely affects the thickness of the LV myocardium, the myocytes proliferation, the expression of cardiac genes as well as cardiac function.

Since Cerl2 is a dedicated antagonist of TGFßs/Nodal/Activin/Smad2 signaling, we observed an increase of Smad2 phosphorylated levels in the *Cerl2*$^{-/-}$ hearts, indicating therefore that ectopic and sustained activation of this signaling pathway may be responsible for the cardiac phenotype in *Cerl2 null* mutants.

The –LD *Cerl2 null* shared the same phenotype such a decreased systolic function in first day of birth. However, we do not known the reasons by which determines the survival and recovering cardiac function in some –LD *Cerl2*$^{-/-}$ as revealed through follow up studies.

We suggest *Cerl2 null* mutant mice as a model to understand the intrinsic mechanism behind the recovery of cardiac function may provide valuable insights towards the identification of potential therapeutic approaches to treat heart failure.

Through systematic morphometry, cellular growth and molecular approaches during embryogenesis and early neonatal age, this study uncovers an important break-through in the role of Cerl2 in the regulation of growth factor activity in cardiogenesis and ultimately use this knowledge to understand the morphogentic mechanisms underlying Congenital Heart Disease.Heart.

6 Future Perspectives

The work presented in this thesis was focused on the definition of the endogenous role of Cerl2 in cardiogenesis, separate from its known role during establishment of L/R asymmetry. The results presented here represent a step forward in the characterization of the role of Cerl2 in heart development. Nonetheless, some questions on the role of Cerl2 remain to be answered. With this in mind, I describe a number of suggestions that may be relevant to deepen the understanding Cerl2 function and its role in the regulation of signaling pathways during cardiac formation.

As complement to the characterization of the role of Cerl2 during the heart formation, presented on chapter 3.2:

Here, it has been demonstrated that *Cerl2* is expressed in the LV until the midgestation (E13). Therefore, it would be informative to show by immunohistochemical analysis the cellular localization of Cerl2 protein in the heart, in particular its localization in myocytes and non-myocytes (fibroblast, vascular smooth muscle cells) and the respective layers i.e. endo-; epi- and myocardium in order to dissect more clearly the role of this gene in heart formation.

We demonstrated the *Cerl2 null* mutants have de-regulated expression of cardiac genes in the heart during the embryogenesis. Since most defects in the *Cerl2* mutants absent of LD are observed in the LV and that until midgestation *Cerl2* is preferentially expressed therein, it would be interesting to separate LV and RV from the mutant hearts to determine whether the expression of cardiac genes, i.e. *Gata-4*, *Nkx2.5*, *c-TNT*, *α-Mhc,* are more severely affected on the LV.

The high magnification of the transverse sections stained with H&E seems to show irregular orientation of the muscle and fibers (Chapter 3.2 Figure 3.5 A',B'). Therefore, transmission electron micrographs could be helpful to analyze the arrangement of the sarcomeres in *Cerl2* mutant hearts and determine whether absence of Cerl2 leads to defective rearrangement of the cardiac cells at the level of the contractile machinery.

The microdissection of the ventricles (RV and LV) followed by tissue dissociation through collagenase and subsequent isolation of specific cardiac cells (myocytes and non-myocytes) using Fluorescence-activated cell sorting (FACS) forward scatter may be useful to the next experiments:

1. It has been demonstrated here that embryonic and neonatal *Cerl2*$^{-/-}$ hearts have increased Smad2 activation. In order to quantify which ventricle and more specifically which cardiac cells express more phospho-Smad2, it would be interesting to perform the dissociation of ventricular cells to study precisely where does the ectopic activation of Tgfβs/Nodal/Activin-Smad2 signaling occurs in the *Cerl2* mutant heart. Alternatively, this could be performed as well trough immunohistochemistry if we would dispose of a good antibody to detect phosphorylated Smad2 in sections.
2. It is known that the heart grows through physiological hyperplasia and hypertrophy. However, the measurement of cell boundaries in embryonic hearts is very difficult. Therefore, in order to determine the physiological/pathological hypertrophy during cardiac formation, measuring cell size through FACS could be helpful to determine cardiomyocyte size at E13 and E15 in *Cerl2* mutants. In addition, it would be also useful to quantify the number of cardiac fibroblasts. This non-cardiac cellular lineage is able to interact with cardiomyocytes and affect their function (Ieda et al., 2010). With these experiments we would be able to understand if absence of Cerl2 affects specifically any of these cardiac cell types.
3. In addition, having the two isolated populations of myocytes and non-myocytes, it would be possible to cultivate them and evaluate cellular processes such as cell proliferation and behavior over the time. This would allow us to determine which cardiac cell type is more affected by the absence of *Cerl2*.

It has been recently reported that Wnt is required to regulate *Cerl2* expression in crown cells in the embryonic node. Furthermore, Cerl2 inhibits the Wnt self-activating loop, thus establishing a interlinked feedback loop (Nakamura et al., 2012; Kitajima et al., 2013). Recent data revealed that Wnt signaling through ß-catenin is responsible for controlling the ventricular cardiomyocyte proliferation mainly in the compact myocardium (Buikema et al., 2013). To investigate the role of this signaling in *Cerl2*$^{-/-}$ during heart formation, it would be interesting to evaluate the presence of active ß-catenin in the right and left ventricular cardiomyocytes. This would allow us to understand if Cerl2 is involved in the regulation of Wnt signaling during ventricular development.

Here, we have demonstrated that Cerl2 is important for correct development of the LV. Recent studies have been reported showing that the endodermal marker, Cerl1, in murine embryonic stem cells is able to induce cardiomyocyte differentiation through inhibition of

Nodal and Bmps (Cai et al., 2013; D'Aniello et al., 2013). Using Mouse Embryonic Stem Cells (mESCs) obtained from *Cerl2*$^{-/-}$ mouse and respective WT control, we could evaluate if *Cerl2*$^{-/-}$ mESC can produce cardiogenic progenitors and if those cells are able to terminally differentiate into cardiac cells (myocytes and non-myocytes). FACS would be used to sort those cells for quantification of cardiac cellular diversity. Furthermore, in order to assess the effect of the Cerl2 overexpression in cardiogenesis, WT mESC could be generated to overexpress Cerl2. This would allow us to elucidate if with the gain and/or loss-of-function of Tgfβs/Nodal/Activin-Smad2 signaling antagonist Cerl2, the mESC commit to cardiac progenitor and to cardiomyocyte fates.

In contrast to *Cerl1* mutant mice where the cardiac formation proceeds normally (Belo et al., 2000), we demonstrated that *Cerl2*$^{-/-}$ present abnormal heart formation, de-regulation of cardiac markers and impaired systolic function. It would be of interest to cross both knockout mouse lines, creating a double *null* mutant line *Cerl1::Cerl2* to study the effects caused by the absence of the both Cer family members in mice. This would allow us to understand if there is any functional redundancy between these two members of the Cer family during mouse (heart) development.

We believe that the cardiac-specific deletion of *Cerl2* using the Cre-loxP system would be relevant to determine its precise contribution during heart formation. For specific Cerl2 deletion in the cardiomyocytes, we would generate a Cerl2 homozygous floxed mice that would then be intercrossed with one mouse strain carrying the Cre recombinase gene under control of the cardiac homeobox gene Nkx2-5 (Stanley et al., 2002) or alfa-MHC (Agah et al., 1997). Briefly, we could create a conditional knockout (CKO) of the *Cerl2* using the same mutation used to target deletion of Cerl2 germline (Marques et al., 2004) where the second exon in this case was replaced by a LacZ cassete. For CKO, the second exon of Cerl2 should be flank by loxP sites, whose excision trough Cre-mediated recombination would create a non-functional protein. These mice would provide us the ultimate proof that Cerl2 is required for proper heart development independently of the role of Cerl2 during establishment of L/R asymmetry.

As complement to the cardiac function characterization in *Cerl2*$^{-/-}$ during postnatal age presented on chapter 3.3:

The evaluation of cardiac function in *Cerl2* mutants during the postnatal age revealed that the dimensions of the LV of the *Cerl2* mutant hearts evolve differently from those of the WT, i.e. in contrast to the WT, the *Cerl2*$^{-/-}$ showed with ageing a thinner LVAW and LVPW. Using speckle-tracking echocardiography (STE) it would be possible to investigate the velocity and direction of myocardial movements, assessing the B-mode images from the left ventricular segmental myocardial strain (circumferential and radial strain) (Peng et al., 2009; Mor-Avi et al., 2011). This would allow us to assess the regional dimensions of LV wall during the cardiac cycles and therefore we could identify both quantitative and qualitative information about tissue deformation and motion.

Moreover, we have demonstrated that the surviving *Cerl2*$^{-/-}$ improve the relative expression of stress cardiac markes (*Bnp* and *Ankrd1*) and most of the systolic function. Our data showed Cerl2 null mutant in adult age are able to partially recovery of the pathological hypertrophy observed at neonatal age. Nevertheless, we showed that the preload seems to be affected in these animals. In order to assess other preload parameters we could evaluate the expression of genes of contractile proteins, like actin, myosins and tropomyosins, of the cardiomyocyte electro-excitability (Patch-Clamp measurements) (Toischer et al., 2010) and measure LV pressure-volume loops (pressure-volume conductance catheter) (Pacher et al., 2008). This would provide us a better perception of myocardium function and elasticity and, therefore, allow us to understand the hemodynamic load in *null* mutants. Moreover, detailed evaluation of cardiomyocyte length and stretch isolated from the IVS and LV walls could be helpful to obtain a better understanding of the regional electro-physiology in *Cerl2*$^{-/-}$ heart.

At P60 *Cerl2* mutants showed improvement of the cardiac function evidenced at early neonatal age. Eventually, it would be interesting to induce a pathological hypertrophy through aortic constriction (ascendant, transversal) to determine whether the *Cerl2*$^{-/-}$ adult mice are able to adapt to LV hypertrophy and cardiac dysfunction of pathological origin.

The prosecution of this work would help to further clarify the cardiac role of Cerl2 during embryogenesis and postnatal age, providing valuable information to better understand the intricate molecular mechanisms underlying the congenital heart diseases and heart failure.

7 References

Abu-issa, R., Kirby, M.L., 2007. Heart Field : From Mesoderm to Heart Tube. Annu. Rev. Cell Dev. Biol. 23, 45–68.

Abu-Issa, R., Smyth, G., Smoak, I., Yamamura, K., Meyers, E.N., 2002. Fgf8 is required for pharyngeal arch and cardiovascular development in the mouse. Development 129, 4613–4625.

Agah, R., Frenkel, P.A., French, B.A., Michael, L.H., Overbeek, P.A., Schneider, M.D., 1997. Gene Recombination in Postmitotic Cells. J. Clin. Invest. 100, 169–179.

Ahuja, P., Sdek, P., Maclellan, W.R., 2007. Cardiac Myocyte Cell Cycle Control in Development, Disease, and Regeneration. Physiol. Rev. 87, 521–544.

Ai, D., Fu, X., Wang, J., Lu, M., Chen, L., Baldini, A., Klein, W.H., Martin, J.F., 2007. Canonical Wnt signaling functions in second heart field to promote right ventricular growth. PNAS 104, 9319–9324.

Akazawa, H., Komuro, I., 2003. Roles of cardiac transcription factors in cardiac hypertrophy. Circ. Res. 92, 1079–1088.

Anderson, R.M., 2012. The Gross Physiology of the Cardiovascular System.

Arai, A., Yamamoto, K., Toyama, J., 1997. Murine Cardiac Progenitor Cells Require Visceral Embryonic Endoderm and Primitive Streak for Terminal Differentiation. Dev. Dyn. 353, 344–353.

Arimura, T., Bos, J.M., Sato, A., Kubo, T., Okamoto, H., Nishi, H., Harada, H., Koga, Y., Moulik, M., Doi, Y.L., Towbin, J.A., Ackerman, M.J., Kimura, A., 2009. Cardiac ankyrin repeat protein gene (ANKRD1) mutations in hypertrophic cardiomyopathy. J. Am. Coll. Cardiol. 54, 334–342.

Babu, D., Roy, S., 2013. Left − right asymmetry : cilia stir up new surprises in the node. Open Biol. 3, 1–10.

Bamford, R., Roessler, E., Burdine, R.D., Saplakoglu, U., dela Cruz, J., Splitt, M., Towbin, J., Bowers, P., MArino, B., Schier, A.F., Shen, M.M., Muenke, M., Casey, B., 2000. Loss-of- function mutations in the EGF-CFC gene CFC1 are associated with hu man left-right laterality defects. Nature. 26, 365–369.

Barrick, C.J., Rojas, M., Schoonhoven, R., Smyth, S.S., Threadgill, D.W., 2007. Cardiac response to pressure overload in 129S1/SvImJ and C57BL/6J mice : temporal- and background-dependent development of concentric left ventricular hypertrophy. Am. J. Physiol. Heart Circ. Physiol. 292, H2119–H2130.

Baumann, P.Q., Sobel, B.E., Tarikuz Zaman, A.K.M., Schneider, D.J., 2008. Gender-dependent differences in echocardiographic characteristics of murine hearts. Echocardiography 25, 739–748.

Becker, J.R., Deo, R.C., Werdich, A.A., Panàkovà, D., Coy, S., MacRae, C.A., 2011. Human cardiomyopathy mutations induce myocyte hyperplasia and activate hypertrophic pathways during cardiogenesis in zebrafish. Dis. Model. Mech. 4, 400–410.

Beddington, R.S., Robertson, E.J., 1999. Axis development and early asymmetry in mammals. Cell 96, 195–209.

Beddington, R.S.P., 1994. Induction of a second neural axis by the mouse node. Development 120, 613–620.

Beddington, R.S.P., Robertson, E.J., 1998. Anterior patterning in mouse. Trends Genet. 14, 277–284.

Belo, J.A., Bachiller, D., Agius, E., Kemp, C., Borges, A.C., Marques, S., Piccolo, S., De Robertis, E.M., 2000. Cerberus-like is a secreted BMP and nodal antagonist not essential for mouse development. Genesis 26, 265–270.

Belo, J.A., Bouwmeester, T., Leyns, L., Kertesz, N., Gallo, M., Follettie, M., De Robertis, E.M., 1997. Cerberus-like is a secreted factor with neutralizing activity expressed in the anterior primitive endoderm of the mouse gastrula. Mech. Dev. 68, 45–57.

Belo, J.A., Silva, A.C., Borges, A.-C., Filipe, M., Bento, M., Gonçalves, L., Vitorino, M., Salgueiro, A.-M., Texeira, V., Tavares, A.T., Marques, S., 2009. Generating asymmetries in the early vertebrate embryo: the role of the Cerberus-like family. Int. J. Dev. Biol. 53, 1399–1407.

Ben-Shachar, G., Arcilla, R.A., Lucas, R. V, Manasek, F.J., 1985. Ventricular trabeculations in the chick embryo heart and their contribution to ventricular and muscular septal development. Circ. Res. 57, 759–766.

Benavides-Vallve, C., Corbacho, D., Iglesias-Garcia, O., Pelacho, B., Albiasu, E., Castaño, S., Muñoz-Barrutia, A., Prosper, F., Ortiz-de-Solorzano, C., 2012. New strategies for echocardiographic evaluation of left ventricular function in a mouse model of long-term myocardial infarction. PLoS One 7, e41691.

Bentham, J., Bhattacharya, S., 2008. Genetic mechanisms controlling cardiovascular development. Ann. N. Y. Acad. Sci. 1123, 10–19.

Bento, M., Correia, E., Tavares, A.T., Becker, J.D., Belo, J.A., 2011. Identification of differentially expressed genes in the heart precursor cells of the chick embryo. Gene Expr. Patterns 11, 437–447.

Bers, D.M., 2002. Cardiac excitation–contraction coupling. Nature 415, 198–215.

Bersell, K., Arab, S., Haring, B., Kühn, B., 2009. Neuregulin1/ErbB4 signaling induces cardiomyocyte proliferation and repair of heart injury. Cell 138, 257–270.

Biben, C., Weber, R., Kesteven, S., Stanley, E., McDonald, L., Elliott, D.A., Barnett, L., Koentgen, F., Robb, L., Feneley, M., Harvey, R.P., 2000. Cardiac Septal and Valvular

Dysmorphogenesis in Mice Heterozygous for Mutations in the Homeobox Gene Nkx2-5. Circ. Res. 87, 888–895.

Bochmann, L., Sarathchandra, P., Mori, F., Lara-Pezzi, E., Lazzaro, D., Rosenthal, N., 2010. Revealing new mouse epicardial cell markers through transcriptomics. PLoS One 5, e11429.

Böttcher, R.T., Niehrs, C., 2005. Fibroblast growth factor signaling during early vertebrate development. Endocr. Rev. 26, 63–77.

Bouwmeester, T., Kim, S.-H., Sasai, Y., Lu, B., De Robertis, E.M., 1996. Cerberus is a head-inducing secreted factor expressed in the anterior endoderm of Spemann's organizer. Nature 382, 595–601.

Bowers, P.N., Brueckner, M., Yost, H.J., 1996. Laterality disturbances. Pediatr. Cardiol. 6, 53–62.

Brade, T., Männer, J., Kühl, M., 2006. The role of Wnt signalling in cardiac development and tissue remodelling in the mature heart. Cardiovasc. Res. 72, 198–209.

Brand, T., 2003. Heart development : molecular insights into cardiac specification and early morphogenesis. Dev. Biol. 258, 1–19.

Brennan, J., Norris, D.P., Robertson, E.J., 2002. Nodal activity in the node governs left-right asymmetry service Nodal activity in the node governs left-right asymmetry. Genes Dev. 2339–2344.

Brunson DB, 1997. Pharmacology of inhalational anesthetics, in: Anesthesia and Analgesia in Laboratory Animals. pp. 29–41.

Buckingham, M., Meilhac, S., Zaffran, S., 2005. Building the mammalian heart from two sources of myocardial cells. Nat. Rev. Genet. 6, 826–835.

Buikema, J.W., Mady, A.S., Mittal, N. V, Atmanli, A., Caron, L., Doevendans, P.A., Sluijter, J.P.G., Domian, I.J., 2013. Wnt/β-catenin signaling directs the regional expansion of first and second heart field-derived ventricular cardiomyocytes. Development 140, 1–12.

Bujak, M., Frangogiannis, N.G., 2007. The role of TGF-beta Signaling in Myocardial Infarction and Cardiac Remodeling. Cardiovasc. Res. 74, 184–195.

Cai, W., Albini, S., Wei, K., Willems, E., Guzzo, R.M., Tsuda, M., Giordani, L., Spiering, S., Kurian, L., Yeo, G.W., Puri, P.L., Mercola, M., 2013. Coordinate Nodal and BMP inhibition directs Baf60c-dependent cardiomyocyte commitment. Genes Dev. 27, 2332–2344.

Cai, W., Guzzo, R.M., Wei, K., Willems, E., Davidovics, H., Mercola, M., 2012. A Nodal-to-TGFβ cascade exerts biphasic control over cardiopoiesis. Circ. Res. 111, 876–881.

Camelliti, P., Borg, T.K., Kohl, P., 2005. Structural and functional characterisation of cardiac fibroblasts. Cardiovasc. Res. 65, 40–51.

Cameron, V.A., Ellmers, L.J., 2003. Minireview: Natriuretic Peptides during Development of the Fetal Heart and Circulation. Endocrinology 144, 2191–2194.

Chen, G., Li, Y., Tian, J., Zhang, L., Jean-Charles, P., Gobara, N., Nan, C., Jin, J.-P., Huang, X.P., 2012. Application of echocardiography on transgenic mice with cardiomyopathies. Biochem. Res. Int. 2012, 1-9.

Chen, H., Shi, S., Acosta, L., Li, W., Lu, J., Bao, S., Chen, Z., Yang, Z., Schneider, M.D., Chien, K.R., Conway, S.J., Yoder, M.C., Haneline, L.S., Franco, D., Shou, W., 2004. BMP10 is essential for maintaining cardiac growth during murine cardiogenesis. Development 131, 2219–2231.

Chen, J., Kubalak, S.W., Chien, K.R., 1998. Ventricular muscle-restricted targeting of the RXR α gene reveals a non-cell- autonomous requirement in cardiac chamber morphogenesis. Development 125, 1943–1949.

Chen, J., Murchison, E.P., Tang, R., Callis, T.E., Tatsuguchi, M., Deng, Z., Rojas, M., Hammond, S.M., Schneider, M.D., Selzman, C.H., Meissner, G., Patterson, C., Hannon, G.J., Wang, D., 2008. Targeted deletion of Dicer in the heart leads to dilated cardiomyopathy and heart failure. Proc. Natl. Acad. Sci. 105, 2111–2116.

Christoffels, V.M., Burch, J.B.E., Moorman, A.F.M., 2004. Architectural plan for the heart: early patterning and delineation of the chambers and the nodes. Trends Cardiovasc. Med. 14, 301–307.

Christoffels, V.M., Habets, P.E., Franco, D., Campione, M., de Jong, F., Lamers, W.H., Bao, Z.-Z., Palmer, S., Biben, C., Harvey, R.P., Moorman, A.F.M., 2000. Chamber formation and morphogenesis in the developing mammalian heart. Dev. Biol. 223, 266–278.

Clark, K.L., Yutzey, K.E., Benson, D.W., 2006. Transcription factors and congenital heart defects. Annu. Rev. Physiol. 68, 97–121.

Collins, K. a, Korcarz, C.E., Lang, R.M., 2003. Use of echocardiography for the phenotypic assessment of genetically altered mice. Physiol. Genomics 13, 227–39.

Collins, K.A., Korcarz, C.E., Shroff, S.G., Bednarz, J.E., Fentzke, R.C., Lin, H., Leiden, J.M., Lang, 2001. Accuracy of echocardiographic estimates of left ventricular mass in mice. Am. J. Physiol. Heart Circ. Physiol. 280, H1954–H1962.

Constantinides, C., 2012. Study of the Murine Cardiac Mechanical Function Using Magnetic Resonance Imaging : The Current Status , Challenges , and Future Perspectives, in: Practical Applications in Biomedical Engineering. pp. 343–386.

Crow, T.J., 2008. The “big bang” theory of the origin of psychosis and the faculty of language. Schizophr. Res. 102, 31–52.

D’Aniello, C., Fiorenzano, A., Iaconis, S., Liguori, G.L., Andolfi, G., Cobellis, G., Fico, A., Minchiotti, G., 2013. The G-protein-coupled receptor APJ is expressed in the second heart field and regulates Cerberus-Baf60c axis in embryonic stem cell cardiomyogenesis. Cardiovasc. Res. 100, 95–104.

Das, B.B., Raj, S., Solinger, R., 2009. Natriuretic peptides in cardiovascular diseases of fetus, infants and children. Cardiovasc. Hematol. Agents Med. Chem. 7, 43–51.

Davidson, B.P., Tam, P.P.L., 2000. The node of the mouse embryo. Curr. Biol. 10, R617–R619.

De Bold, A.J., Bruneau, B.G., Kuroski de Bold, M.L., 1996. Mechanical and neuroendocrine regulation of the endocrine heart. Cardiovasc. Res. 31, 7–18.

DeRuiter, M.C., Poelmann, R.E., Vries, I.V., Mentink, M.M.T., Groot, A.C.G., 1992. The development of the myocardium and endocardium in mouse embryos. Fusion of two heart tubes? Anat. Embryol. (Berl). 185, 461–473.

Dorey, K., Amaya, E., 2010. FGF signalling: diverse roles during early vertebrate embryogenesis. Development 137, 3731–3742.

Dorn Il, G.W., 2007. The Fuzzy Logic of Physiological Cardiac Hypertrophy. Hypertension 49, 962–970.

Dunwoodie, S.L., 2007. Combinatorial signaling in the heart orchestrates cardiac induction , lineage specification and chamber formation. Semin. Cell Dev. Biol. 18, 54–66.

Durocher, D., Charron, F., Warren, R., Schwartz, R.J., Nemer, M., 1997. The cardiac transcription factors Nkx2-5 and GATA-4 are mutual cofactors. EMBO J. 16, 5687–5696.

Euler-Taimor, G., Heger, J., 2006. The complex pattern of SMAD signaling in the cardiovascular system. Cardiovasc. Res. 69, 15–25.

Evans, S.M., Yelon, D., Conlon, F.L., Kirby, M.L., 2010. Myocardial lineage development. Circ. Res. 107, 1428–1444.

Feng, X.-H., Derynck, R., 2005. Specificity and versatility in tgf-beta signaling through Smads. Annu. Rev. Cell Dev. Biol. 21, 659–93.

Foley, A.C., Korol, O., Timmer, A.M., Mercola, M., 2007. Multiple functions of Cerberus cooperate to induce heart downstream of Nodal. Dev. Biol. 303, 57–65.

Foryst-Ludwig, A., Kreissl, M.C., Sprang, C., Thalke, B., Böhm, C., Benz, V., Gürgen, D., Dragun, D., Schubert, C., Mai, K., Stawowy, P., Spranger, J., Regitz-Zagrosek, V., Unger, T., Kintscher, U., 2011. Sex differences in physiological cardiac hypertrophy are associated with exercise-mediated changes in energy substrate availability. Am. J. Physiol. Heart Circ. Physiol. 301, H115–H122.

Fox, P.R., Sisson, D., Moise, N.S., 1999. Echocardiography and doppler imaging, in: In Textbook of Canine and Feline Cardiology. pp. 130–171.

Francis, R.J.B., Christopher, A., Devine, W.A., Ostrowski, L., Lo, C., 2012. Congenital heart disease and the specification of left-right asymmetry. Am. J. Physiol. Heart Circ. Physiol. 302, H2102–H2111.

Franco, D., Lamers, W.H., Moorman, A.F.M., 1998. Patterns of expression in the developing myocardium: towards a morphologically integrated transcriptional model. Cardiovasc. Res. 38, 25–53.

Franco, D., Meilhac, S.M., Christoffels, V.M., Kispert, A., Buckingham, M., Kelly, R.G., 2006. Left and right ventricular contributions to the formation of the interventricular septum in the mouse heart. Dev. Biol. 294, 366 – 375.

Francou, A., Saint-Michel, E., Mesbah, K., Théveniau-Ruissy, M., Rana, M.S., Christoffels, V.M., Kelly, R.G., 2013. Second heart field cardiac progenitor cells in the early mouse embryo. Biochim. Biophys. Acta 1833, 795–798.

Fuster, V., Alexander, Wayne, R., Alaxander, F., Wellens, H.J.J., 2000. Hurst ' s The Heart.

Gao, S., Ho, D., Vatner, D.E., Vatner, S.F., 2011. Echocardiography in Mice. Curr. Protoc. Mouse Biol. 1, 71–83.

Gao, X.-M., Dart, A.M., Dewar, E., Jennings, G., Du, X.-J., 2000. Serial echocardiographic assessment of left ventricular dimensions and function after myocardial infarction in mice. Cardiovasc. Res. 45, 330–338.

Garne, E., Olsen, M.S., Johnsen, S.P., Hjortdal, V., Andersen, H.O., Nissen, H., Sondergaard, L., Videbaek, J., 2012. How Do We Define Congenital Heart Defects for Scientific Studies? Congenit. Heart Dis. 7, 46–49.

Garry, D.J., Olson, E.N., 2006. A Common Progenitor at the Heart of Development. Cell 127, 1101–1104.

Gesmhwnd, N., Levitsky, W., 1968. Human Brain : Left-Right Asymmetries in Temporal Speech Region. Science (80-.). 161, 186–187.

Ghanem, A., Willi, R., Hashemi, T., Dewald, O., Djoufack, P.C., Fink, K.B., Schrickel, J., Lewalter, T., Luderitz, B., Tiemann, K., 2006. Echocardiographic Assessment of Left Ventricular Mass in Neonatal and Adult Mice : Accuracy of Different Echocardiographic Methods. Echocardiography 23, 900–907.

Giummelly, P., Lartaud-Idjouadiene, I., Marque, V., Niederhoffer, N., Chillon, J.-M., Capdeville-Atkinson, C., Atkinson, J., 1999. Effects of Aging and Antihypertensive Treatment on Aortic Internal Diameter in Spontaneously Hypertensive Rats. Hypertension 34, 207–211.

Goldberg, R.L., Smith, S.W., 1994. Multilayer piezoelectric ceramics for two-dimensional array transducers. IEEE Trans. Ultrason. Ferroelectr. Freq. Control 41, 761–771.

Graham, R.M., Harvey, R.P., 2011. The Ontogeny of Cardiac Regeneration. Circ. Res. 108, 1304–1305.

Grant, A.O., 2009. Cardiac ion channels. Circ. Arrhythm. Electrophysiol. 2, 185–194.

Grego-Bessa, J., Luna-Zurita, L., del Monte, G., Bolós, V., Melgar, P., Arandilla, A., Garratt, A.N., Zang, H., Mukouyama, Y.-S., Chen, H., Shou, W., Ballestar, E., Esteller, M., Rojas, A., Pérez-Pomares, J.M., de la Pompa, J.L., 2007. Notch signaling is essential for ventricular chamber development. Dev. Cell 12, 415–429.

Greyson, C.R., 2010. The Right Ventricle and Pulmonary Circulation : Basic Concepts. Rev. Esp. Cardiol. 81–95.

Guo, X., Xiao-Fan, W., 2009. Signaling cross-talk between TGF-B/BMP and other pathways. Cell Res. 19, 71–88.

Hamada, H., 2010. Molecular Mechanisms of Left – Right Development, in: Heart Development and Regeneration. Elsevier Inc., pp. 297–306.

Hamada, H., Meno, C., Saijoh, Y., Adachi, H., Yashiro, K., Sakuma, R., Shiratori, H., 2001. Role of Asymmetric Signals in Left-Right Patterning in the Mouse. Am. J. Med. Genet. 101, 324–327.

Hang, C.T., Yang, J., Han, P., Cheng, H.-L., Shang, C., Ashley, E., Zhou, B., Chang, C.-P., 2010. Chromatin regulation by Brg1 underlies heart muscle development and disease. Nature 466, 62–67.

Harris, I.S., Black, B.L., 2010. Development of the endocardium. Pediatr. Cardiol. 31, 391–399.

Hartley, C.J., Taffet, G.E., Reddy, A.K., Entman, M.L., Michael, L.H., 2002. Noninvasive cardiovascular phenotyping in mice. ILAR J. 43, 147–158.

Hashimoto, H., Rebagliati, M., Ahmad, N., Muraoka, O., Kurokawa, T., Hibi, M., Suzuki, T., 2004. The Cerberus/Dan-family protein Charon is a negative regulator of Nodal signaling during left-right patterning in zebrafish. Development 131, 1741–1753.

Hatfield, A., Bodenham, A., 1999. Portable ultrasound for difficult central venous access. Br. J. Anaesth. 82, 822–826.

Heymann, M.A., Iwamoto, H.S., Rudolph, A.M., 1981. Factors affecting changes in the neonatal systemic circulation. Annu. Rev. Physiol. 43, 371–383.

Hinton, R.B., Alfieri, C.M., Witt, S.A., Glascock, B.J., Khoury, P.R., Benson, D.W., Yutzey, K.E., 2008. Mouse heart valve structure and function : echocardiographic and morphometric analyses from the fetus through the aged adult. Am. J. Physiol. Heart Circ. Physiol. 294, H2480–H2488.

Hirokawa, N., Tanaka, Y., Okada, Y., 2009. Left-right determination: involvement of molecular motor KIF3, cilia, and nodal flow. Cold Spring Harb. 1, a000802.

Hirokawa, N., Tanaka, Y., Okada, Y., 2012. Cilia, KIF3 molecular motor and nodal flow. Curr. Opin. Cell Biol. 24, 31–39.

Hirschy, A., Schatzmann, F., Ehler, E., Perriard, J., 2006. Establishment of cardiac cytoarchitecture in the developing mouse heart. Dev. Biol. 289, 430–441.

Ho, S.Y., Rigby, M.L., Anderson, R.H., 2005. Echocardiography in Congenital Heart Disease Made Simple.

Hoffman, J.I.E., Kaplan, S., 2002. The Incidence of Congenital Heart Disease. J. Am. Coll. Cardiol. 39, 1890–1900.

Hoodless, P.A., Pye, M., Chazaud, C., Labbé, E., Attisano, L., Rossant, J., Wrana, J.L., 2001. FoxH1 (Fast) functions to specify the anterior primitive streak in the mouse. Genes Dev. 15, 1257–1271.

Horsthuis, T., Christoffels, V.M., Anderson, R.H., Moorman, A.F.M., 2009. Can recent insights into cardiac development improve our understanding of congenitally malformed hearts? Clin. Anat. 22, 4–20.

Hsu, S.-C., Galceran, J., Grosschedl, R., 1998. Modulation of Transcriptional Regulation by LEF-1 in Response to Wnt-1 Signaling and Association with β -Catenin. Mol. Cell. Biol. 18, 4807–4818.

Huang, Y., Guo, X., Kassab, G.S., 2006. Axial nonuniformity of geometric and mechanical properties of mouse aorta is increased during postnatal growth. Am. J. Physiol. Heart Circ. Physiol. 290, H657–H664.

Huelsken, J., Birchmeier, W., 2001. New aspects of Wnt signaling pathways in higher vertebrates J. Curr. Opin. Genet. Dev. 11, 547–553.

Hutson, M.R., Zeng, X.L., Kim, A.J., Antoon, E., Harward, S., Kirby, M.L., 2010. Arterial pole progenitors interpret opposing FGF/BMP signals to proliferate or differentiate. Development 137, 3001–3011.

Icardo, J.M., 1988. Heart anatomy and developmental biology. Experientia 44, 910–919.

Ieda, M., Tsuchihashi, T., Ivey, K.N., Ross, R.S., Hong, T., Shaw, R.M., Srivastava, D., 2010. Cardiac Fibroblasts Regulate Myocardial Proliferation through ổBeta1 Integrin Signaling. Dev. Cell 16, 233–244.

Ikenishi, A., Okayama, H., Iwamoto, N., Yoshitome, S., Tane, S., Nakamura, K., Obayashi, T., Hayashi, T., Takeuchi, T., 2012. Cell cycle regulation in mouse heart during embryonic and postnatal stages. Dev. Growth Differ. 54, 731–738.

Inácio, J.M., Marques, S., Nakamura, T., Shinohara, K., Meno, C., Hamada, H., Belo, J.A., 2013. The dynamic right-to-left translocation of Cerl2 is involved in the regulation and termination of Nodal activity in the mouse node. PLoS One 8, e60406.

Ip, H.S., Wilson, D.B., Heikinheimo, M., Tang, Z., Ting, C.-N., Simon, M.C., Leiden, J.M., Parmacek, M.S., 1994. The GATA-4 transcription factor transactivates the cardiac muscle-specific troponin C promoter-enhancer in nonmuscle cells. Mol. Cell. Biol. 14, 7517–7526.

Janssen, B.J.A., De Celle, T., Debets, J.J.M., Brouns, A.E., Callahan, M.F., Smith, T.L., 2004. Effects of anesthetics on systemic hemodynamics in mice. Am. J. Physiol. Heart Circ. Physiol. 287, H1618–H1624.

Jones, W.K., Grupp, I.L., Doetschman, T., Grupp, G., Osinska, H., Hewett, T.E., Boivin, G., Gulick, J., Ng, W.A., Robbins, J., 1996. Ablation of the Murine alpha Myosin Heavy Chain Gene Leads to Dosage Effects and Functional Deficits in the Heart. J. Clin. Invest. 98, 1906–1917.

Kathiriya, I.S., Srivastava, D., 2000. Left-Right Asymmetry and Cardiac Looping : Implications for Cardiac Development and Congenital Heart Disease. Am. J. Med. Genet. 97, 271–279.

Kawabata, M., Imamura, T., Miyazono, K., 1998. Signal transduction by bone morphogenetic proteins. Cytokine Growth Factor Rev. 9, 49–61.

Kawasumi, A., Nakamura, T., Iwai, N., Yashiro, K., Saijoh, Y., Belo, J.A., Shiratori, H., Hamada, H., 2011. Left-right asymmetry in the level of active Nodal protein produced in the node is translated into left-right asymmetry in the lateral plate of mouse embryos. Dev. Biol. 353, 321–330.

Kelly, R.G., Brown, N.A., Buckingham, M.E., 2001. The Arterial Pole of the Mouse Heart Forms from Fgf10-Expressing Cells in Pharyngeal Mesoderm. Dev. Cell 1, 435–440.

Kelly, R.G., Buckingham, M.E., 2002. The anterior heart-forming field: voyage to the arterial pole of the heart. Trends Genet. 18, 210–216.

Keyes, W.M., Logan, C., Parker, E., Sanders, E.J., 2003. Expression and function of bone morphogenetic proteins in the development of the embryonic endocardial cushions. Anat. Embryol. (Berl). 207, 135–147.

Kiatchoosakun S., Restivo J., Kirkpatrick D., Hoit B. D. 2002. Assessment of left ventricular mass in mice: comparison between two-dimensional and m-mode echocardiography. Echocardiography. 19:199–204

Kirby, M.L., 2007. Cardiac Development.

Kitajima, K., Oki, S., Ohkawa, Y., Sumi, T., Meno, C., 2013. Wnt signaling regulates left – right axis formation in the node of mouse embryos. Dev. Biol. 380, 222–232.

Kitamura, R., Takahashi, T., Nakajima, N., Isodono, K., Asada, S., Ueno, H., 2007. Stage-Specific Role of Endogenous Smad2 Activation in Cardiomyogenesis of Embryonic Stem Cells. Circ. Res. 101, 78–87.

Kohl, P., Camelliti, P., Burton, F.L., Smith, G.L., 2005. Electrical coupling of fibroblasts and myocytes: relevance for cardiac propagation. J. Electrocardiol. 38, 45–50.

Kohn, A.D., Moon, R.T., 2005. Wnt and calcium signaling: beta-catenin-independent pathways. Cell Calcium 38, 439–446.

Kolettis, M., Jenkins, B.S., Webb-Peploe, M.M., 1976. Assessment of left ventricular function by indices derived from aortic flow velocity. Br. Heart J. 38, 18–31.

Krupinski, P., Chickarmane, V., Peterson, C., 2011. Simulating the mammalian blastocyst--molecular and mechanical interactions pattern the embryo. PLoS Comput. Biol. 7, e1001128.

Kusunose, K., Penn, M.S., Zhang, Y., Cheng, Y., Thomas, J.D., Marwick, T.H., Popović, Z.B., 2012. How similar are the mice to men? Between-species comparison of left ventricular mechanics using strain imaging. PLoS One 7, e40061.

Lai, D., Liu, X., Forrai, A., Wolstein, O., Michalicek, J., Ahmed, I., Garratt, A.N., Birchmeier, C., Zhou, M., Hartley, L., Robb, L., Feneley, M.P., Fatkin, D., Harvey, R.P., 2010. Neuregulin 1 sustains the gene regulatory network in both trabecular and nontrabecular myocardium. Circ. Res. 107, 715–727.

Lamers, W.H., Moorman, A.F.M., 2002. Cardiac Septation: A Late Contribution of the Embryonic Primary Myocardium to Heart Morphogenesis. Circ. Res. 91, 93–103.

Laugwitz, K.-L., Moretti, A., Caron, L., Nakano, A., Chien, K.R., 2008. Islet1 cardiovascular progenitors: a single source for heart lineages? Development 135, 193–205.

Lavine, K.J., Ornitz, D.M., 2008. Fibroblast growth factors and Hedgehogs: at the heart of the epicardial signaling center. Trends Genet. 24, 33–40.

Lavine, K.J., Ornitz, D.M., 2009. Shared circuitry: developmental signaling cascades regulate both embryonic and adult coronary vasculature. Circ. Res. 104, 159–169.

Lavine, K.J., Yu, K., White, A.C., Zhang, X., Smith, C., Partanen, J., Ornitz, D.M., 2005. Endocardial and epicardial derived FGF signals regulate myocardial proliferation and differentiation in vivo. Dev. Cell 8, 85–95.

Le, V.P., Knutsen, R.H., Mecham, R.P., Wagenseil, J.E., 2011. Decreased aortic diameter and compliance precedes blood pressure increases in postnatal development of elastin-insufficient mice. Am. J. Physiol. Heart Circ. Physiol. 301, H221–H229.

Le, V.P., Wagenseil, J.E., 2012. Echocardiographic Characterization of Postnatal Development in Mice with Reduced Arterial Elasticity. Cardiovasc. Eng. Technol. 3, 424–438.

Lenhart, K.F., Holtzman, N.G., Williams, J.R., Burdine, R.D., 2013. Integration of Nodal and BMP Signals in the Heart Requires FoxH1 to Create Left – Right Differences in Cell Migration Rates That Direct Cardiac Asymmetry. PLoS Genet. 9, e1003109.

Leonard, C.M., Eckert, M.A., 2009. Asymmetry and Dyslexia. Dev Neuropsychol. 33, 663–681.

Li, F., Wang, X., Capasso, J.M., Gerdes, A.M., 1996. Rapid transition of cardiac myocytes from hyperplasia to hypertrophy during postnatal development. J. Mol. Cell. Cardiol. 28, 1737–1746.

Li, J.-M., Brooks, G., 1999. Cell cycle regulatory molecules (cyclins , cyclin-dependent kinases and cyclin-dependent kinase inhibitors) and the cardiovascular system. Potential targets for therapy? Eur. Heart J. 20, 406–420.

Li, Y.Y., Feng, Y.Q., Kadokami, T., McTiernan, C.F., Draviam, R., Watkins, S.C., Feldman, A.M., 2000. Myocardial extracellular matrix remodeling in transgenic mice overexpressing tumor necrosis factor alpha can be modulated by anti-tumor necrosis factor alpha therapy. Proc. Natl. Acad. Sci. U. S. A. 97, 12746–12751.

Liang, Q., De Windt, L.J., Witt, S.A., Kimball, T.R., Markham, B.E., Molkentin, J.D., 2001. The transcription factors GATA4 and GATA6 regulate cardiomyocyte hypertrophy in vitro and in vivo. J. Biol. Chem. 276, 30245–30253.

Liao, Y., Ishikura, F., Beppu, S., Asakura, M., Takashima, S., Asanuma, H., Sanada, S., Kim, J., Ogita, H., Kuzuya, T., Node, K., Kitakaze, M., Hori, M., 2002. Echocardiographic assessment of LV hypertrophy and function in aortic-banded mice: necropsy validation. Am. J. Physiol. Heart Circ. Physiol. 282, H1703–H1708.

Lin, C.-J., Lin, C.-Y., Chen, C.-H., Zhou, B., Chang, C.-P., 2012. Partitioning the heart: mechanisms of cardiac septation and valve development. Development 139, 3277–3299.

Livak, K.J., Schmittgen, T.D., 2001. Analysis of relative gene expression data using real-time quantitative PCR and the 2(-Delta Delta C(T)) Method. Methods 25, 402–408.

Loepke, A.W., Istaphanous, G.K., McAuliffe, J.J., Miles, L., Hughes, E.A., McCann, J.C., Harlow, K.E., Kurth, C.D., Williams, M.T., Vorhees, C. V, Danzer, S.C., 2009. The effects of neonatal isoflurane exposure in mice on brain cell viability, adult behavior, learning, and memory. Anesth. Analg. 108, 90–104.

Lough, J., Sugi, Y., 2000. Endoderm and Heart Development. Dev. Dyn. 217, 327–342.

Luxán, G., Casanova, J.C., Martínez-Poveda, B., Prados, B., D'Amato, G., MacGrogan, D., Gonzalez-Rajal, A., Dobarro, D., Torroja, C., Martinez, F., Izquierdo-García, J.L., Fernández-Friera, L., Sabater-Molina, M., Kong, Y.-Y., Pizarro, G., Ibañez, B., Medrano, C., García-Pavía, P., Gimeno, J.R., Monserrat, L., Jiménez-Borreguero, L.J., de la Pompa, J.L., 2013. Mutations in the NOTCH pathway regulator MIB1 cause left ventricular noncompaction cardiomyopathy. Nat. Med. 19, 193–201.

Magga, J., Vuolteenaho, O., Tokola, H., Marttila, M., Ruskoaho, H., 1997. Involvement of Transcriptional and Posttranscriptional Mechanisms in Cardiac Overload–Induced Increase of B-Type Natriuretic Peptide Gene Expression. Circ. Res. 81, 694–702.

Mäkikallio, K., Rounioja, S., Vuolteenaho, O., Paakkari, J., Hallman, M., Räsänen, J., 2006. Fetal cardiac natriuretic peptide expression and cardiovascular hemodynamics in endotoxin-induced acute cardiac dysfunction in mouse. Pediatr. Res. 59, 180–184.

Manabe, I., Shindo, T., Nagai, R., 2002. Gene Expression in Fibroblasts and Fibrosis: Involvement in Cardiac Hypertrophy. Circ. Res. 91, 1103–1113.

Männer, J., Pérez-Pomares, J.M., Macías, D., Muñoz-Chápuli, R., 2001. The origin, formation and developmental significance of the epicardium: a review. Cells. Tissues. Organs 169, 89–103.

Marikawa, Y., Alarcón, V.B., 2010. Establishment of trophectoderm and inner cell mass lineages in the mouse embryo. Mol. Reprod. Dev. 76, 1019–1032.

Marques, S., Borges, A.C., Silva, A.C., Freitas, S., Cordenonsi, M., Belo, J.A., 2004. The activity of the Nodal antagonist Cerl-2 in the mouse node is required for correct L/R body axis. Genes Dev. 18, 2342–2347.

Martin-Puig, S., Wang, Z., Chien, K.R., 2008. Lives of a heart cell: tracing the origins of cardiac progenitors. Cell Stem Cell 2, 320–331.

Matsuoka, R., 2007. GATA4 mutation and congenital cardiovascular diseases : Importance of phenotype and genetic background clarification. J. Mol. Cell. Cardiol. 43, 667 – 669.

Mcelhinney, D.B., Geiger, E., Blinder, J., Benson, D.W., Goldmuntz, E., 2003. NKX2.5 Mutations in Patients With Congenital Heart Disease. J. Am. Coll. Cardiol. 42, 1650–1655.

McFadden, D.G., Barbosa, A.C., Richardson, J. a, Schneider, M.D., Srivastava, D., Olson, E.N., 2005. The Hand1 and Hand2 transcription factors regulate expansion of the embryonic cardiac ventricles in a gene dosage-dependent manner. Development 132, 189–201.

Mcgrath, J., Brueckner, M., 2003. Cilia are at the heart of vertebrate left – right asymmetry. Curr. Opin. Genet. Dev. 385–392.

Mcgrath, J., Somlo, S., Makova, S., Tian, X., Brueckner, M., 2003. Two Populations of Node Monocilia Initiate Left-Right Asymmetry in the Mouse. Cell 114, 61–73.

McNally, E., Dellefave, L., 2009. Sarcomere mutations in cardiogenesis and ventricular noncompaction. Trends Cardiovasc. Med. 19, 17–21.

Meilhac, S.M., Esner, M., Kerszberg, M., Moss, J.E., Buckingham, M.E., 2004. Oriented clonal cell growth in the developing mouse myocardium underlies cardiac morphogenesis. J. Cell Biol. 5, 97–109.

Meno, C., Takeuchi, J., Sakuma, R., Koshiba-Takeuchi, K., Ohishi, S., Saijoh, Y., Miyazaki, J., ten Dijke, P., Ogura, T., Hamada, H., 2001. Diffusion of nodal signaling activity in the absence of the feedback inhibitor Lefty2. Dev. Cell 1, 127–138.

Mercola, M., Ruiz-Lozano, P., Schneider, M.D., 2011. Cardiac muscle regeneration: lessons from development. Genes Dev. 25, 299–309.

Mikawa, T., Brand, T., 2010. Epicardial Lineage : Origins and Fates, in: Heart Development and Regeneration. Elsevier Inc., pp. 325–344.

Mikhailov, A.T., Torrado, M., 2008. The enigmatic role of the ankyrin repeat domain 1 gene in heart development and disease. Int. J. Dev. Biol. 52, 811–821.

Miller, J.R., 2001. Protein family review The Wnts Gene organization and evolutionary history. Genome Biol. 3, 1–15.

Minchiotti, G., 2005. Nodal-dependant Cripto signaling in ES cells: from stem cells to tumor biology. Oncogene 24, 5668–5675.

Miquerol, L., Beyer, S., Kelly, R.G., 2011. Establishment of the mouse ventricular conduction system. Cardiovasc. Res. 91, 232–242.

Misra, C., Sachan, N., Mcnally, C.R., Koenig, S.N., Nichols, H.A., Guggilam, A., Lucchesi, P.A., Pu, W.T., Srivastava, D., Garg, V., 2012. Congenital Heart Disease – Causing Gata4 Mutation Displays Functional Deficits In Vivo. PLoS Genet. 8, e1002690.

Molkentin, J.D., Lin, Q., Duncan, S.A., Olson, E.N., 1997. Requirement of the transcription factor GATA4 for heart tube formation and ventral morphogenesis. Genes Dev. 11, 1061–1872.

Mollova, M., Bersell, K., Walsh, S., Savla, J., Das, T.L., Park, S.-Y., Silbertein, L.E., dos Remedios, C.G., Graham, D., Colan, S., Kuhn, B., 2012. Cardiomyocyte proliferation contributes to heart growth in young humans. PNAS 110, 1446–1451.

Moorman, A., Webb, S., Brown, N.A., Lamers, W., Anderson, R.H., 2003. Development of the heart : (1) formation of the cardiac chambers and arterial trunks. Heart 89, 806–814.

Moorman, A.F.M., Christoffels, V.M., 2003. Cardiac chamber formation: development, genes, and evolution. Physiol. Rev. 83, 1223–1267.

Mor-Avi, V., Lang, R.M., Badano, L.P., Belohlavek, M., Cardim, N.M., Derumeaux, G., Galderisi, M., Marwick, T., Nagueh, S.F., Sengupta, P.P., Sicari, R., Smiseth, O.A., Smulevitz, B., Takeuchi, M., Thomas, J.D., Vannan, M., Voigt, J.-U., Zamorano, J.L., 2011. Current and evolving echocardiographic techniques for the quantitative evaluation of cardiac mechanics: ASE/EAE consensus statement on methodology and indications endorsed by the Japanese Society of Echocardiography. Eur. J. Echocardiogr. 12, 167–205.

Morris, S.A., Teo, R.T.Y., Li, H., Robson, P., Glover, D.M., Zernicka-Goetz, M., 2010. Origin and formation of the first two distinct cell types of the inner cell mass in the mouse embryo. Proc. Natl. Acad. Sci. U. S. A. 107, 6364–6349.

Moss, R.L., Fitzsimons, D.P., 2002. Frank-Starling Relationship: Long on Importance, Short on Mechanism. Circ. Res. 90, 11–13.

Moustakas, a, Souchelnytskyi, S., Heldin, C.H., 2001. Smad regulation in TGF-beta signal transduction. J. Cell Sci. 114, 4359–4369.

Mysliwiec, M.R., Bresnick, E.H., Lee, Y., 2011. Endothelial Jarid2/Jumonji is required for normal cardiac development and proper Notch1 expression. J. Biol. Chem. 286, 17193–17204.

Nahrendorf, M., Badea, C., Hedlund, L.W., Figueiredo, J.-L., Sosnovik, D.E., Johnson, G.A., Weissleder, R., 2007. High Resolution Imaging of Murine Myocardial Infarction With Delayed Enhancement and Cine Micro-CT. Am. J. Physiol. Heart Circ. Physiol. 292, H3172–H3178.

Nakajima, Y., 2010. Second lineage of heart forming region provides new understanding of conotruncal heart defects. Congenit. Anom. (Kyoto). 50, 8–14.

Nakamura, T., Hamada, H., 2012. Left-right patterning: conserved and divergent mechanisms. Development 139, 3257–3262.

Nakamura, T., Saitoh, D., Kawasumi, A., Shinohara, K., Asai, Y., Takaoka, K., Dong, F., Takamatsu, A., Belo, J.A., Mochizuki, A., Hamada, H., 2012. Fluid Flow and Interlinked Feedback Loops Establish Left-Right Asymmetric Decay of Cerl2 mRNA in the Mouse Embryo. Nat. Commun. 3, 1- 48.

Nemer, M., 2008. Genetic insights into normal and abnormal heart development. Cardiovasc. Pathol. 17, 48 – 54.

Niessen, K., Karsan, A., 2008. Notch signaling in cardiac development. Circ. Res. 102, 1169–1181.

Nihoyannopoulos, P., Kisslo, J., 2009. Echocardiography.

Nishii, K., Morimoto, S., Minakami, R., Miyano, Y., Hashizume, K., Ohta, M., Zhan, D.-Y., Lu, Q.-W., Shibata, Y., 2008. Targeted disruption of the cardiac troponin T gene causes sarcomere disassembly and defects in heartbeat within the early mouse embryo. Dev. Biol. 322, 65–73.

Nishikimi, T., Maeda, N., Matsuoka, H., 2006. The role of natriuretic peptides in cardioprotection. Cardiovasc. Res. 69, 318–328.

Nonaka, S., Shiratori, H., Saijoh, Y., Hamada, H., 2002. Determination of left – right patterning of the mouse embryo by artificial nodal flow. Nature 418, 96–99.

Norris, D.P., 2012. Cilia , calcium and the basis of left-right asymmetry. BMC Biol. 10, 1–8.

Norton, J.M., 2001. Toward Consistent Definitions For Preload and Afterload. Adv. Phisiology Educ. 25, 53–61.

Nusse, R., 2005. Wnt signaling in disease and in development. Cell Res. 15, 28–32.

Odiete, O., Hill, M.F., Sawyer, D.B., 2012. Neuregulin in cardiovascular development and disease. Circ. Res. 111, 1376–1385.

Okada, Y., Takeda, S., Tanaka, Y., Izpisúa Belmonte, J.-C., Hirokawa, N., 2005. Mechanism of nodal flow: a conserved symmetry breaking event in left-right axis determination. Cell 121, 633–644.

Oki, S., Kitajima, K., Marques, S., Belo, J.A., Yokoyama, T., Hamada, H., Meno, C., 2009. Reversal of left-right asymmetry induced by aberrant Nodal signaling in the node of mouse embryos. Development 136, 3917–3925.

Oosterhout, M.F.M. Van, Arts, T., Bassingthwaighte, J.B., Reneman, R.S., Prinzen, F.W., 2002. Relation between local myocardial growth and blood flow during chronic ventricular pacing. Cardiovasc. Res. 53, 831–840.

Oosterhout, M.F.M. Van, Prinzen, F.W., Arts, T., Schreuder, J.J., Vanagt, W.Y.R., Cleutjens, J.P.M., Reneman, R.S., 1998. Asynchronous Electrical Activation Induces Asymmetrical Hypertrophy of the Left Ventricular Wall. Circulation 98, 588–595.

Pacher, P., Nagayama, T., Mukhopadhyay, P., Bátkai, S., Kass, D.A., 2008. Measurement of cardiac function using pressure–volume conductance catheter technique in mice and rats. Nat. Protoc. 3, 1422–1434.

Parisi, S., D'Andrea, D., Lago, C.T., Adamson, E.D., Persico, M.G., Minchiotti, G., 2003. Nodal-dependent Cripto signaling promotes cardiomyogenesis and redirects the neural fate of embryonic stem cells. J. Cell Biol. 163, 303–314.

Park, E.J., Watanabe, Y., Smyth, G., Miyagawa-Tomita, S., Meyers, E., Klingensmith, J., Camenisch, T., Buckingham, M., Moon, A., 2008. An FGF autocrine loop initiated in second heart field mesoderm regulates morphogenesis at the arterial pole of the heart. Development 135, 3599–3610.

Parthenakis, F.I., Kanakaraki, M.K., Kanoupakis, E.M., Skalidis, E.I., Diakakis, G.F., Filippou, O.K., Vardas, P.E., 2002. Value of Doppler index combining systolic and diastolic myocardial performance in predicting cardiopulmonary exercise capacity in patients with congestive heart failure: effects of dobutamine. Chest 121, 1935–1941.

Pashmforoush, M., Lu, J.T., Chen, H., Amand, T.S., Kondo, R., Pradervand, S., Evans, S.M., Clark, B., Feramisco, J.R., Giles, W., Ho, S.Y., Benson, D.W., Silberbach, M., Shou, W., Chien, K.R., 2004. Nkx2-5 Pathways and Congenital Heart Disease : Loss of Ventricular Myocyte Lineage Specification Leads to Progressive Cardiomyopathy and Complete Heart Block. Cell 117, 373–386.

Pasumarthi, K.B.S., Field, L.J., 2002. Cardiomyocyte Cell Cycle Regulation. Circ. Res. 90, 1044–1054.

Peng, Y., Popovic, Z.B., Sopko, N., Drinko, J., Zhang, Z., Thomas, J.D., Penn, M.S., 2009. Speckle tracking echocardiography in the assessment of mouse models of cardiac dysfunction. Am. J. Physiol. Heart Circ. Physiol. 297, H811–H820.

Pennisi, D.J., Ballard, V.L.T., Mikawa, T., 2003. Epicardium is required for the full rate of myocyte proliferation and levels of expression of myocyte mitogenic factors FGF2 and

its receptor, FGFR-1, but not for transmural myocardial patterning in the embryonic chick heart. Dev. Dyn. 228, 161–172.

Pérez-Pomares, J.M., González-Rosa, J.M., Muñoz-Chápuli, R., 2009. Building the vertebrate heart - an evolutionary approach to cardiac development. Int. J. Dev. Biol. 53, 1427–1443.

Piccolo, S., Eric, A., Luc, L., Bhattacharyya, S., Grunz, H., Bouwmeester, T., De Robertis, E.M., 1999. The head inducer Cerberus is a multifunctional antagonist of Nodal, BMP and Wnt signals. Nature 397, 707–710.

Pikkarainen, S., Tokola, H., Kerkelä, R., Ruskoaho, H., 2004. GATA transcription factors in the developing and adult heart. Cardiovasc. Res. 63, 196–207.

Popović, Z.B., Sun, J.P., Yamada, H., Drinko, J., Mauer, K., Greenberg, N.L., Cheng, Y., Moravec, C.S., Penn, M.S., Mazgalev, T.N., Thomas, J.D., 2005. Differences in left ventricular long-axis function from mice to humans follow allometric scaling to ventricular size. J. Physiol. 568, 255–265.

Porrello, E.R., Mahmoud, A.I., Simpson, E., Hill, J.A., Richardson, J.A., Olson, E.N., Sadek, H.A., 2011. Transient regenerative potential of the neonatal mouse heart. Science 331, 1078–80.

Prall, O.W.J., Menon, M.K., Solloway, M.J., Watanabe, Y., Bajolle, F., Biben, C., Mcbride, J.J., Robertson, B.R., Stennard, F.A., Wise, N., Schaft, D., Wolstein, O., B, M., Shiratori, H., Chien, K.R., Hamada, H., Black, B.L., Robertson, E.J., Buckingham, M.E., Harvey, R.P., 2010. An Nkx2-5/Bmp2/Smad1 negative feedback loop controls second heart field progenitor specification and proliferation. Cell 128, 947–959.

Pu, W.T., Ishiwata, T., Juraszek, A.L., Ma, Q., Izumo, S., 2004. GATA4 is a dosage-sensitive regulator of cardiac morphogenesis. Dev. Biol. 275, 235–244.

Qi, X., Yang, G., Yang, L., Lan, Y., Weng, T., Wang, J., Wu, Z., Xu, J., Gao, X., Yang, X., 2007. Essential role of Smad4 in maintaining cardiomyocyte proliferation during murine embryonic heart development. Dev. Biol. 311, 136–146.

Qiu, Z., Cang, Y., Goff, S.P., 2010. c-Abl tyrosine kinase regulates cardiac growth and development. Proc. Natl. Acad. Sci. 107, 1136–1141.

Ramsdell, A.F., 2005. Left-right asymmetry and congenital cardiac defects: getting to the heart of the matter in vertebrate left-right axis determination. Dev. Biol. 288, 1–20.

Randall, V., Mccue, K., Roberts, C., Kyriakopoulou, V., Beddow, S., Barrett, A.N., Vitelli, F., Prescott, K., Shaw-Smith, C., Devriendt, K., Bosman, E., Steffes, G., Steel, K.P., Simrick, S., Basson, M.A., Illingworth, E., Scambler, P.J., 2009. Great vessel development requires biallelic expression of Chd7 and Tbx1 in pharyngeal ectoderm in mice. J. Clin. Invest. 119, 3301–3310.

Reffelmann, T., Kloner, R.A., 2003. Transthoracic echocardiography in rats. Basic Res. Cardiol. 98, 275–284.

Risebro, C.A., Riley, P.R., 2006. Formation of the ventricles. Sci. World J. 6, 1862–1880.

Rochais, F., Mesbah, K., Kelly, R.G., 2009. Signaling pathways controlling second heart field development. Circ. Res. 104, 933–942.

Rodríguez Esteban, C., Capdevila, J., Economides, A.N., Pascual, J., Ortiz, Á., Izpisúa Belmonte, J.C., 1999. The novel Cer-like protein Caronte mediates the establishment of embryonic left-right asymmetry. Nature 401, 243–251.

Rohini, A., Agrawal, N., Koyani, C.N., Singh, R., 2010. Molecular targets and regulators of cardiac hypertrophy. Pharmacol. Res. 61, 269–280.

Rossant, J., Tam, P.P.L., 2009. Blastocyst lineage formation , early embryonic asymmetries and axis patterning in the mouse. Development 713, 701–713.

Roth, D.M., Swaney, J.S., Dalton, N.D., Gilpin, E.A., Ross, J., 2002. Impact of anesthesia on cardiac function during echocardiography in mice. Am. J. Physiol. Heart Circ. Physiol. 282, H2134–H2140.

Rottman, J.N., Ni, G., Brown, M., 2007. Echocardiographic Evaluation of Ventricular Function in Mice. Echocardiography 24, 83–89.

Rottman, J.N., Ni, G., Khoo, M., Wang, Z., Zhang, W., Anderson, M.E., Madu, E.C., 2003. Temporal Changes in Ventricular Function Assessed Echocardiographically in Conscious and Anesthetized Mice. J. Am. Soc. Echocardiogr. 16, 1150–1157.

Rubart, M., Field, L.J., 2006. Cardiac Regeneration: Repopulating the Heart. Annu. Rev. Physiol. 68, 29–49.

Rumiantsev, P.P., Bruce, M.C., 1991. Growth and hyperplasia of cardiac muscle cells., in: London, U.K.: Harwood Academic Publishers.

Sahn D.J., DeMaria A., Kisslo J., Weyman A., 1978. Recommendations regarding quantitation in M-mode echocardiography: results of a survey of echocardiographic echocardiographic measurements. Circulation. 58:1072–1083.

Satir, P., Christensen, S.T., 2007. Overview of structure and function of mammalian cilia. Annu. Rev. Physiol. 69, 377–400.

Satir, P., Christensen, S.T., 2008. Structure and function of mammalian cilia. Histochem. Cell Biol. 129, 687–693.

Schier, A.F., 2003. Nodal Signaling in Vertebrate Development. Annu. Rev. Cell Dev. Biol. 19, 589–621.

Schier, A.F., 2009. Nodal morphogens. Cold Spring Harb. Perspect. Biol. 1, a003459.

Schlueter, J., Brand, T., 2011. Origin and fates of the proepicardium. Aswan Hear. Centre, Sci. Pract. Ser. 11, 1–18.

Schneider, J.E., Stork, L.-A., Bell, J.T., ten Hove, M., Isbrandt, D., Clarke, K., Watkins, H., Lygate, C.A., Neubauer, S., 2008. Cardiac structure and function during ageing in energetically compromised Guanidinoacetate N-methyltransferase (GAMT)-knockout mice - a one year longitudinal MRI study. J. Cardiovasc. Magn. Reson. 10, 1–9.

Sedmera, D., 2010. Factors in ventricular and atrioventricular valve growth: An embryologist's perspective. Prog. Pediatr. Cardiol. 29, 11–14.

Sedmera, D., 2011. Function and form in the developing cardiovascular system. Cardiovasc. Res. 91, 252–259.

Sedmera, D., Hu, N., Weiss, K.M., Keller, B.B., Denslow, S., Thompson, R.P., 2002. Cellular changes in experimental left heart hypoplasia. Anat. Rec. 267, 137–145.

Sedmera, D., Pexieder, T., Vuillemin, M., Thompson, R.P., Anderson, R.H., 2000. Developmental Patterning of the Myocardium. Anat. Rec. 258, 319–337.

Sedmera, D., Reckova, M., DeAlmeida, A., Coppen, S.R., Kubalak, S.W., Gourdie, R.G., Thompson, R.P., 2003. Spatiotemporal pattern of commitment to slowed proliferation in the embryonic mouse heart indicates progressive differentiation of the cardiac conduction system. Anat. Rec. A. Discov. Mol. Cell. Evol. Biol. 274, 773–777.

Sedmera, D., Thompson, R.P., 2011. Myocyte proliferation in the developing heart. Dev. Dyn. 240, 1322–1334.

Seidman, J.G., Seidman, C., 2001. The Genetic Basis for Cardiomyopathy : from Mutation Identification to Mechanistic Paradigms. Cell 104, 557–567.

Semeniuk, L.M., Kryski, A.J., Severson, D.L., 2002. Echocardiographic assessment of cardiac function in diabetic db/db and transgenic db/db-hGLUT4 mice. Am. J. Physiol. Heart Circ. Physiol. 283, H976–H982.

Shen, M.M., 2007. Nodal signaling: developmental roles and regulation. Development 134, 1023–1034.

Shiraishi, I., Ichikawa, H., 2012. Human Heterotaxy Syndrome-From Molecular Genetics to Clinical Features, Managemens, and Prognosis-. Circ. J. 76, 2066–2075.

Shiratori, H., Hamada, H., 2006. The left-right axis in the mouse : from origin to morphology. Development 133, 2095–2104.

Shiratori, H., Sakuma, R., Watanabe, M., Hashiguchi, H., Mochida, K., Sakai, Y., Nishino, J., Saijoh, Y., Whitman, M., Hamada, H., 2001. Two-step regulation of left-right asymmetric expression of Pitx2: initiation by nodal signaling and maintenance by Nkx2. Mol. Cell 7, 137–49.

Simpson, E.M., Linder, C.C., Sargent, E.E., Davisson, M.T., Mobraaten, L., Sharp, J.J., 1997. Genetic variation among 129 substrains and its importance for targeted mutagenesis in mice. Nat. Genet. 16, 19–27.

Smith, T.K., Bader, D.M., 2007. Signals from both sides: Control of cardiac development by the endocardium and epicardium. Semin. Cell Dev. Biol. 18, 84–89.

Soonpaa, M.H., Kim, K.K., Pajak, L., Franklin, M., Field, L.J., 1996. Cardiomyocyte DNA synthesis and binucleation during murine development. Am. Physiol. Soc. 271, H2183–H2189.

Stankunas, K., Hang, C.T., Tsun, Z.-Y., Chen, H., Lee, N. V, Wu, J.I., Shang, C., Bayle, J.H., Shou, W., Iruela-Arispe, M.L., Chang, C.-P., 2008. Endocardial Brg1 represses ADAMTS1 to maintain the microenvironment for myocardial morphogenesis. Dev. Cell 14, 298–311.

Stanley, E.G., Biben, C., Elefanty, A., Barnett, L., Koentgen, F., Robb, L., Harvey, R.P., 2002. Efficient cre-mediated deletion in cardiac progenitor cells con- ferred by a 3 ' UTR-ires-Cre allele of the homeobox gene Nkx2-5. Int. J. Dev. Bio 46, 431–439.

Stennard, F.A., Harvey, R.P., 2010. T-box transcription factors and their roles in regulatory hierarchies in the developing heart. Development 132, 4897–4910.

Strizzi, L., Hardy, K.M., Kirsammer, G.T., Gerami, P., Hendrix, M.J.C., 2011. Embryonic signaling in melanoma: potential for diagnosis and therapy. Lab. Investig. 91, 819–824.

Stypmann, J., Engelen, M.A., Epping, C., van Rijen, H.V.M., Milberg, P., Bruch, C., Breithardt, G., Tiemann, K., Eckardt, L., 2006. Age and gender related reference values for transthoracic Doppler-echocardiography in the anesthetized CD1 mouse. Int. J. Cardiovasc. Imaging 22, 353–362.

Stypmann, J., Engelen, M.A., Troatz, C., Rothenburger, M., Eckardt, L., Tiemann, K., 2009. Echocardiographic assessment of global left ventricular function in mice. Lab. Anim. 43, 127–137.

Sugihara, M., Odagiri, F., Suzuki, T., Murayama, T., Nakazato, Y., Unuma, K., Yoshida, K., Daida, H., Sakurai, T., Morimoto, S., Kurebayashi, N., 2013. Usefulness of running wheel for detection of congestive heart failure in dilated cardiomyopathy mouse model. PLoS One 8, e55514.

Supp, D.M., Witte, D.P., Potter, S.S., Brueckner, M., 1997. Mutation of an axonemal dynein affects left–right asymmetry in inversus viscerum mice. Nature 389, 963–966.

Sutton, M., Maniet, A.R., 2003. Normal transesophageal echocardiographic examination, in: Atlas of Multiplane Transesophageal Echocardiography.

Swynghedauw, B., 1999. Molecular mechanisms of myocardial remodeling. Physiol. Rev. 79, 1577–1584.

Syed, F., Diwan, A., Hahn, H.S., 2005. Murine echocardiography: a practical approach for phenotyping genetically manipulated and surgically modeled mice. J. Am. Soc. Echocardiogr. 18, 982–990.

Takaoka, K., Hamada, H., 2012. Cell fate decisions and axis determination in the early mouse embryo. Development 139, 3–14.

Takaoka, K., Yamamoto, M., Hamada, H., 2011. Origin and role of distal visceral endoderm, a group of cells that determines anterior-posterior polarity of the mouse embryo. Nat. Cell Biol. 13, 743–752.

Takeuchi, J.K., Ohgi, M., Koshiba-Takeuchi, K., Shiratori, H., Sakaki, I., Ogura, K., Saujih, Y., Ogura, T., 2003. Tbx5 specifies the left / right ventricles and ventricular septum position during cardiogenesis. Development 130, 5953–5964.

Tam, P.P.L., Behringer, R.R., 1997. Mouse gastrulation : the formation of a mammalian body plan. Mech. Dev. 68, 3–25.

Tanaka, C., Sakuma, R., Nakamura, T., Hamada, H., Saijoh, Y., 2007. Long-range action of Nodal requires interaction with GDF1. Genes Dev. 21, 3272–3282.

Tanaka, N., Dalton, N.D., Mao, L., Rockman, H.A., Peterson, K.L., Gottshall, K.R., Hunter, J.J., Chien, K.R., Ross, J.J., 1996. Transthoracic echocardiography in models of cardiac disease in the mouse. Circulation 94, 1109–1117.

Tanaka, Y., Okada, Y., Hirokawa, N., 2005. FGF-induced vesicular release of Sonic hedgehog and retinoic acid in leftward nodal flow is critical for left-right determination. Nature 435, 172–177.

Tardiff, J.C., Hewett, T.E., Palmer, B.M., Olsson, C., Factor, S.M., Moore, R.L., Robbins, J., Leinwand, L.A., 1999. Cardiac troponin T mutations result in allele-specific phenotypes in a mouse model for hypertrophic cardiomyopathy. J. Clin. Invest. 104, 469–481.

Targoff, K.L., Schell, T., Yelon, D., 2008. Nkx genes regulate heart tube extension and exert differential effects on ventricular and atrial cell number. Dev. Biol. 322, 314–321.

Ten Dijke, P., Hill, C.S., 2004. New insights into TGF-beta-Smad signalling. Trends Biochem. Sci. 29, 265–273.

Thierfelder, L., Watkins, H., MacRae, C., Lamas, R., McKenna, W., Vosberg, H.-P., Seidman, J.G., Seidman, C.E., 1994. Alpha-tropomyosin and cardiac troponin T mutations cause familial hypertrophic cardiomyopathy: a disease of the sarcomere. Cell 77, 701–712.

Thomas, T., Yamagishi, H., Overbeek, P.A., Olson, E.N., Srivastava, D., 1998. The bHLH factors, dHAND and eHAND, specify pulmonary and systemic cardiac ventricles independent of left-right sidedness. Dev. Biol. 196, 228–236.

Tiemann, K., Weyer, D., Djoufack, P.C., Ghanem, A., Lewalter, T., Dreiner, U., Meyer, R., Grohe, C., Fink, K.B., 2003. Increasing myocardial contraction and blood pressure in C57BL/6 mice during early postnatal development. Am. J. Physiol. Heart Circ. Physiol. 284, H464–H474.

Toischer, K., Rokita, A.G., Unsöld, B., Zhu, W., Kararigas, G., Sossalla, S., Reuter, S.P., Becker, A., Teucher, N., Seidler, T., Grebe, C., Preub, L., Gupta, S.N., Schmidt, K., Lehnart, S.E., Krüger, M., Wolfgang, L., Backs, J., Regitz-Zagrosek, V., Schäfer, K., Field, L.J., Maier, L.S., Hasenfuss, G., 2010. Differential Cardiac Remodeling in Preload. Circulation 122, 993–1003.

Torres-Padilla, M.-E., Richardson, L., Kolasinska, P., Sigolène, M.M., Luetke-Eversloh, M.V., Zernicka-Goetz, M., 2007. The anterior visceral endoderm of the mouse embryo is established from both preimplantation precursor cells and by de novo gene expression after implantation. Dev. Biol. 309, 97–112.

Tortora, G. & Grabowski, S. 2000. Principles of Anatomy & Physiology. Wiley & Sons.

Uosaki, H., Andersen, P., Shenje, L.T., Fernandez, L., Christiansen, S.L., Kwon, C., 2012. Direct contact with endoderm-like cells efficiently induces cardiac progenitors from mouse and human pluripotent stem cells. PLoS One 7, e46413.

Van den Berg, G., Abu-Issa, R., de Boer, B.A., Hutson, M.R., de Boer, P.A.J., Soufan, A.T., Ruijter, J.M., Kirby, M.L., van den Hoff, M.J.B., Moorman, A.F.M., 2009. A caudal proliferating growth center contributes to both poles of the forming heart tube. Circ. Res. 104, 179–188.

Van Nierop, B.J., van Assen, H.C., van Deel, E.D., Niesen, L.B.P., Duncker, D.J., Strijkers, G.J., Nicolay, K., 2013. Phenotyping of left and right ventricular function in mouse models of compensated hypertrophy and heart failure with cardiac MRI. PLoS One 8,

Van Rooij, E., Sutherland, L.B., Qi, X., Richardson, J.A., Hill, J., Olson, E.N., 2007. Control of Stress-Dependent Cardiac Growth and Gene Expression by a MicroRNA. Science 316, 575–579.

Van Vliet, P., Wu, S.M., Zaffran, S., Pucéat, M., 2012. Early cardiac development: a view from stem cells to embryos. Cardiovasc. Res. 96, 352–362.

Van Weerd, J.H., Koshiba-Takeuchi, K., Kwon, C., Takeuchi, J.K., 2011. Epigenetic factors and cardiac development. Cardiovasc. Res. 91, 203–211.

Van Wijk, B., Moorman, A.F.M., van den Hoff, M.J.B., 2007. Role of bone morphogenetic proteins in cardiac differentiation. Cardiovasc. Res. 74, 244–255.

Vandenberg, L.N., Levin, M., 2013. A unified model for left-right asymmetry? Comparison and synthesis of molecular models of embryonic laterality. Dev. Biol. 379, 1–15.

Veerkamp, J., Rudolph, F., Cseresnyes, Z., Priller, F., Otten, C., Renz, M., Schaefer, L., Abdelilah-Seyfried, S., 2013. Unilateral Dampening of Bmp Activity by Nodal Generates Cardiac Left-Right Asymmetry. Dev. Cell 24, 1–8.

Villapol, S., Logan, T.T., Symes, A.J., 2013. Role of TGF-β Signaling in Neurogenic Regions After Brain Injury. INTECH 1, 3–36.

Vincent, S.D., Buckingham, M.E., 2010. How to make a heart: the origin and regulation of cardiac progenitor cells. Curr. Top. Dev. Biol. 90, 1–41.

Vincentz, J.W., Barnes, R.M., Firulli, B.A., Conway, S.J., Firulli, A.B., 2008. Cooperative interaction of Nkx2.5 and Mef2c transcription factors during heart development. Dev. Dyn. 237, 3809–3819.

Vincentz, J.W., McWhirter, J.R., Murre, C., Baldini, A., Furuta, Y., 2005. Fgf15 is required for proper morphogenesis of the mouse cardiac outflow tract. Genesis 41, 192–201.

Vinereanu, D., Nicolaides, E., Boden, L., Payne, N., Jone, C.J., G, F.A., 2003. Conduit arterial stiffness is associated with impaired left ventricular subendocardial function. Heart 89, 449–451.

Vinhas, M., Araújo, A.C., Ribeiro, S., Rosário, L.B., Belo, J.A., 2013. Transthoracic echocardiography reference values in juvenile and adult 129/Sv mice. Cardiovasc. Ultrasound 11, 1–10.

Vitarelli, A., Terzano, C., 2010. Do we have two hearts? New insights in right ventricular function supported by myocardial imaging echocardiography. Heart Fail. Rev. 15, 39–61.

Voelkel, N.F., Quaife, R.A., Leinwand, L.A., Barst, R.J., McGoon, M.D., Meldrum, D.R., Dupuis, J., Long, C.S., Rubin, L.J., Smart, F.W., Suzuki, Y.J., Gladwin, M., Denholm, E.M., Gail, D.B., 2006. Right ventricular function and failure: report of a National Heart, Lung, and Blood Institute working group on cellular and molecular mechanisms of right heart failure. Circulation 114, 1883–1891.

Von Gise, A., Lin, Z., Schlegelmilch, K., Honor, L.B., Pan, G.M., Buck, J.N., Ma, Q., Ishiwata, T., Zhou, B., Camargo, F.D., Pu, W.T., 2012. YAP1, the nuclear target of Hippo signaling, stimulates heart growth through cardiomyocyte proliferation but not hypertrophy. Proc. Natl. Acad. Sci. U. S. A. 109, 2394–2399.

Wagenseil, J.E., Mecham, R.P., 2009. Vascular Extracellular Matrix and Arterial Mechanics. Physiol. Rev. 80, 957–989.

Wagner, M., Siddiqui, M.A.Q.S., 2007. Signal Transduction in Early Heart Development (I): Cardiogenic Induction and Heart Tube Formation. Exp. Biol. Med. 232, 852–865.

Waldo, K.L., Hutson, M.R., Ward, C.C., Zdanowicz, M., Stadt, H.A., Kumiski, D., Abu-Issa, R., Kirby, M.L., 2005. Secondary heart field contributes myocardium and smooth muscle to the arterial pole of the developing heart. Dev. Biol. 281, 78–90.

Waldo, K.L., Kumiski, D.H., Wallis, K.T., Stadt, H. a, Hutson, M.R., Platt, D.H., Kirby, M.L., 2001. Conotruncal myocardium arises from a secondary heart field. Development 128, 3179–88.

Walsh, S., Ponte, A., Fleischmann, B.K., Jovinge, S., 2010. Cardiomyocyte cell cycle control and growth estimation in vivo — an analysis based on cardiomyocyte nuclei. Cardiovasc. Res. 86, 365–373.

Wang, G., Yeh, H.I., Lin, J.J., 1994. Characterization of cis-regulating elements and trans-activating factors of the rat cardiac troponin T gene. J. Biol. Chem. 269, 30595–30603.

Wessels, A., Sedmera, D., 2003. Developmental anatomy of the heart: a tale of mice and man. Physiol. Genomics 15, 165–176.

Wiesmann, F., Ruff, J., Hiller, K.-H., Rommel, E., Haase, A., Neubauer, S., 2000. Developmental changes of cardiac function and mass assessed with MRI in neonatal, juvenile, and adult mice. Am. J. Physiol. Heart Circ. Physiol. 278, H652–H657.

Wilkins, L.W.&, 2011. ECG Interpretation made incredibly easy!

Wu, J., Bu, L., Gong, H., Jiang, G., Li, L., Ma, H., Zhou, N., Chen, Z., Ye, Y., Niu, Y., Sun, A., Ge, J., Zou, Y., 2010. Timing on High-ResolutionEffects of Heart Rate and Anesthetic Timing on High-Resolution Echocardiographic Assessment Under Isoflurane Anesthesia in Mice. Jounal Utrasound Med. 29, 1771–1778.

Xavier-Neto, J., Shapiro, M.D., Houghton, L., Rosenthal, N., 2000. Sequential Programs of Retinoic Acid Synthesis in the Myocardial and Epicardial Layers of the Developing Avian Heart. Dev. Biol. 219, 129–141.

Xu, C., Liguori, G., Persico, M.G., Adamson, E.D., 1999. Abrogation of the Cripto gene in mouse leads to failure of postgastrulation morphogenesis and lack of differentiation of cardiomyocytes. Development 126, 483–494.

Yamamoto, M., Saijoh, Y., Perea-gomez, A., Shawlot, W., Behringer, R.R., Ang, S., Hamada, H., Meno, C., 2004. Nodal antagonists regulate formation of the anteroposterior axis of the mouse embryo. Nature 428, 387–392.

Yang, X.-P., Liu, Y.-H., Rhaleb, N.-E., Kurihara, N., Kim, H.E., Carretero, O.A., 1999. Echocardiographic assessment of cardiac function in conscious and anesthetized mice. Am. J. Physiol. Heart Circ. Physiol. 277, H1967–H1974.

Yared, K., Noseworthy, P., Weyman, A.E., McCabe, E., Picard, M.H., Baggish, A.L., 2011. Pulmonary artery acceleration time provides an accurate estimate of systolic pulmonary arterial pressure during transthoracic echocardiography. J. Am. Soc. Echocardiogr. 24, 687–692.

Yoshiba, S., Shiratori, H., Kuo, I.Y., Kawasumi, A., Shinohara, K., Nonaka, S., Asai, Y., Sasai, G., Belo, J.A., Sasaki, H., Nakai, J., Dworniczak, B., Ehrlich, B.E., Pennekamp, P., Hamada, H., 2013. Cilia at the node of mouse embryos sense fluid flow for left-right determination via Pkd2. Science 338, 226–231.

Yoshioka, H., Meno, C., Koshiba, K., Sugihara, M., Itoh, H., Ishimaru, Y., Inoue, T., Ohuchi, H., Semina, E. V, Murray, J.C., Hamada, H., Noji, S., 1998. Pitx2 , a Bicoid-Type Homeobox Gene , Is Involved in a Lefty-Signaling Pathway in Determination of Left-Right Asymmetry. Cell 94, 299–305.

Yuan, S.-M., Jing, H., 2010. Cardiac pathologies in relation to Smad-dependent pathways. Interact. Cardiovasc. Thorac. Surg. 11, 455–460.

Yutzey, K.E., Robbins, J., 2007. Principles of genetic murine models for cardiac disease. Circulation 115, 792–799.

Zaffran, S., Frasch, M., 2002. Early Signals in Cardiac Development. Circ. Res. 91, 457–469.

Zaffran, S., Kelly, R.G., Meilhac, S.M., Buckingham, M.E., Brown, N.A., 2004. Right Ventricular Myocardium Derives From the Anterior Heart Field. Circ. Res. 95, 261–268.

Zamora, M., Männer, J., Ruiz-Lozano, P., 2007. Epicardium-derived progenitor cells require beta-catenin for coronary artery formation. Proc. Natl. Acad. Sci. U. S. A. 104, 18109–18114.

Zeisberg, E.M., Ma, Q., Juraszek, A.L., Moses, K., Schwartz, R.J., Izumo, S., Pu, W.T., 2005. Morphogenesis of the right ventricle requires myocardial expression of Gata4. J. Clin. Invest. 115, 1522–1531.

Zheng, B., Wen, J.K., Han, M., 2003. Regulatory Factors Involved in Cardiogenesis. Biochem. 68, 650–657.

Zheng-Fischhöfer, Q., Ghanem, A., Kim, J.-S., Kibschull, M., Schwarz, G., Schwab, J.O., Nagy, J., Winterhager, E., Tiemann, K., Willecke, K., 2006. Connexin31 cannot functionally replace connexin43 during cardiac morphogenesis in mice. J. Cell Sci. 119, 693–701.

Zhou, B., Ma, Q., Rajagopal, S., Wu, S.M., Domian, I., Rivera-Feliciano, J., Jiang, D., von Gise, A., Ikeda, S., Chien, K.R., Pu, W.T., 2008. Epicardial progenitors contribute to the cardiomyocyte lineage in the developing heart. Nature 454, 109–113.

Zhou, Y., Foster, F.S., Parkes, R., Adamson, S.L., 2003. Developmental changes in left and right ventricular diastolic filling patterns in mice environment. Am. J. Physiol. Heart Circ. Physiol. 285, H1563–H1575.

Zhu, L., Marvin, M.J., Gardiner, A., Lassar, A.B., Mercola, M., Stern, C.D., Levin, M., 1999. Cerberus regulates left-right asymmetry of the embryonic head and heart. Curr. Biol. 9, 931–938.